Titre: Title:	Compressive Strength of Truss Bridge Members Made of Laced Built-Up Sections
Auteur: Author:	Oudom Chhoeng
Date:	2025
Type:	Mémoire ou thèse / Dissertation or Thesis
Référence: Citation:	Chhoeng, O. (2025). Compressive Strength of Truss Bridge Members Made of Laced Built-Up Sections [Thèse de doctorat, Polytechnique Montréal]. PolyPublie. https://publications.polymtl.ca/72074/

URL de PolyPublie: PolyPublie URL:	https://publications.polymtl.ca/72074/
Directeurs de recherche: Advisors:	Mahdi Ben Ftima
Programme: Program:	Génie civil

POLYTECHNIQUE MONTRÉAL

affiliée à l'Université de Montréal

Compressive Strength of Truss Bridge Members Made of Laced Built-Up Sections

OUDOM CHHOENG

Département des génies civil, géologique et des mines

Thèse présentée en vue de l'obtention du diplôme de *Philosophiæ Doctor*

Génie civil

Décembre 2025

POLYTECHNIQUE MONTRÉAL

affiliée à l'Université de Montréal

Cette thèse intitulée :

Compressive Strength of Truss Bridge Members Made of Laced Built-Up Sections

présentée par **Oudom CHHOENG**

en vue de l'obtention du diplôme de *Philosophiæ Doctor*

a été dûment acceptée par le jury d'examen constitué de :

Bruno MASSICOTTE, président
Mahdi BEN FTIMA, membre et directeur de recherche
Robert TREMBLAY, membre et codirecteur de recherche
Nicolas BOISSONNADE, membre et codirecteur de recherche
Sanda KOBOEVIC, membre
Kyle TOUSIGNANT, membre externe

DEDICATION

To my grandmothers, whose wisdom and prayer always guided me,

To my parents, for their unconditional love, support, and sacrifices,

To my wife, Kanhara, for her unwavering support, patience, and love throughout this journey …

ACKNOWLEDGEMENTS

Pursuing a PhD has been a dream of mine since I was young. At the time, I did not fully understand what it truly meant, but my curiosity and passion for learning always inspired me to continue my studies. Over the years, as I delved deeper into research, I came to understand the true meaning of a PhD – a journey of discovery, challenges and growth. Along this journey, I have been fortunate to receive the guidance, encouragement and support of many remarkable people, without whom this work would not have been possible.

First and foremost, I would like to express my sincere gratitude to my supervisor, Prof. Robert Tremblay. Our first contact was during a virtual meeting, where his kindness and openness left a strong impression. I still remember the first day I arrived in Montreal – new to the city and uncertain, I even missed our first in-person meeting. Despite this rocky start and the many challenges along the way, Prof. Tremblay has been generous with his guidance, advice, and support, providing invaluable insights and skills related to my research topic. I truly appreciated his patience, understanding, and encouragement throughout my PhD journey.

I am also deeply grateful to my co-supervisor, Prof. Nicolas Boissonade. From the very beginning, he has been consistently approachable and supportive. I always felt comfortable seeking his advice, discussing ideas, and sharing challenges, and he generously dedicated his time and expertise to guiding my research. Prof. Boissonade has been a mentor and academic role model for me, and his encouragement, thoughtful feedback, and constant support have been a source of motivation and inspiration throughout my PhD journey.

I would like to thank Prof. Mahdi Ben Ftima for taking over supervisory responsibilities after Prof. Tremblay's retirement. His careful review, constructive feedback, and insightful comments greatly contributed to improving this thesis. I also thank Prof. Bruno Massicotte for his support with admission and the testing program.

I would like to sincerely thank the professors Sanda Koboevic and Kyle Tousignant for kindly agreeing to serve as the chair and members of my thesis examination jury.

Many people contributed to making my time in Montreal productive and memorable. I wish to thank my colleagues, friends, and technicians at Polytechnique Montréal, especially Morane and

Kamrul, who were more than colleagues and friends, for sharing ideas, providing valuable advice, and helping me navigate life in a new city.

I am profoundly thankful to my family for their love, encouragement, and support. To my parents, who raised me with curiosity and a passion for learning, and to my siblings for always believing in me – your support has been a foundation for my journey. I am especially grateful to my wife, Kanhara, whose unwavering patience, care, and encouragement sustained me through the toughest moments. Your love and support have been my anchor throughout this journey.

Finally, I wish to acknowledge the funding provided by Jacques Cartier and Champlain Bridge Incorporated, which made this research possible. I also thank everyone who, directly or indirectly, contributed to my learning, growth, and the completion of this thesis.

RÉSUMÉ

Les pièces en acier assemblées, fréquemment utilisés dans les ponts en treillis et les structures métalliques lourdes, sont généralement constituées de sections en C ou de cornières reliées entre elles par des plaques discontinues, des plaques perforées, ou des barres de liaison. Durant la décennie 1950-1960 ces configurations assemblées constituaient une solution efficace pour former des éléments de grande section et de résistance élevée. Toutefois, leur comportement au flambement est particulièrement complexe, étant régi par l'interaction entre le voilement local de la section transversale, le flambement global des membrures longitudinales et le flambement d'ensemble de la pièce assemblée. Ces interactions sont souvent mal prises en compte dans les règlements actuels, créant une incertitude quant à la prédiction de leur résistance ultime et de leur fiabilité.

Cette thèse s'inscrit dans un projet de recherche lancé par Les Ponts Jacques-Cartier et Champlain Incorporée (PJCCI) dans le cadre de la déconstruction de l'ancien pont Champlain à Montréal. L'objectif principal est de proposer une méthode de conception rationnelle permettant d'évaluer la résistance en compression des pièces assemblées avec étrésillons, tout en tenant compte du voilement local, du flambement global et du flambement d'ensemble, ainsi que de leurs interactions. Pour y parvenir, une méthodologie basée sur des modèles par éléments finis (EF) est développée afin de reproduire fidèlement le comportement au flambement observé dans des essais expérimentaux de la littérature. Une fois validée, cette méthodologie est utilisée pour réaliser une vaste étude paramétrique, menant à l'élaboration d'équations de dimensionnement pratiques pour les membrures principales et leur système de liaison.

Le programme de recherche est structuré en trois études principales. La première propose une nouvelle équation pour estimer les efforts tranchants dans les pièces assemblés avec des systèmes de liaison simples (diagonales) et doubles (X). Les méthodes proposées dans les deuxième et troisième études reposent sur le concept d'interaction globale connu sous l'acronyme O.I.C. (*Overall Interaction Concept*) : la deuxième étude développe une approche de conception pour déterminer la résistance en compression des pièces assemblés à doubles liaisons (X) soumis à un flambement dans le plan, tandis que la troisième étend cette approche au flambement hors plan.

Les résultats montrent que les efforts tranchants de second ordre dans les pièces assemblées sont fortement influencés par la configuration des liaisons, l'élancement des sections et des barres de

liaison, ainsi que par la longueur de l'élément. Pour les éléments à élancement intermédiaire, ces efforts peuvent dépasser les valeurs minimales couramment supposées dans les normes, suggérant que ces hypothèses peuvent être insuffisantes pour les pièces élancées et trop conservatrices pour les pièces courtes. Les résultats démontrent également que l'interaction entre le voilement local, le flambement global des éléments longitudinaux et le flambement de l'ensemble influence significativement la résistance en compression des pièces assemblées. Les équations de conception existantes se révèlent non conservatrices pour certaines configurations, en particulier pour les sections et pièces très élancées. À travers les trois études, les équations proposées offrent une précision, une fiabilité et une performance prédictive nettement améliorées pour une large gamme de pièces assemblées avec barres de liaison, y compris celles qui ne respectent pas les limites géométriques ou d'élancement imposées par les normes actuelles.

Par ailleurs, les analyses de fiabilité réalisées conformément à l'EN 1990 et selon le cadre de l'AISC-LRFD, confirment que les règles de conception proposées offrent une méthode fiable et robuste pour la conception des pièces assemblés à liaisons. Les résultats contribuent ainsi au développement de directives de conception améliorées pour les pièces comprimés assemblés dans les structures en acier.

Mots-clés : résistance en compression, pièces en acier assemblées avec étrésillons, effort tranchant du second ordre, concept d'interaction globale (O.I.C.), interactions de flambement local/global/assemblé, flambement dans le plan, flambement hors plan, méthode de dimensionnement.

ABSTRACT

Built-up steel members, commonly used in truss bridges and heavy steel structures, are typically composed of C-shaped (channels) or angle-based sections (plates connected with angles to form a C-shape) connected by batten plates, lacing bars, or perforated plates. At the time, such built-up configurations were an efficient means of forming members with large cross-sections and high resistance. However, their buckling behaviour is highly complex, governed by the interaction between local buckling of the cross-section, global buckling of the chords, and the overall built-up buckling of the members. These interactions are often not fully captured in current design provisions, leading to uncertainty in predicting their ultimate strength and reliability.

This thesis is part of a research project initiated by Jacques Cartier and Champlain Bridge Incorporated (JCCBI) in relation to the deconstruction of the Original Champlain Bridge in Montreal, Canada. The primary objective of this thesis is to provide a rational design approach capable of evaluating the compressive resistance of laced built-up members while accounting for local, global, and overall built-up buckling, as well as their interactions. To achieve this, a methodology based on finite element (FE) models is developed to accurately replicate the buckling behaviour observed in laboratory tests from literature. The validated methodology is then used to perform extensive parametric studies, leading to the formulation of practical design equations for such members, including their lacing systems and main chords. The research is structured into three core studies. The first introduces a new design equation for estimating the shear force in laced built-up members with single (diagonal) and double (X) lacing systems. The second and third studies build upon the extended Overall Interaction Concept: the former proposes a design approach for evaluating the compressive resistance of double-X laced members under in-plane buckling, while the latter extends this approach to out-of-plane buckling.

The results show that second-order shear forces in laced built-up members are significantly influenced by lacing arrangement, lacing and chord slenderness, and member length. For members with intermediate slenderness, these shear forces can exceed the commonly assumed minimum values prescribed by design codes, indicating that these assumptions may be insufficient for slender members and overly conservative for short members. The findings further demonstrate that the interaction between local, global, and built-up buckling has a substantial effect on the overall capacity of built-up members. Existing design equations exhibit unconservative predictions for

certain configurations, particularly for sections and members with high slenderness. Across the three studies, the proposed equations consistently provide improved accuracy, reliability, and predictive capability for a broad range of laced built-up members, including cases outside the geometric and slenderness limits of current design standards. Furthermore, reliability analyses incorporating the tail approximation technique, conducted in accordance with EN 1990 and the AISC-LRFD framework, confirmed that the proposed design rules offer a safe and reliable method for designing laced built-up columns. The findings contribute to the development of improved design guidelines for built-up compression members in steel structures.

Keywords: compressive strength, laced built-up steel members, 2nd order shear force, Overall Interaction Concept, Local/Global/Built-up buckling interactions, in-plane buckling, out-of-plane buckling, design proposal.

TABLE OF CONTENTS

LIST OF TABLES

LIST OF FIGURES

LIST OF SYMBOLS AND ABBREVIATIONS

AASHTO	American Association of State Highway and Transportation Officials
AISC	American Institute of Steel Construction
AS	Australian Standard
C.o.V.	Coefficient of Variation
C.S.M	Continuous Strength Method
D.S.M.	Direct Strength Method
E.W.M.	Effective Width Method
EC 3	Eurocode EN 1993-1-1
F.E.	Finite Element
G.M.N.I.A.	Geometrically and Materially Non-linear with Imperfections Analysis
L.B.A.	Linear Buckling Analysis
O.I.C.	Overall Interaction Concept
T.A.	Tail Approximation

A, A_g, A_s	Total area of built-up section
A_{ch}, A_i	Area of individual chord section
$A_{ch,eff}$	Effective area of individual chord, calculated using E.W.M.
A_d	Area of diagonal lacing
A_{eff}	Effective cross-sectional area, calculated using E.W.M.
A_h, A_v	Area of horizontal lacing/member
a	Distance between lacing connections
a_L	Half-wavelength of local imperfections
$a_{i,f}$	Buckling length of flange plate

$a_{i,w}$	Buckling length of web plate
b	Width of C-sections (section geometry); mean value of the correction factor (reliability analysis)
b_o	Total width of cross-section
b_p	Width of tie-plate
C_r	Compressive resistance
D	Dead load
D_m	Mean value of dead load
d	Length of lacing member measured from connection point to connection point
E	Young's modulus
e	End distance from end of built-up member to edge of end tie-plate, measured along axial direction of built-up member
e_0	initial bow of imperfections
$e_{0,B}$, $e_{0,global}$	Amplitude of global imperfection in overall built-up member
$e_{0,G}$	Amplitude of global imperfection in individual chord segment between connectors
$e_{0,L}$, $e_{0,local,i}$	Amplitude of local imperfection in cross-section
$e_{0,L,f}$	Amplitude of local imperfection in flange plate
$e_{0,L,w}$	Amplitude of local imperfection in web plate
$e_{0,lacing}$	Amplitude of global imperfection in lacing bar
F_e	Elastic critical stress
F_m	Mean ratio of actual-to-specified plastic section modulus
F_n	Nominal stress
$f_{G/B}$	Interaction factor accounting for influences of global buckling on built-up buckling
$f_{L/G}$	Interaction factor accounting for influences of local buckling on global buckling

$f_{L/GB}$	Interaction factor accounting for influences of local buckling on built-up buckling
$f_{L/G/B}$	Interaction factor accounting for local, global, and built-up buckling interactions
f_y	Yield strength
$f_{y,mean}$	Mean value of yield strength
$f_{y,nom}$	Nominal value of yield strength
f_u	Ultimate tensile strength
G	Shear modulus
GA	Shear stiffness
$GA_{s,a}$	Shear stiffness resulting from the axial stiffness
$GA_{s,f}$	Shear stiffness resulting from flexural stiffness
h	Total height of cross-section
h_o	Distance between centroids of chords
h_p	Length of tie-plate
I, I_o	Second moment of area of built-up section
I_b	Second moment of area of horizontal lacing
I_c, I_{ch}	Second moment of area of individual chord section
I_{eff}	Effective second moment of area
K	Effective length factor
$k_{d,n}$	Design fractile factor
k_L	Factor accounting for the influence of local buckling
L	Length of test specimen (geometry); live load (reliability analysis)
L_B	Length of built-up member
L_{ch}	Buckling length of chord
L_G	Length of chord segment between connectors

L_L	Length of stub column
L_{lacing}	Length of lacing member measured between the centers of connection points
L_m	Mean value of live load
M_{Ed}	Design value of applied bending moment
M^I_{Ed}	Moment at mid-length of the built-up member without considering 2nd order effects
M_m	Mean ratio of actual-to-specified yield stress
N	Axial compression load
N_1, N_2	Compressive force in a truss chord
$N_{ch,Ed}$	Design axial force for each chord
N_{cr}	Elastic critical load
$N_{cr,e}$	Euler critical load
$N_{cr,B}$	Elastic critical load corresponding specifically to built-up buckling
$N_{cr,G}$	Elastic critical load corresponding specifically to global buckling of chords segment between connectors
$N_{cr,L}$	Elastic critical load corresponding specifically to local buckling of cross-section
N_{Ed}	Design axial compression axial force
N_{pl}	Plastic capacity of built-up section
$N_{pl,ch}$	Plastic capacity of individual chord section
N_u	Ultimate load or peak load
$N_{u,F.E.}$	Ultimate load predicted by F.E. analysis
$N_{u,L+G}$	Ultimate load considering local and global buckling
$N_{u,L+B}$	Ultimate load considering local and built-up buckling
$N_{u,L+G+B}$	Ultimate load considering local, global, and built-up buckling
$N_{u,Test}$	Ultimate load recorded during testing

n	Number of cases; factors depending on material and buckling curve; number of lacing plans; curve-fitting parameter
n_{tail}	Number of cases using T.A. technique
$P_{cr,e}$	Euler elastic critical load
P_m	Mean ratio of test-to-predicted resistance
P_n	Nominal compressive strength
P_{nl}	Local ultimate strength
P_{ne}	Nominal global axial strength
P_y	Full plastic resistance
$R_{b,L}$	Load ratio to reach local ultimate strength
$R_{cr,L}$	Load ratio to reach the critical instability limit
R_m	Mean value of resistance
R_n	Nominal value of resistance
R_{pl}	Load ratio to reach the limit plastic resistance
S_V	Shear stiffness
$S_{v,double}$	Shear stiffness of member with double (X) lacing system
$S_{v,single}$	Shear stiffness of member with single (diagonal) lacing system
r, r_i, $r_{i,b}$	Fillet radius (section geometry); radius of gyration (section property)
t_f	Thickness of flange plate
t_p	Thickness of tie-plate
t_w	Thickness of web plate
V, V_{Ed}	Shear force
V_F	C.o.V. of fabrication
V_{geom}	C.o.V. of section geometry

V_M	C.o.V. of material property (AISC-LRFD approach)
V_{mat}	C.o.V. of material property (European approach)
V_P	C.o.V. of professional judgment
V_Q	C.o.V. of load effect
V_R	C.o.V. of resistance
V_r	Combined C.o.V. of design model and basic variables
$V_{r,t}$	Combined C.o.V. of material and geometry variables
V_u, $V_{u,2nd}$	2nd order shear force
$V_{u,ext}$	Shear force due to external transverse load
V_δ	C.o.V. of uncertainty of numerical and experimental resistance
x_1, x_2	Factor of residual stress
$x_o - x_o$	Strong axis of built-up section
$y_o - y_o$	Weak axis of built-up section
α	Imperfection factor (buckling curve); separation factor (reliability analysis); amplitude of residual stress
α_B	Generalized imperfection factor for built-up buckling of overall member
α_e	Parameter for curve fitting
α_G	Generalized imperfection factor for global buckling of chord segments between connectors
α_L	Generalized imperfection factor for local buckling of cross-section
β	Factor accounting for possible strain hardening effects (material behaviour); safety index (reliability analysis); Factor associated with type of lacing configuration
β_1 β_2, β_3	Amplitude of residual stress
γ_V	Parameter accounting for sensitivity of web and flange plate buckling

ε_0, ε_{LB}	Strain value
γ_M	Partial safety factor (EC 3 format)
δ	Factor accounting for potential post-buckling effect
χ	Generalized reduction factor
χ_B	Generalized reduction factor for built-up buckling of overall member
χ_G	Generalized reduction factor for global buckling of chord segments between connectors
χ_L	Generalized reduction factor for local buckling of cross-section
χ_{G+B}	Generalized reduction factor accounting for global and built-up buckling
χ_{L+G}	Generalized reduction factor accounting for local and global buckling
χ_{L+B}	Generalized reduction factor accounting for local and built-up buckling
χ_{L+G+B}	Generalized reduction factor accounting for local, global, and built-up buckling
λ	Slenderness value corresponding to relevant buckling mode
$\overline{\lambda}_0$	Length of plateau of buckling curve
$\overline{\lambda}_B$	Generalized relative slenderness of built-up buckling of overall member
λ_c	Relative member slenderness
$\overline{\lambda}_G$	Generalized relative slenderness of global buckling of chord segments between connectors
$\overline{\lambda}_{G+B}$	Generalized relative slenderness of members including influence of global and built-up buckling
$\overline{\lambda}_L$	Generalized relative slenderness of local buckling of cross-section
λ_{lacing}	Relative slenderness ratio of lacing member
$\overline{\lambda}_{L+G}$	Generalized relative slenderness of members including influence of local and

	global buckling
$\bar{\lambda}_{L+B}$	Generalized relative slenderness of members including influence of local and Built-up buckling
$\bar{\lambda}_{L+G+B}$	Generalized relative slenderness of members including influence of local, global, and built-up buckling
λ_n	Relative member slenderness
λ_p	Relative plate slenderness
ϕ	Resistance factor (AISC format)
ϕ_2	Constant resistance factor
ϕ_B	Key parameter to determine χ_B
ϕ_G	Key parameter to determine χ_G
ϕ_L	Key parameter to determine χ_L
ϕ_{L+G}	Key parameter to determine χ_{L+G}
ρ_e	Equivalent slenderness ratio
ρ_i	Maximum slenderness ratio of individual components between connectors
ρ_o	Slenderness ratio of overall built-up member
$\sigma_{\max}$	Amplitude of residual stress
σ_{LB}	Local buckling stress

CHAPTER 1 INTRODUCTION

1.1 Background and motivation

This research project was launched by Jacques Cartier and Champlain Bridges Incorporated (JCCBI) in relation to the dismantling of the Original Champlain Bridge (1962–2019). Figure 1.1 illustrates the view of the Original Champlain Bridge before its deconstruction. The Original Champlain Bridge was a 3.4 km long structure crossing the St-Lawrence River that was completed in 1962 to link the Island of Montreal to its south shore suburbs. The portion of the bridge passing over the U.S.–Canada St-Lawrence Seaway channel was a 763.5 m long steel truss bridge structure that comprised two simply supported 78.3 m long approach spans on either side of a 450.5 m long cantilever bridge structure. The bridge included one central truss and two outer trusses that are spaced 22.1 m o/c. The remaining of the bridge consisted of 40 approach spans constructed with precast pre-stressed concrete girders.

Figure 1.1 The Original Champlain Bridge before its deconstruction [3].

Constructed in the early 1960s, the bridge provided a crucial link between Montreal and the South Shore. It featured a steel truss cantilever main span with prestressed concrete approach viaducts,

distinguished by its large scale and structural complexity, reflecting the engineering practices of its time. The cantilevered steel truss, combined with concrete viaducts, allowed for a long span over the Saint Lawrence River while accommodating heavy vehicular traffic. Its clearance beneath the deck ensured safe passage for maritime vessels, a key consideration for this major waterway [1], [2].

Despite the common deterioration of structures from this era, the Original Champlain Bridge's distinctive design made rehabilitation particularly difficult, ultimately leading to its replacement. The main contributing factors were:

- Complex original design: the cantilevered steel truss combined with prestressed concrete viaducts limited conventional repair methods, such as slab or beam replacement;
- Aging infrastructure: after more than 50 years in service, many structural components showed significant wear and degradation;
- Severe climatic and usage conditions: exposure to harsh winters, de-icing salts, and heavy traffic accelerated corrosion and material fatigue;
- Safety and reliability concerns: inspections indicated declining structural reliability, making long-term operation increasingly risky;
- Practicality of replacement: replacing the bridge was deemed more feasible and cost-effective than extensive rehabilitation, ensuring compliance with modern design standards and future traffic demands.

To take advantage of the Original Champlain Bridge deconstruction and given that JCCBI manages several major engineering structures in Canada, the organization launched a research initiative aimed at developing innovative techniques to enhance the durability of the infrastructure under its responsibility. The deconstruction of the Champlain Bridge provides a unique opportunity to advance knowledge of infrastructure performance and sustainability. Following a competition among Canadian research bodies in June 2019, JCCBI selected ten projects to be carried out during the deconstruction. Among the ten selected projects, ours focuses on *developing rational calculation methods and tools to evaluate the compressive strength of members in large steel truss bridges*, such as the Original Champlain Bridge. The knowledge gained from this bridge will be applied to assess the capacity of other structures managed by JCCBI, including the Jacques Cartier Bridge in Montreal (Figure 1.2) and similar bridges across Canada.

Figure 1.2 The Jacques Cartier Bridge [4].

1.2 Overall research problems

1.2.1 Built-up members in the Original Champlain and Jacques Cartier Bridges

The Original Champlain Bridge, completed in 1962, and the Jacques Cartier Bridge, opened in 1930, are two prominent examples of steel bridge construction in Montréal that employed different types of built-up members. Both bridges incorporated built-up steel members within their truss systems, yet the configuration of these members varied notably between the two structures.

As shown in Figure 1.1 and Figure 1.3, the Original Champlain Bridge adopted several configurations of built-up members within its truss system. The main truss members were built-up sections with batten plates, each consisting of two C-shaped sections joined by battens. These C-shaped sections were typically fabricated from two angle sections riveted to a continuous plate,

forming a C-section. The secondary truss members followed a similar arrangement, comprising two channel sections connected by battens. The bracing systems of the Original Champlain Bridge consisted of laced built-up members, formed either by closely spaced back-to-back C-shaped sections connected with diagonal lacing bars, or by members composed of four angles interconnected on all sides using diagonal lacing. These members primarily acted as tension braces, mobilizing axial tensile forces under lateral loading to restrain transverse displacements of the truss joints and to transfer lateral loads to the main load-resisting system, thereby enhancing the overall lateral stability of the truss structures.

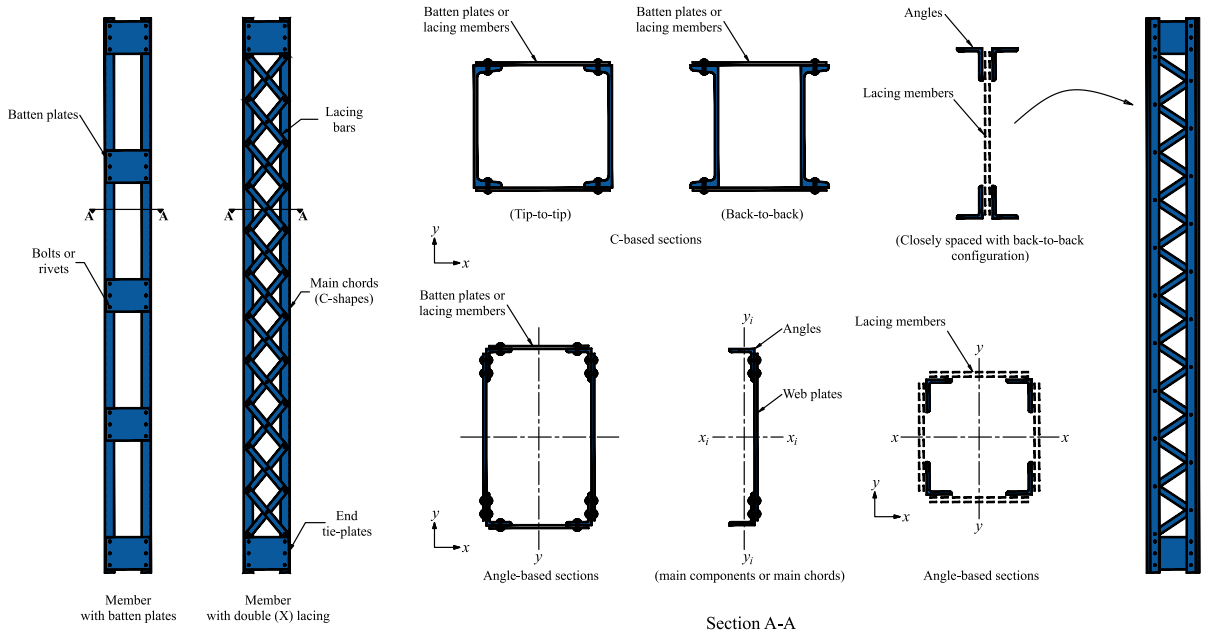

Figure 1.3 Typical built-up members used in the Original Champlain and Jacques Cartier Brides.

In contrast, the Jacques Cartier Bridge, shown in Figure 1.2 and Figure 1.3, adopted similar built-up member configurations for its primary truss members; however, lacing systems were used instead of batten plates to connect the main components. The use of different built-up member types, such as battened and laced members, underscore the challenges associated with buckling and the failure behaviour of built-up members, thereby motivating the overall research project. Figure 1.4 presents the possible failure modes of built-up members with batten plates and lacings. It shows the complex buckling behaviour resulting from the interaction between local buckling of the cross-section, global buckling of the chords, and overall built-up buckling of the member. Such interactions pose significant research challenges, as they are often overlooked in current design

approaches. A detailed discussion of these limitations and their implications for design is presented in the next sections.

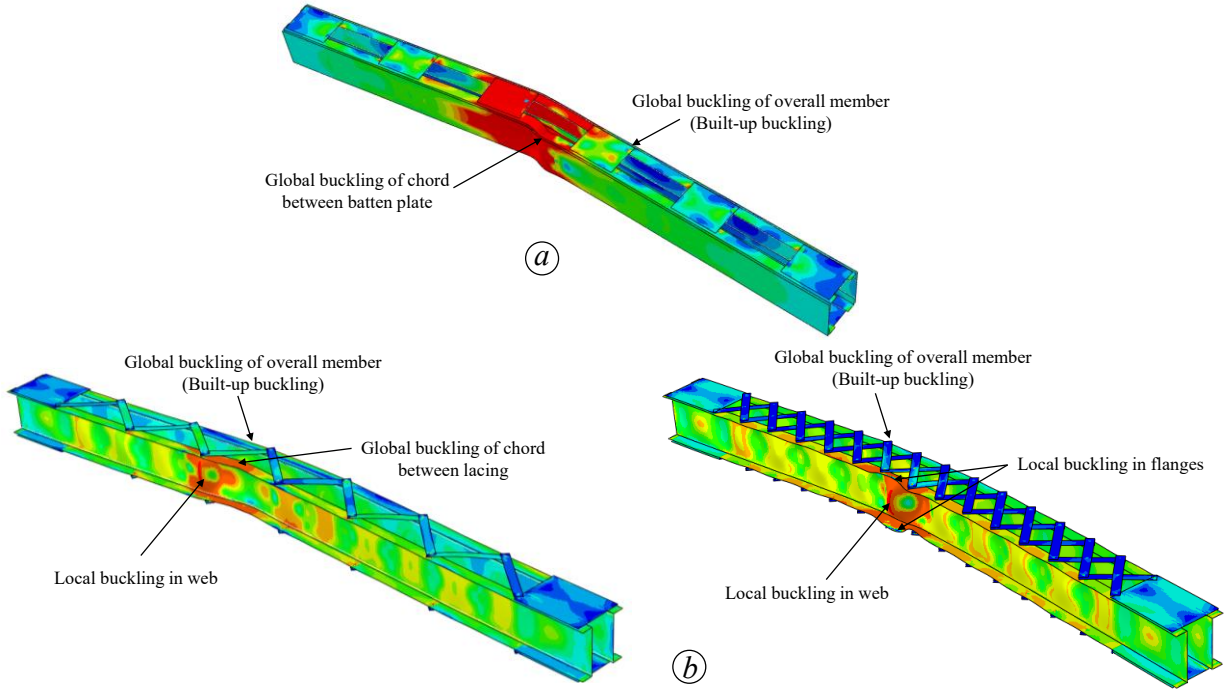

Figure 1.4 Failure modes of built-up members: (a) with batten plates – (b) with lacings.

1.2.2 Limitations of current design approach

The current design approaches for built-up compression members, as provided in major design codes such as the American Institute of Steel construction (AISC), Eurocode 3 (EC3), the Canadian Standards Association (CSA S16), and the American Association of State Highway and Transportation Officials (AASHTO), are primarily based on simplified assumptions and empirical formulations developed decades ago. These methods often treat built-up members as equivalent single, non-built-up members, neglecting the interaction of chord buckling (which usually occurs between connectors) and the overall buckling of the built-up member. Moreover, the code also imposes fabrication limitations for secondary members, such as batten plates and lacing, as well as for the built-up member itself. As a result, these simplifications can lead to either conservative or unconservative predictions of compressive resistance, particularly for members that do not comply with the construction limitations specified by the standards. Besides, the interaction between

different buckling modes – such as local buckling of the cross-section, global buckling of individual chords, overall buckling of the built-up member, and the premature buckling or failure of the secondary system (lacing and batten plates) – can significantly reduce the compressive resistance of the built-up member. Further details on the limitation and the performance of the current design approach will be detailed in Chapters 3, 4, and 5.

1.2.3 Overall research questions

The overall research project aims to address the following key questions:

1. Geometric and fabrication constraints:
    - Are the geometric and fabrication details of the built-up compression members used in historical truss bridges consistent with the geometric limits and slenderness limitations defined in current design codes?
    - Do the geometry and fabrication of batten plates and lacing systems in historical truss bridges meet the limits and slenderness criteria of current design codes?
2. Initial imperfections and residual stresses:
    - What are the typical magnitudes and distributions of geometric imperfections and residual stresses in built-up members fabricated during the early construction period of steel bridges?
    - How do these imperfections differ from those of modern welded or hot-rolled members, and how do they influence the overall buckling behaviour?
3. Strength of secondary elements (batten plates and lacing systems):
    - What is the actual contribution of batten plates and lacing systems to the overall stiffness, load-carrying capacity, and 2nd order shear forces of built-up members?
    - Are the simplified assumptions used in modern design codes adequate to represent the true behaviour of these connection systems, particularly for members where fabrication limitations are not respected?
    - How do factors such as lacing configuration and section arrangement influence the behaviour of these secondary elements?
4. Strength of the main chord and buckling interaction:

- How does the axial strength of the built-up chord members compare with theoretical predictions when considering the effects of residual stresses, fabrication tolerances, and aged material properties?
- Do existing design provisions underestimate or overestimate the true strength of these historical members?
- How do different buckling modes – local buckling of individual plates, buckling of individual chords between connectors, and overall global buckling of the built-up member – interact in laced or battened configurations?
- Can the interaction between these buckling modes be accurately predicted using current analytical or numerical models?

1.3 Overall research objectives

The general objective of this research project is to reduce uncertainties in evaluating the load-carrying capacity of steel members in aging bridges. This will support more accurate investigation, assessment, and rehabilitation efforts, thereby ensuring the long-term sustainability of JCCBI's infrastructure assets. Accordingly, the project aims to develop equations that provide reliable and realistic estimates of the compressive strength of truss bridge members composed of built-up sections. It focuses on built-up members consisting of two longitudinal chords connected by either batten plates or lacing members.

1.4 Specific research objectives

Given the extensive scope of the research project, it was divided into collaborative sub-projects. This thesis focuses specifically on *built-up members with lacing*, addressing their buckling behaviour and design. The aim is to develop equations capable of accurately predicting the axial compressive strength of laced built-up members, particularly those similar to the members of the Jacques Cartier Bridge. Accordingly, the specific objectives of this thesis are to:

(i) develop *finite element (FE) models* that accurately reproduce the buckling behaviour observed in laboratory tests on laced built-up members; and

(ii) use the validated numerical model to conduct a comprehensive parametric study on laced built-up members, ultimately leading to the development of design equations for these

members, including their lacing system and main chords. The goal is *to provide a practical design approach* capable of evaluating the compressive resistance of laced built-up members by accounting for their *complex buckling behaviour – local, global, built-up buckling, and their interactions*.

1.5 Research methodology

To address the research objectives outlined previously, the methodology proposed in this thesis is structured into five main steps. Figure 1.5 presents the research methodology flowchart adopted in this thesis. Each step corresponds to a specific phase of study designed to investigate, model, and ultimately improve the design of laced built-up members. These steps encompass numerical modeling, model validation, parametric studies, development of new design equations, and reliability analysis, with the aim of providing a comprehensive and robust framework for both understanding the behaviour of built-up members and guiding their practical design. Together, these steps allow for the systematic evaluation of key factors influencing buckling and failure, the validation of numerical and analytical models, and the development of design recommendations that are consistent with modern engineering practice and code requirements.

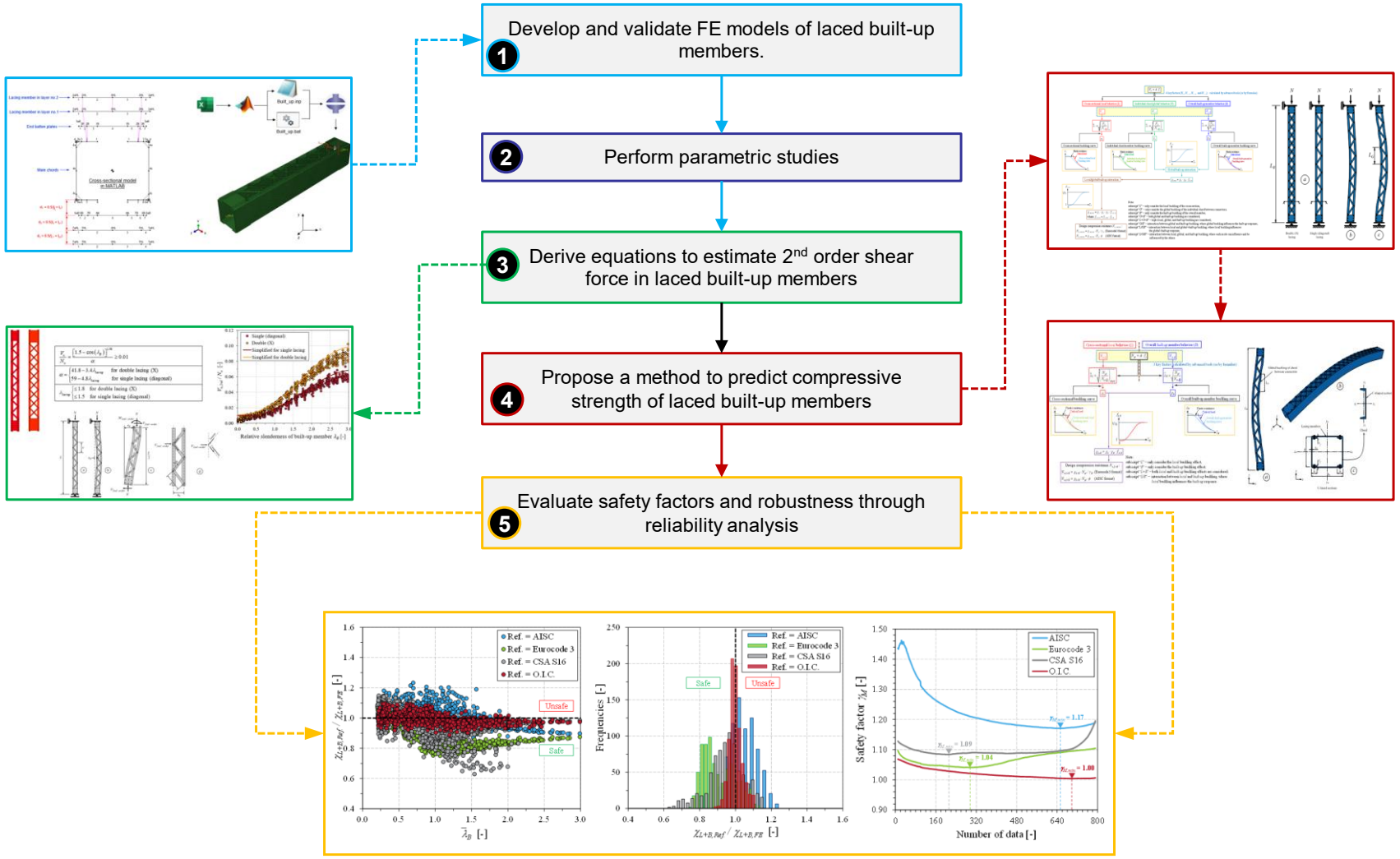

Figure 1.5 Research methodology adopted in thesis.

Step 1: develop and validate detailed finite element models to simulate the structural response of built-up compression members. The numerical modeling is performed using ABAQUS, with input files automatically generated through customized MATLAB scripts. The use of MATLAB enables the automated creation of complex models efficiently, which is essential given the large number of simulations required for parametric studies. To compensate for the lack of newly obtained experimental data, the FE models are calibrated using available experimental results reported in the literature, comprising 23 tests conducted across four different laboratories. Geometric imperfections were derived from these experimental datasets, while residual stress patterns were adopted from previously published findings. This step ensures that the developed FE model accurately reproduces the observed buckling and failure behaviour, particularly the ultimate load capacity of the laced built-up members.

Step 2: perform parametric studies. Once the FE model is validated, the automated modeling framework enables the execution of thousands of simulations, allowing a systematic parametric analysis of key variables such as yield strength, section classification, section geometry, member slenderness, connector spacing, chord arrangement, lacing slenderness, and lacing configuration. In this step, a large set of numerical models is generated based on selected built-up member geometries representative of the truss bridge members currently managed by JCCBI. This step provides a deeper understanding of the key parameters influencing the buckling and failure behaviour, particularly those affecting the ultimate load capacity of the laced built-up members. The data obtained from the parametric study serves as the foundation for developing the proposed design methodology.

Step 3: develop new design equations to estimate the second-order shear force in laced built-up members. The purpose of this step is to derive the forces in the lacing system, which primarily arise from the initial deflection of the overall built-up member, generating 2nd order shear forces acting in the transverse direction. These forces are transferred from one chord to another through the lacing system. Therefore, it is essential to accurately quantify the magnitude of these forces in relation to the axial design resistance (V_u / N_u). This allows the design of the lacing system to ensure it does not fail prior to the main components of the built-up member.

Step 4: propose a new design approach to determine the compressive strength of laced built-up members. This approach is based on the adopted Overall Interaction Concept (O.I.C.) method,

which has been extended in this thesis to account for the triple interaction of local, global, and built-up buckling modes (L/G/B). The purpose of this step is to provide a practical and reliable framework for designing the main components of laced built-up members while considering the combined effects of multiple buckling and their interaction. By integrating the results from the experimental studies, FE modeling, and parametric analyses, the proposed approach allows designers to predict the ultimate load capacity of the main components more accurately, ensuring safety and efficiency even for members with complex geometries that may not comply with current code limitations.

Step 5: perform reliability analysis to determine the safety factors. This step aims to quantify the level of structural safety and to assess the robustness of the proposed design approach. The analysis is conducted using both the European framework (EN 1990) and the American AISC-LRFD methodology, allowing a comparison of reliability levels under different code recommendations. By incorporating variability in material properties, section geometry, and the professional judgment, the reliability study provides a systematic evaluation of the probability of failure and helps to establish appropriate partial safety factors. This ensures that the proposed design method not only predicts the ultimate compressive strength accurately but also satisfies rigorous safety and reliability requirements for practical engineering applications.

1.6 Main original contributions

The original contributions of this thesis are:

Article 1 (Chapter 4): *Stability and design of built-up columns: effect of 2nd order shear forces.*

- Investigation of the influence of chord and lacing arrangements on the ultimate load (N_u) and the shear force-to-ultimate load ratio (V_u / N_u) of laced built-up members;
- Assessment of lacing slenderness on the ultimate load (N_u) and the shear force-to-ultimate load ratio (V_u / N_u) of laced built-up members;
- Development of a systematic method to evaluate second-order shear forces in laced built-up members, accounting for lacing slenderness, lacing arrangement (single and double lacing), and cross-section slenderness across a wide range of member lengths;
- Addressing a gap in the literature, as many existing bridge members may exceed code-specified slenderness and geometric limits;

- Proposal for two sets of design equations for lacing forces:
- An equation, accounting for both cross-section slenderness and lacing effects, applicable for a broad range of member geometries;
- A simplified equation for practical design, valid within a defined range of cross-section slenderness (γ_V).

Article 2 (Chapter 5): *O.I.C.-based design for local/global/built-up interaction in laced built-up steel columns.*

- Development of a comprehensive FE modeling framework for laced built-up members incorporating combined imperfections at multiple levels, including: (i) cross-sectional plate imperfections, (ii) out-of-straightness of individual chords between lacing points, (iii) initial curvature of lacing members, and (iv) global imperfections of the overall built-up member;
- Calibration of the amplitude of geometric imperfections based on available experimental results to ensure realistic representation of the tested behaviour;
- Identification of the primary buckling modes of laced built-up members under compression loads, and its influence on the elastic critical load (N_{cr}) and ultimate load (N_u) of laced built-up members;
- Proposal for an extended Overall Interaction Concept (O.I.C.) approach to capture the interaction effect of local, global, and overall built-up member buckling, offering practical design equations and highlighting failure-governing factors often neglected in conventional design approaches;
- Reliability studies of the proposed design equations using both European (EN1990) and American (AISC-LRFD) frameworks to assessed safety factors and demonstrated the robustness and applicability of the proposed formulations for practical engineering design.

Article 3 (Chapter 6): *O.I.C. design of laced built-up steel columns for out-of-plane flexural buckling.*

- Investigation of the influence of key parameters such as yield strength, cross-section geometry, inclination angle of lacing, and lacing slenderness ratio on the ultimate load of laced built-up members, particularly for members exhibiting out-of-plane buckling of the lacing system;

- Comparison the effects of global buckling of chords between lacing connectors on the ultimate load of laced built-up members with respect to in-plane and out-of-plane buckling behaviour;
- Examination of the influence of local buckling of cross-sectional elements on the ultimate load of laced built-up members, considering both in-plane and out-of-plane buckling modes;
- Proposal for a reduced O.I.C. interaction framework for the design of laced built-up members subjected to out-of-plane buckling, providing an effective and practical set of design equations;
- Reliability analyses of the proposed design equations using both the European (EN 1990) and American (AISC-LRFD) frameworks to evaluate safety factors and demonstrate the robustness and applicability of the proposed formulations for engineering design practice.

CHAPTER 2 RESEARCH METHODOLOGY AND STRUCTURE OF THESIS IN RELATION TO RESEARCH OBJECTIVES

2.1 Introduction

This chapter presents the overall research process and illustrates how the individual articles included in this thesis contribute to achieving the research objectives. Its purpose is to provide a coherent view of the study, demonstrating the logical progression from problem identification to results and conclusions.

2.2 Research framework

The research is structured in a series of interrelated stages as outlined in the workflow illustrated in Figure 2.1. The main stages can be summarized as follows:

- *Chapter 1. Introduction*: This chapter introduces the research problem, defines the objectives, and outlines the scope and significance of the study, while highlighting the key challenges in evaluating the compressive strength of laced built-up truss members;
- *Chapter 2. Research approach and document structure:* This chapter describes the overall research workflow and presents the rationale behind the organization of the thesis. It explains how the individual articles are integrated and aligned with the research objectives to form a coherent body of work;
- *Chapter 3. Literature review:* This chapter reviews relevant research on built-up steel members, truss bridges, and lacing systems. It identifies knowledge gaps and justifies the methodology adopted in this study;
- *Chapter 4. Article 1 – Stability and design of built-up columns: effect of 2nd order shear forces:* This study developed practical equations (V_u / N_u) to predict the shear forces in lacing members, enabling a rational design of the lacing system for built-up columns. The approach accounts for the effects of lacing arrangement, lacing slenderness, member slenderness, and initial imperfections, capturing phenomena that current design standards do not fully address;
- *Chapter 5. Article 2 – O.I.C.-based design for local/global/built-up interaction in laced built-up steel columns:* This study proposed equations to determine the axial capacity N_u of

laced built-up members using the extended O.I.C. approach, explicitly accounting for local, global, and built-up buckling interactions. A design safety factor was then defined and calibrated based on EN 1990 and the AISC-LRFD methodology. Various section geometries, chord arrangements, and member slenderness were considered to ensure the equations' broad applicability;

- *Chapter 6. Article 3 – O.I.C. design of laced built-up steel columns for out-of-plane flexural buckling:* This study investigated the out-of-plane flexural buckling of laced built-up columns with X-shaped lacing, emphasizing members with low overall height-to-width ratios that increase susceptibility to out-of-plane failure. A validated finite element model was used to examine local, built-up, and interaction effects. Based on these results, a design approach using the O.I.C. was proposed, providing reliable and conservative predictions compared to AISC, Eurocode 3, and CSA S16. Reliability analyses following EN 1990 and AISC-LRFD confirmed the approach's suitability for practical design;
- *Chapter 7. General discussion:* This chapter synthesizes results from all studies, highlights the significance of the findings, discusses limitations, and relates the outcomes to existing research;
- *Chapter 8. Conclusion and recommendations:* This chapter summarizes the main conclusions, outlines contributions to the field, and provides recommendations for practical applications and future research.

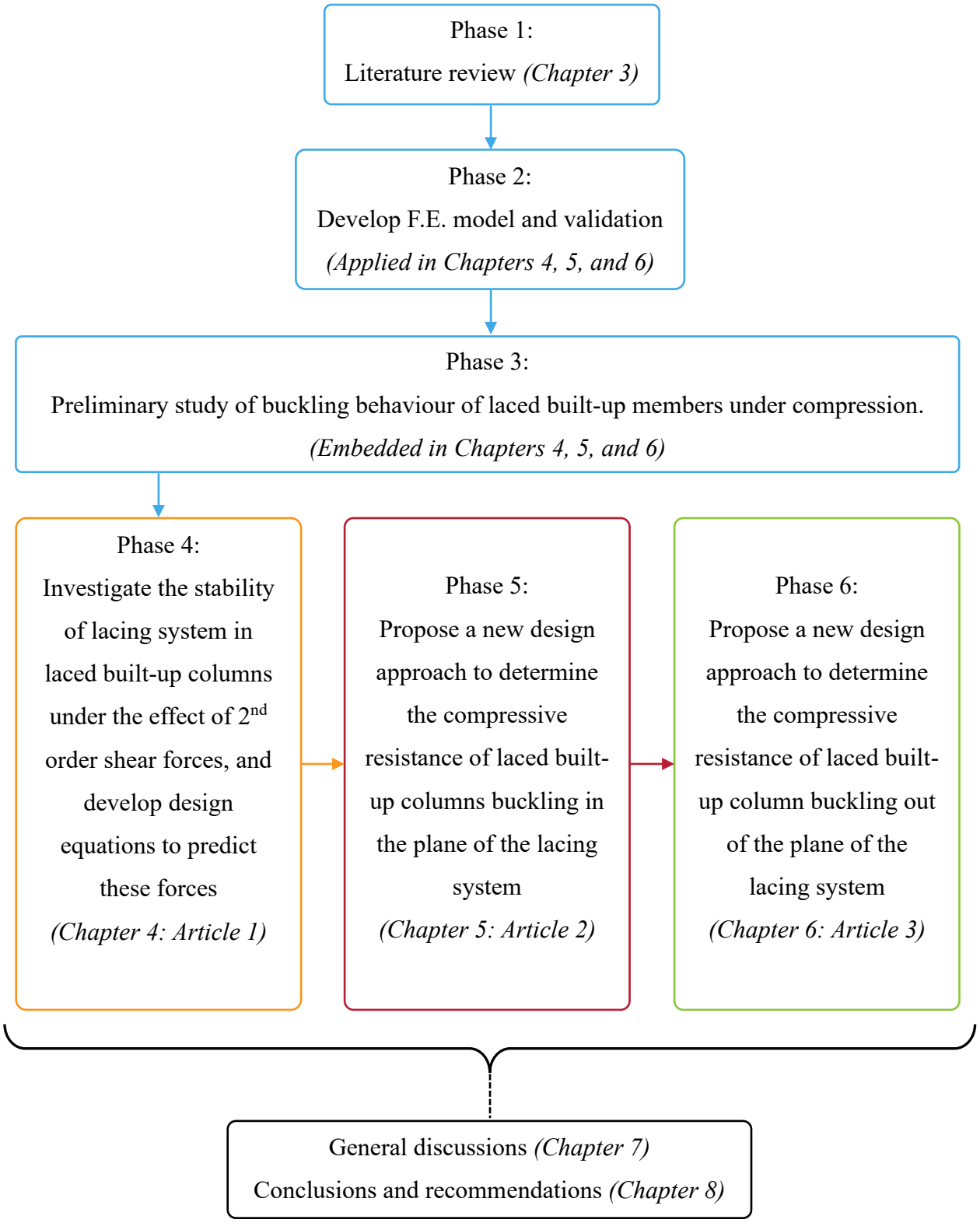

Figure 2.1 Schematic representation of the overall organization of the thesis.

2.3 Organization and coherence of papers

Each article included in the thesis addresses a specific research objective while contributing to the overall goals of the study. Table 2.1 presents an overview of the thesis articles, outlining each article's research objective, key contribution, and their interrelation to ensure coherence with the overall research goals. This structure allows the reader to understand how the articles are interrelated and how they collectively address the research questions posed at the beginning of the study.

Table 2.1 Mapping of articles to research objectives.

Article	Objective addressed	Key contribution	Connection to other articles
1	Predict 2nd order shear forces of laced built-up columns under compression.	Developed practical equations (V_u / N_u) for the design of lacing systems, accounting for lacing arrangement, lacing slenderness, member slenderness, and cross-sectional slenderness.	Provides the foundation for Article 2 by enabling rational design of lacing system.
2	Determine axial capacity (N_u) considering local/global/built-up interactions.	Proposed equations using the extended O.I.C. approach, applicable to various geometries and member slenderness.	Leads to Article 3 by providing the framework for out-of-plane flexural buckling analysis.
3	Address out-of-plane flexural buckling in laced built-up columns.	Developed equations using the reduced O.I.C. approach to account for local/built-up interactions.	Builds on Article 2, integrating findings for a complete design framework covering both in-plane and out-of-plane buckling.

CHAPTER 3 LITERATURE REVIEW

3.1 Introduction

Built-up sections were widely used in the construction of steel truss bridges, particularly before the 1950s. The primary benefit of using built-up members is their ability to achieve a high load-carrying capacity by effectively combining individual slender components. These built-up sections often consist of at least two parallel main chords interconnected by discontinuous plates (batten plates), perforated cover plates, or lacing. Figure 3.1 illustrates typical built-up sections used in old steel truss bridges constructed in the late 19th and early 20th centuries. Additionally, their resistance can significantly exceed the total axial resistances of the individual components, which may, in turn, be substantially limited by instability phenomena within the range of standard products.

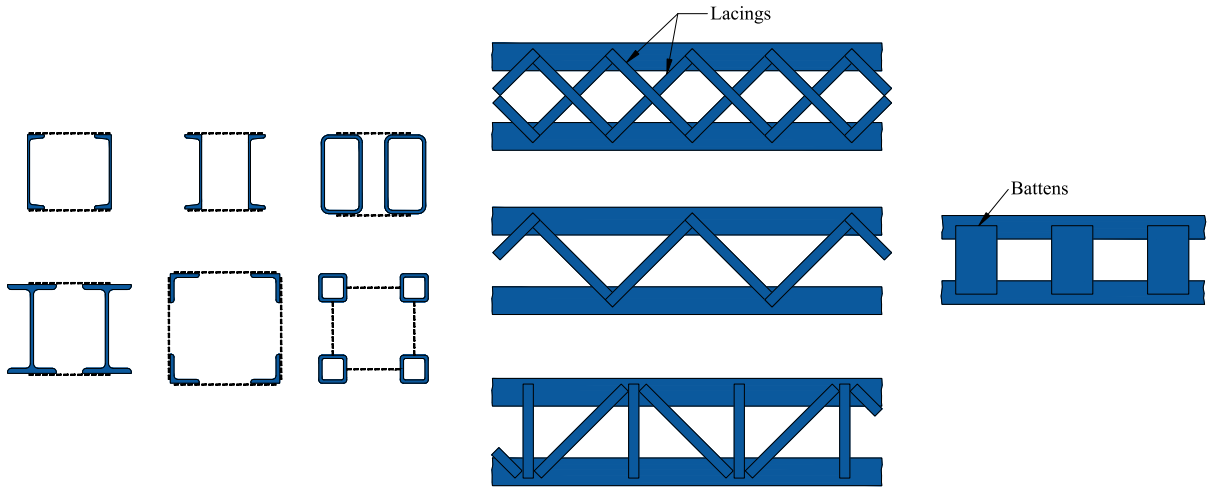

Figure 3.1 Typical built-up sections used in steel truss bridges.

3.2 Brief historical overview of buckling in built-up columns

While built-up compression members are often used in structural design, their complex buckling behaviour still requires careful investigation. These highlight that the primary issues with built-up compression members are their shear flexibility and, in theory, the potential for simultaneous global buckling of the individual chords between the interconnectors and the built-up buckling of the overall member. This section provides an overview of the existing main developments in this topic.

3.2.1 Effect of shear in built-up columns

The critical importance of designing shear-resisting elements in built-up columns was tragically underscored by the collapse of the first Quebec Bridge during its construction in 1907, as previously noted by Galambos [5]. This incident was documented by the Royal Commission for the Quebec Bridge Inquiry [6] and analyzed by Engesser [7], leading to numerous in-depth investigations into the behaviour of built-up columns. Engesser [8] derived approximate formulas for critical buckling loads, later refined by Ziegler [9], Timoshenko [10], and Bleich [11]. Engesser developed the elastic critical load formulas for built-up columns, taking into account the effect of shear deformation.

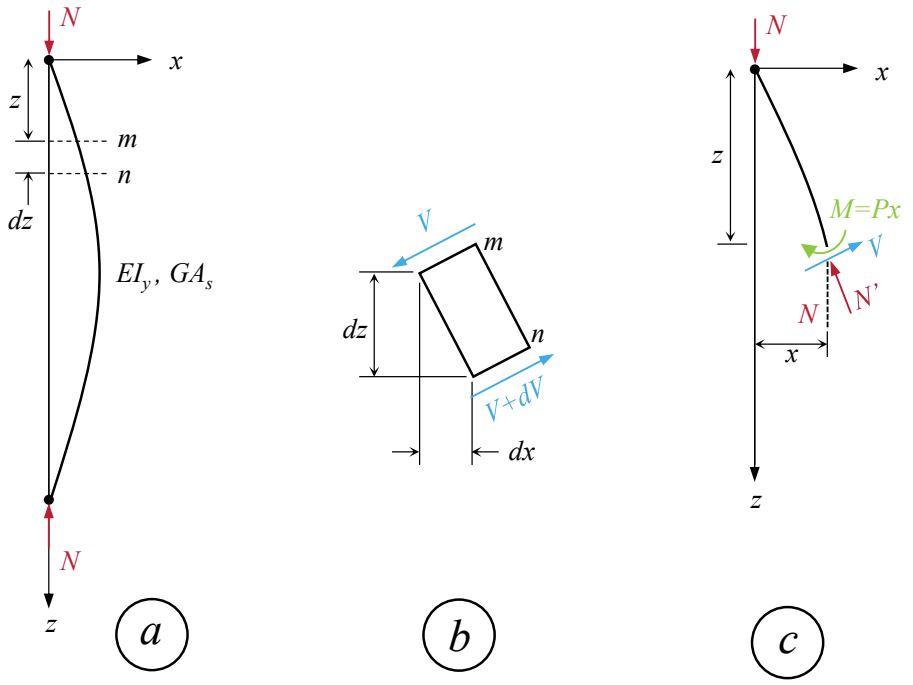

Figure 3.2 Effect of shear force acting on the cross-section of the column.

As shown in Figure 3.2, the current derivations of the critical load equations adopt the differential equation of the column in its deformed configuration, considering the effect of shear force acting on the cross-section. Consider a shear force V acting over an element of length dz between two cross-sections, m and n. The magnitude of this force is:

$$V = N\frac{dx}{dz} \tag{3.1}$$

For a built-up column, the shear force is not carried by a solid web, necessitating a secondary system, such as batten plates or lacings. During buckling, the variation in the slope of the deflection curve caused by the shear force is represented by V / GA_s, where G is the shear modulus and A_s is the total shear area of the cross-section. The shear force V induces an additional curvature, reflected as a change in the slope, and is given by:

$$\frac{1}{GA_s}\frac{dV}{dz} = \frac{N}{GA_s}\frac{d^2x}{dz^2} \tag{3.2}$$

The total curvature of the deflection curve results from both bending and shear. For a pin-ended column, the deflection is described by the following equation:

$$\frac{d^2x}{dz^2} = -\frac{Nx}{EI_y} + \frac{N}{GA_s}\frac{d^2x}{dz^2} \tag{3.3}$$

This can be written as:

$$\frac{d^2x}{dz^2} + k^2x = 0 \tag{3.4}$$

where $k = \sqrt{\dfrac{N}{\left(1-\dfrac{N}{GA_s}\right)EI_y}}$.

The solution of Eq. (3.4) is

$$\frac{N_{cr}L^2}{\left(1-\dfrac{N_{cr}}{GA_s}\right)EI_y} = \pi^2 \tag{3.5}$$

where N_{cr} is the elastic critical load of the column and L is the total length of the column. By rewriting the expression and introducing the Euler critical load of the column as $N_{cr,e}$ where K is the effective length factor, the result becomes:

$$N_{cr} = \frac{N_{cr,e}}{1 + \dfrac{N_{cr,e}}{GA_s}} \tag{3.6}$$

where $N_{cr,e} = \dfrac{\pi^2 EI_y}{(KL)^2}$.

It is evident that the effect of shear forces reduces the critical load by a factor of $1/\left(1 + N_{cr,e}/GA_s\right)$. This ratio is close to one for solid columns, such as those with rectangular or I-shaped cross sections, however it becomes practically significant in built-up columns. The expression in Eq. (3.6), derived by Engesser, defines GA_s as the shear stiffness of the built-up columns. For various types of built-up sections, the shear stiffness GA_s of lacings should be taken from Figure 3.3.

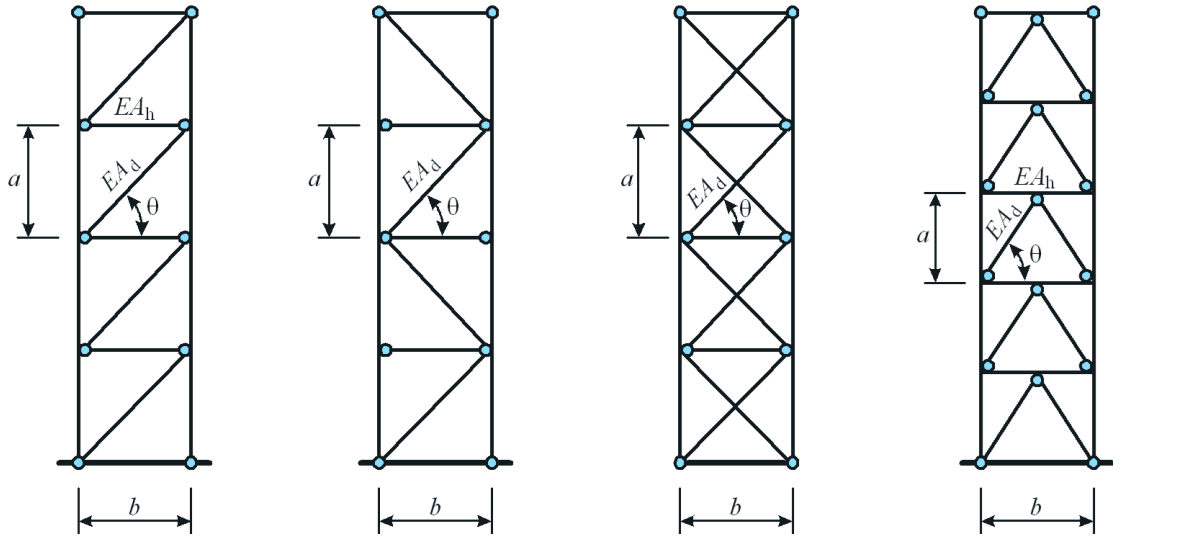

Figure 3.3 Shear stiffness of lacings of built-up members.

In the case of laced built-up members comprising vertical and horizontal chords with rigid connections and diagonal members, the shear stiffness GA_s can be obtained as the sum of the shear stiffness $GA_{s,f}$ resulting from the bending stiffness of the horizontal and vertical chords, and the shear stiffness $GA_{s,a}$ resulting from the axial stiffness of the diagonal and horizontal members. For example, for a V-configuration as illustrated in Figure 3.4:

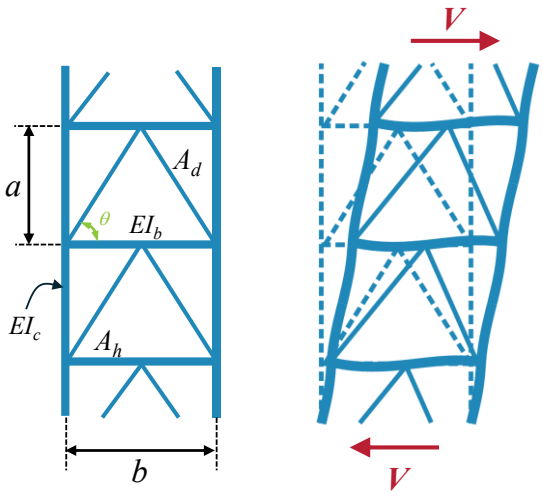

$$\text{Flexural deformations: } \frac{1}{GA_{s,f}} = \frac{a\,b}{12\,EI_b} + \frac{a^2}{24\,EI_c}$$

$$\text{Axial deformations: } \frac{1}{GA_{s,a}} = \frac{b}{a}\left(\frac{1}{4EA_h} + \frac{1}{4EA_d\cos^3\theta}\right)$$

$$\text{Total deformations: } GA_s = GA_{s,f} + GA_{s,a}$$

Figure 3.4 Laced built-up members with rigid vertical and horizontal chords.

After Engesser's foundational work on the critical load of built-up columns, many researchers tried to further refine the analysis by modeling the column as a framework, i.e., a system composed of interconnected members, like in trusses or latticed structures. The goal was to find exact formulations for the column's critical load to be more precise than previous approximations. As demonstrated in the classical textbook by Bleich [11], such studies include the works of Mann [12], Ljungberg [13], von Mises and Ratzersdorfer [14], [15], Chwalla [16], and Wentzel [17]. However, these studies reinforced confidence in Engesser's work, rather than advancing the theory further. One important difference is that only the exact solutions explicitly include the number of lacing panels (segments created by transverse connectors like lacing or batten plates) in calculating critical loads. The approximate methods do not include this detail. A built-up column can be treated as an ordinary column when the number of lacing panels exceeds four, as reported by Tall [18]. Relevant issues of built-up columns were also investigated by Müller-Breslau [19], Petermann [20], [21], Young [22], Holt [23], and Pippard [24], [25].

Bleich [11] employed energy methods to analyze the buckling behaviour of built-up columns, including those with laced and battened systems. He derived expressions to estimate the effective length factor and equivalent slenderness ratio considering shear deformation in the connectors. He thoroughly investigated both types and analyzed how the type of web system affects overall stability. He also proposed guidelines and requirements for the design of lacing systems, such as allowable slenderness of lacing bars, angle of inclination, and required stiffness, to prevent premature failure of the lacing system relative to the main chords.

Timoshenko and Gere [26] investigated the influence of shear deformation in the bracing systems of built-up columns, particularly its effect on overall buckling behaviour. They derived analytical expressions to quantify the impact of shear flexibility in laced and battened configurations and introduced corresponding correction factors and equivalent slenderness ratios. In their analysis, inflection points were assumed at the midpoints of the main members within each panel. Based on this assumption, they formulated expressions for the critical buckling load, incorporating the contribution of the shear-flexible web system.

Other researchers have contributed to the study of built-up columns, expanding both theoretical understanding and practical design approaches. Ng [27], [28] conducted foundational analyses on the buckling behaviour of built-up columns. Jones [29] developed theoretical models for members with lattice or battened configurations. Koenigsberger and Mohsin [30] and Mohsin [31], [32] investigated stability and design considerations under various loading conditions. Tamayo and Ojalvo [33] analyzed the buckling behaviour of three-legged columns with batten plate, while Williamson and Margolin [34] addressed shear deformation effects in built-up columns. Lin et al. [35] applied Haringx's method to study laced columns, and Johnston [36] provided experimental data on spaced built-up columns to validate theoretical models. Kennedy and Madugula [37] explored buckling behaviour in angle members, including those in built-up assemblies. Ballio and Mazzolani [38] contributed finite element analyses that generalized buckling solutions, and Gioncu [39] studied coupled instabilities in thin-walled built-up members.

Libove [40] reported that the post-buckling behaviour of built-up columns with two and three interconnectors was unstable. Unlike solid columns, which remain stable after buckling, built-up columns can become highly sensitive to imperfections due to their unstable post-buckling behaviour. Similar conclusions were reported by Chang [41]. Chang [42] adapted the Engesser-Shanley tangent modulus theory of inelastic buckling [43] to analyze his model consisting of three interconnectors.

Numerous studies have examined the behaviour and configuration of double-angle struts, notably those by Temple et al. [44], [45], [46] and Krige and Wolmarans [47]. Temple et al. [44] investigated the buckling behaviour of back-to-back starred angles. Based on experimental results, the authors recommended using two interconnectors placed at the third point along the member length for optimal performance. Similar recommendations were later made by the same authors for

boxed angles [45] and back-to-back double angles [46]. Krige and Wolmarans [47] subsequently suggested a minimum of three bolted interconnectors: one at mid-length and one at each sixth or quarter points, arranged in a plane perpendicular to that of the mid-height interconnector.

Research on the seismic performance of double-angle bracing was conducted by Astaneh and Goel [48], [49] and Astaneh et al. [50]. Astaneh and Goel [48] studied the in-plane buckling behaviour of back-to-back double-angle braces under cyclic loading, identifying premature failures in some cases and highlighting the need for improved seismic design. Aslani and Goel [51] expanded this work by demonstrating that reducing the width-to-thickness ratio improved ductility, while stitch spacing had a lesser effect.

Gjelsvik [52], [53] developed an analytical method to evaluate the stability of built-up columns by modeling the chords as beams connected through a shear panel that simulates a web. This formulation leads to a sixth-order differential equation, which requires additional boundary conditions compared to traditional fourth-order models. The analysis accounts for the presence of stay plates at the ends of the column, which increases shear stiffness where shear forces are most critical and help reduce deformation. His findings show that these end connectors significantly enhance the buckling resistance, and that the overall buckling load is influenced by both the shear and bending stiffness as well as the relative stiffness between the chords and the full member. Paul [54], [55], [56] extended Gjelsvik's analytical model by treating the web of a built-up column as continuously connected to the chords, allowing it to share both axial and flexural stresses. This approach provided a more comprehensive understanding of the interaction between the web and chords, leading to improved predictions of buckling behaviour. Toossi [57] investigated the torsional-flexural buckling behaviour of built-up columns, focusing on how the interaction between torsion and flexure affects the stability of these members. His work contributed to the development of more accurate design methods for columns susceptible to such combined buckling modes. Kitipornchai and Lee [58] conducted studies on the torsional-flexural buckling of built-up columns, analyzing the effects of various parameters on their stability. Their research provided valuable insights into the design and analysis of built-up columns under complex loading conditions.

3.2.2 The modified slenderness ratio

The equivalent slenderness ratio, originally developed by Timoshenko and Gere [26] and Bleich [11], has been incorporated into various design codes, with several adjustments over time. It was

first introduced in the AISC-LRFD [59] Specification for Structural Steel Buildings. Zahn and Haaijer [60], [61] provided supporting background for these provisions, which were based on experimental work by Zandonini [62] and further supported by studies from Astaneh et al. [50]. Zandonini conducted two experimental series on back-to-back channels, one connected with welded filler plates and the other with snug tight bolted filler plates. The test results were compared with the SSRC curve proposed by Galambos [5], using specimens that had an initial out of straightness equal to L / 1000, as shown in Figure 3.5. Astaneh et al. performed cyclic loading tests on back-to-back double angle members, with the first cycle yielding valuable data.

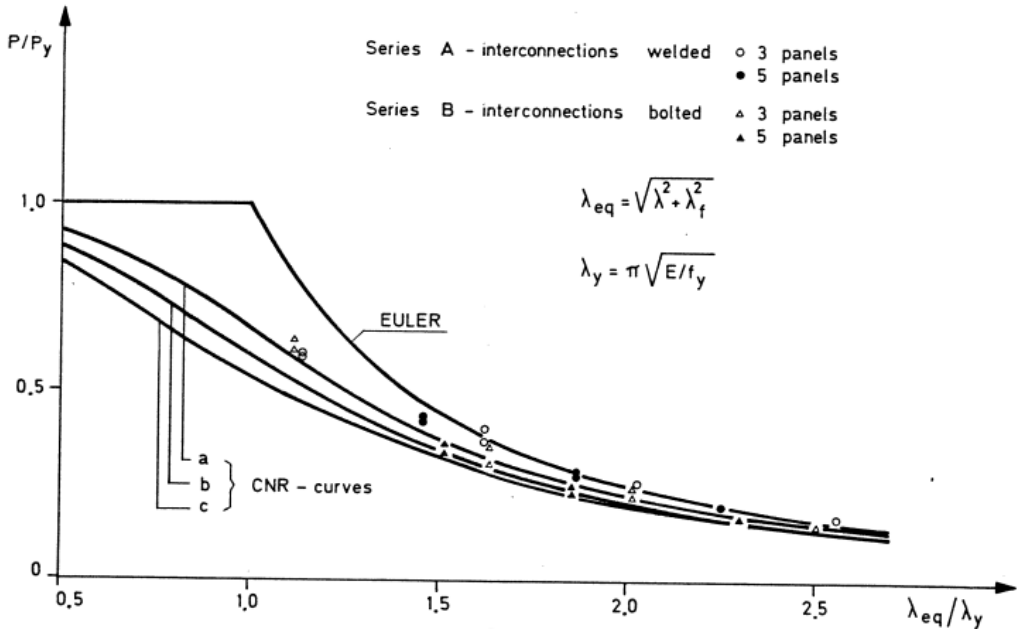

Figure 3.5 Results of experimental test conducted in [62].

Aslani and Goel [49] investigated built-up columns with both welded and bolted connectors. In their study, they proposed a generalized form of the analytical equation originally developed by Bleich [11]. For built-up members with general end conditions, they suggested that the modified slenderness ratio is given by:

$$\left(\frac{KL}{r}\right)_m = \sqrt{\left(\frac{L}{r_o}\right)^2 + \frac{\pi^2 I_o}{12I}\left(\frac{a}{r_i}\right)^2} \tag{3.7}$$

where L / r_o is the overall slenderness of built-up column, a / r_i is the slenderness ratio of individual chord between connectors, $I_o = A_i b^2 / 2$ represents the second moment of area of the built-up section

about the buckling axis with considering the second moment of area of the individual chords, A_i is the cross-section of individual chord, b is the distance between centroids of individual chords, and I is the total second moment of area of the integral section about the axis of buckling (see for annotations). In addition, Aslani and Goel [49] introduced the term $0.82\alpha^2 / (1+ \alpha^2)$ to replace $\pi^2 I_o / 12I$ in Eq. (3.7), resulting in the following form:

$$\left(\frac{KL}{r}\right)_m = \sqrt{\left(\frac{L}{r_o}\right)^2 + 0.82\left(\frac{\alpha^2}{1+\alpha^2}\right)\left(\frac{a}{r_i}\right)^2} \tag{3.8}$$

This formulation was proposed based on assuming that $\pi^2/ 12 \approx 0.82$ and $I_o / I = \alpha^2 / (1+ \alpha^2)$, where the separation factor $\alpha = b / 2\, r_i$. The factor $\alpha^2 / (1+ \alpha^2)$ in Eq. (3.8) accounts for the effect of the spacing between the main chords. When the chords are widely spaced, resulting in a large value of α, the ratio $\alpha^2 / (1+ \alpha^2)$ approaches unity. However, when α is small due to closely spaced sections, this effect becomes significant and must be considered. This equation was validated by a parametric study and test results and was adopted by the 1993 edition of the AISC-LRFD Specification [63].

Several researchers have proposed alternative values for the factor in the second term of the radicand in Eq. (3.8). Ballio and Mazzolani [38] recommended adjusting the original value of 0.82 by multiplying it by 0.8, resulting in a factor of 0.66. This adjustment accounts for the global flexural behaviour of built-up members such as compound struts, where the bending of the chords plays an important role and cannot be neglected. Experimental studies conducted by Temple and Elmahdy [64], [65] on struts made of bars joined by welded battens, as well as on built-up columns made from face-to-face channels with welded battens, showed that applying an effective length factor of 0.65 in the second term of Eq. (3.8) was not conservative. As a result, the 1994 edition of the Canadian Standard CAN/CSA-S16.1 retained the existing effective length factor for compact built-up struts. However, for built-up members consisting of two rolled shapes connected by lacing or batten plates, the maximum slenderness of the components between connectors was determined using an effective length factor of 1.0, regardless of whether snug-tight bolts, pretensioned bolts, or welds were used.

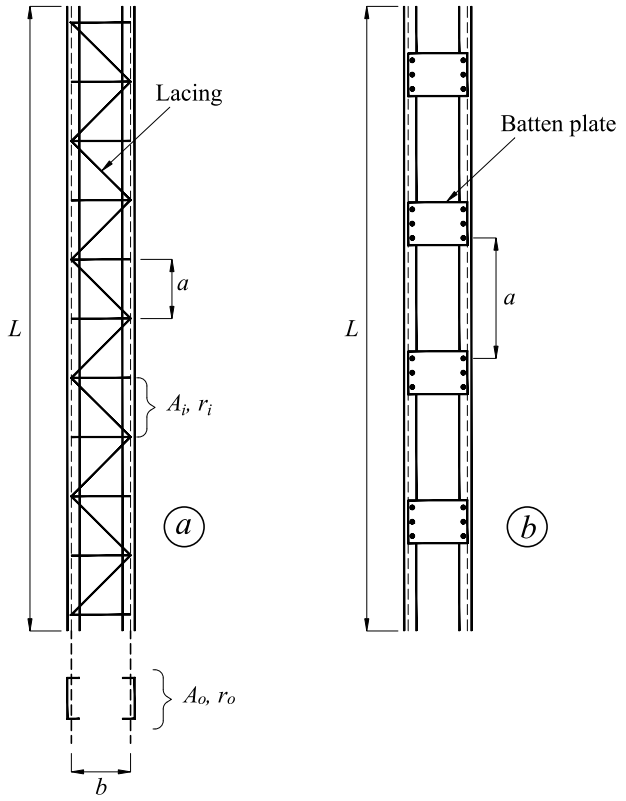

Figure 3.6 Notations for typical built-up columns – (a) member with lacings – (b) member with batten plates.

3.2.3 Effect of interaction buckling

An important aspect of column buckling behaviour is the interaction between local plate buckling and global buckling in compression members with slender cross-sections, which may experience flexural failure, torsional-flexural buckling, and local buckling. This problem has been studied extensively, beginning with the foundational work of Koiter [66], and further developed by van der Neut [67], Graves-Smith [68], Koiter and Kuiken [69], Thompson and Lewis [70], Svensson and Croll [71], and Fan [72]. The interaction between local buckling and global column failure in thin-walled compression members was among the earliest analytically modeled by van der Neut [67] who adopted an idealized system consisting of two flanges of width w and thickness t, separated by a distance 2 c and connected by webs. These webs were assumed to be rigid in shear and laterally stiff but low in longitudinal stiffness which can provide simple support to the flanges. The author showed that the post-buckling reduction in longitudinal stiffness of the flanges significantly influences the overall column strength. In perfect columns, this interaction may cause a sudden

failure at a load higher than the Euler critical load $N_{cr,e}$, whereas columns without imperfections can experience a rapid failure at the local buckling load $N_{cr,L}$, occurring within a range where the ratio $N_{cr,e}$ / $N_{cr,L}$ exceeds one, where $N_{cr,e}$ represents Euler global critical load. In addition, when $N_{cr,e}$ / $N_{cr,L}$ approaches unity, the column strength is significantly reduced. A similar study case involving a square tube with thin walls was investigated by Graves-Smith [68]. Koiter and Kuiken [69] validated van der Neut's results using Koiter's general non-linear elastic stability theory, which produced nearly identical numerical outcomes along with valuable asymptotic expressions. The model developed by van der Neut was also employed by Thompson and Lewis [70] to examine the validity of simultaneous buckling as a design optimization criterion for compression members. They found that even small imperfections could significantly reduce and shift the optimal design point. Building on this, Svensson and Croll [71] revealed that although designing for the interaction between local and global buckling in box columns may appear theoretically optimal, the presence of imperfections and plasticity effects substantially reduces its effectiveness. These factors lead to a significant reduction in the critical load compared to the ideal prediction. Fan [72] worked on a similar issue in stiffened panels with symmetric cross-sections. The influence of small shape imperfections on the interactive buckling strength was also investigated by Palassopoulos [73], [74], [75] and Ikeda and Murota [76].

Many researchers investigated the interaction of local plate buckling and global buckling of symmetrical and monosymmetric steel columns such as Migita et al. [77], Gioncu et al. [78], Pignataro and Luongo [79], Rasmussen and Hankcock [80], [81]. Migita et al. [77] conducted experimental studies on polygonal-section steel columns to examine the interaction between local and global buckling under axial compression. Pignataro and Luongo [79] analyzed the effects of local-overall interaction on the post-buckling behaviour of uniformly compressed channels, providing insights into the imperfection sensitivity of such structures. Rasmussen and Hancock [80], [81] investigated the local and overall buckling behaviour of stainless steel I-columns, contributing to the understanding of buckling interactions in such members.

However, in built-up columns, the individual chords may buckle between the connectors. This phenomenon was discussed by Thompson and Hunt [82], [83] and is illustrated in Figure 3.7. The modes of buckling as shown Figure 3.7 in involving global buckling of the main chord between lacing bars and overall global buckling of the built-up column. Studies by Thompson and Hunt [82], [83] showed that the interaction between local and global buckling leads to significant

sensitivity to imperfections, particularly at the point where both buckling modes interact. The critical load is most affected in this region, consistent with findings by Koiter and Kuiken [69].

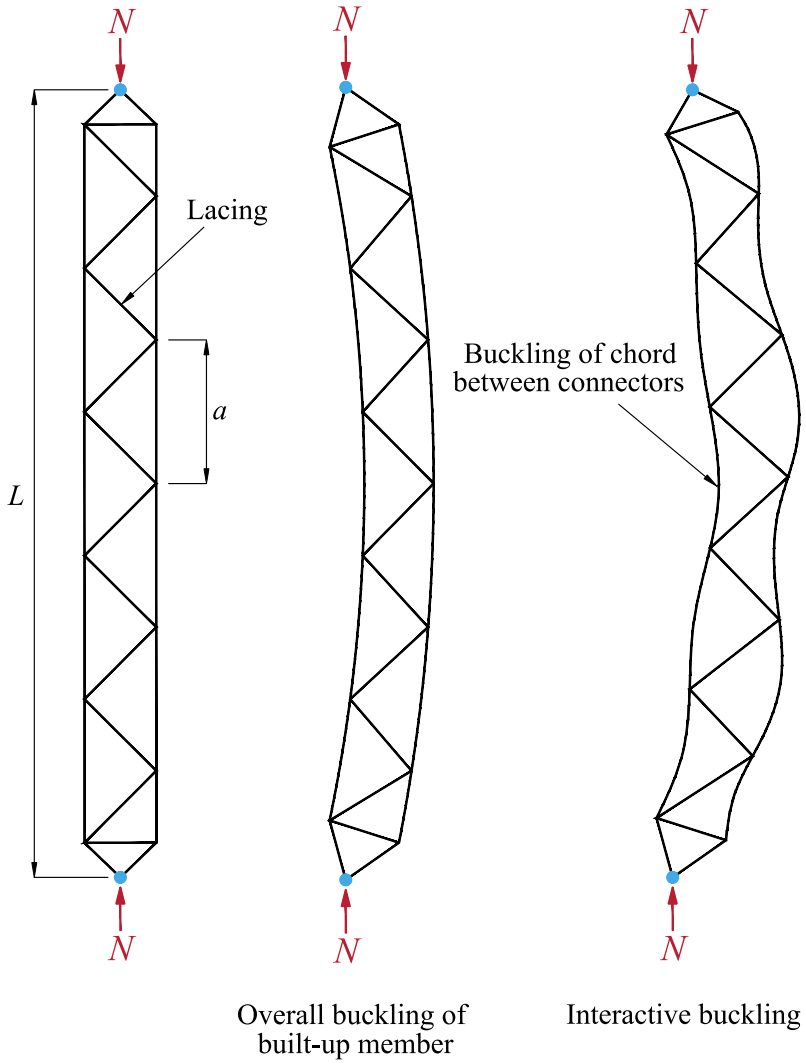

Figure 3.7 Interactive buckling in Thompson and Hunt's reticulated laced built-up columns [82], [83].

Several other researchers have addressed the issue of interactive buckling in latticed columns, including Crawford and Hedgepeth [84], Byskov [85], Miller and Hedgepeth [86], Crawford and Benton [87], Svensson and Kragerup [88], [89], Bälut et al. [90], Gioncu [39], [91], and Tong and Chen [92].

Crawford and Hedgepeth [84] studied the effects of initial imperfections on the strength and design of built-up columns, highlighting the sensitivity of laced built-up columns to such imperfections. Byskov [85] investigated interactive buckling phenomena in thin-walled structures, providing

foundational insights into buckling behaviour. Miller and Hedgepeth [86] conducted an analysis to evaluate the buckling load of triangular laced columns considering random imperfections. They found that in these columns, a slight overall curvature along the centerline causes the compressive end load to increase stress in the local members, leading to early crippling of those elements. Conversely, local imperfections in the cross section reduce the effective bending stiffness of the column, causing premature global buckling. The authors suggested that effective design of slender lattice columns must address the combined influence of random local imperfections and deterministic overall imperfections. Their study examined how various magnitudes of local and overall imperfections together affect the buckling load. Hence, they developed statistical estimators for the mean and standard deviation of the buckling load, providing a reliable method for predicting the minimum buckling capacity.

Bälut et al. [90] proposed limiting the slenderness ratio of the chords in laced built-up columns in order to reduce the loss of bending stiffness and the resulting decrease in buckling strength. They found that the sensitivity to imperfections becomes particularly significant when the ratio of a / r_i to $(L / r_o)_e$ is close to one, where $(L / r_o)_e$ represents the equivalent slenderness of the perfect laced column. In such cases, the buckling capacity may be reduced by up to 50% of the overall buckling load. To limit this reduction, the authors recommended the following restrictions on slenderness ratios:

(i) For $(L / r_o)_e \leq 40$

$$\left(\frac{a}{r_i}\right) \leq 40 - 10\frac{210}{f_y} \tag{3.9}$$

(ii) For $(L / r_o)_e > 40$

$$\left(\frac{a}{r_i}\right) \leq 40 - 0.5\frac{210}{f_y}\left[\left(\frac{L}{r_o}\right)_e - 60\right] \tag{3.10}$$

The above expressions apply to built-up columns in which the main chords are channel sections.

Gioncu [91] investigated the interaction behaviour of monosymmetric cross-sections subjected to compressive loads. The author reported that buckling interaction leads to unstable post-critical behaviour, which significantly increases imperfection sensitivity.

Tong and Chen [92] examined the interactive buckling effect of built-up columns by considering the various influences of imperfections. In this context, Bažant and Cedolin [93] conducted an analysis to estimate the imperfection sensitivity of laced columns. As reported by Koenigsberger and Mohsin [30], many researchers provided a constraint to minimize this effect. Ng [27] limited a / r_i to 50 associated with $(a / r_i) / (L / r_o) \approx 0.6$. Petermann [20], [21] suggested a / r_i to 40 based on the experimental tests conducted by Müller-Breslau [19], and 30 corresponding to $(a / r_i) / (L / r_o) \approx 0.75$.

As reported by Koenigsberger and Mohsin [30], several researchers proposed constraints to minimize this effect. Ng [27] limited the ratio a / r_i to 50, corresponding to $(a / r_i) / (L / r_o) \approx 0.6$. Petermann [20], [21] recommended a value of 40 for a / r_i, based on experimental tests conducted by Müller-Breslau [19], and later suggested a value of 30, corresponding to $(a / r_i) / (L / r_o) \approx 0.75$.

The interaction between the global buckling of individual chords between connectors and the overall global buckling of built-up members, known as compound buckling, was studied by Duan et al. [94] in relation to the compressive strength of built-up members. They developed a β factor, formulated as a function of the separation factor, expressed in terms of a / r_i and L / r_o. This factor was introduced to calculate the critical load, accounting for the influence of buckling interaction.

$$N_{cr} = \frac{N_{cr,e}}{\beta^2} = \frac{\pi^2 EI}{(\beta L)^2} \tag{3.11}$$

In Eq. (3.11), $N_{cr,e} = \pi^2 EI / L^2$ is the elastic critical load and N_{cr} is buckling load considering the effect of buckling interaction. For simply supported columns, β can be solved through iterative calculation and written as the following:

$$\beta^2 = \frac{1+\alpha^2}{1+\dfrac{\alpha^2}{1+\dfrac{(\delta_0 / a)^2 (a / r_i)^2}{2\left(1-\dfrac{(a / r_i)^2}{(\beta L / r_o)^2}\right)^3}}} \tag{3.12}$$

where α is the separation factor and δ_o / a is the out-of-straightness. In case the spacing between the connectors is significant, β becomes:

$$\beta^2 = 1 + \frac{\left(\delta_0 / a\right)^2 \left(a / r_i\right)^2}{2\left(1 - \frac{\left(a / r_i\right)^2}{\left(\beta L / r_o\right)^2}\right)^3} \tag{3.13}$$

Solution to Eq. (3.12) are illustrated in Figure 3.8, Figure 3.9, and Figure 3.10. Figure 3.8 presents the effect of separation ratio (α) on the value of β across six curves, each corresponding to increasing values of α. It is clearly shown that the variation of α has minor impact on the β value, particularly when $\alpha > 5$. Figure 3.9 shows the effect of global slenderness ratio of the overall built-up member on the β factor. Similarly, six curves corresponding to various L / r_o values ranging from 20 to 120 are plotted. The results indicate that all values of L / r_o influence the β factor, with the effect of interaction buckling being more sensitive to member slenderness. Additionally, the effects of initial geometric imperfection are illustrated in Figure 3.10, corresponding to $\delta_0 / a = 500$, $\delta_0 / a = 1000$, and $\delta_0 / a = 1500$. The figure is plotted for a specific slenderness ratio ($L / r_o = 20$), and the results showed that the interaction effect is significant, particularly when $(a / r_i)^2 / (L / r_o)^2 > 0.5$. In contrast, interaction effect is negligible when $(a / r_i)^2 / (L / r_o)^2 < 0.5$.

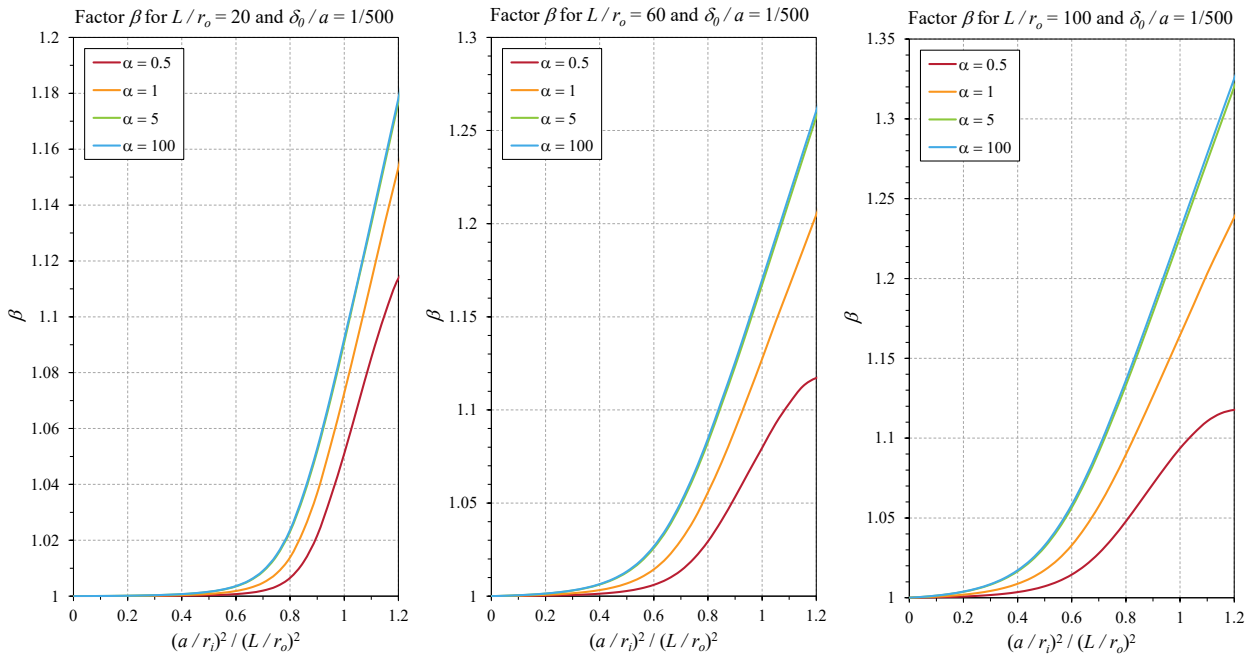

Figure 3.8 Effects of separation ratio on β factor (reproduced from [94]).

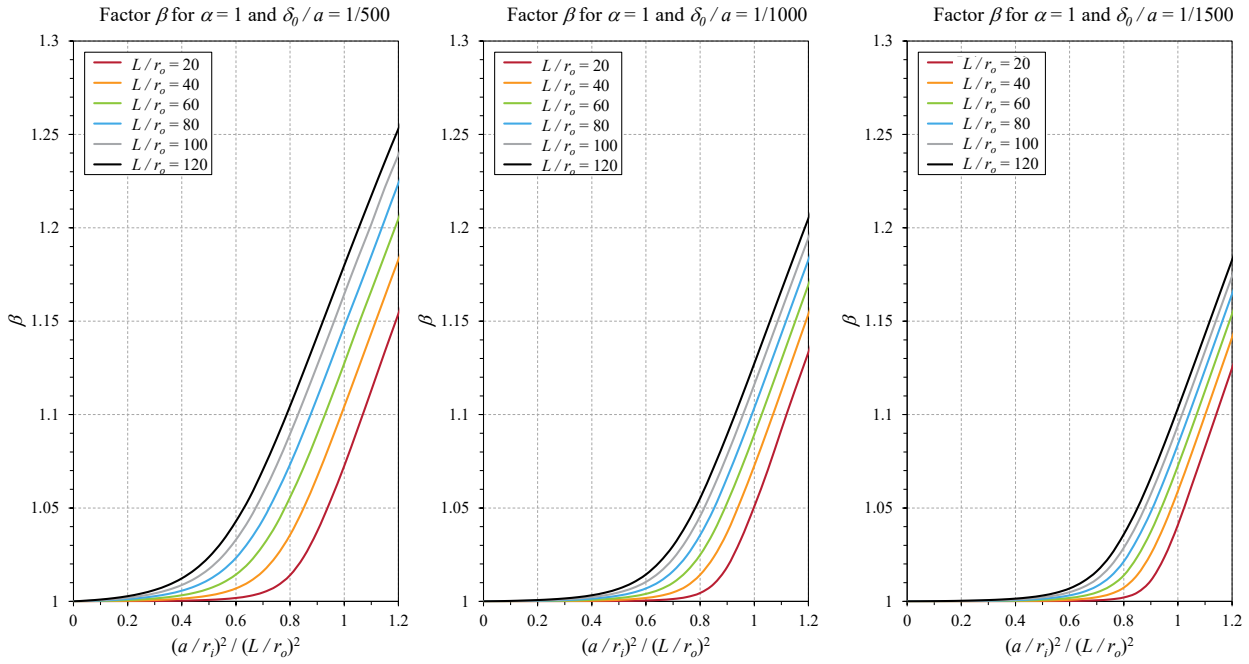

Figure 3.9 Effects of global slenderness ratio on β factor (reproduced from [94]).

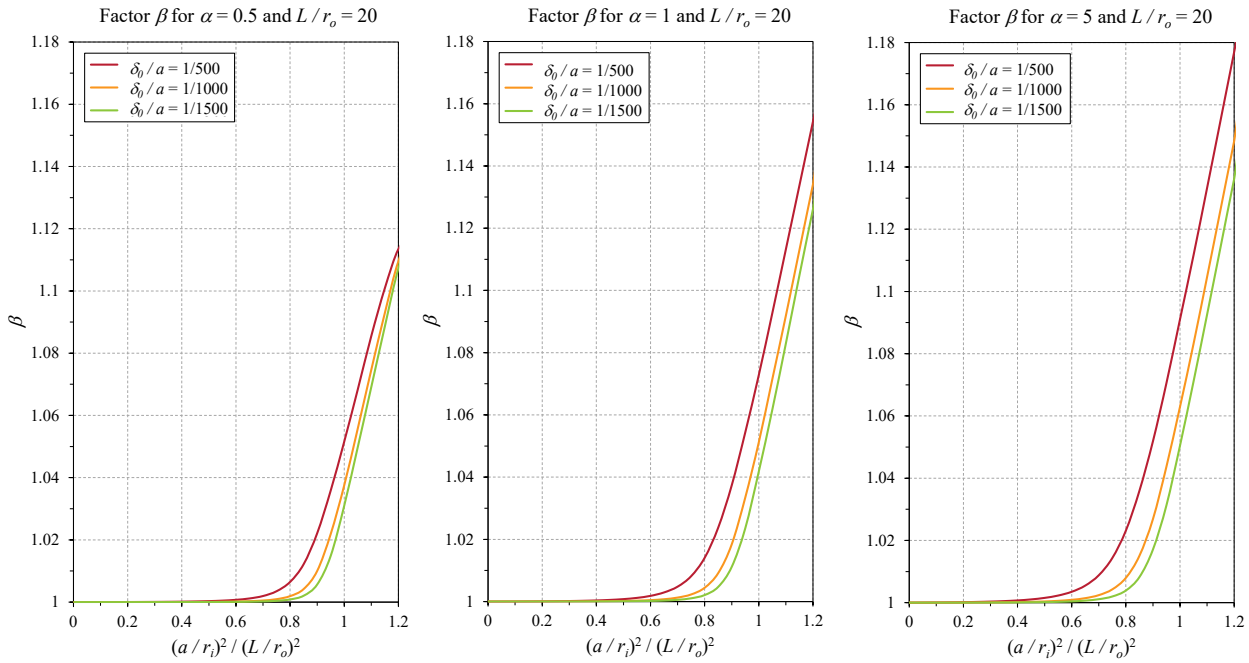

Figure 3.10 Effects of initial imperfections on β factor (reproduced from [94]).

3.3 Factors affecting buckling strength

3.3.1 Effect of residual stresses

Residual stresses are internal stresses that remain in a structure even in the absence of external loads. They arise due to internal constraints within a section that prevent the natural development of elastic strain relief, such as compression, tension, or relaxation, during events like phase transformations, thermal gradients, or mechanical processing. These internal constraints cause tensile and compressive stresses to develop within the same section, which remain in equilibrium because no external axial force is acting on the member.

Figure 3.11 illustrates the residual stresses effects in an I-section under compression. When the member is subjected to axial compression, the orientation and magnitude of the residual stresses can influence its behaviour. In compressed regions, residual stress may increase the total compressive stress, leading to an earlier onset of yielding and a reduction in stiffness. In contrast, in regions with residual tension, these stresses may offset some of the applied compression and provide a stabilizing effect. Overall, residual stress can reduce compressive resistance by causing earlier local yielding, lowering stiffness, and negatively impacting structural stability.

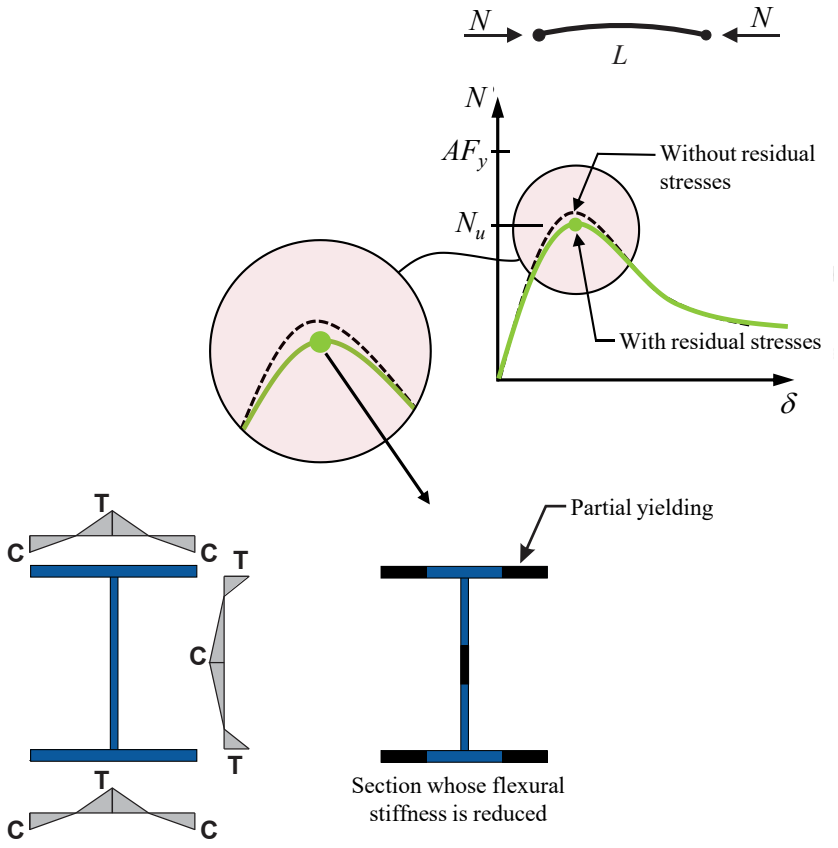

Figure 3.11 Effect of residual stresses on an I-section compression member.

Residual stresses have a significant impact on brittle fracture, fatigue, stress corrosion, and buckling strength in structural steel sections. Additional sources include welding, flame cutting (such as oxygen cutting), straightening, cold bending, and other finishing operations, as noted by Ziemian [95]. For hot-rolled members, Beedle and Tall [96] reported that both the magnitude and distribution of residual stresses depend on steel properties, cross-sectional shape, and manufacturing parameters including rolling temperature, straightening methods, and cooling conditions. Može et al. [97] further highlighted that longitudinal residual stresses have a more pronounced effect on buckling behaviour compared to those acting in the transverse direction. The residual stresses distribution models for hot-rolled equal angles, as adopted in American and European design codes, are reported by Ban et al. [98] and Može et al. [97], and are illustrated in Figure 3.12.

For the American standards, the stress distribution is defined by $\beta_1 = \beta_3 = -0.3$ and $\beta_2 = 0.3$, while for the European code, the values are $\beta_1 = -0.22$, $\beta_2 = 0.24$ and $\beta_3 = -0.25$.

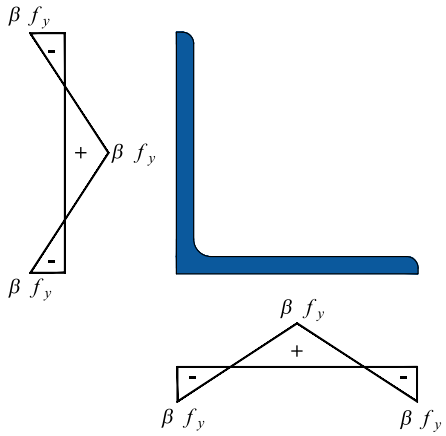

Figure 3.12 Residual stress distribution model of hot-rolled steel equal angle in the American and European codes.

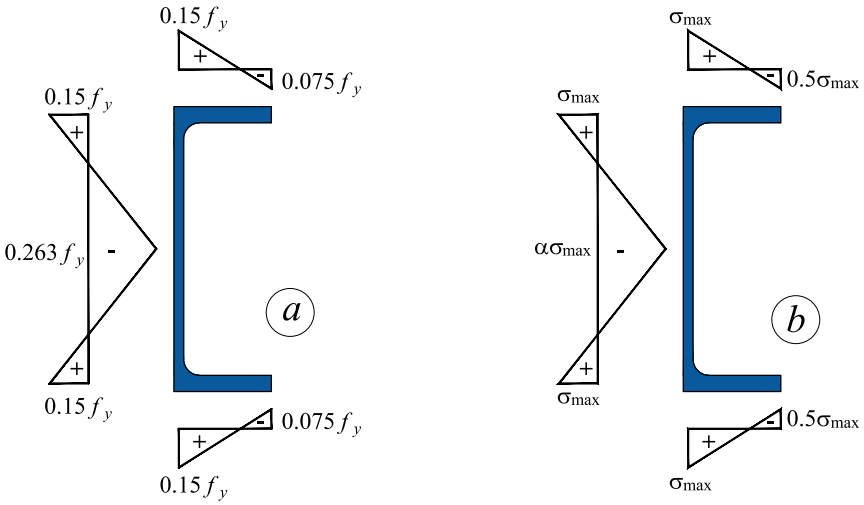

Figure 3.13 Residual stress in hot-rolled C-shaped section – (a) Pattern proposed by Lindner and Glitsch [99] – (b) Pattern proposed by Beyer et al. [100].

Lindner and Glitsch [99] discussed the influence of residual stresses on the behaviour of hot-rolled sections, but detailed stress patterns were derived from earlier experimental studies. The authors proposed a methodology to extract residual stresses patterns from I shape sections and subsequently adjusted them to suit channel sections (see Figure 3.13a). These residual stresses patterns were later further investigated by Beyer et al. [100], who proposed residual stresses distribution patterns in finite element models for UPE sections subjected to major-axis bending (see Figure 3.13b). A critical aspect of their method involved ensuring self-equilibrium within each plate of the channel section. Their results show that residual stresses could be neglected in Geometrically and

Materially Nonlinear Analysis with Imperfections Analysis (GMNIA) simulations for major-axis bending, as calculations without residual stresses were generally in good agreement with experimental tests and represented a lower bound solution compared to experimental tests. The definition of σ_{max} and α coefficient are described in Eq. (3.14).

$$\sigma_{max} = 0.15 f_y \tag{3.14}$$

$$\alpha = 1 + \frac{b t_f}{h t_w} \tag{3.15}$$

where b is the width of C-section, h represents the total height of the section, and t_w and t_f are the thickness of web and flange, respectively.

For rolled plates, the average longitudinal residual stress through the thickness typically follows a parabolic distribution, with tension at the center and compression near the edges [101]. In flame-cut plates, residual stresses induce tensile stress approximately equal to the yield strength in a narrow strip adjacent to the cut edge. Figure 3.14 illustrates the residual stress distribution for (a) a rolled plate, (b) a flame-cut plate with one cut edge, and (c) a flame-cut plate with two cut edges.

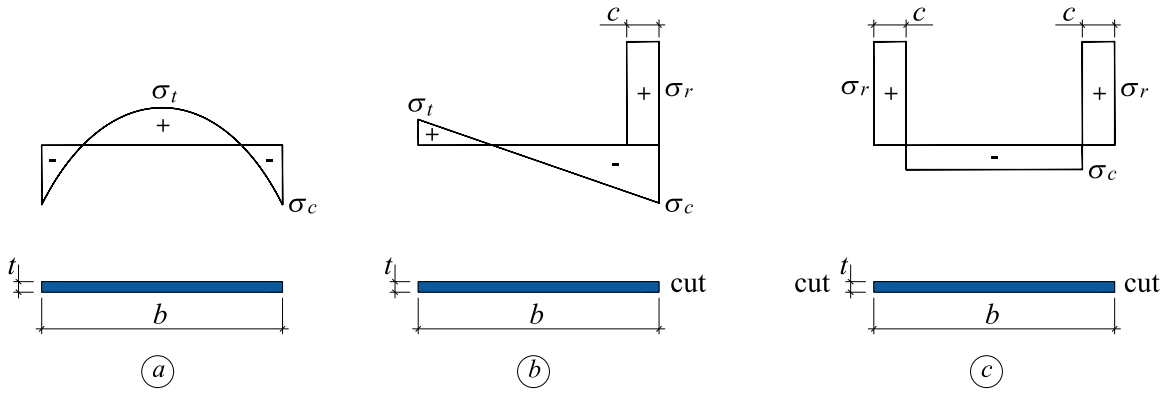

Figure 3.14 Residual stresses in steel plates, as reported in [101].

3.3.2 Effect of initial geometric imperfections

Another important parameter influencing column behaviour is the initial geometric imperfections. Generally, structural members are never perfect as they usually exhibit geometric imperfections such as initial out-of-straightness induced by fabrication processes. Figure 3.15 shows the influence effect of residual stress and geometric imperfection on the ultimate strength of compressive members. Behaviour. Geometric imperfections promote premature buckling and trigger the nonlinear beam–column response, in which the member is subjected to axial force and second-order bending, while residual stresses modify its stiffness and yielding behaviour. When acting together, these effects amplify each other, accelerating plasticity and instability, and lowering the strength of real members compared to idealized models.

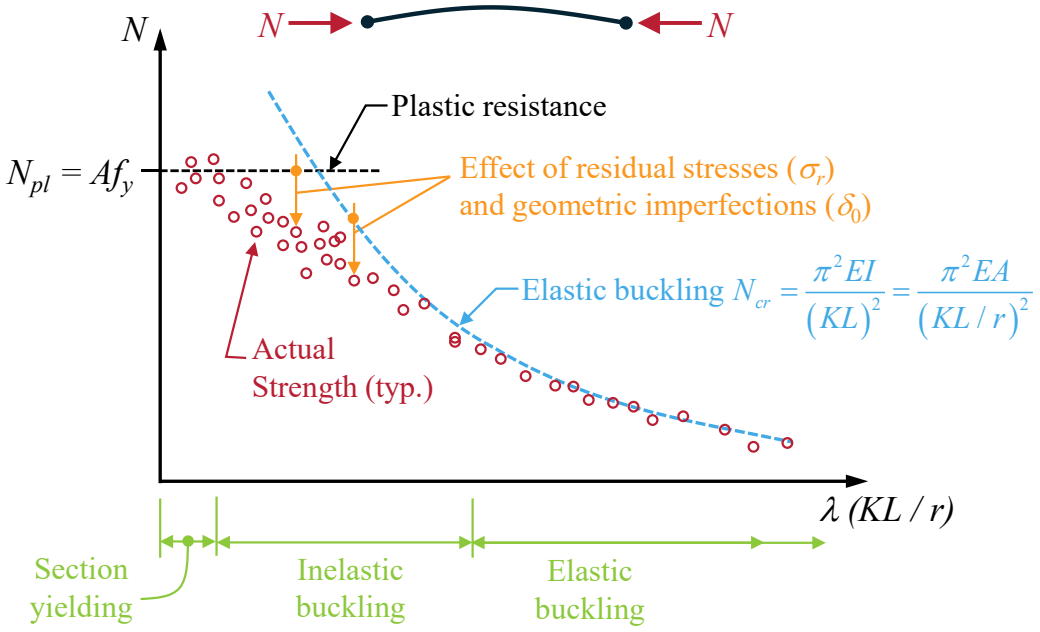

Figure 3.15 Effect of residual stress and geometric imperfections.

Crawford and Benton [87] investigated the strength of laced columns with initial waviness, providing insights into the influence of initial geometric imperfections on buckling behaviour. Svensson and Kragerup [88] studied the effect of local and overall global geometric imperfections on laced columns. They reported that a linear-elastic column is likely to behave like a shell upon reaching the collapse load and, therefore, is sensitive to imperfections. They showed that local and overall imperfections are most significant when the critical load and overstress coincide, and that realistic imperfections can reduce the approximated capacity by about 50%. Similarly, Geng-Shu

and Shao-Fan [102] showed that a highly unfavorable interaction occurs between local and global deformations when the equivalent slenderness of the built-up column is close to the local slenderness ratio of the chord.

Duan et al. [103] further studied the influence of initial geometric imperfections in laced or battened members. They assumed that the initial imperfection follows a sinusoidal form and introduced an imperfection amplitude factor, α, defined as a function of the separation factor. Their results showed that initial imperfections can significantly reduce the compressive strength of built-up members, potentially affecting the outcomes of structural optimization.

Kalochairetis and Gantes [104] also considered the effect of initial geometric imperfections in their analytical method for determining the collapse load of laced built-up members. They incorporated local imperfections by reducing the effective bending rigidity of the members and deriving the critical force from the maximum total deflection. Their study highlighted that the maximum strength reduction occurs when local and global Euler critical stresses coincide with the yield stress, and that this loss becomes more pronounced when imperfections reach magnitudes of 50%.

El Aghoury et al. [105], [106] experimentally investigated cold-formed steel battened column members composed of four equal slender angles, accounting for residual stress and geometric imperfections in the chords. Their results showed that the interaction between the initial imperfections of the individual angles and those of the overall column, significantly affects local buckling and the ultimate collapse load.

Recently, Li et al. [107] investigated the elastic compound buckling of laced columns with three lacing systems (X-lacing, E-lacing, and K-lacing) under simply supported and cantilever conditions, considering the effects of eccentric loading. Local imperfections due to bending displacement and initial twisting imperfection were introduced in sinusoidal form. The authors found that local imperfections reduce the critical buckling load of all laced columns. They also reported that the K-lacing system under simply supported conditions is more sensitive to local buckling than the X-lacing and E-lacing systems, while local imperfections have almost no effect on the critical load of any of the three lacing systems under cantilever conditions. More recently, Li et al. [108] modeled four-legged latticed columns to investigate the influence of lacing bar imperfections on the buckling load under three loading conditions. They proposed four imperfection models for the lacing bars: Mode 1, a single sine wave on the outer lacing plane;

Mode 2, a double sine wave on the inner lacing plane; Mode 3, a double sine wave on the outer lacing plane; and Mode 4, a single sine wave on the outer lacing plane with multiple lacing bars. Their results showed that lacing bar imperfections significantly affect the critical buckling load of four-legged latticed columns, with the outer lacing plane imperfection model having the greatest effect, leading to the largest reduction in buckling capacity.

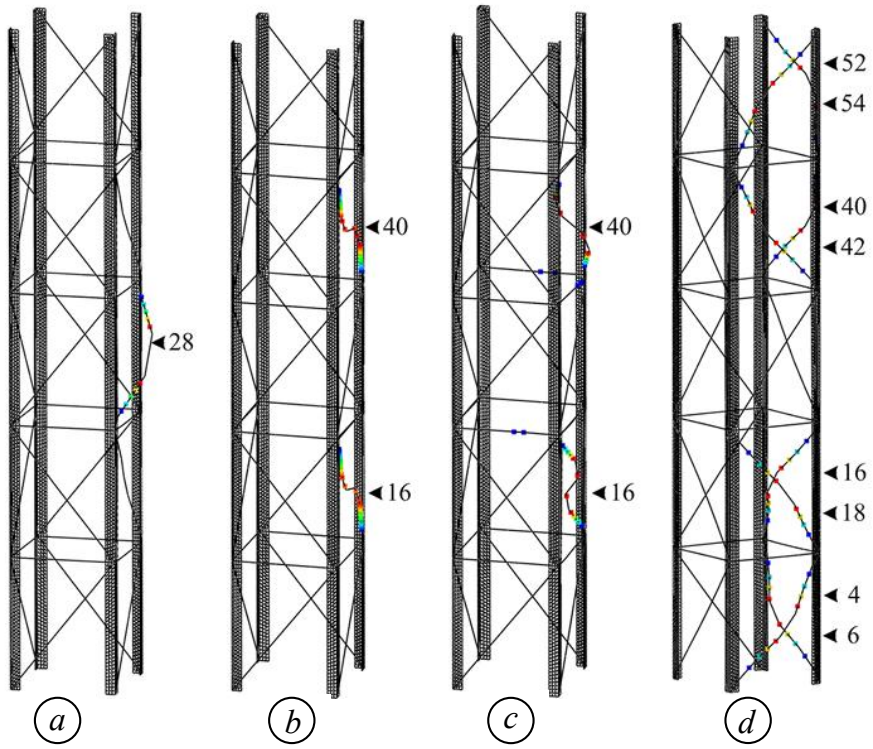

Figure 3.16 Imperfection shapes of lacing bars adopted in [108] – (a) Mode 1, single sin wave outer lacing plane – (b) Mode 2, double sin waves inner lacing plane – (c) Mode 3, double sin wave outer lacing plane – (d) Mode 4, single sin wave outer lacing plane.

3.3.3 Effective length factor in truss structures

In truss structures, joints connected by welds or bolts develop secondary stresses due to changes in joint angles. These stresses have a negligible effect on member buckling strength, as local yielding in the extreme fibers near the joints allows secondary moments to dissipate progressively under increasing load, and can therefore be neglected in buckling analysis [109]. For in-plane buckling of compression members, the effective length factor is generally taken as 1.0, since simultaneous attainment of factored resistance by all members implies no member restrains another. Effective

length factors for compression members not braced perpendicular to the truss plane are also provided by Ziemian [95].

$$K = 0.75 + 0.25\left(\frac{N_1}{N_2}\right) \tag{3.16}$$

where $N_2 < N_1$. This expression is applied when the compressive forces N_1 and N_2 in a truss chord changes at a subpanel point that is not braced perpendicular to the plane of the main truss (see Figure 3.17), the chord may be susceptible to out-of-plane buckling.

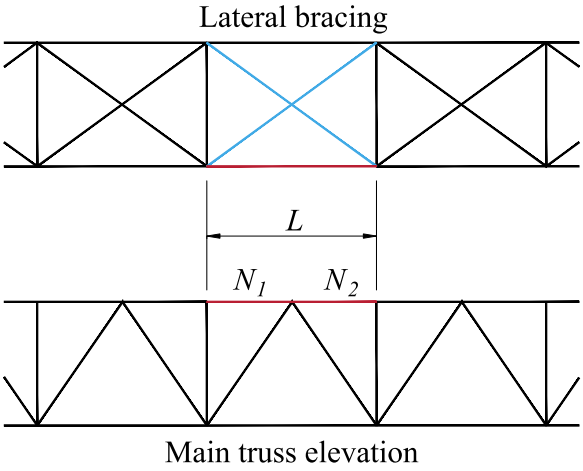

Figure 3.17 Effective length factor in compression chords of truss structure, as reported in [95].

Higgins et al. [110] conducted experimental tests on large-scale bridge-type gusset plates, focusing on their sway-buckling behaviour. The study investigated the effects of plate thickness, the flexural stiffness of compression diagonals, and initial out-of-plane imperfections. Their results showed that the maximum observed effective length factor, K, of 0.8, which can be applied in the analysis of gusset plates governed by sway-dominated behaviour. Most recently, Zheng et al. [111] investigated the in-plane effective length factor of web members in steel trusses. Their study accounted for the effects of stiffness contributions from non-adjacent members, joint rigidity, and load variations specified in design codes by developing a finite element model based on the Steel Truss Atlas in Abaqus. The authors recommended using effective length factors of 0.8 for support web members and 0.7 for other web members when evaluating in-plane buckling of steel trusses.

3.4 Current standard practices for the design of laced built-up columns

3.4.1 American Standards (AISC 360)

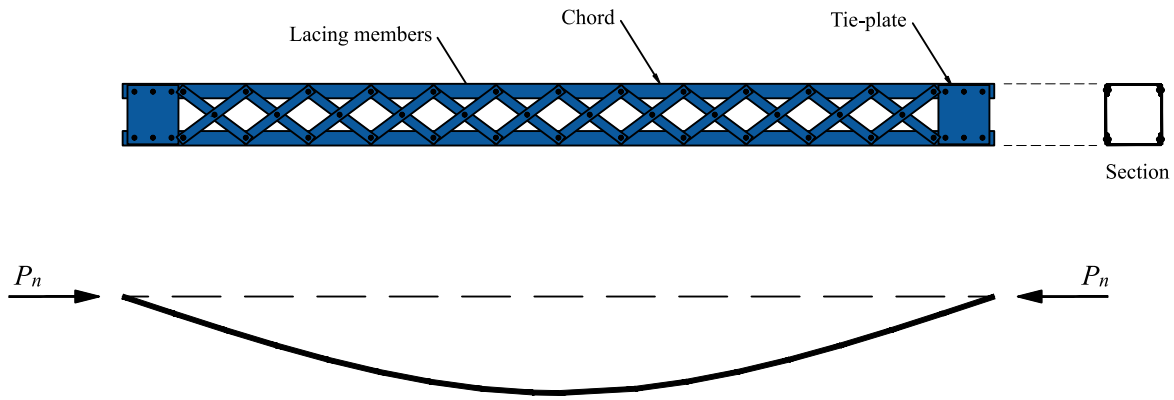

Figure 3.18 Typical laced built-up column subjected to compression.

According to AISC 360-22 [112], the compressive strength of a built-up member composed of two shapes interconnected by lacing and tie plates (see Figure 3.18) is determined using the modified slenderness ratio approach, with the nominal compressive strength, P_n, evaluated based on the flexural buckling limit state.

$$P_n = F_n A_g \tag{3.17}$$

where F_n represents the nominal stress which is calculated as follows:

(i) When $\left(\frac{KL}{r}\right)_m \le 4.71\sqrt{\frac{E}{F_y}}$ or $\frac{F_y}{F_e} \le 2.25$

$$F_n = \left(0.658^{\frac{F_y}{F_e}}\right) F_y \tag{3.18}$$

(ii) Otherwise

$$F_n = 0.877 F_e \tag{3.19}$$

where A_g denotes the total gross area of the built-up section, E is the modulus elasticity, and F_e represents the elastic buckling stress, given by $F_e = \dfrac{\pi^2 E}{\left(\dfrac{KL}{r}\right)_m^2}$.

When the buckling mode involves relative shear deformation between lacing segments, the modified slenderness ratio, $(KL/r)_m$, is determined as follows:

(i) When lacing members are connected using snug-tight bolts

$$\left(\frac{KL}{r}\right)_m = \sqrt{\left(\frac{KL}{r}\right)_o^2 + \left(\frac{a}{r_i}\right)^2} \tag{3.20}$$

(ii) When lacing members are connected by pre-tensioned bolts (i.e., with Class A or B faying surfaces) or by welding

$$\left(\frac{KL}{r}\right)_m = \sqrt{\left(\frac{KL}{r}\right)_o^2 + \left(\frac{a}{r_i}\right)^2} \quad \text{if } \frac{a}{r_i} \le 40 \tag{3.21}$$

$$\left(\frac{KL}{r}\right)_m = \sqrt{\left(\frac{KL}{r}\right)_o^2 + \left(\frac{K_i a}{r_i}\right)^2} \quad \text{if } \frac{a}{r_i} > 40 \tag{3.22}$$

where $(KL/r)_o$ represents the slenderness ratio of the overall built-up member, and (a/r_i) is the slenderness ratio of an individual chord between lacing segments, a is the distance between lacing connectors, r_i is the minimum radius of gyration, and K_i is a modification factor with values of 0.50 for back-to-back angles, 0.75 for back-to-back channels, and 0.86 for all other cases.

It should be noted that Eq. (3.17) applied to built-up sections composed of non-slender elements. To account for local buckling, i.e., section with slender elements, the gross area A_g is replaced by the effective area A_e, which is the sum of the effective areas of each cross-sectional element (flange, web) based on their reduced widths, b_e. Further details on the calculation of b_e are provided in Clause E7.1 of AISC 360-22.

Similarly to AISC 360-22, the AASHTO 2020 LRFD Bridge Design Specifications (9th Edition) [113] adopted a comparable approach; however, when lacing members connected by welding or fully-tensioned bolted, the modified slenderness ratio is determined as follows:

$$\left(\frac{KL}{r}\right)_m = \sqrt{\left(\frac{KL}{r}\right)_o^2 + 0.82\left(\frac{\alpha^2}{1+\alpha^2}\right)\left(\frac{a}{r_{ib}}\right)^2} \tag{3.23}$$

where α is the separation ratio, given by $\alpha = h / 2\ r_{ib}$ and r_{ib} is the radius of gyration of an individual chord relative to its centroidal axis parallel to the member axis of buckling. For other types of lacing connectors, including built-up members with riveted connections on existing bridges, Eq. (3.20) should be applied.

For steel buildings, AISC 360-22 allows a slenderness ratio $(KL / r)_m$ of up to 200. However, for truss bridge members subjected to pure compression, the AASHTO provisions limit $(KL / r)_m$ to 120 for primary members and 140 for secondary members. In addition, both provisions impose further constraints to limit the effect of shear deformation, expressed as $\frac{a}{r_i} \le 0.75\left(\frac{KL}{r}\right)_o$.

Furthermore, AISC 360-22 includes the following additional requirements:

(i) Tie plates shall be provided at each end of the built-up member or at intermediate points if the lacing is interrupted. End tie plates must be at least as long as the distance between fastener or weld lines, while intermediate plates must be at least half this length. Plate thickness shall not be less than 1 / 50th of the distance between attachment lines;

(ii) For welded tie plates, each weld line must extend over at least one-third of the plate length. For bolted tie plates, fasteners should be spaced at most six diameters apart along the stress direction, with a minimum of three fasteners connecting each segment;

(iii) The lacing system shall resist a shear force (V) perpendicular to the axis of the built-up member equal to 2% of its nominal compressive strength, i.e., $V = 0.02P_n$;

(iv) The inclination of lacing bars to the axis of the built-up member shall be at least 60° for single lacing and 45° for double (X) lacing. The slenderness ratio of the lacing bars, $(L / r)_{lacing}$, shall not exceed 140 for single lacing and 200 for double lacing. If the distance between the lines of welds or fasteners is large, double (X) lacing or lacing using angles shall be provided.

3.4.2 Canadian Standards (CSA S16)

The unfactored compressive resistance of built-up members, calculated in accordance with CSA S16-24 [114], is expressed as follows:

$$C_r = \frac{AF_y}{\left(1+\lambda^{2n}\right)^{\frac{1}{n}}} \tag{3.24}$$

where n = 1.34 for hot-rolled or fabricated sections and non-stress-relieved HSS per CSA G40.20 Class C or ASTM A1085; and n = 2.24 for welded three-plate members with oxy-flame-cut flanges and stress-relieved HSS per CSA G40.20 Class H. The non dimensional slenderness parameter λ is defined by $\lambda = \sqrt{\frac{F_y}{F_e}}$, while the elastic buckling stress F_e for doubly symmetric sections can be calculated as $F_e = \frac{\pi^2 E}{\rho_e^2}$. Here, ρ_e denotes the equivalent slenderness ratio of the built-up member, determined from Eq. (3.25) using the modified slenderness ratio approach, similar to the method in the American standard.

$$\rho_e = \sqrt{\rho_o^2 + \rho_i^2} \tag{3.25}$$

where ρ_e is the equivalent slenderness ratio of the built-up member, ρ_o is the slenderness ratio of the member considered as an integral unit, and ρ_i is the maximum slenderness ratio of individual components between interconnectors. Similarly, Eq. (3.25) can be rewritten as:

$$\left(\frac{KL}{r}\right)_e = \sqrt{\left(\frac{KL}{r}\right)_o^2 + \left(\frac{K_i a}{r_i}\right)^2} \tag{3.26}$$

where $\left(\frac{K_i a}{r_i}\right) \leq \left(\frac{KL}{r}\right)_o$.

Note that, the effective length factor, K_i, for a component between interconnectors that are in contact or separated only by a filler plate is 1.0 for snug-tight bolts and 0.65 for pretensioned bolts

or welds. If the component is separated by batten plates or lacing, K_i is taken as 1.0 even if both bolts and welds are used.

In Eq. (3.24), A shall be taken as the full gross area, A_g, for non-slender sections, and as the effective area, A_e, for slender sections. For steel buildings, CSA S16-24 permits a slenderness ratio $(KL / r)_m$ of up to 200. However, for truss bridge members subjected to pure compression, the Canadian Highway Bridge Design Code, CSA S6-24 [115] provisions limit $(KL / r)_m$ to 120 for primary members and 160 for secondary and bracing members.

Moreover, CSA S16-24 provisions specify further requirements for the design of tie plates and the lacing system, as follows:

(i) Lacing systems shall have diaphragms such as tie plates or shapes in the plane of the lacing and as near to the ends as practicable as well as at intermediate points where lacing is interrupted;

(ii) Tie plates shall have at least a length equal to the distance between the lines of bolts or welds connecting them to the main member components. Intermediate tie plates must be at least one-half the length of the end tie plates;

(iii) The plate thickness shall be no less than 1 / 60 of the width between the lines of bolts or welds, with the longitudinal spacing of bolts or the clear spacing between welds not exceeding 150 mm. Each tie plate shall be fastened to each main component with at least three bolts, or, alternatively, a total weld length of at least one-third the tie plate length shall be provided;

(iv) The lacing system shall resist a shear force (V) perpendicular to the axis of the built-up member equal to 2.5% of total axial load plus the additional shear due to external transverse loads, i.e., $V = 0.025\ C_u + V_{u,ext}$;

(v) The lacing shall be inclined at not less than 45° to the axis of the built-up member, with a slenderness ratio, $(L / r)_{lacing}$, not exceeding 140.

3.4.3 European Standards (Eurocode 3)

The verification of built-up sections is addressed in Eurocode 3 [116], which provides guidance for uniform built-up members with hinged ends, laterally supported, and subjected to compression. The code requires consideration of initial bow imperfections $e_0 = L / 500$, where L denotes the length of the built-up member. The provisions apply to uniform built-up members consisting of

lacing or batten systems formed by equal panels with parallel chords, with a minimum requirement of three panels per member. As shown in Figure 3.19,the design effect of an element comprising two parallel chords shall be determined as follows:

$$N_{ch,Ed} = 0.5N_{Ed} + \frac{M_{Ed} h_0 A_{ch}}{2I_{eff}} \tag{3.27}$$

where N_{Ed} is the design value of the compression force acting on the built-up member, A_{ch} is the cross-sectional area of one chord, I_{eff} is the effective moment of inertia of the built-up member, h_0 is the distance between the centroids of the chords, and M_{Ed} can be determined as:

$$M_{Ed} = \frac{N_{Ed} e_0 + M_{Ed}^I}{1 - \frac{N_{Ed}}{N_{cr}} - \frac{N_{Ed}}{S_v}} \tag{3.28}$$

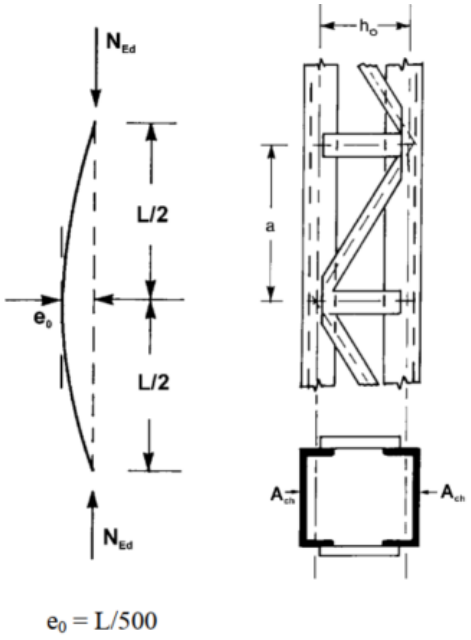

Figure 3.19 Uniform built-up column with lacings [116].

The term M_{Ed}^I refers to the design value of the maximum moment at mid-length of the built-up member without considering second-order effects, S_v denotes the shear stiffness of the lacing or battened panels, and N_{cr} represents the effective critical force of the built-up member, which is defined as:

$$N_{cr} = \frac{\pi^2 EI_{eff}}{L^2} \tag{3.29}$$

where L is the effective length and I_{eff} is the effective moment of inertia of laced built-up member, calculated as:

$$I_{eff} = 0.5 h_0^2 A_{ch} \tag{3.30}$$

In Eq. (3.30), I_{ch} denotes the in-plane second moment of area of one chord. The shear stiffness, S_v, is defined as given in Table 3.1. In this context, n refers to the number of lacing planes, A_d denotes the cross-sectional area of the intermediate diagonal lacing, A_v represents the cross-sectional area of the horizontal lacing, and a is the spacing between lacing connectors.

For design verification, Eq. (3.27) represents the design axial force in a chord at the mid-length of the built-up member. This force should be checked against the chord's design buckling resistance, $N_{b,Rd}$, using the following criterion:

$$\frac{N_{ch,Ed}}{N_{b,Rd}} \leq 1.0 \tag{3.31}$$

where $N_{b,Rd}$ is calculated assuming a buckling length $L_{ch} = a$ for the laced built-up member composed of two main chords.

Additionally, the standard specifies further constructional details for lacing systems, as summarized below:

(i) For built-up members with two parallel laced planes, the single lacing systems on opposite faces should be arranged correspondingly so that one plane mirrors the other. If they are oriented in opposite directions, the resulting torsional effects on the member must be considered;

(ii) Tie panels shall be provided at lacing ends, interruptions, and joints with other members;

(iii) Lacing in built-up members should be checked at the end panels, taking into account the shear force in the member, V_{Ed}, which is given by $V_{Ed} = \pi M_{Ed} / L$.

Table 3.1 Shear stiffness for different lacing systems in built-up members.

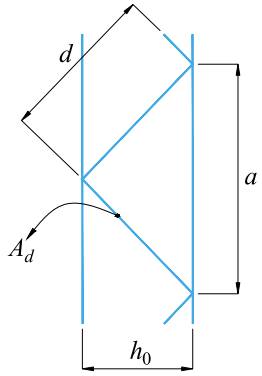	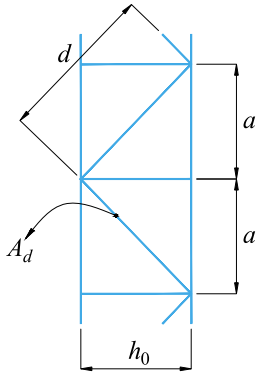	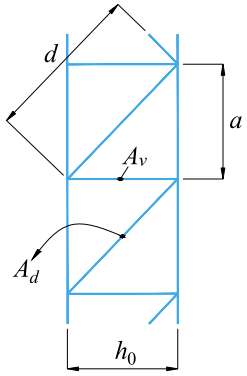
$S_v = \frac{nEA_d a h_0^2}{2d^3}$	$S_v = \frac{nEA_d a h_0^2}{d^3}$	$S_v = \frac{nEA_d a h_0^2}{d^3\left(1+\frac{A_d h_0^3}{A_v d^3}\right)}$

3.5 Overview of modern design approaches for coupled instabilities

3.5.1 The Continuous Strength Method (C.S.M.)

The Continuous Strength Method (C.S.M.) was introduced by Gardner in 2008 [117]; it evaluates the cross-sectional capacity of a member based on the material's strain limits. The method incorporates non-linear material behaviour and strain hardening, thereby eliminating the need for the Effective Width Method (E.W.M.) for slender sections. For stocky members, which can undergo substantial deformations beyond the plastic limit, strain-based approaches like the C.S.M. provide a more accurate estimate of actual capacity. Additionally, this method is particularly suitable for sections that benefit from strain hardening, such as compact hot-rolled, cold-formed, stainless steel, and certain high-strength steel sections. However, the advantages of strain hardening are limited for many high-strength steel members. While C.S.M. effectively captures local strength, its influence on global member behaviour is negligible, as only a small portion of fibers typically reach strain-hardening levels. For members with high local slenderness, failure is predominantly governed by local buckling and subsequent post-buckling behaviour. Although residual stresses and stress concentrations can induce some plasticity even in slender sections, differences in cross-

sectional slenderness may produce similar strain levels, meaning that the C.S.M. can provide only an approximate estimate of local strength in these cases. Besides, the average relative strain at ultimate load, $\varepsilon_{LB} / \varepsilon_0$ (ε_{LB} at peak load, $\varepsilon_0 = F_y / E$ is related to the maximum plate slenderness, λ_p, depending on the cross-section type (CHS, I, or H) and loading condition [117]. These experimentally derived relationships account for inelastic buckling, imperfections, and post-buckling behaviour. The C.S.M. involves the following steps:

(i) Identify the maximum plate slenderness based on the cross-section;

(ii) Calculate the average strain ratio, $\varepsilon_{LB} / \varepsilon_0$, using the relevant formulas or curves;

(iii) Determine the local buckling stress, σ_{LB}, from the material constitutive law (σ–ε relationship);

(iv) Evaluate the cross-sectional resistance according to the loading condition, using the relationship between external forces and internal stresses.

While the C.S.M. provides notable improvements over conventional code formulations, its practical advantage disappears in the vast majority of cases (approximately 95%) where members do not reach strain-hardening conditions. For slender sections, buckling often occurs before strain hardening develops, limiting the method's benefits. In such cases, cross-sectional resistance may be better estimated directly from the slenderness ratio. Moreover, C.S.M. relies on interaction formulas for combined loading, which overlooks the need for continuity. A similar review also been reporting in [118].

3.5.2 The Direct Strength Method (D.S.M.)

The Direct Strength Method (D.S.M.), introduced by Schafer [119], is a design approach that determines member strength by accounting for resistance-stability interactions, which are then incorporated into cross-sectional strength formulas. Depending on whether a section is susceptible to local or distortional buckling, different equations, derived from experimental and numerical studies, are applied.

Originally developed for very slender cold-formed sections such as C- and Z-shapes under axial compression [119], D.S.M. was later extended to standard hot-rolled sections [120]. Research has further adapted D.S.M. to combined loading conditions, with available formulas also addressing pure bending and lateral-torsional buckling. More recently, B. Young [121] and P.B. Dinis [122]

proposed an extension of the D.S.M. for triple interaction in cold-formed sections, introducing a validated approach to predict column failure under complex loading. Their work expanded the original D.S.M., which focused on double interaction modes, by incorporating design rules for cold-formed columns subjected to lateral/distortional/global (L/D/G) interaction.

For the design of columns under axial loading, the nominal global axial strength, P_{ne}, corresponding to flexural, torsional, or combined buckling is first calculated based on the relative member slenderness, $\lambda_c = \sqrt{P_y / P_{cre}}$, where P_y is the full plastic resistance and P_{cre} the elastic buckling load. The local ultimate strength, P_{nl}, is then obtained by combining the nominal axial strength and the local elastic buckling load of a short element. Similarly, distortional ultimate strength can be determined using corresponding equations. The D.S.M. offers several advantages: it provides a direct estimate of member strength, distinguishes the contributions of different buckling modes (global, local or distortional), eliminates the need for complex calculations associated with the E.W.M. for slender sections, and can yield higher strength predictions compared to traditional design approaches.

However, D.S.M. also has limitations. It is less suitable for compact sections without adjustments, relies primarily on elastic capacity with equations valid only up to the elastic limit, which may misestimate strength when plastic reserve becomes significant, and, similarly to code-based approaches for combined loading, it uses interaction formulas that can disrupt the continuity of the design. Similar observations also reported in [118].

3.5.3 The Overall Interaction Concept (O.I.C.)

The O.I.C. is based on the well-established resistance-instability interaction, utilizing a definition of generalized relative slenderness. It eliminates the need for cross-section classification and the E.W.M., treating all cross-section shapes uniformly at both the section and member levels. This method was proposed by Boissonnade et al. [123], who described its mechanical background, principles, and application steps. The concept was initially developed for hollow sections subjected to pure compression, pure bending, and combined loading. Figure 3.20 illustrates the principle of the O.I.C. and the application steps for the cross-section resistance.

For such section resistance, the O.I.C. framework is founded on the interaction of two fundamental phenomena that govern section capacity: plasticity and instability. For compact sections, resistance

is primarily controlled by plastic capacity (see blue curve in Figure 3.20), while for slender sections it is limited by instability (see red curve in Figure 3.20). Sections with intermediate slenderness are influenced by both effects, as well as by imperfections, and their behaviour follows the "real behaviour" or "buckling" curve illustrated in Figure 3.20. This curve integrates the key factors affecting resistance, namely material yielding, local buckling, and imperfections. Within this framework, the plastic capacity serves as the reference strength, and a penalty factor, χ_L, is introduced to capture the influence of buckling, imperfections, and their interaction with plastic behaviour. The factor χ_L is expressed as a continuous function of local slenderness, λ_L, thereby defining the buckling curve shown in Figure 3.20; however, it may not be strictly limited to local buckling behavior. In addition to summarizing these principles, Figure 3.20 presents the stepwise procedure adopted in the O.I.C. for predicting local resistance.

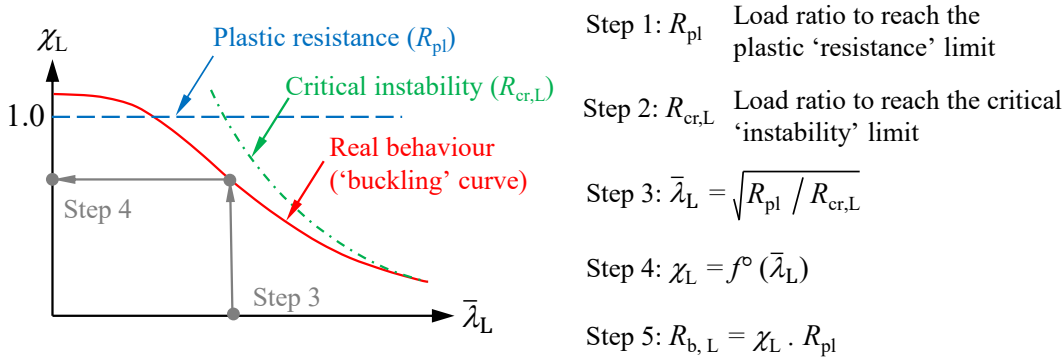

Figure 3.20 Principles of the O.I.C. and application steps for cross-section resistance, as proposed in [123].

The O.I.C. framework employs a systematic five-step procedure for predicting the resistance of general cross-section shapes under compressive or combined loading. It is applicable to all forms of buckling and does not depend on boundary conditions.

(i) Plastic capacity (R_{pl}) – Evaluate the section's plastic capacity through the plastic load ratio, R_{pl}, defined as the multiplier of the applied load required to reach plastic resistance;

(ii) Local critical resistance ($R_{cr,L}$) – Determine the local buckling resistance through the critical load ratio, $R_{cr,L}$, which represents the multiplier of the applied load leading to reach elastic critical load for local buckling;

(iii) Local slenderness (λ_L) – Define a generalized local relative slenderness parameter, λ_L, which balances the competing effects of plasticity and instability;

(iv) Penalty factor (χ_L) – Compute the reduction factor χ_L, expressed as a function of λ_L, to account for the influence of local instability and imperfections;

(v) Ultimate resistance ($R_{b,L}$) – Establish the final resistance through the load ratio $R_{b,L} = \chi_L \cdot R_{pl}$, thereby incorporating the combined effects of plasticity, instability, and imperfections.

The O.I.C. was originally developed for hot-rolled square and hollow sections [124], [125], covering a range from compact (stocky sections) to slender sections, but its concept applies to all cross-section shapes. It provides a direct prediction of resistance, incorporates all types of member continuity, and allows the use of tools for evaluating key R ratios. The approach can be implemented as a semi-analytical or fully analytical method, offering a flexible and comprehensive procedure for structural assessment. Recently, O.I.C-based design approaches have been extended to various hot-rolled sections, including bi-symmetric I-sections [122]–[125], mono-symmetric I-sections [130], and T-sections [131]. More recently, the O.I.C. method has also been applied to aluminum structures [128]–[130], demonstrating its capability to deliver highly accurate predictions while maintaining safety and economic efficiency compared to existing design proposals. The results demonstrate that the O.I.C-based design rules provide more reliable and consistent predictions compared to current design standards. These studies also show that the O.I.C. effectively accounts for complex coupling interaction effects, such as local/global interactions in hot-rolled sections.

3.6 Summary and research gaps

An extensive review of the literature was undertaken to assess the current requirements for designing laced built-up steel members. This review highlighted the progress achieved in resolving the well-recognized inconsistencies within design codes, which can serve as a basis for directing future research. The focus was on collecting and analyzing existing studies and recent knowledge related to this thesis, covering aspects from the design of the primary components of built-up members to the configuration of their lacing systems. Unlike non-built-up columns, whose resistance is primarily governed by local buckling of the cross-section, global buckling of the member, or a combination of both, the resistance of built-up columns is also influenced by shear

deformations. The reason is that shear deformations introduce an additional buckling mode in built-up columns, specifically the global buckling of the chord between the connectors, which results in a more complex buckling behaviour compared to non-built-up columns.

To address this issue, researchers developed the modified slenderness ratio design, which accounts for the additional flexibility of chord segments between connectors with the overall behaviour of the built-up member to capture the effect of shear deformations. This concept has been widely adopted by many current design standards. However, instead of accounting for the full interaction between these modes, current standards impose additional constraints to minimize the interaction between the flexural buckling of the overall built-up member and the buckling of chord segments between connectors caused by shear deformation. This approach can lead to inaccurate estimates of resistance, particularly for built-up members fabricated for older steel bridges, as they may not comply with the limitations imposed by the current design rules. Furthermore, members fabricated for older steel bridges were typically assembled from plates, angles, or C-sections to form the built-up section. These elements are often very slender, so local buckling of the cross-section can significantly influence the member's resistance as well as its interaction with other buckling modes. As a result, the effect of coupled instability becomes highly sensitive and can also have a substantial impact on the overall resistance of the built-up member.

Table 3.2 summarizes the possible buckling and failure modes of non-built-up and laced built-up compressive members, along with how current design codes treat them. Non-built-up members are primarily checked for local and global buckling, while laced built-up members require additional consideration of chord buckling between connectors, overall built-up buckling, and the strength of lacing members. The table compares AISC 360-22, AASHTO 2020, CSA S16-24, and Eurocode 3, highlighting whether each code includes local, global, and built-up buckling effects and whether interactions between these modes are considered. It also notes specific design requirements for the lacing system to ensure shear transfer and chord stability. This highlights the need for a design method capable of considering all relevant buckling modes simultaneously to ensure accurate assessment of member stability. In addition, two modern design concepts that explicitly account for buckling interactions, namely D.S.M. and O.I.C., were briefly discussed in the previous section. While C.S.M. is mainly developed for local behavior, its capability to capture interaction effects has not been conclusively demonstrated. Their main characteristics for compressive members are

summarized in Table 3.3. Accordingly, D.S.M. is a strength-based approach that calculates member strength from separate buckling modes, i.e., local, distortional, and global, but does not explicitly model interactions between these modes. The C.S.M., a strain-based method, computes member strength from continuous strain distributions.

Table 3.2 Buckling modes and design considerations of non-built-up vs laced built-up members.

<table>
<tr><td colspan="2">Category</td><td>Non-built-up members</td><td>Laced built-up members</td></tr>
<tr><td colspan="2">Possible buckling / failure modes</td><td>1. Local buckling of cross-sections;
2. Global buckling of the overall members.</td><td>1. Local buckling of cross-sections;
2. Global buckling of chord segments between lacing connectors;
3. Built-up buckling of the overall members;
4. Failure of lacing members.</td></tr>
<tr><td rowspan="4">Current design rules</td><td>AISC 360-22</td><td rowspan="4">Local and global buckling included.</td><td>Global and built-up buckling included through modified slenderness ratio, excluding interaction effects; lacing must resist shear and prevent chord buckling.</td></tr>
<tr><td>AASHTO 2020</td><td>Similar to AISC 360-22 with additional constraints on member slenderness.</td></tr>
<tr><td>CSA S16-24</td><td>Similar to AISC 360-22.</td></tr>
<tr><td>Eurocode 3</td><td>Built-up buckling of the overall member included; member capacity governed by individual chords with effective length equal to spacing between lacing; interaction of local, global, and built-up buckling excluded; lacing designed for shear transfer and chord stability.</td></tr>
</table>

While originally intended for compact cross-section resistance, subsequent extensions allowed it to address local or global buckling individually; however, interaction effects are not explicitly included. In contrast, O.I.C. systematically accounts for the coupled behaviour of local and global

instabilities, making it capable of accurately assessing members with a wide range of section slenderness.

Table 3.3 Comparison of modern design approaches.

Aspect	D.S.M.	C.S.M.	O.I.C.
Design approach	Strength-based design	Strain-based design	Strength-based design
Basis	Experimental data and numerical simulations	Experimental data and numerical simulations	Experimental data and numerical simulations
Applicability	Cold formed slender sections	Compact sections exhibiting strain-hardening	Sections ranging from compact to slender
Buckling interaction	Local, global, and distortional interactions not explicitly modeled	Local and global interactions not explicitly modeled	Local and global interactions considered systematically
Determination of compressive strength	Minimum nominal strength from each buckling mode	Maximum axial load before yielding/buckling	Coupled analysis of local and global modes

The literature indicates that conventional design codes and methods provide guidance for individual member types. D.S.M. is capable of modeling interactions among local, distortional, and global buckling modes; however, interactions involving built-up buckling of built-up members remain unaccounted for. C.S.M., in contrast, primarily targets local or global behavior and does not explicitly consider mode interactions. This limitation is particularly critical for laced or slender built-up members, where coupled instabilities can significantly affect overall strength and stability. While methods such as the O.I.C. have been developed to account for local/global interaction, they have not yet been extended to include built-up buckling. Therefore, there is a research opportunity to explore or develop methods capable of evaluating the compressive strength of built-up members with complex buckling interactions. Such approaches could provide a more comprehensive assessment of member stability and performance and may guide future design and analysis practices.

CHAPTER 4 ARTICLE 1: STABILITY AND DESIGN OF BUILT-UP COLUMNS: EFFECT OF 2ND ORDER SHEAR FORCES

Oudom Chhoeng[a], Morane Chloé Mefande Wack[a], Robert Tremblay[a], Nicolas Boissonnade[b, *]

[a] Polytechnique Montréal, H3T 1J4, Montréal, QC, Canada

[b] Université Laval, G1V 0A6, Québec, QC, Canada

[*] Corresponding author

Email: oudom.chhoeng@polymtl.ca (O. Chhoeng), morane-chloe.mefande-wack@polymtl.ca (M. Wack), robert.tremblay@polymtl.ca (R. Tremblay), nicolas.boissonnade@gci.ulaval.ca (N. Boissonnade).

The paper has been published in the *Journal of Constructional Steel Research on 24 October 2025* (https://doi.org/10.1016/j.jcsr.2025.110052).

Abstract: Current design standards for built-up steel members often overlook buckling effects, particularly when 2nd order shear forces in the lacing are substantial. This oversight can lead to overestimated member capacities and inaccurate force predictions. This study explores various nonlinear finite element (FE) models of laced built-up members fabricated from pairs of hot rolled C shaped sections connected by either double (X) or single (diagonal) flat lacing bars. It further investigates the influence of member properties and lacing configurations on the overall stability of the lacing system, explicitly considering axial forces both in compression and tension acting on the lacing elements. The developed FE models were carefully developed and rigorously validated against existing experimental data. A series of parametric studies was performed, and the numerical results were used to evaluate a newly proposed shear force design formula for laced built-up members with both double and single lacing systems. The assessment demonstrates that the proposed formulas provide more adaptable, accurate, and reliable predictions compared to those specified in Eurocode 3, Australian, and American design standards, and are also simpler than the current design rules.

Keywords: 2nd order**,** Shear force, Lacing members, Built-up sections, Double and single lacing systems.

4.1 Introduction

Built-up members are often used in steel truss bridges. They are typically composed of C-based sections (channels) or angle-based sections (plates connected with angles to form a C-shape), joined by batten plates, lacing bars, or perforated plates (see Figure 4.1). When angles are used, lacing bars may be placed on all four sides, or the angles can be paired with continuous web plates to form two C-sections. This study focuses on laced built-up members consisting of two C-sections interconnected with double (X) or single (diagonal) lacing bars, where main chords are connected to lacing members through rivets or bolts.

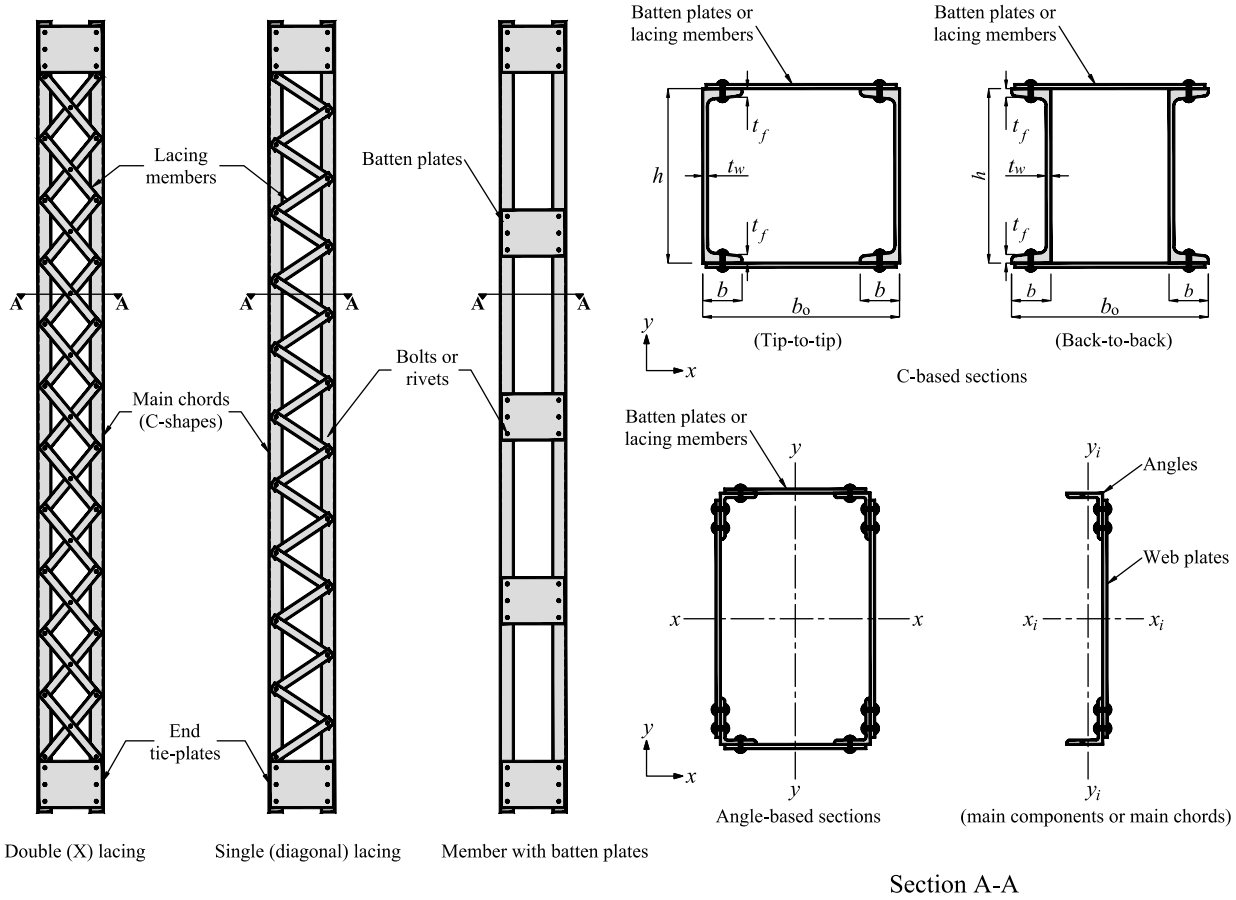

Figure 4.1 Symbols and examples of built-up structural members typically found in steel truss bridges.

For a built-up member subjected to compression, as shown in Figure 4.2a, the lacing system must withstand internal forces before the member reaches failure. When considering initial global imperfections (Figure 4.2b), the lacing system should be designed with reference to the deformed configuration using 2nd order analysis (Figure 4.2c). This ensures that internal forces account for 2nd order effects, distributing moment and shear along the diagonal lacing members, which may be subjected to either tension or compression (Figure 4.2d). Based on current design approaches, the main components of a built-up section should be designed to fail before the transverse members, which primarily serve to unify the main components for increased capacity and to resist shear from bending and external transverse loads [135]–[137].

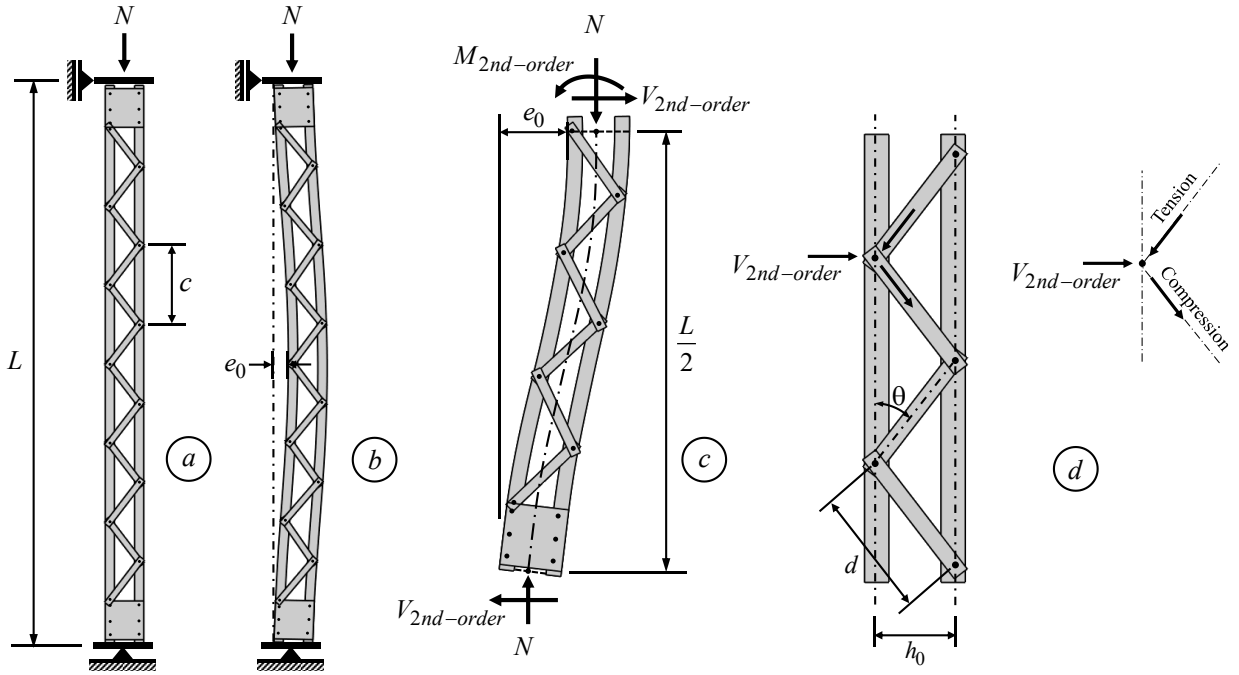

Figure 4.2 Effect of 2nd order actions in laced built-up columns.

Early investigations into the buckling behaviour of built-up columns were prompted by the collapse of the first Quebec Bridge, leading to the Royal Commission's inquiry [6] and subsequent research on shear deformations. Engesser [8] derived approximate formulas for critical buckling loads, later refined by Ziegler [9], Timoshenko [26], and Bleich [11]. Bleich's modified slenderness ratio approach was initially developed for hinged-end conditions and later extended by Aslani and Goel [49] to general boundary conditions. Additional studies by Duan and Chen [138], Sato and Uang [139], Razdolsky [140], and Gjelsvik [141] further examined the stability of built-up members. Despite these efforts, most research primarily focused on the buckling capacity of built-up

members rather than the capacity of their lacing system to withstand the shear force induced by 2nd order effects.

Several studies have examined the buckling capacity of the lacing system of built-up members. Geng-Shu and Shao-Fan [102] proposed an equation to predict shear force in built-up columns under compression loads using the finite integral method. Their studies relied on a perfectly elastic column theory. To account for the effect of initial imperfections, they assumed a sine-shaped deflection curve by adopting the concept of reduced axial rigidity for an imperfect bar and modeled the built-up members with a sandwich cross-section. Another set of analytical equations to calculate the 2nd order bending moment and shear force for laced built-up columns with various end conditions, subjected to both axial and lateral loads, was developed by Gantes and Kalochairetis [142]. Their formulations were based on the theory of imperfect "Timoshenko" members which treat columns as an imperfect solid member. Therefore, the stability of the lacing system was not considered. Besides, many investigators [106], [107], [143], [144] have reported that these factors affect the buckling load of built-up columns and therefore, similarly impact the 2nd order shear force. Recent numerical studies have further explored these effects. Baláž et al. [145], [146] performed 2nd order analyses on laced built-up members under combined axial and bending loads, validating their results against Eurocode 3 recommendations. Dar et al. [143] and El Aghoury et al. [144], [106] examined cold-formed steel built-up columns, finding that lacing member slenderness and the width-to-thickness ratio of the main components significantly impact buckling capacity. Li et al. [108] showed that initial deflections in lacing bars could reduce axial capacity by up to 20%, depending on imperfection modes.

While some studies have addressed the seismic performance of built-up members [147]–[153], research on the influence of the lacing system stability on the shear capacity of built-up members remains limited. Existing approaches primarily rely on the imperfect Timoshenko beam theory [139], [142] to calculate the 2nd order shear force in built-up members. However, this approach entirely neglects the influence of lacing system buckling when determining 2nd order internal forces. Additionally, some current design codes, such as the American and Australian standards, assume 2% of the column's ultimate load as the shear capacity of built-up members. A more detailed discussion of these design rules is provided in Section 4.2.

It is clearly observed that current investigations into the buckling load of the lacing system of laced built-up members, induced by 2nd order shear force, are quite limited. In the current study, numerical investigations are employed to analyze the buckling performance and 2nd order shear forces of hot-rolled laced built-up members composed of two C sections under compression. Advanced numerical models are built, capable of taking into account the effect of combined buckling modes such as overall buckling of the built-up member, global buckling of the chord between connectors, cross-sectional local buckling and global buckling of the lacing member. The study examines how chord arrangement, lacing slenderness, and the with-to-thickness ratio of the cross-section influence the ultimate load and 2nd order shear forces in both double (X) and single (diagonal) lacing systems. Firstly, a review of current design rules, including design methods specified in the American standards, Eurocode 3 and the Australian standards is discussed in Section 4.2. Numerical modeling assumptions, procedures, and validation are detailed in Section 4.3. A series of parametric studies are then conducted to investigate the influence of channel arrangement, lacing arrangement, and slenderness of lacing on the ultimate load and the 2nd order shear force in built-up columns. Then, in Section 4.4, suitable equations are proposed for predicting the 2nd order shear force at the end of built-up members for both double lacing systems and single lacing systems. Finally, performance assessments of the proposed equations are carried out, comparing them to the results of the non-linear finite element (FE) analyses and to the current design methods.

4.2 Determination of shear forces in built-up members according to current design codes

This section provides a detailed examination of how to determine shear forces in built-up members, along with additional construction guidelines for lacing systems as outlined in Eurocode 3 (EC 3) [154], the Australian Standard (AS 4100) [155], and American Standards (AISC and AASHTO) [112], [113]. Table 4.1 summarizes the formulas these standards recommend for predicting the shear force V_u in built-up members. According to EC 3, the shear force should be calculated based on the maximum 2nd order moment occurring at the member's midsection. This moment arises from a specified initial deflection of the entire built-up member. For built-up compression members with hinged supports, the 2nd order moment is calculated considering an initial bow imperfection e_0 and the 1st order bending moment at midsection M^I, where $e_0 = L / 500$. The EC 3 formula

incorporates a sinusoidal mid-span deflection to account for its amplifying effect on the design compression force N. The elastic shear deformation of the lacing system is assumed to be continuous and is derived from the column's shear stiffness S_v, which varies depending on the lacing configuration. Further details on calculating S_v can be found in [154]. Note that the notations used in Table 4.1 follow the conventions of the respective standards. Specifically, N_u denotes the axial resistance of the member, M_u the ultimate moment, N_{cr} the Euler critical load, A the cross-sectional area, f_y the yield stress, and λ_n the non-dimensional slenderness ratio of the built-up member.

In contrast with the EC 3 methodology, the Australian Standards approach the calculation of design shear force in built-up members by relating it to their nominal compressive strength. This strength is derived using a theoretical formulation that introduces a modified slenderness ratio, intended to reflect the influence of shear deformation. As a result, the slenderness value increases when compared to non-built-up members. This method is applicable only when the slenderness of the lacing members remains below 140, with required lacing angles between 50° and 70° for single lacing and 40° and 50° for double lacing configurations.

Meanwhile, the AISC standards adopt a more simplified design approach. They prescribe that built-up members with single or double lacing should resist a minimum shear force equal to 2% of their compressive capacity, provided that the slenderness ratio stays within 140 for single lacing and 200 for double. These requirements apply when the lacing is inclined at no less than 60° for single lacing and 45° for double lacing relative to the member's longitudinal axis. Unlike AISC, the AASHTO guidelines do not define a specific shear force requirement. However, they incorporate an AISC-based restriction that limits the built-up member's overall slenderness to 120 for primary truss elements and 140 for secondary ones. In line with AISC and AS provisions, AASHTO also mandates the use of tie plates at both ends of the lacing system.

Although these standards define geometric constraints for lacing design, their shear force equations are inherently limited, as they depend heavily on the physical proportions of the lacing components. This limitation presents challenges when evaluating older built-up truss members, especially those constructed during the 1950s, that often do not comply with modern slenderness requirements. Moreover, current formulas do not fully capture the impact of shear-related deformations caused by flexural buckling within the lacing members themselves. Thus, refinement of existing design

provisions is warranted. These updates should better incorporate the potential for lacing instability and acknowledge the varying influence of different lacing layouts on 2nd order shear behaviour.

Table 4.1 2nd order shear force design of built-up members in compliance with existing approaches.

Standards	Design shear force
EC 3	$V_u = \frac{\pi M_u}{L}$ Where $M_u = \frac{N \cdot e_0 + M^I}{1 - N / N_{cr} - N / S_v}$
AS 4100	$V_u = \frac{\pi\left(Af_y / N_u - 1\right)N}{\lambda_n} \geq 0.01N$
AISC & AASHTO	$V_u = 0.02N_u$

4.3 Numerical evaluation

4.3.1 Key assumptions of numerical models

Built-up steel members commonly consist of two hot-rolled, widely spaced profiles functioning as the primary load-carrying components (main chords). These chords are positioned either tip-to-tip or back-to-back and are interconnected by flat lacing bars, arranged in either X-shaped (double lacing) or diagonal (single lacing) patterns along their length. Tie plates are provided at both ends to connect the main chords and to stabilize the ends of the lacing system. These types of configurations are typical of truss bridge construction, where connections are often riveted. In this study, three-dimensional FE models were developed using the non-linear analysis software ABAQUS [156]. The models were based on the centerline geometry of the cross-sections. Four-node shell elements (S4R) were used to discretize the main chords, lacing elements, and tie plates. This element type has demonstrated strong performance in prior research involving both mono-symmetric and double-symmetric members [130], [131], [157], [158]. Before finalizing the mesh, a sensitivity analysis was carried out within the framework of Geometrically and Materially Nonlinear Analysis with Imperfections (GMNIA). A mesh size equal to 1/20th of the web depth of the main chord (Figure 4.3) was adopted, as it provided an optimal compromise between solution accuracy and computational cost and was thus selected for all subsequent simulations.

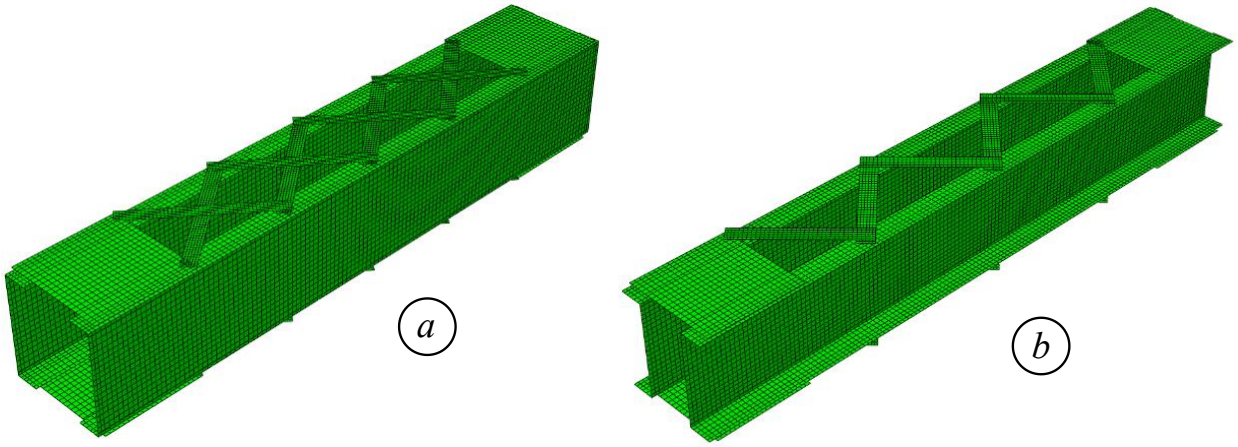

Figure 4.3 Typical numerical modeling – (a) Tip-to-tip section with a double lacing system – (b) Back-to-back section with a single lacing system.

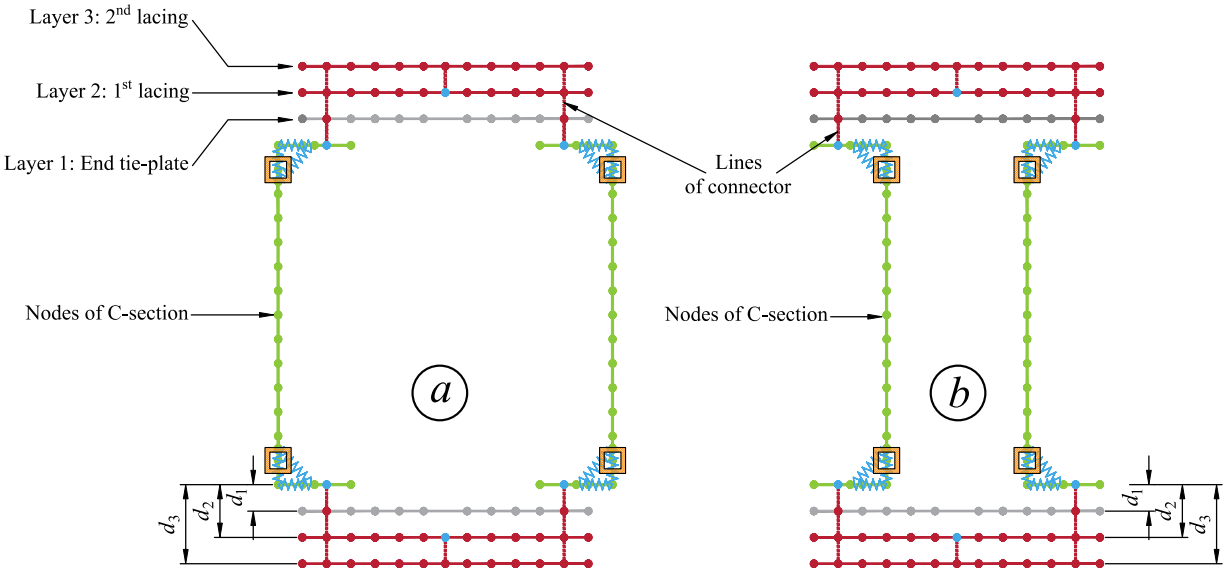

Figure 4.4 FE modeling of cross-sections – (a) Tip-to-tip configuration – (b) Back-to-back configuration.

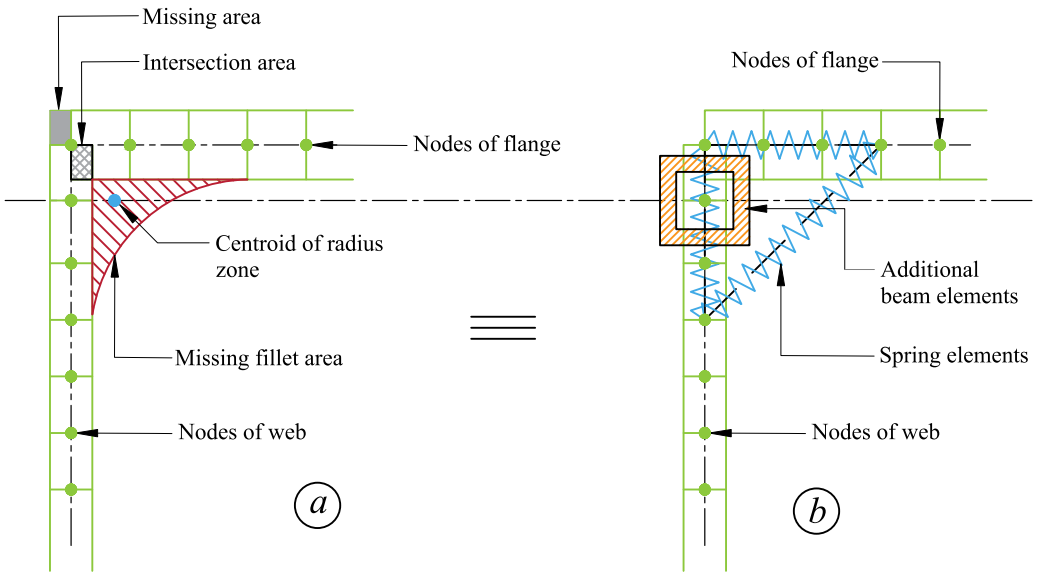

Figure 4.5 Modeling of the web-flange area in a C component – a) Real section – b) FE model.

Figure 4.4 illustrates the numerical model considered for laced built-up members. The FE cross-sectional model comprises two C-sections oriented in either tip-to-tip ([ ]) or back-to-back (] [) configurations. Adjacent to each top and bottom flange of the main components (C-sections) are three additional layers. The first layer, closest to the flanges of the Cs, represents a tie-plate positioned offset from the center flange by a distance d_1, with the offset distance calculated as $\left(t_f + t_p\right)/2$, where t_f is the flange thickness of the main C components and t_p represents the thickness of the tie-plate. The second and third layers correspond to lacing members, strategically placed at distances d_2 and d_3 respectively, from the chord flange. The offset distances for these lacing members are determined to accurately reflect the actual geometry of the member. Specifically, the distance d_2 is equal to $\left(t_f + t_d\right)/2$, where t_d is the thickness of the lacing member, while the distance $d_3 = d_2 + t_d$, ensures precise alignment with the intended structural configuration. The tie-plates and lacing bars are connected to the flanges of the main C-shaped members via continuous rows of connectors. In the FE model, the cross-section of each main chord was represented using three shell components of uniform thickness. However, this simplification omits the curved fillet regions at the web-flange junctions and introduces overlapping at these intersections (see Figure 4.5a). For hot-rolled sections, neglecting the fillet radius can lead to an underestimation of both the cross-sectional moment of inertia and the torsional rigidity, particularly affecting St. Venant torsional stiffness [126]. To better approximate the true geometry, additional

square hollow sections were introduced (see Figure 4.5a), effectively restoring the cross-sectional area typically provided by the fillet zones. This approach was adopted since it allows restoring not only the missing cross-sectional area but also the torsional stiffness contributed by the fillets. Specifically, the two geometric parameters of a hollow square, i.e., width and thickness, can be determined such that both the area and the torsional constant of the original section (including fillet zones) are matched. In this way, the modified model correctly reproduces both the actual cross-sectional area and the torsional stiffness, ensuring a realistic representation of global buckling, including torsional modes, which would otherwise be misrepresented if the fillets were neglected [128], [130], [131], [159]. Additionally, high-stiffness spring elements were inserted at the web-flange junctions to inhibit unrealistic local deformations in those areas, with their stiffness calibrated to be mechanically rigid yet numerically stable, depending on the section size. This approach ensured that any local buckling behaviour would develop outside the fillet zones, reflecting the response of the cross-sectional buckling.

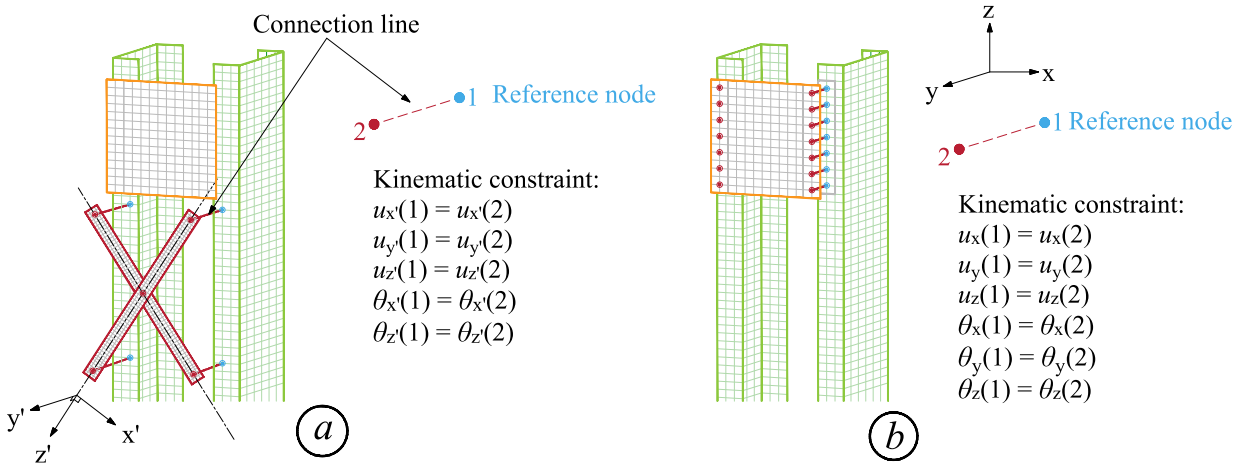

Figure 4.6 Connection modeling details – (a) Lacing-to-chord connection – (b) Tie plate-to-chord connection.

The rivet connectors were idealized to allow free in-plane rotation at the lacing bar ends, thereby replicating realistic articulation within the lacing system. As shown in Figure 4.6a, the rivet connection was simulated by a constraint line linking a pair of nodes – one on the lacing element and the other on the chord member. A multi-point kinematic coupling was defined along this line, constraining both nodes (i.e., the reference node and the associated coupling node) to share identical translational degrees of freedom along the local axes x', y', and z', and rotational degrees of freedom about the x' and z' axes. Notably, rotational freedom about the rivet's longitudinal

axis (y') was intentionally left unrestrained to allow realistic relative rotation between the lacing and the chord. The coupling node's full motion was governed with respect to the reference node located on the chord surface. For the end connections, tie-plates were coupled to the chord components via tie constraints, representing mechanical fasteners such as rivets or bolts [160]. As illustrated in Figure 4.6b, an analogous approach was adopted for batten plate connections, wherein equivalent kinematic constraints were enforced to ensure uniform displacement and rotation across all interacting nodes within the joint region. Similar approach was also adopted in [161].

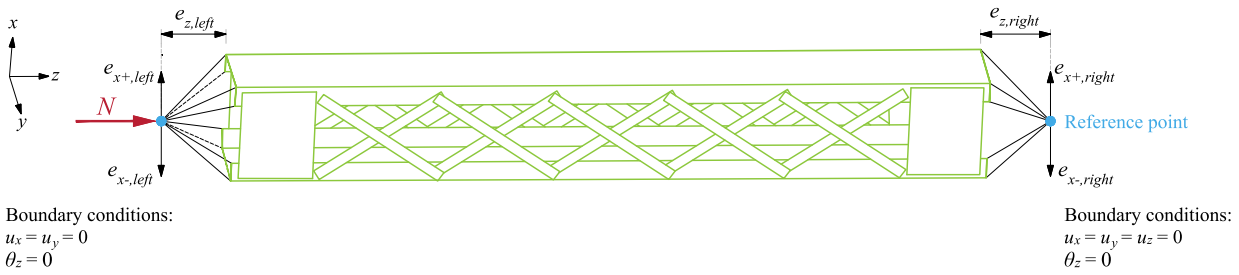

Figure 4.7 FE model boundary conditions settings for built-up members.

The support conditions of laced built-up column were modeled as simply supported at both ends, as illustrated in Figure 4.7. To simulate this, all nodes at each extremity of the member were kinematically coupled to a reference point positioned at the cross-sectional centroid. Rotational restraint about the longitudinal axis (θ_z) and translational restraints in the lateral directions (u_x and u_y) were imposed at both ends, enforcing $u_x = u_y = \theta_z = 0$. Axial loading was introduced at one end of the column by applying a force at the reference point in the longitudinal (z) direction, while the opposite end was constrained against axial displacement ($u_z = 0$). To accurately replicate the physical boundary conditions used in experimental testing (see Section 4.3.2), the location of the reference point could be offset by defined eccentricities in the transverse (e_x) and longitudinal (e_z) directions, thereby allowing refined control over support and loading alignment in the numerical simulations.

The material behaviour was defined using a quad-linear stress-strain model [162]. This constitutive relationship was converted into true stress versus logarithmic plastic strain format to comply with input requirements for implementation in the ABAQUS FE environment. Residual stresses are inherently induced in hot-rolled steel members during fabrication, primarily due to non-uniform cooling rates across the plate elements. Modeling these stresses in C-shaped sections presents a particular challenge, as experimental data specific to hot-rolled channels remains scarce. In light

of this limitation, researchers have commonly relied on adapting residual stress profiles from better-documented shapes, such as hot-rolled I-sections. A notable example is the work by Linder and Glitsch [99], who developed a procedure to derive residual stress distributions from I-sections and modified them to approximate the behaviour in channel sections (see Figure 4.8a). This adapted stress pattern was later utilized by Beyer et al. [100] to propose residual stress distributions within FE models of UPE sections subjected to major-axis bending. A key feature of their approach was the enforcement of self-equilibrium within each constituent plate of the cross-section. Their findings suggested that residual stresses have a limited influence under major-axis bending in GMNIA simulations, as models that exclude these effects still produce conservative and reasonably accurate results when compared with experimental data. In the present study, however, residual stresses were incorporated into the FE models, using the distribution proposed by Beyer et al. [100], as the C-shaped sections forming the built-up members are also subjected to weak-axis bending, where their influence can be more significant.

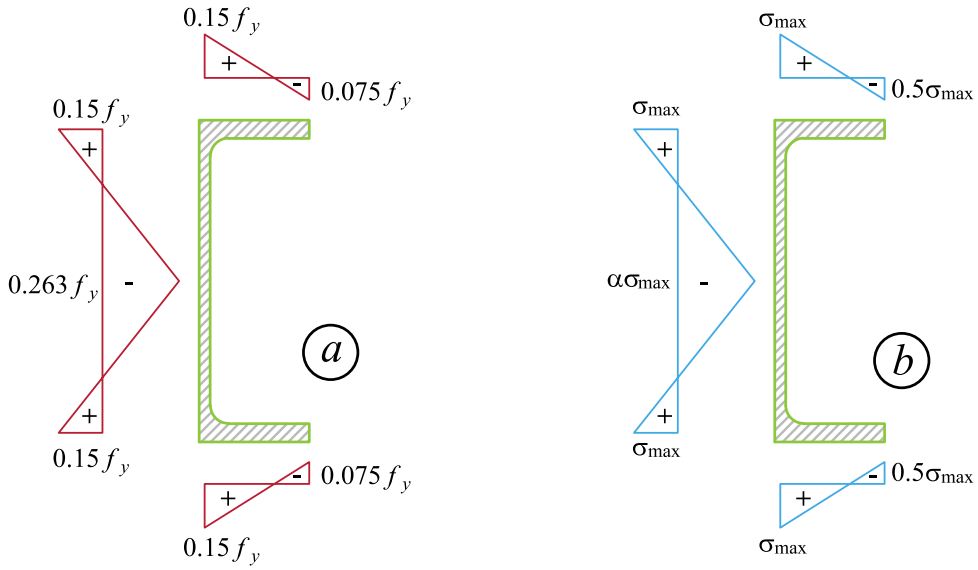

Figure 4.8 Residual stresses patterns for C-sections – (a) Residual stresses from [99] – (b) Residual stress distribution proposed in [100].

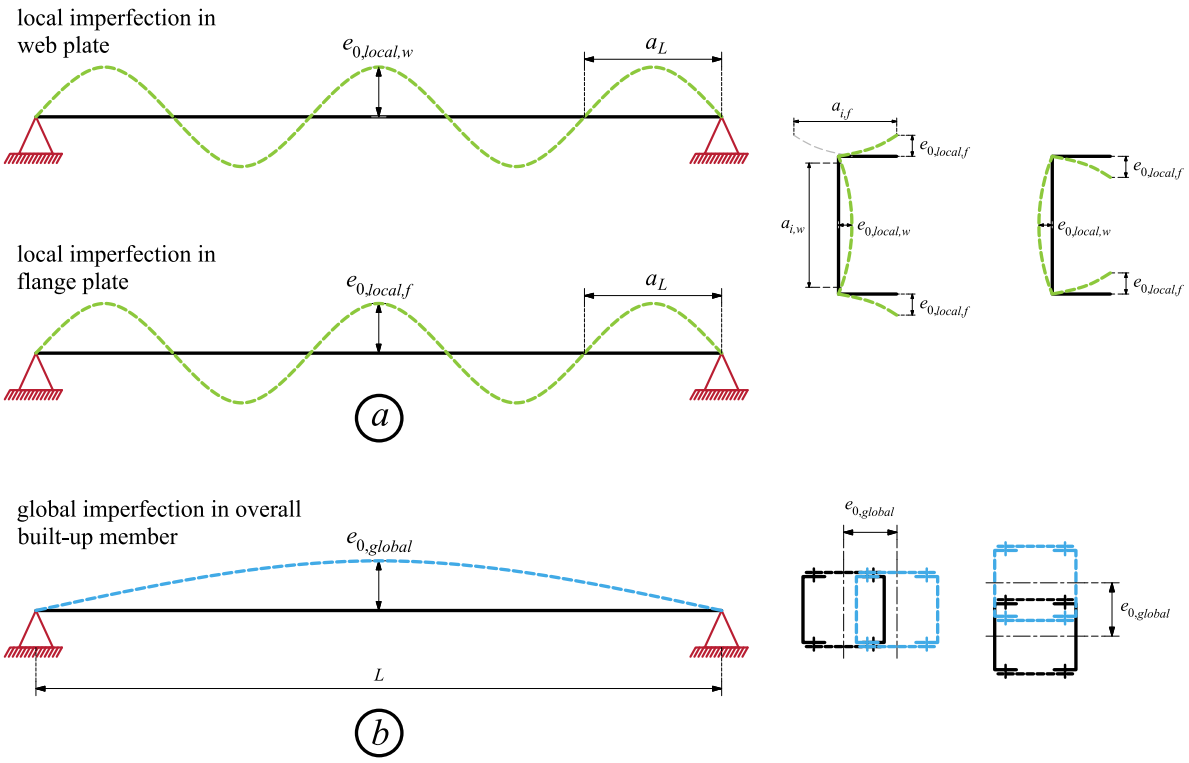

Figure 4.9 Description of geometric imperfections – (a) Local – (b) Global.

Both global and local imperfections were simulated by perturbing nodal coordinates using predefined sinusoidal waveforms, as shown in Figure 4.9. Local imperfections were imposed individually on the web and flange plates, based on their respective buckling length – denoted as $a_{i,w}$ for the web and $a_{i,f}$ for the flange. These lengths were calculated as $a_{i,w} = h - 2\left(t_f + r\right)$ and $a_{i,f} = 2\left(b - t_w - r\right)$, where h, b, t_f, t_w, and r represent the section geometry parameters. The amplitude of local imperfections, $e_{0,local,i}$, was set equal to a_i / 400 and a_i / 200, in accordance with the recommendations provided in Eurocode 3 Part 1.5 and the work of Gérard [128] on I-shaped sections. These imperfection amplitudes were independently assigned to each plate, ensuring localized buckling effects were appropriately captured for each element. To introduce a representative characteristic length, the average of the web and flange buckling lengths was defined as $a_L = \left(a_{i,w} + a_{i,f}\right)/2$. It should be noted that the imperfection shape was generated by repeating the local buckling mode based on a_L. For a given member length L, a_L was slightly adjusted so that L was fully covered by an integer number of half-waves. Previous studies [126], [131], [159] have demonstrated that using this average length provide reasonable and appropriate resistance

predictions. As illustrated in Figure 4.9a, an odd number of half sine waves was selected along the member's length, ensuring that the location of maximum imperfection – and thus the weakest cross-section – was situated at mid-span. For global imperfection, $e_{0,global}$ was introduced along the minor axis, aligned with the plane of the lacing system. This alignment was particularly important for accurately capturing 2nd order shear effects within the bracing layout.

4.3.2 Numerical model validation

Table 4.3 includes three tests from [148], [149] using specimens that simulate the back-to-back laced members from the San Francisco-Oakland Bay Bridge (SFOBB), with riveted lacing systems. These specimens were axially loaded with pinned-pinned supports and varying eccentricities, e_x, (381 *mm*, 127 *mm*, and 0 *mm*). The study reported in [150] involved 12 diagonal bracing members, but only 7 were considered valid for FE model validation due to section and setup considerations. These included By8-60, By8-120, By16-60, By16-120, Bx8-120, Bx816-60, and Bx16-120, which represent widely spaced, C-shaped built-up sections based on actual bridge designs. The lacing bars in these specimens were bolted to the main chords. All specimens were mounted in rigid frames and subjected to lateral shear forces and loaded under displacement-controlled loading, following the ATC-24 cyclic protocol [163] (Case 1). However, to align with the objective of evaluating static behaviour in compressive members, static loading conditions (Case 2) were also examined.

Table 4.2 Sections, cross-section dimensions, profiles, and material properties of each component of laced built-up members.

Specimens	Sections and geometric dimensions		Main chords			Lacing system and end tile-plates	
	Section	Cross-section dimensions	Profile / F_y / F_u [MPa]				
		b_o x h x L x c x e [mm]	Channel	Angle	Web plate [PL b_p x t_p]	Lacing [PL b x t_p]	End tile-plate [PL b_p x h_p x t_p]
Specimen 1 [148], [149]	4L+2P	437 x 337 x 7146 x 365 x 530	-	L76x76x8 / 338 / 489	PL 330x8 / 324 / 478	PL 38x8 / 327 / 484	PL 441x553x7 / 327 / 484
Specimen 2 [148], [149]							
Specimen 3 [148], [149]							
By8-60 [150]	4L+2P	121 x 121 x 2445 x 108 x 0	-	L25x25x3.2 / 361 / 475	PL 121x3.3 / 323 / 384	PL 19x3.2 / 323 / 384	PL 121x495x9.5 / 253 / 349
By8-120 [150]		121 x 121 x 5035 x 108 x 0		L25x25x3.2 / 361 / 475	PL 121x3.3 / 323 / 384	PL 19x3.2 / 323 / 384	PL 121x495x9.5 / 253 / 349
By16-60 [150]		133 x 133 x 1838 x 95 x 0		L51x51x3.2 / 352 / 470	PL 133x3.3 / 323 / 384	PL 24x3.2 / 323 / 384	PL 133x560x9.5 / 253 / 349
By16-120 [150]		133 x 133 x 3835 x 95 x 0		L51x51x3.2 / 352 / 470	PL 133x3.3 / 323 / 384	PL 24x3.2 / 323 / 384	PL 133x560x9.5 / 253 / 349
Bx8-120 [150]		114 x 76 x 3683 x 102 x 0		L25x25x3.2 / 361 / 475	PL 76x3.3 / 323 / 384	PL 19x3.2 / 323 / 384	PL 114x394x9.5 / 253 / 349
Bx16-60 [150]		165 x 105 x 2432 x 133 x 0		L51x51x3.2 / 352 / 470	PL 105x3.3 / 323 / 384	PL 24x3.2 / 323 / 384	PL 165x527x9.5 / 253 / 349
Bx16-120 [150]		165 x 105 x 5055 x 133 x 0		L51x51x3.2 / 352 / 470	PL 105x3.3 / 323 / 384	PL 24x3.2 / 323 / 384	PL 165x527x9.5 / 253 / 349
L140B8(R1) [164]	2C	80 x 60 x 1400 x 56 x 0	UNP60 / 278 / 405	-	-	PL 10x3 / 278 / 405	PL 200x80x10 / 278 / 405
L140B8(R2) [164]		80 x 60 x 1400 x 56 x 0					
L140B8(R3) [164]		80 x 60 x 1400 x 56 x 0					
L140B10(R1) [164]		100 x 60 x 1400 x 56 x 0					
L170B7(R1) [164]		70 x 60 x 1700 x 56 x 0					
L170B7(R2) [164]		70 x 60 x 1700 x 56 x 0					
L170B7(R3) [164]		70 x 60 x 1700 x 56 x 0					
L170B8(R2) [164]		80 x 60 x 1700 x 56 x 0					
L170B8(R3) [164]		80 x 60 x 1700 x 56 x 0					
Group 1 [165]	2C	218 x 60 x 2020 x 400 x 0	UNP60 / 338 / 435	-	-	L25x25x3	-
Group 2 [165]		218 x 60 x 2020 x 200 x 0	UNP60 / 338 / 435				
Group 4 [165]		218 x 60 x 2020 x 400 x 0	UNP60 / 335 / 435				
Group 5 [165]		218 x 60 x 2020 x 400 x 0	UNP60 / 302 / 435				

Note: b_o = total width of cross section, h = total height of cross section, L = total length of member, c = distance between connector of lacing measured in the axial direction of built-up member, e = end distance from end of built-up member to edge of end tie-plate measured in axial direction of built-up member, b_p = width of plate, h_p = length of plate, t_p = thickness of plate.

Table 4.3 Comparison of ultimate loads from FE analysis and experimental tests for specimens subjected to cyclic loading.

Reference	Specimens	Section / Lacing	Test loadings	Loading positions				Ultimate loads and ratios		
				$e_{x,left}$ [mm]	$e_{z,left}$ [mm]	$e_{x,right}$ [mm]	$e_{z,right}$ [mm]	$N_{u,test}$ [kN]	Case 1: static loading $N_{u,FE} / N_{u,test}$ [-]	Case 2: cyclic loading $N_{u,FE} / N_{u,test}$ [-]
Kleiser and Uang [148], [149]	Specimen 1	Back-to-back / Double	Cyclic ($N + M_y$)	381	400	0	400	928.79	1.017	0.960
	Specimen 2		Cyclic ($N + M_y$)	127	400	0	400	1633.83	1.012	1.012
	Specimen 3		Cyclic (N)	0	400	0	400	2885.12	0.990	0.954
Lee and Bruneau [150]	By8-120	Back-to-back / Single	Cyclic (V)	0	0	0	0	295.81	0.952	0.952
	By16-60		Cyclic (V)	0	0	0	0	521.64	0.912	0.911
	By16-120		Cyclic (V)	0	0	0	0	447.00	0.981	0.977
	Bx8-60		Cyclic (V)	0	0	0	0	267.16	1.041	1.047
	Bx8-120		Cyclic (V)	0	0	0	0	213.51	1.113	1.110
	Bx16-60		Cyclic (V)	0	0	0	0	506.87	1.090	1.094
	Bx16-120		Cyclic (V)	0	0	0	0	409.50	1.024	1.024
								Mean	1.013	1.004
								C.o.V.	5.9 %	6.5 %
								Min.	0.912	0.911
								Max.	1.113	1.110

Table 4.4 Comparison of ultimate loads from FE analysis and experimental results for specimens under static loading.

Reference	Specimens	Section / Lacing	Test loadings	Loading positions				Ultimate loads and ratios (Case 2)		
				$e_{x,left}$ [mm]	$e_{z,left}$ [mm]	$e_{x,right}$ [mm]	$e_{z,right}$ [mm]	$N_{u,test}$ [kN]	$N_{u,FE}$ [kN]	$N_{u,FE}$ / $N_{u,test}$ [-]
Bonab et al. [164]	L140B8(R1)	Back-to-back / Single	Static (N)	0	140	0	140	204.76	199.62	0.97
	L140B8(R2)		Static (N)	0	140	0	140	183.86	185.91	1.01
	L140B8(R3)		Static (N)	0	140	0	140	159.09	160.88	1.01
	L140B10(R1)		Static (N)	0	95	0	95	289.05	253.81	0.88
	L170B7(R1)		Static (N)	0	95	0	95	151.95	136.04	0.90
	L170B7(R2)		Static (N)	0	95	0	95	135.19	138.34	0.88
	L170B7(R3)		Static (N)	0	95	0	95	124.32	113.17	0.91
	L170B8(R2)		Static (N)	0	95	0	95	162.40	153.10	0.94
	L170B8(R3)		Static (N)	0	95	0	95	146.29	141.82	0.97
Kalochairetis et al. [165]	Group 1	Tip-to-tip / Double	Static ($N + M_y$)	100	162.5	100	162.5	200.00	211.12	1.06
	Group 2		Static ($N + M_y$)	100	162.5	100	162.5	206.00	215.29	1.05
	Group 4		Static ($N + M_y$)	100	162.5	-80	162.5	230.00	246.73	1.07
	Group 5		Static ($N + M_y$)	50	162.5	50	162.5	247.00	250.24	1.01
									Mean	0.985
									C.o.V.	6.3 %
									Min.	0.880
									Max.	1.070

Table 4.4 includes specimens originally tested under static conditions. The test series reported from [164] included 9 back-to-back members with single lacing systems while the tests conducted in [165], also cited in [160], consisted of five groups of double-laced members. Since Group 3 used I-sections instead of C-sections, only Groups 1, 2, 4, and 5 – each made with tip-to-tip C-sections – were used for model validation. All specimens in Table 4.4 had their main components welded to the lacing members. For these welded connections, an extra rotational boundary condition, $\theta_{y'}(1) = \theta_{y'}(2)$, was applied, as shown in Figure 4.6a. The specimens were tested under simply supported conditions, with the distance from the support to the member end defined as e_z, and subjected to axial compression (N). The specimens from [165] also experienced combined loading (axial and bending), denoted as $N + M_y$. Additionally, all specimens in Table 4.4 were laterally restrained at mid-height to prevent out-of-plane movement ($u_x = 0$).

Due to incomplete data on initial geometrical imperfections and the absence of residual stress measurements across all tests, a sensitivity analysis was carried out to determine suitable magnitudes for local and global imperfections for use in subsequent parametric studies. This was based on the residual stresses distribution of C-sections shown in Figure 4.8b, where $\sigma_{\max} = 0.15 f_y$ and $\alpha = 1 + bt_f / \left(ht_w\right)$, as proposed by Beyer et al. [100]. Although direct measurements of residual stresses are scarce in the literature, the distribution considered in this study follows the proposal in [100], providing a reasonable representation. Any deviations from the true residual stresses are expected to have a negligible impact on the results. Figure 4.10 presents a comparison of FE results with experimental data for various assumed imperfection amplitudes. Results from Bonab et al. [164] were omitted from this comparison since their specimens developed imperfections due to repeated loading, and these were quantified using a modified Southwell plot [166]. Geometric imperfections were introduced into the model as described in the previous section, i.e., through modified node coordinates. Three key parameters were varied: half-wavelengths of local imperfection a_L, amplitudes of local imperfections $e_{0,local}$ and amplitudes of global imperfection $e_{0,global}$. To simplify the analysis, only one amplitude for local imperfections $a_L = (a_{i,w} + a_{i,f}) / 2$, was considered. Consequently, eight sets of imperfections were generated, including (i) two amplitudes of local imperfections (a_i / 400 and a_i / 200), and (ii) four amplitudes of global imperfections (L / 500, L / 1000, L / 1500, and L / 3000).

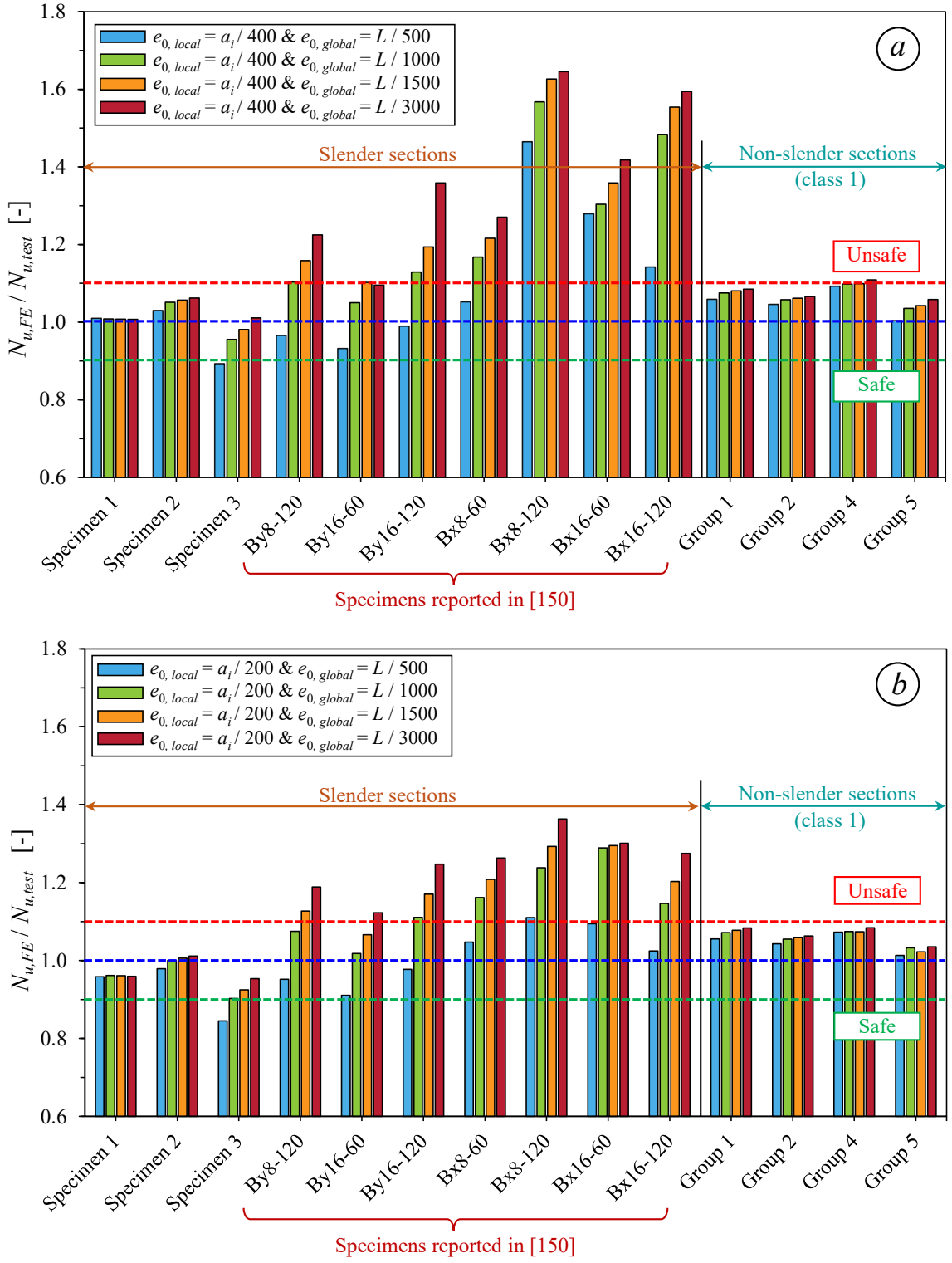

Figure 4.10 Comparison of test and FE results with various amplitudes of local and global imperfections – (a) $e_{0,local} = a_i / 400$ – (b) $e_{0,local} = a_i / 200$.

Figure 4.10 reports the ratios of numerical-to-experimental capacities $N_{u,FE}$ / $N_{u,test}$ on the vertical axis for each specimen (horizontal axis). As expected, the figure reveals distinct patterns: lower amplitudes of global imperfections generally lead to higher capacity for all specimens. This effect is notably significant for members subjected to pure compression (Specimen 3 and all specimens reported in [150]), but less so for members subjected to combined loading ($N + M_y$). By adopting local imperfection amplitudes of a_i / 400 with global imperfection amplitudes of L / 500, 11 out of 14 specimens fall within an acceptable zone, defined as a ratio between 0.9 and 1.1, with 3 specimens achieving nearly perfect agreement (close to 100%) between FE and test results. The results show, however, significant improvements when relying on a local imperfection of a_i / 200. Improved results are therefore identified based on both a mean ratio closer to unity and a reduced Coefficient of Variation (C.o.V.). Specifically, the mean ratio of $N_{u,FE}$ / $N_{u,test}$ decreases from 1.07 (a_i / 400) to 1.01 (a_i / 200). The corresponding C.o.V. reduces from 13.8% to 7.3%, indicating closer agreement with experiments. This increase in prediction performance is more pronounced for sections with slender elements, particularly for members with small to medium slenderness ratios (λ_B ranges from 0.2 to 1.5). The effect of local imperfections becomes less influential for specimens with non-slender elements, i.e., members with class 1 sections (Group 1, Group 2, Group 4, and Group 5). Therefore, adopting a combined amplitude of $e_{0,local,i} = a_i$ / 200 with $e_{0,global} = L$ / 500 results in good agreement across all cases. Note that this imperfection set only underestimated the capacity of Specimen 3 since the specimens reported were fabricated under an allowable out-of-straightness of L / 1500, whereas the actual imperfections in the specimens were about L / 3000 at the middle length, as specified by the authors in [148] and [149]. Consequently, amplitude combinations of $e_{0,local,i} = a_i$ / 200 for local imperfections with $e_{0,global} = L$ / 500 for built-up members have been adopted in the following. These imperfections were also used for specimens without imperfection measurements. Since the effect of local imperfections for the specimens reported in [164] is minimal due to the compactness of the cross-section, Figure 4.11 shows load-displacement curves illustrating only the influence of varying global imperfection amplitudes for specimen L170B7(R2). The figure proves that the local imperfection amplitude of a_i / 200, applied plate-per-plate with a global imperfection of the built-up member of L / 500 leads to a reasonable strength prediction with a difference lower than 3%.

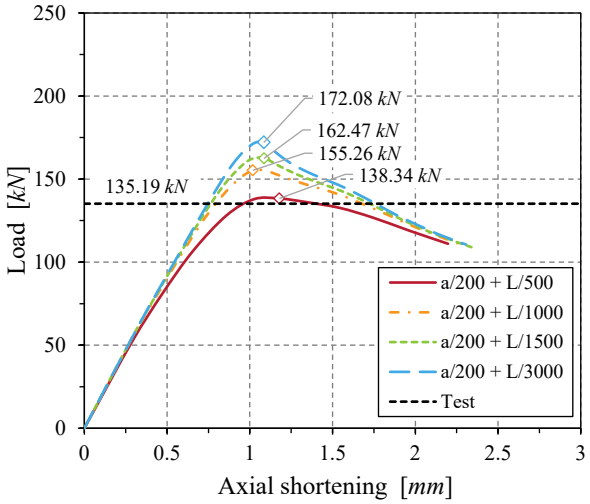

Figure 4.11 Influence of local and global imperfection on ultimate resistance of specimen L170B7(R2) reported in [164].

As presented in Table 4.3, FE models subjected to cyclic loads show excellent agreement with experimental results, with an average $N_{u,FE}$ / $N_{u,test}$ ratio of 1.013 and a C.o.V. of 5.9% for cyclic loading (Case 1). For static loading conditions (Case 2), the results also show improvement, with an average $N_{u,FE}$ / $N_{u,test}$ ratio of approximately 1.0, with a C.o.V. of 6.5%. Figure 4.12 shows that the hysteresis of Specimen 3 and Specimen By16-120 obtained from the FE model superimposed with the hysteresis of test results.

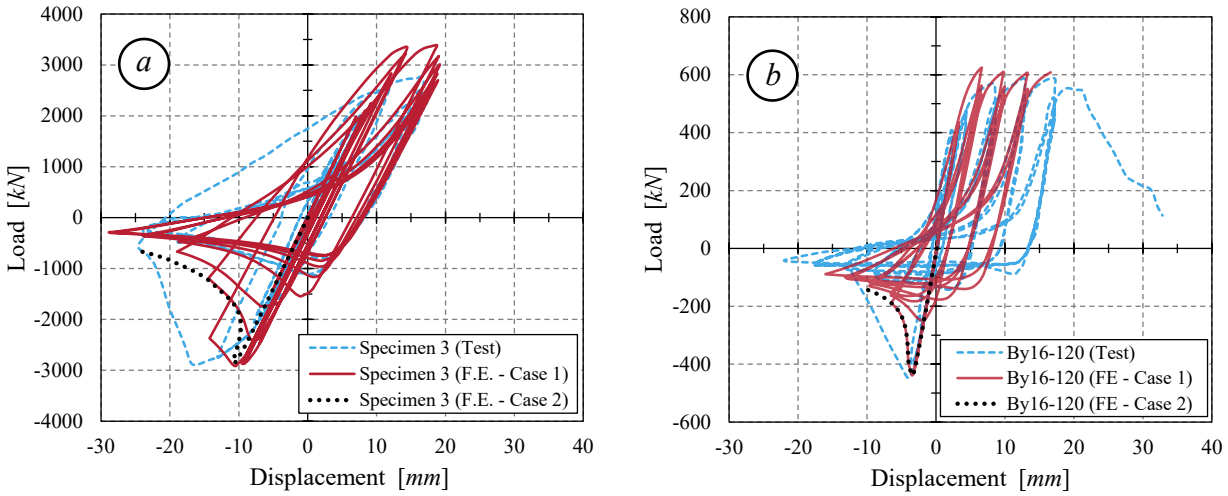

Figure 4.12 Comparison between test and FE – (a) Hysteretic curve for specimen 3 reported [148] and [149] – (b) Hysteretic curve for specimen By16-120 reported in [150].

As shown in Table 4.3, the FE models subjected to cyclic loading exhibit strong correlation with the experimental outcomes, achieving an average load ratio $N_{u,FE}$ / $N_{u,test}$ of 1.013 and a coefficient

of variation (C.o.V.) of 5.9% under Case 1 loading. Under static loading conditions (Case 2), the agreement remains consistent, with an average load ratio close to 1.0 and a C.o.V. of 6.5%. Figure 4.12 illustrates the hysteresis loops for Specimen 3 and By16-120 from the FE analysis overlaid with the corresponding experimental hysteresis curves. As expected, the hysteresis of both specimens is two-sided, as it displays loops on both the positive side (tension) and negative side (compression). A sharp decline in compressive strength occurred immediately after the initial yielding, coinciding with the ultimate load. Differences in stiffness and strain hardening during the post-yield phase were noticeable, reflecting the material model's different behaviour under cyclic compared to static loading. Similar behaviour was also reported in [161] for Specimen 3. The ultimate compressive capacity is reached at the point of initial yielding. Yet, the initial stiffness and ultimate compressive resistance from the FE modeling closely match the experimental results, indicating that the effect of discontinuous yielding is minimal when using quad-linear stress–strain models during the early yielding phase. Furthermore, Figure 4.13 shows that the failure mode of Specimen 3 obtained from FE closely corresponds to the test result.

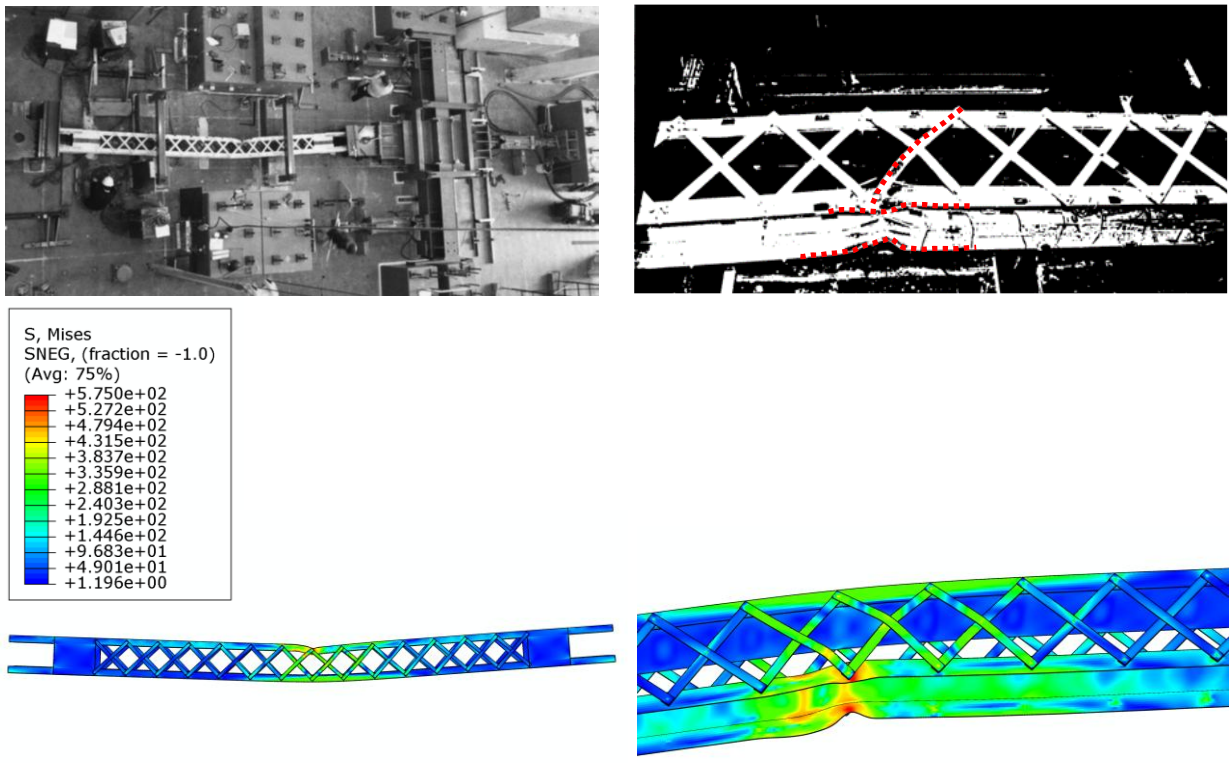

Figure 4.13 Comparison of failure modes from tests and FE analysis for Specimen 3, as reported in [148] and [149] (von Mises stress shown in *ksi*).

As reported in Table 4.4, a strong agreement between FE predictions and experimental results is also obtained for all specimens tested by Bonab et al. [164] and Kalochairetis et al. [165]. The average value of the $N_{u,FE}$ / $N_{u,test}$ ratio is 0.985, with a coefficient of variation of 6.3 %. This ratio ranges from 0.88 to 1.07, indicating that the FE model provides predictions within a reasonable range, neither too conservative nor overly optimistic, which confirms the reliability of the model. The FE simulations accurately reproduce the initial stiffness, ultimate strength, and post-peak behaviour of the tested specimens, as demonstrated by the load and displacement curves for specimens in Group 2 and Group 5 in Figure 4.14. Taken together, these results confirm that the developed numerical models are capable of reliably predicting ultimate resistance and effectively capturing the buckling behaviour of laced built-up members. This supports their suitability for additional parametric studies and further numerical parametric studies.

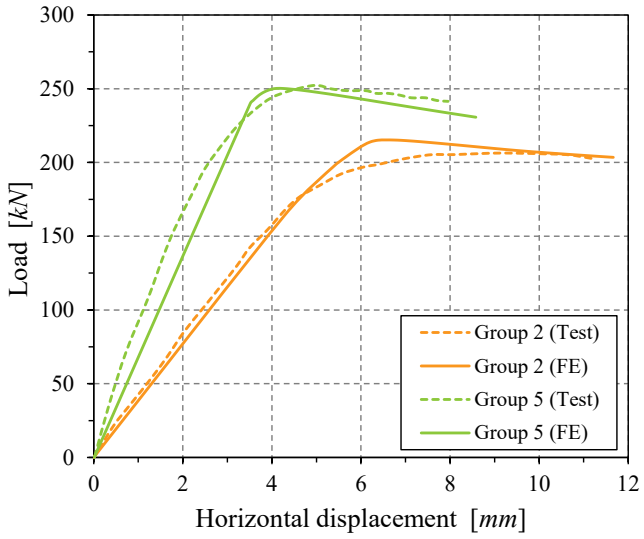

Figure 4.14 Comparison of load–displacement curves from FE analysis and experimental tests for specimen Groups 2 and 5, based on [165].

4.3.3 Influence of chord and lacing arrangement

After validation of the numerical models, FE parametric studies are conducted in this section to assess the impact of chord and lacing arrangements on the ultimate resistance and the acting shear force in lacing systems is examined. The objective is to identify the critical parameters for further numerical parametric studies. The studies examine members of varying lengths, so nondimensional parameters are introduced to represent relative slenderness. The relative slenderness of the lacing

members is expressed as λ_{lacing}, while that of the built-up members is denoted as λ_B, and can be determined as:

$$\lambda_{lacing} = \sqrt{\frac{A_d f_y}{\pi^2 EI_d / d^2}} \tag{4.1}$$

$$\lambda_B = \sqrt{\frac{A_g f_y}{\pi^2 EI_g / L^2}} \tag{4.2}$$

where A_d and A_g represent the total cross-sectional areas of the lacing bar and the built-up member, respectively; I_d is the minimum second moment of inertia of the lacing bar, and I_g is the overall second moment of inertia of the built-up member; while d and L represent the lengths of the lacing bar and built-up member, respectively.

This study analyzes 53 numerical models of laced built-up steel columns made from CSA G40.4 steel ($F_y = 230\ MPa$). Each column consists of two C380x50.4 channel sections configured either tip-to-tip or back-to-back. The chords are braced with single or double (X) flat lacing bars, each having a slenderness ratio of $\lambda_{lacing} = 1.45$ and inclined at 48 degrees to the column axis. The spacing of the chords was such that $h / b_o > 1$ and $I_y < I_x$, where h and b_o are the total height and total width of the built-up section, respectively (Figure 4.1). This ensured that the member is always buckled around the axis perpendicular to the plane of the lacing. Results are presented in Figure 4.15a, showing the influence of lacing arrangement on ultimate capacity, and in Figure 4.15b, illustrating the influence on shear force in the lacing systems, with the shear force recorded at the end of the built-up member. The results clearly indicate that:

- For built-up members with identical lacing systems, back-to-back sections exhibit lower ultimate resistance compared to tip-to-tip sections. This difference is notable, particularly for intermediate length ($\lambda_B \approx 0.75$) to long members ($\lambda_B > 1.5$), where the resistance can be up to 18% and 25% lower, respectively. The lower ultimate resistance of back-to-back sections is attributed to their reduced moment of inertia, resulting in a higher slenderness value compared to tip-to-tip sections;
- When comparing different lacing systems, no significant differences in ultimate resistances are observed for tip-to-tip built-up sections, with variations lower than 5%. However, the

effect of lacing arrangement is more pronounced for back-to-back built-up sections, where differences can reach approximately 10% for low-length members ($\lambda_B \approx 0.75$);

- Single lacing systems consistently show lower resistances, especially for back-to-back built-up sections. This can be attributed to (i) the lower performance of individual chords between connectors in a single lacing system, which reduces shear stiffness, and to (ii) lower torsional rigidities in open built-up sections (back-to-back) compared to closed built-up sections (tip-to-tip);
- As expected, long members with higher λ_B values exhibit increased shear forces ($V_{u,2nd}$) due to more important 2nd order bending moments resulting from initial deflection of the members. As illustrated in Figure 4.15b, shear force-to-ultimate member capacity ratio increases slightly for short members ($\lambda_B < 0.5$) yet more significantly for members with $\lambda_B > 0.75$;
- Shear force-to-ultimate capacity can significantly exceeds 2% for members with $\lambda_B > 1$ or $(L / r) > 95$. This indicates that the minimum required shear force for designing lacing systems – as suggested by the AISC approach – may be insufficient for members with a slenderness ratio $L / r > 95$ and too conservative for those with $L / r < 50$;
- As expected, built-up members with a single lacing system generally exhibit lower shear forces compared to those with a double lacing system, especially for tip-to-tip configurations. The difference in shear force increases from short to long members, reaching up to an average of 40% for tip-to-tip sections composed of C380x50.4. For back-to-back sections, however, the difference in the shear-to-ultimate capacity ratio between single and double lacing systems is smaller, averaging around 7% for members with $\lambda_B < 1.5$. This reduced impact is due to the influence of lacing arrangements on the ultimate load value of back-to-back built-up sections, as shown in Figure 4.15a. It should be noted that the results plotted in Figure 4.15 may vary if these parameters change, as they represent built-up members composed of C380x50.4 chord sections. A more detailed discussion on the influence of various section dimensions is provided in Section 4.4.

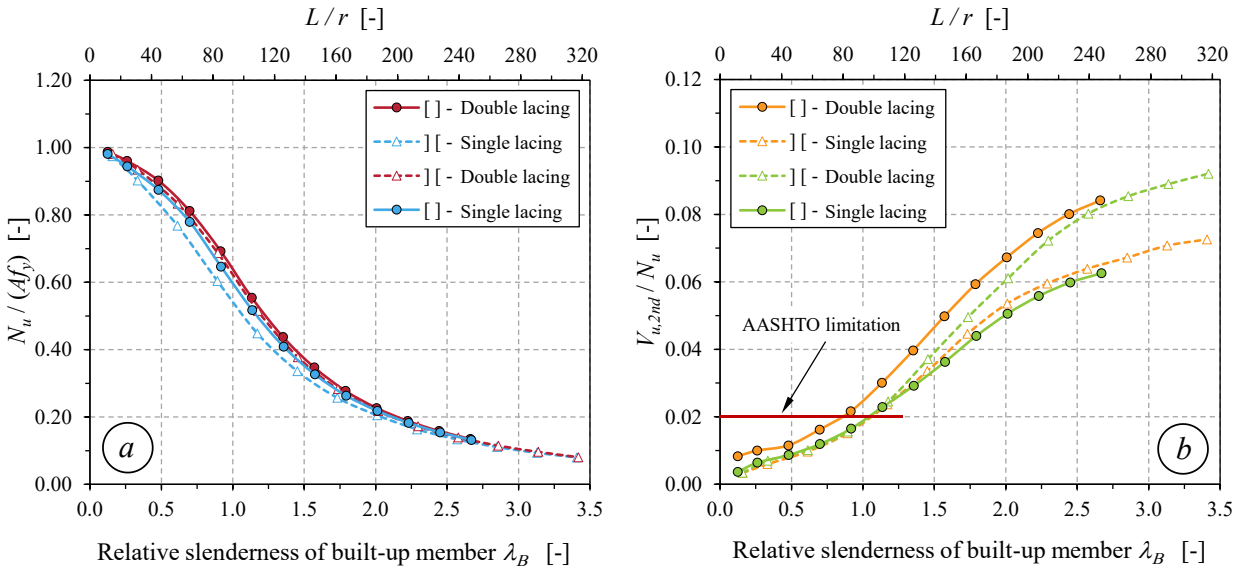

Figure 4.15 Influence of chord and lacing arrangement on – (a) ultimate load – (b) shear force in lacing systems.

4.3.4 Influence of lacing member slenderness

Using the same built-up configuration and material properties described earlier, this section examines how the slenderness of the lacing members affects both the ultimate load capacity and the ratio of shear force to ultimate load in built-up members. As clearly shown in the previous analysis, accurate determination of shear force is more critical for tip-to-tip built-up members compared to back-to-back sections; therefore, tip-to-tip configurations are the focus of this study. A total of 168 numerical simulations were carried out on laced built-up columns with both single and double lacing configurations, where λ_{lacing} ranged from 0.5 to 2.5. Figure 4.16 presents the relationship between the overall slenderness of the built-up members (λ_B) and their normalized ultimate strength (N_u / Af_y). Figure 4.17 further illustrates how λ_B influences the ratio of 2nd order shear force to ultimate load ($V_{u,2nd}$ / N_u), depending on the slenderness of the lacing members. A detailed analysis of these results is provided in the following discussion:

- The slenderness of lacing members significantly affects the compressive strength of built-up columns with single lacing systems. For columns with λ_B values between 0.6 and 1.5, increasing the lacing slenderness leads to noticeable reductions in load-carrying capacity. As shown in Figure 4.16a, a 10% drop in strength occurs between λ_{lacing} values of 0.54 and 1.08, and up to a 20% drop is observed when comparing λ_{lacing} values of 0.54 and 2.51. In

contrast, built-up columns with double lacing systems are less affected by lacing instability. This difference arises because shear forces are transmitted along the axial direction of the lacing bars, and in single lacing configurations, those members primarily resist compressive forces, making their slenderness more critical to global stability;

- As expected, double lacing systems offer improved stability by allowing one lacing member to resist compression while the other carries tension. This interaction enhances the support of the compressed member and introduces greater redundancy. In contrast, single lacing systems rely on a single diagonal to resist both tension and compression, making them more sensitive to flexural buckling due to the lack of load-sharing between lacing elements;
- For both single and double lacing systems, the slenderness of the lacing members has a minimal effect on shear force in built-up members when $\lambda_B < 0.75$. However, this effect becomes increasingly significant as $\lambda_B > 1$, particularly when the lacing members have higher slenderness values;
- Before reaching maximum load-carrying capacity, built-up members with single lacing systems often experience early buckling in the lacing members, particularly when λ_{lacing} exceeds 1.5 or when $(L / r)_{lacing} > 140$. As shown in Figure 4.17a, for $\lambda_B \approx 1.25$, the ratio $V_{u,2nd} / N_u$ increases with λ_{lacing} but then drops sharply beyond this threshold. This behaviour, highlighted by the red ellipse, indicates that early buckling in the braces begins to affect the shear capacity of the built-up member;
- For double lacing systems, no buckling of the lacing members is observed when the built-up member has a slenderness λ_B less than 1.5, confirming the stabilizing effect of having two lacing bars. This is clearly demonstrated at λ_B around 1.25 (see green ellipse in Figure 4.17b), where the ratio of $V_{u,2nd} / N_u$ consistently increases. However, similar to single lacing systems, buckling in the lacing members is first observed at $\lambda_B = 1.75$ when λ_{lacing} reaches 1.88 (see red ellipse in Figure 4.17b). This behaviour is attributed to a loss of redundancy in the double lacing system, particularly when the diagonal under tension fails, causing the remaining compressed diagonal to buckle.

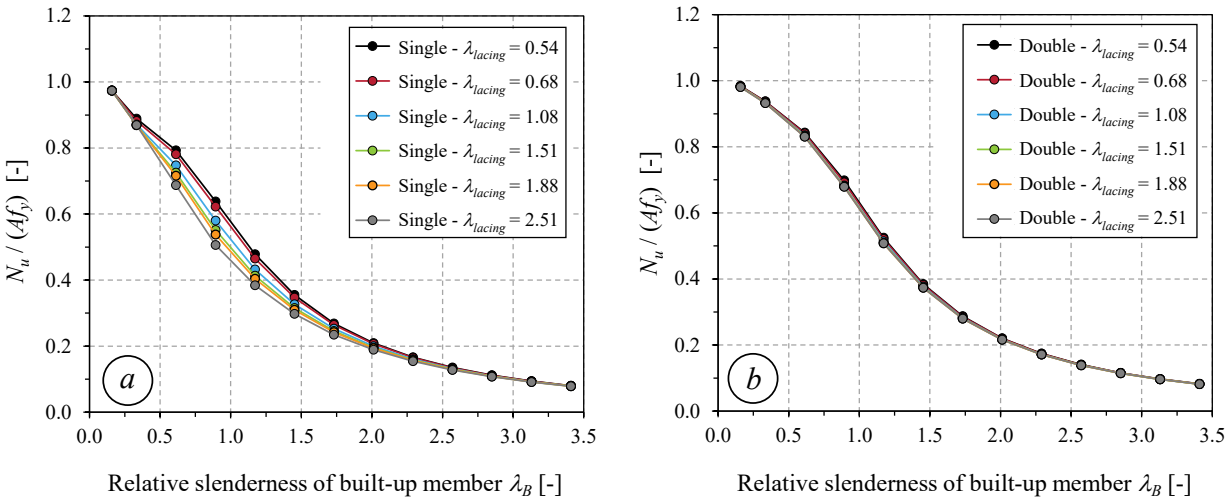

Figure 4.16 Effect of lacing slenderness on ultimate load– (a) Single (diagonal) lacing system – (b) Double (X) lacing system.

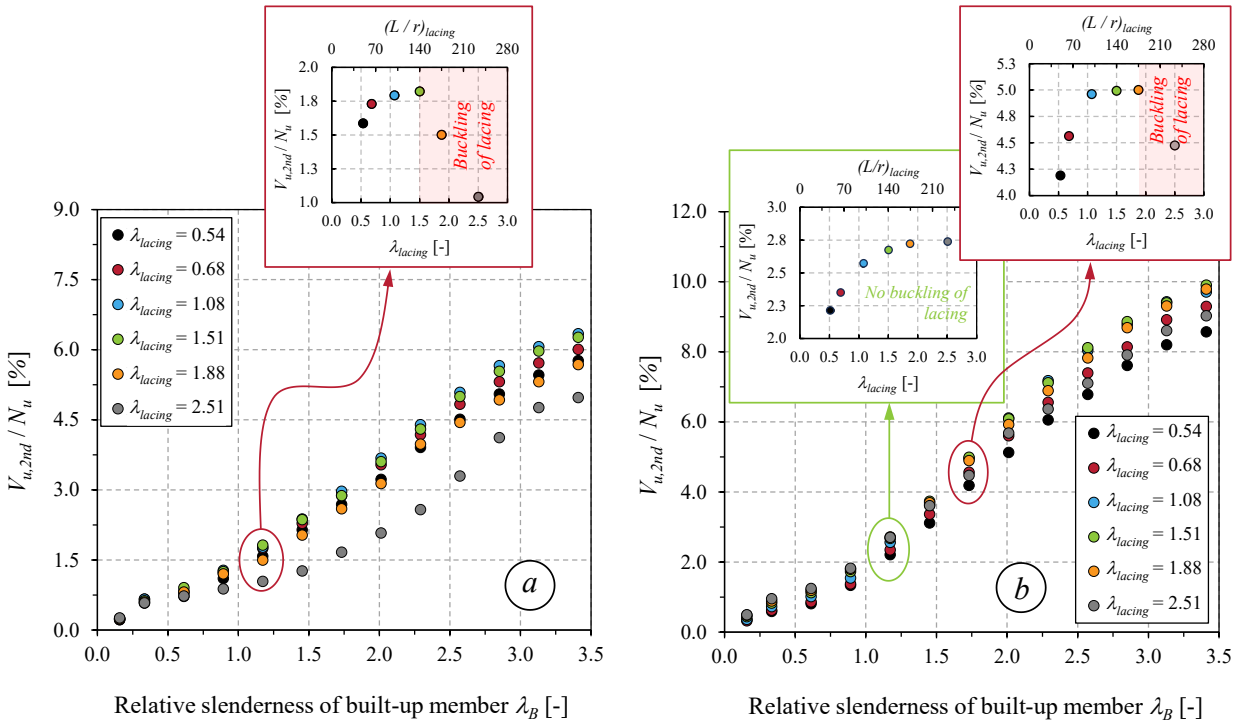

Figure 4.17 Effect of lacing slenderness on shear force in built-up members – (a) Single (diagonal) lacing system – (b) Double (X) lacing system.

4.3.5 Parametric studies

The extensive parametric study, involving around 2 000 numerical models of laced built-up columns, was conducted to evaluate how variations in section geometry and slenderness affect compressive resistance and shear demand. All models used CSA G40.4 steel (f_y = 230 MPa) for both main components and connecting elements, which reflects the mild steels commonly used in North American bridges built during 1950s. The built-up members consist of two C-shaped sections arranged as tip-to-tip and back-to-back, with height-to-width ratios (h / b) ranging from 2.3 to 9. These sections include both non-slender and slender elements, characterized by web slenderness ratios (h / t_w) between 6 and 65.8, and flange slenderness ratios (b / t_f) ranging from 4.9 to 20. Flat lacing bars, arranged in X or diagonal patterns, connect the widely spaced chords, while tie-plates are placed at the ends. Five lacing slenderness ratios (λ_{lacing} ranges from 0.5 to 1.88) and eight overall member slenderness values (λ_B) were considered. The results provide insight into structural behaviour and support the development of equations to estimate 2nd shear forces in laced built-up members, which will be presented in the next sections. Although this study primarily considers riveted or bolted lacing bars, the conclusions are also applicable to columns with welded diagonals, as the minor-axis buckling behaviour and ultimate capacities of the lacing bars are largely unaffected, with only a slightly lower diagonal force possible in some cases.

4.4 Development of design equations

4.4.1 Members with double (X) lacing system

As a key aspect of the proposed approach, improving the performance of the equation by accounting for all relevant effects is essential. This improvement led to the identification of a geometric parameter, denoted as γ_V (see Eq.(4.3)), which is responsible for the scatter observed in the results. The parameter γ_V is introduced to account for the sensitivity of web and flange plate buckling in transferring shear force between chords. For example, in built-up members composed of two main chords interconnected by X-shaped lacing bars, the shear force is transmitted from one chord to the other through the lacing system. Since the effectiveness of this force transfer is also influenced by the slenderness of the plate elements, γ_V reflects their role in the overall shear

behaviour of the member. Accordingly, a series of equations dependent on γ_V has been developed for built-up members with both double and single lacing systems.

$$\gamma_V = \frac{\left(h/t_w\right)^2}{\left(b/t_f\right)} \tag{4.3}$$

In Eq. (4.3), h denotes the web height of the C-section, b represents the flange width, and t_w and t_f are the respective thicknesses of the web and flange. A higher value of the parameter indicates that the web is considerably more slender than the flange, making it more susceptible to local buckling. Conversely, a lower value implies either comparable slenderness between the web and flange or a dominant flange effect in the structural response. As illustrated in Figure 4.18a, increasing this parameter correlates with a rising V_u / N_u ratio, highlighting the growing influence of web slenderness on shear resistance. However, when the shear force acts in a direction parallel to the flange of the C-shaped members, the flange becomes more critical in resisting shear, which typically corresponds to a lower value of the parameter. It should be noted that the parameter γ_V accounts for the influence of section geometry – specifically the relative stiffness of the web and flanges – on the shear force distribution in the lacing system. In built-up sections of existing bridge members, often composed of multiple channels or plates connected with angles to form a C-shape, these plates are frequently slender, and including this effect allows more precise calculation of shear forces and understand how close the bridge is to its ultimate limit. Typical values of γ_V depend on the section dimensions and lie within a narrow range for most members considered. Therefore, its influence is minimal, and retaining it does not significantly improve accuracy. In Section 4.4.3, a simplified proposal eliminates this factor.

Table 4.5 Summary of parameters involved in the proposed equation for double (X) lacing configurations.

<table>
<tr><td>For $\lambda_B \le 0.25$</td><td colspan="4">For $0.25 < \lambda_B < 2.5$</td></tr>
<tr><td rowspan="4">$\frac{V_u}{N_u} = 0.01$</td><td colspan="4">$\frac{V_u}{N_u} = \frac{\left[1.5 - \cos\left(\lambda_B\right)\right]^{1/n}}{\alpha_e \beta} \ge V_{u,\min}$</td></tr>
<tr><td colspan="4">$\alpha_e = 41.8 - 3.4\lambda_{lacing} - 0.0017\gamma_V$</td></tr>
<tr><td>β</td><td>γ_V</td><td>n</td><td>λ_{lacing}</td></tr>
<tr><td>1.0</td><td>$\left(h/t_w\right)^2 / \left(b/t_f\right)$</td><td>$0.7 + \lambda_B / 50$</td><td>$\le 1.8$</td></tr>
</table>

Table 4.5 presents the proposed equations for calculating the design shear force in built-up members. In these equations, γ_V represents the influence of plate slenderness in the main structural components on the resulting shear force. The variables n, α_e, and β correspond to a curve-fitting coefficient where n and α_e are the equivalent factors accounting for the influence of lacing slenderness based on numerical calibration, and β is the factor associated with the type of lacing configuration.

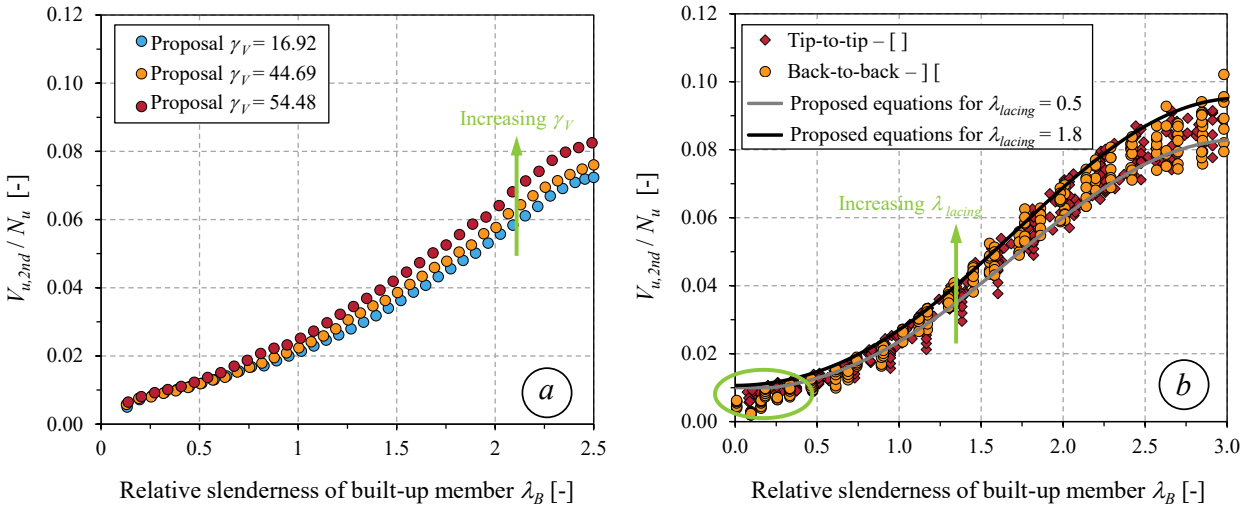

Figure 4.18 (a) Section geometry parameter (γ_V) – (b) Proposed equations for laced built-up sections with double (X) lacing system.

Figure 4.18b presents the proposed design shear force for laced built-up members with double (X) lacing system. The plot is shown in V_u / N_u – λ_B format, with the proposed V_u / N_u curves displayed over a range of lacing member slenderness values (λ_{lacing}). It could be observed that as λ_{lacing} increases, the V_u / N_u ratio tends to rise due to earlier buckling of lacing elements, causing a slight decrease in the resistance of built-up members. To avoid the earlier failure of lacing, λ_{lacing} is limited to 1.8. Besides, for very short members (λ_B < 0.25), strain hardening can cause the ultimate axial strength (N_u) to exceed the plastic resistance, which reduces the V_u / N_u ratio (see green ellipse). This behaviour is especially noticeable in members with fewer than three lacing modules (lacing segments). To ensure realistic and safe design values, a minimum V_u / N_u ratio of 1% is enforced.

4.4.2 Members with single (diagonal) lacing system

Figure 4.19 illustrates the proposed design equation obtained from the numerical results for built-up members with single (diagonal) lacing systems for both lacing configurations, tip-to-tip and

back-to-back. In Figure 4.19, the plot includes various curves, specifically representing proposed equations for $\lambda_{lacing} = 0.5$ and 1.5. As expected, the trend reveals a clear increase in V_u / N_u as λ_B increases, with more slender lacing (higher value of λ_{lacing}) resulting in higher shear demands. Additionally, at low λ_B values (see green ellipse), the $V_u / \mathrm{N_u}$ ratio is minimal, reflecting reduced 2nd shear effects for short column. It also reveals that built-up members with double lacing systems exhibit higher shear force compared to those with single lacing (see Figure 4.18b and Figure 4.19a). This is evidenced by determining the ratio $[V/N]_{u,double} / [V/N]_{u,single}$, as reported in Figure 4.19b, to further investigate the relative performance of double and single lacing systems. It clearly shows that double laced systems consistently produce higher shear responses, with the ratio generally ranging from 1.4 to 1.5 when $\lambda_B > 0.75$. For short column, especially $\lambda_B \approx 0.5$, the ratio slightly drops below 1.4, likely due to the presence of fewer than three modules in the built-up configuration, which reduces structural interaction and amplification. Besides, the relative difference is primarily due to the greater shear stiffness (S_v) provided by the double lacing configuration. To capture this difference, a constant lower-bound factor $\left(\beta_{\min} \approx \sqrt{S_{v,double} / S_{v,single}} \approx 1.41\right)$ is introduced (see solid black line in Figure 4.19b), serving as a modified factor to adapt equations derived for double lacing to single lacing cases by adjusting for the reduction in shear stiffness.

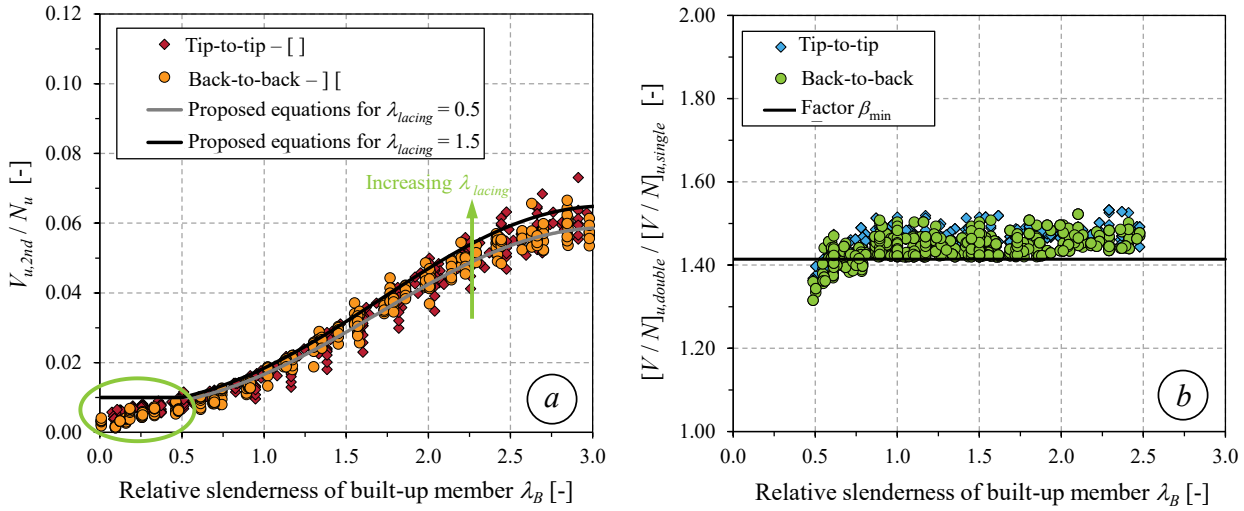

Figure 4.19 (a) Proposed design for laced built-up sections with a single lacing system – (b) Parameter representing the lacing layout (β).

The proposed equations for laced built-up members with single (diagonal) lacing systems are detailed in Table 4.6, where certain parameters have been adjusted to reflect the behaviour of these

members. Similarly to built-up members with a double lacing system, a minimum threshold of 1% for the V_u / N_u ratio is maintained. Additionally, the slenderness of lacing elements is capped at $\lambda_{lacing} \leq 1.5$ to prevent earlier failure of lacing members. Note that the formulas in Table 4.5 and 4.6 are derived from the mechanical behaviour of the lacing system, with minor adjustments through local curve fitting to achieve a practical balance between simplicity and accuracy.

Table 4.6 Summary of parameters involved in the proposed equation for single (diagonal) lacing configurations.

<table>
<tr><td>For $\lambda_B \leq 0.5$</td><td colspan="4">For $0.5 < \lambda_B < 2.5$</td></tr>
<tr><td rowspan="4">$\frac{V_u}{N_u} = 0.01$</td><td colspan="4">$\frac{V_u}{N_u} = \frac{\left[1.5 - \cos\left(\lambda_B\right)\right]^n}{\alpha_e \beta} \geq V_{u,\min}$</td></tr>
<tr><td colspan="4">$\alpha_e = 41.8 - 3.4\lambda_{lacing} - 0.0017\gamma_V$</td></tr>
<tr><td>β</td><td>γ_V</td><td>n</td><td>λ_{lacing}</td></tr>
<tr><td>$\sqrt{2}$</td><td>$\left(h / t_w\right)^2 / \left(b / t_f\right)$</td><td>$1 / \left(0.7 + \lambda_B / 50\right)$</td><td>$\leq 1.5$</td></tr>
</table>

Overall, the proposed design shear force in laced built-up members with double and single lacing systems relies on the same base equation for predicting V_u / N_u, allowing the model to capture the buckling behaviour across various lacing types and chord geometries. Besides, the equation is also applicable to a range of lacing slenderness values, making it suitable for considering bending effects in the lacing. Since the equations include several variables, such as the curve fitting factor n, they are slightly more complex than typical design rules. To make them easier to adopt, a simplified version is presented in the next section by combining the less important terms into the curve fitting factor.

4.4.3 Simplified design equations

To provide a more practical and efficient approach, a simplified expression is proposed by eliminating the factors γ_V, β, and α_e, which are originally used to account for shear amplification and cross-sectional geometric effects. Instead, the curve fitting factor n is modified to compensate for the influence of these parameters. Additionally, the factor b and α_e are combined into a single modified term where $\alpha = \alpha_e \times \beta$, which is imposed in the simplified expression. The proposed coefficient is calibrated based on γ_V values ranging from 2.6 to 1080, corresponding to various cross-sections typically used in steel truss bridges and extracted from standard sections. The

analysis indicates that n was found to vary between 1.36 and 1.39. Among these, $n = 1.38$ was chosen as it minimizes the discrepancy between the original formulation and the proposed simplified expression.

The comparison between the first formulation (as introduced in Section 4.4.2) and the simplified version using $n = 1.38$ is illustrated in Figure 4.20. For this figure, a worst-case scenario is considered, where $\gamma_V = 1080$ and $\lambda_{lacing} = 1.5$ for single lacing and 1.8 for double lacing. The simplified equation provides a difference of approximately 5% for single lacing and less than 6% for double lacing. A negative value indicates that the simplified expression is slightly less conservative than the original, whereas a positive value suggests the opposite. This confirms that the proposed simplification maintains acceptable accuracy while offering greater practicality for design applications.

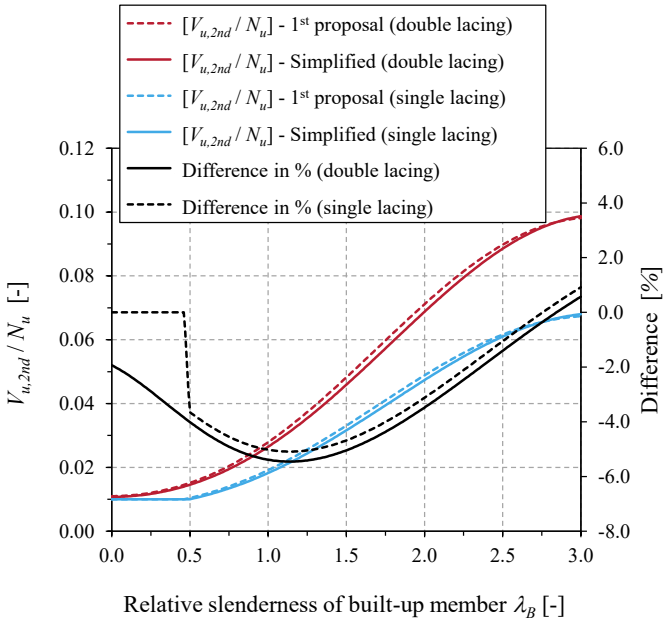

Figure 4.20 Evaluation of the first proposed equation against the simplified one ($n = 1.38$), including percent difference.

Table 4.7 Summary of proposed simplified equations for predicting shear force in laced built-up members.

$\frac{V_u}{N_u} = \frac{\left[1.5 - \cos\left(\lambda_B\right)\right]^{1.38}}{\alpha} \geq 0.01$
$\alpha = \begin{cases} 41.8 - 3.4\lambda_{lacing} & \text{for double lacing (X)} \\ 59 - 4.8\lambda_{lacing} & \text{for single lacing (diagonal)} \end{cases}$
$\lambda_{lacing} \begin{cases} \leq 1.8 & \text{for double lacing (X)} \\ \leq 1.5 & \text{for single lacing (diagonal)} \end{cases}$

The summarized results of the simplified V_u / N_u equations are presented in Table 4.7, which includes two distinct α coefficients – one for laced built-up with single (diagonal) lacing systems and another for double (X) lacing systems. Additionally, Figure 4.21 presents a further comparison between the first and simplified equations using the proposed n = 1.38, for λ_{lacing} = 1.5 and 1.8 for single and double lacing, respectively. By adopting distinct α coefficients, the figure illustrates that the V_u / N_u values for laced built-up members with double lacing system are consistently higher than those with single lacing system, indicating that double-laced members provide greater shear stiffness. The results show a close match between the two formulations, confirming the accuracy of the simplified approach.

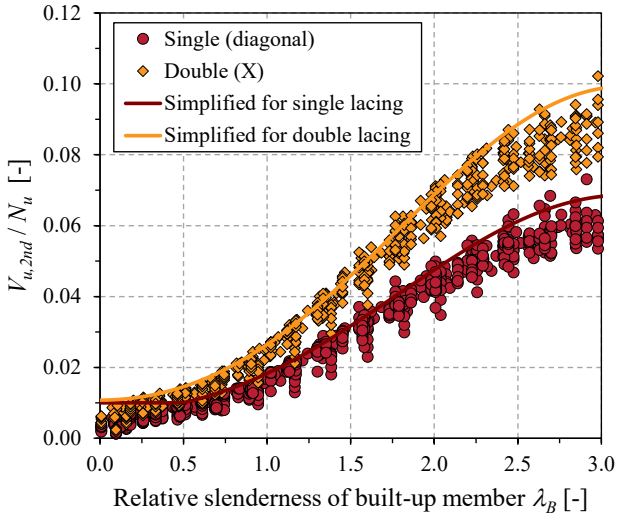

Figure 4.21 Comparison of different lacing configurations using simplified formulas.

4.4.4 Assessment of proposed equations and current design practices

The accuracy and performance of the proposed shear force prediction equations for laced built-up members were evaluated by comparison with three current design codes: EC 3, AS 4100, and American Standards (AASHTO, which incorporates recommendations from AISC). The evaluation covered both double and single lacing systems, with results presented in Figure 4.22 and 4.23 and summarized in Table 4.8.

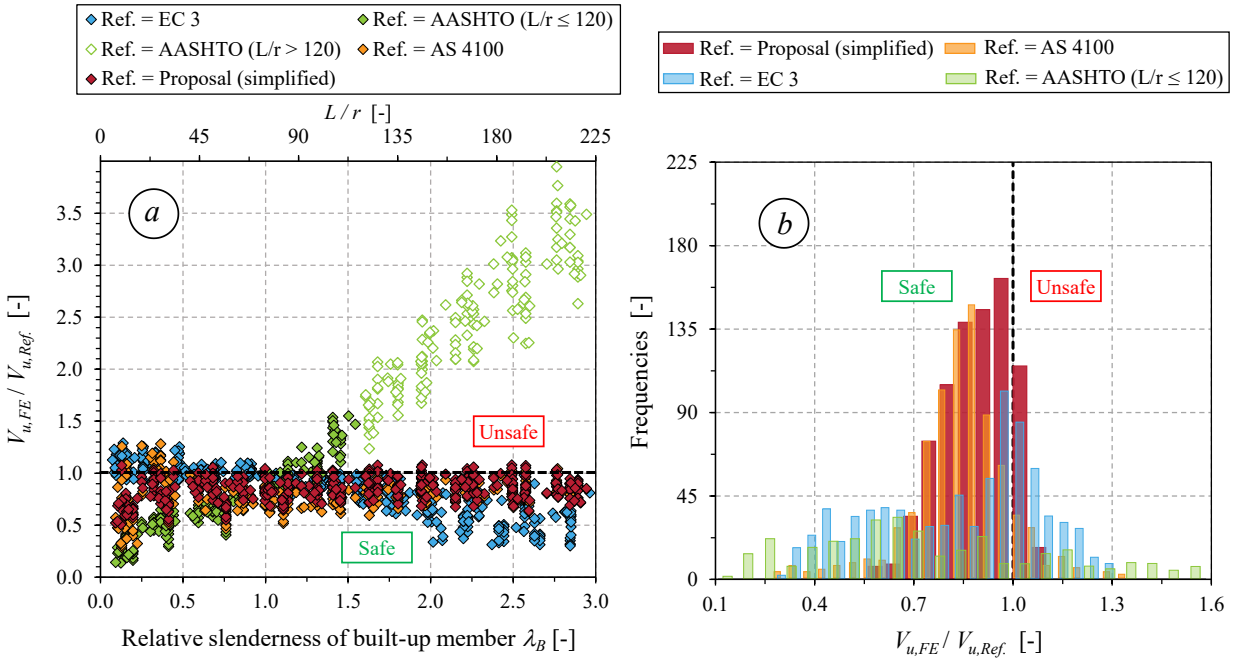

Figure 4.22 Assessment of double lacing systems: design standards compared with FE results.

For laced built-up members with double (X) lacing systems, the proposed equations demonstrate relatively accurate and consistent performance. The mean ratio of FE results to proposed predictions, $V_{u,FE} / V_{u,Proposal}$, is approximately 0.90, with a C.o.V. of 12.1%, and the maximum unsafe deviation is limited to 8%. In comparison, EC 3 and AS 4100 exhibit less accurate predictions, with a mean $V_{u,FE} / V_u$ ratio of about 0.82 and higher variability (C.o.V.s of 30.1% and 17.2%, respectively). Although both standards tend to be more conservative, with results around 8% safer than the proposed equations, they also exhibit significant unsafe predictions for members with $\lambda_B < 0.75$, where the maximum $V_{u,FE} / V_u$ ratio reaches approximately 1.30. Specifically for EC 3, among all results obtained from the parametric study, around 16% of the predictions fall on the unsafe side with $V_{u,FE} / V_{u,EC\,3} > 1.05$, and 10% exceed 1.10.

Besides the AASHTO provisions, which follow AISC recommendations, the performance was examined in two groups based on slenderness (L / r):

- For members with $L / r \leq 120$, the AASHTO predictions are overly conservative but exhibit significant scatter, with a mean $V_{u,FE} / V_{u,AASHTO}$ ratio of 0.72 and a C.o.V. of 48.3%. This indicates both low precision and consistency, especially for short members where $L / r < 30$. However, with the L / r range of 90 to 120, the AASHTO provisions provide unsafe predictions, with $V_{u,FE} / V_{u,AASHTO}$ ratio reaching up to 1.55 on the unconservative side, suggesting limited reliability in this range.
- For members with $L / r > 120$, which exceeds the AASHTO limit but falls within the AISC allowable range, the mean $V_{u,FE} / V_{u,AASHTO}$ ratios rise sharply to 1.49 and 2.28 for single and double lacing systems, respectively, with C.o.V.s above 20%. This reflects severe underestimation of shear forces and poor reliability, with more than 23% of the parametric results lying on the unsafe side.

In addition, for laced built-up members with single lacing system (diagonal), all design codes generally give conservative results. Specifically, the AASHTO is the most conservative and scattered, with a mean $V_{u,FE} / V_{u,AASHTO}$ ratio of 0.46 and a C.o.V. of 50.4%, particularly for members with $L / r < 30$. This results from assuming a constant V_u / N_u ratio of 2% for all member lengths, which is overly cautious for shorter members. Accordingly, EC 3 offers more accurate and consistent predictions than the AS 4100 and AASHTO, primarily due to its consideration of the shear stiffness factor (S_v) for various lacing arrangements – a factor omitted by AASHTO and AS 4100. However, for laced built-up members with single lacing systems, the proposed equations give more accurate and consistent results than all current codes, with a mean ratio of 0.82 and a C.o.V. of 15.2%, which represents an improvement of more than 10% over existing standards.

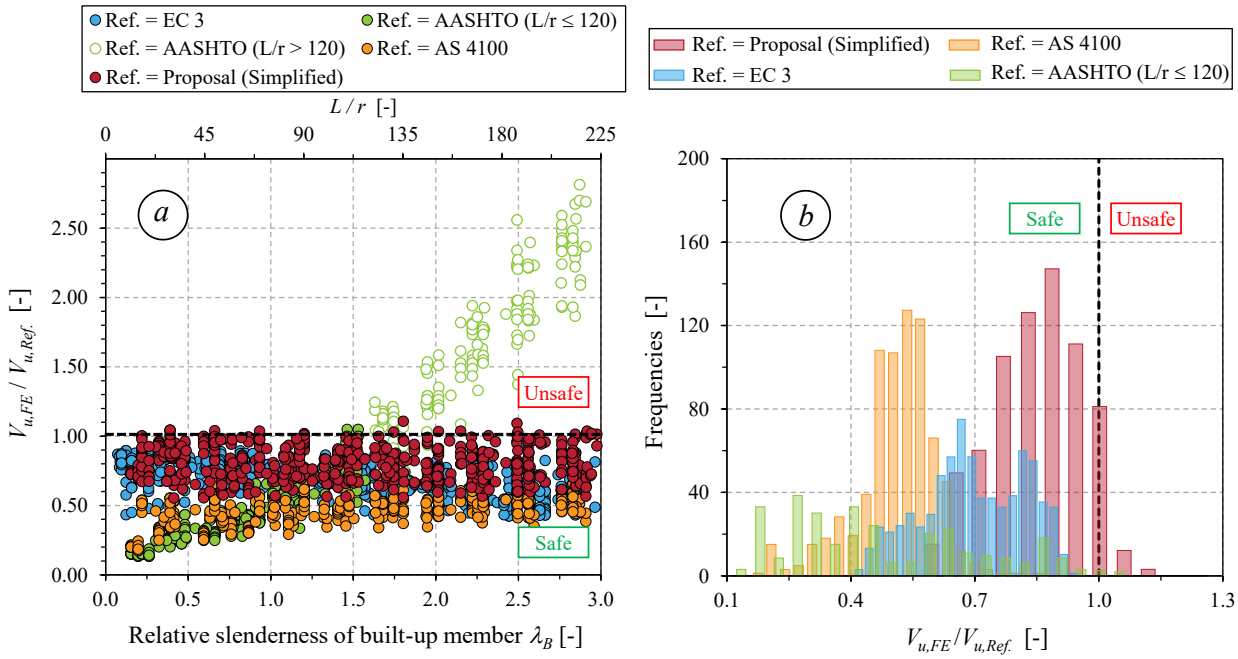

Figure 4.23 Assessment of single lacing systems: design standards compared with FE results.

In summary, the proposed shear force prediction equations are shown to be more accurate, consistent, and simpler to use for both double and single laced built-up members. Various section shapes, lacing slenderness, and chord layouts are considered, and possible buckling of lacing members is taken into account. Although Eurocode 3 and the Australian Standards are found to be safe but conservative, and AASHTO is found to be inconsistent for certain of member slenderness ranges, better precision and reliability are achieved by the proposed equations across a wide range of sections, lacings, and member lengths.

Table 4.8 Summary statistics of $V_{u,FE}$ / $V_{u,Ref}$ values.

Lacing arrangements	References	Mean	C.o.V. [%]	Max.	Min.	>1.05 [%]	>1.1 [%]	>1.3 [%]
Double lacings	EC 3	0.82	30.1	1.29	0.30	15.6	10.3	0.0
	AASHTO ($L/r \leq 120$)	0.72	48.3	1.55	0.14	7.9	6.9	3.4
	AASHTO ($L/r > 120$)	2.28	23.4	3.53	1.03	27.4	27.4	27.1
	AS 4100	0.82	17.2	1.28	0.29	3.4	2.4	0.0
	Proposal (simplified)	0.90	12.1	1.08	0.51	2.4	0.0	0.0
Single lacings	EC 3	0.69	18.1	0.92	0.42	0.0	0.0	0.0
	AASHTO ($L/r \leq 120$)	0.46	50.4	1.05	0.14	0.0	0.0	0.0
	AASHTO ($L/r > 120$)	1.49	29.2	2.56	0.54	23.3	22.5	15.7
	AS 4100	0.50	19.0	0.83	0.18	0.0	0.0	0.0
	Proposal (simplified)	0.82	15.2	1.14	0.55	1.1	0.4	0.0

4.5 Conclusions

This study investigated the behaviour of laced built-up members composed of two C-shaped sections under axial compression, with particular attention to second-order shear forces induced by initial imperfections. Validated numerical models were developed and validated against 23 experimental data and subsequently used to conduct both preliminary and parametric studies. Based on these analyses, practical equations were developed to predict the shear force-to-ultimate load ratio (V_u / N_u) while capturing the effects of lacing instability for both built-up members with single (diagonal) and with double (X) lacing systems. The key findings and contributions of this work are summarized as follows:

(i) The second-order shear forces in laced built-up members were found to be significantly influenced by lacing arrangement, lacing slenderness, chord slenderness, and member length;

(ii) Shear force-to-ultimate load ratios were shown to exceed 2% for members with intermediate slenderness, indicating that commonly assumed minimum shear forces may be insufficient for slender members and overly conservative for short members;

(iii) Two sets of design equations were proposed: a complete equation, accounting for cross-section slenderness and lacing effects, and a simplified equation for practical use. The simplification was shown to be valid for a defined range of cross-section slenderness γ_v, while the complete equation remains applicable beyond this range, ensuring broad usability.

The proposed equations were demonstrated to predict V_u / N_u reliably across a wide range of laced built-up members, effectively capturing lacing instability, which current standards do not fully address. Improved accuracy, consistency, and applicability were achieved, while the simplified formulation enhances practical use without loss of reliability.

4.6 Acknowledgements

This research and development project would not have been possible without the contribution and collaboration of The Jacques Cartier and Champlain Bridges Incorporated.

CHAPTER 5 ARTICLE 2: O.I.C.-BASED DESIGN FOR LOCAL/GLOBAL/BUILT-UP INTERACTION IN LACED BUILT-UP STEEL COLUMNS

Oudom Chhoeng[a], Morane Chloé Mefande Wack[a], Robert Tremblay[a], Nicolas Boissonnade[b, *]

[a] Polytechnique Montréal, H3T 1J4, Montréal, QC, Canada

[b] Université Laval, G1V 0A6, Québec, QC, Canada

[*] Corresponding author

Email: oudom.chhoeng@polymtl.ca (O. Chhoeng), morane-chloe.mefande-wack@polymtl.ca (M. Wack), robert.tremblay@polymtl.ca (R. Tremblay), nicolas.boissonnade@gci.ulaval.ca (N. Boissonnade).

The paper was submitted to *Thin-Walled Structures* on 27 October 2025.

Abstract: This paper investigates the ultimate strength of laced built-up columns that buckle in the plane of the lacing system, where shear deformations significantly reduce the load-carrying capacity. These members are influenced by Local/Global/Built-up (L/G/B) buckling phenomena and their interactions. The built-up section consists of two C-shaped chords connected by double (X) flat lacing bars. Three main buckling modes are examined through detailed numerical analyses: (i) Local buckling of the cross-section, (ii) Global buckling of individual chords between connectors, (iii) Built-up buckling of the overall member and (iv) coupling/interactions between these modes. For members with slender elements, local buckling and its interaction with other modes are not adequately captured by current design codes, resulting in unconservative strength predictions. Similar issues are observed for global buckling of the chord. To address these limitations, this study extends the existing Overall Interaction Concept (O.I.C.), which was originally developed for Local/Global interactions, to include more complex Local/Global/Built-up interaction behaviour. The extended O.I.C.-based approach demonstrates a strong ability to capture these complex interaction effects. Its accuracy and consistency are confirmed through comparisons with numerical results from validated shell finite element models. The proposed method provides more accurate, consistent, and safer strength predictions than the

recommendations provided by Eurocode 3 and the American Standards for both tip-to-tip and back-to-back built-up sections. Its reliability is also supported by statistical analyses in accordance with EN 1990 guidelines.

Keywords: Laced built-up columns, In-plane buckling, Overall Interaction Concept, Local/Global/Built-up buckling interactions.

5.1 Introduction

This paper focuses on the design of laced built-up columns subjected to axial compression, specifically those that buckle within the plane of the lacing system. These types of members were frequently used in truss bridge design during the late 19th and early 20th centuries. Due to the limitations of steel manufacturing and fabrication techniques at the time, engineers combined smaller components like plates, angles, and channels to create larger, stronger structural elements. This method was cost-effective, optimized material usage, and made transportation and assembly of large bridge components easier. While these designs provided benefits such as increased bending stiffness, they also introduced challenges, such as shear flexibility, which compromised buckling resistance. Today, steel built-up members like those used in early truss bridges are rarely seen, as they have been largely replaced by heavy structural sections from rolling mills or welded shapes produced by steel manufacturers. Despite this, many of these older bridges remain in use, with components that often do not conform to modern design codes. This creates difficulties in assessing the structural integrity of the built-up members in these existing truss bridges, a concern underscored by historical failures such as the collapse of the Quebec Bridge, which tragically highlighted the consequences of inadequate understanding of built-up member buckling.

Following the first collapse of built-up members in the Quebec Bridge, the impact of shear deformations on the buckling capacity of built-up sections became a significant concern [6]. This issue was investigated by numerous researchers. To clearly illustrate the buckling behaviour of built-up members, Figure 5.1 presents various configurations: Figure 5.1a shows a typical built-up member under axial compression, Figure 5.1b depicts buckling under flexure, and Figure 5.1c shows buckling involving both flexure and shear deformations. As shown in Figure 5.1c, when buckling occurs about the y_o axis of the section (buckling in-plane of lacing system), the members may deform due to a combination of flexural and shear effects. In this scenario, flexural deformations arise from the overall global buckling of the built-up member (built-up buckling),

while the shear deformations result from the global flexural buckling of the individual chords between the lacings (global buckling) around their minor-axis of bending. These additional shear deformations lead to a reduction in the member's buckling load.

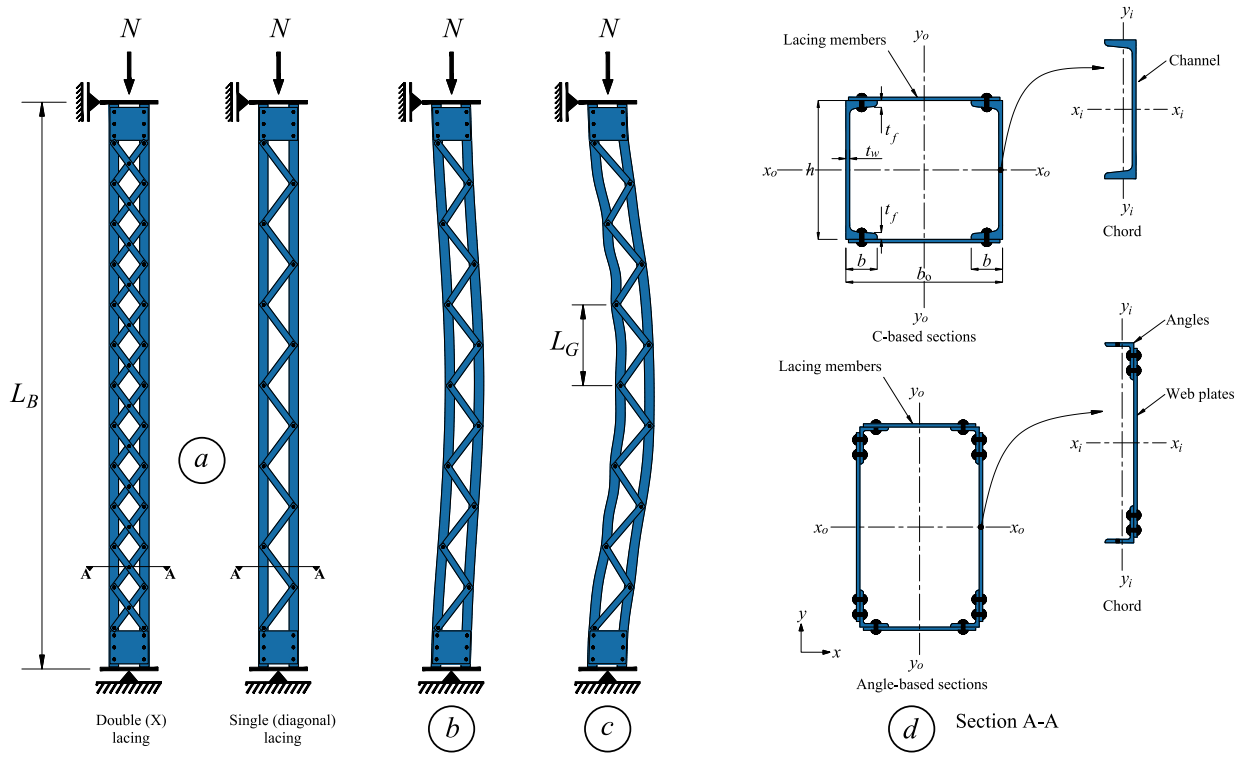

Figure 5.1 Buckling of a built-up member involving shear deformation – (a) typical built-up member under axial compression – (b) buckling under flexure – (c) buckling involving flexural and shear deformations – (d) cross-sections.

This issue was first investigated by Engesser [8] and later by Timoshenko [10], who proposed an equation to determine the critical load causing elastic buckling in a member with pinned supports. Timoshenko's critical load equation considered the combined effects of built-up buckling in flexure and global buckling of individual chords between connectors due to shear. These equations can be found in classical textbooks on structural stability [26], [11]. Expanding on this, Aslani and Goel [49] extended the formulation to account for general boundary conditions and proposed a theory-based version of the modified slenderness ratio for built-up members. This theory was later adopted by most current design codes, which address Built-up (B) buckling and Global (G) buckling of the chord between connectors independently, without properly accounting for their interaction – so called "Global/Built-up (G/B) interaction". The interaction between built-up buckling of overall members and global buckling of individual chords between lacing connection points was studied by Svensson and Kragerup [88], Geng-Shu and Shao-Fan [167], Duan et al. [103], and more

recently, by Li et al. [107]. These researchers focused on the combined effects of geometric imperfections in both the overall built-up member and the individual chords between connectors, rather than directly addressing the G/B interaction that governs member strength. Nevertheless, their findings demonstrate that such combined imperfections can significantly reduce the resistance of built-up members.

While the current design standards [112], [113], [155] incorporate G/B interaction effects using modified slenderness ratios, the interaction between local, global, and built-up buckling is not fully addressed and is often overlooked. These standards also impose additional constraints to reduce G/B interaction, which, if not controlled, could significantly decrease the resistance of member, as highlighted in [103]. A detailed discussion of these design provisions is presented in Section 5.3. Besides, the behaviour of Local (L) buckling of the cross-section is frequently not adequately considered in these standards, especially regarding the Local/Global/Built-up (L/G/B) interaction. In the current design rules, the effect of local buckling of the cross-section is typically addressed using the Effective Width Method (E.W.M.) [168], which calculates the effective area of the cross-section. This effective area is then incorporated with member buckling curves to account for the impact of local buckling on member stability. While the E.W.M. is commonly employed in most current design practices, it has several limitations, mainly its failure to account for the interaction between plate elements [123], [126], [169], [170] and the need for complicated iterations. Additionally, the method is better suited for members with large width-to-thickness ratios, as reported in the experimental investigation described in [171].

Research on the G/B and L/G/B interaction phenomena in built-up members is still limited. Little investigation has been conducted into how local buckling of the cross-section, global buckling of the individual chord between connectors and built-up buckling of the overall member interact with one another. Typical buckling modes for each mode shape of laced built-up members are illustrated in Figure 5.2.

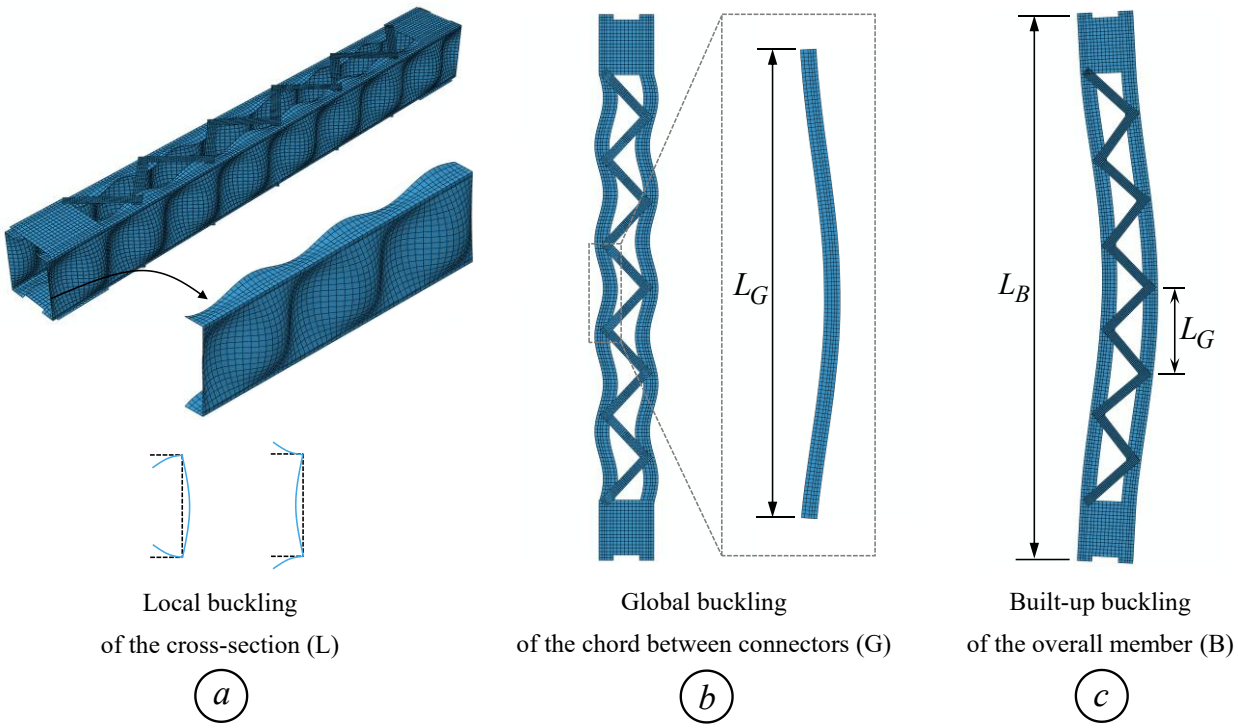

Figure 5.2 Buckling mode shapes of tip-to-tip laced built-up columns – (a) Local – (b) Global – (c) Built-up buckling.

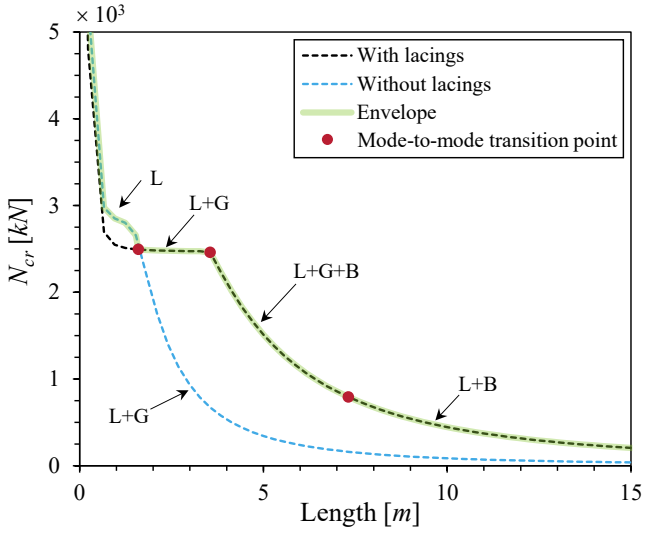

Figure 5.3 Typical elastic buckling behaviour of laced built-up columns with lacings and without lacings.

To address this gap, preliminary analyses incorporating relevant features, as described in Section 5.4, provided the results shown in Figure 5.3. Figure 5.3 presents the elastic buckling load of laced built-up columns under simply supported conditions. The built-up section consists of two

MC310 × 21.3 channel sections arranged tip-to-tip ([ ]). The member is sensitive to local buckling as well as to buckling about the minor axis ($y_o - y_o$), where shear deformations play a significant role. Consequently, the interaction between the local buckling of the cross-section, global buckling of the individual chord, and built-up buckling of the overall member is inevitable. The chords were interconnected by double (X) flat lacing bars, with the lacing angle to the longitudinal axis of the built-up member set at approximately 30 degrees. To address the pure local buckling behaviour, particularly for short columns, an additional series of analyses was performed on members without lacing bars. With an increase in column length, the results reveal that for short columns ($L_B < 1.6\ m$), the elastic critical load (N_{cr}) is significantly influenced by the local buckling of the cross-section. Red dots in Figure 5.3 indicate mode-to-mode transition points, where the dominant elastic buckling mode changes as the column length increases. In typical L/G interaction, two distinct stages can be observed for columns with and without lacing. For columns with lacing and lengths between 2 m and 4 m, the critical load shows a slight decrease, resulting in an almost horizontal plateau. In contrast, for columns without lacings, the critical load drops significantly, indicating that the spacing between lacing connectors (L_G) plays a crucial role in the L/G interaction. Additionally, for columns with lacings, the critical load maintains an almost horizontal trend before transitioning to a steeply descending branch at $L_B \approx 2.5\ m$ (intermediate columns), which is associated with L/G/B interactions. It is clearly observed that for long columns ($L_B > 7\ m$), the global buckling mode of individual chords has minimal influence, while the local buckling mode continues to interact slightly with the built-up buckling mode. It is therefore evident that built-up columns are highly susceptible to many instability phenomena, which include local, global and built-up buckling. Preliminary results indicate that local buckling of the cross-section plays a significant role across various column lengths, influencing the L/G/B interaction buckling modes. This complex interaction may significantly affect the post-buckling behaviour and ultimate strength of built-up columns, depending on the dimensions of the built-up section, spacing of the connectors, and the column's length.

Yet, various modern design methods, such as the Continuous Strength Method (C.S.M.) [172], the Direct Strength Method (D.S.M.) [119] and the Overall Interaction Concept (O.I.C.) [123] provide guidance for designing steel members to account for complex interactive buckling. However, existing literature and design methodologies on the coupling effects involving the interaction of three buckling modes are limited, with most studies focusing on cold-formed steel columns. Young

and Rasmussen [173] conducted a series of experimental tests on cold-formed lipped channel columns, providing evidence of a combined failure mode due to a tiple interaction, i.e., Local-Distortional-Global (L/D/G) interaction. This L/D/G interaction refers to the simultaneous coupling of local buckling of the cross-section, distortional buckling involving flange–lip deformations, and global flexural or flexural–torsional buckling of the global member, resulting in a complex and interactive instability behaviour. Further investigations into the behaviour of columns with cold-formed sections undergoing triple interaction can be found in the works of Young and Yan [174], Dinis and Camotim [175], Dinis et al. [176], [177], Santos et al. [178], [179], Cava et al. [180], and more recently in Young et al. [121] and Kumar and Kalyanaraman [181]. In summary, these studies above were primarily aimed at developing early concepts for design considerations, as highlighted in the report by Camotim et al. [182]. The first comprehensive design method for triple interaction in cold-formed sections was recently proposed by Dinis et al. [122], who introduced a more reliable and validated method using the D.S.M. to predict the failure loads of columns under complex loading conditions. The authors extended the D.S.M., which was initially focused on double interaction modes, by incorporating design rules to address cold-formed section columns affected by the L/D/G interaction. However, the D.S.M. was originally developed for thin-walled cold-formed sections [119] and is primarily based on elastic principles. As a result, it is less suitable for stocky sections, which are more governed by plastic and ductile behaviour [126]. In the same way, the C.S.M. was specifically applied to cold-formed stainless-steel members. This method was developed to take advantage of the strain hardening benefits, especially for very stocky sections.

Besides, the O.I.C. was originally developed for hot-rolled sections, covering a range from compact (stocky sections) to slender sections. This method was proposed by Boissonnade et al. [123], who described its mechanical background, principles, and application steps. A more detailed discussion of the O.I.C. design procedure will be provided in Section 5.2. Since its introduction, O.I.C.-based design approaches have been extended to various hot-rolled sections, including square and hollow sections [124], [125], bi-symmetric I-sections [126] –[129], mono-symmetric I-sections [130], and T-sections [131]. The results demonstrate that the O.I.C.-based design rules provide more reliable and consistent predictions compared to current design standards. These studies also show that the O.I.C. effectively accounts for complex coupling interaction effects, such as local/global interactions in hot-rolled sections. More recently, the O.I.C. method has also been applied to

aluminum structures [128]–[130], demonstrating its capability to deliver highly accurate predictions while maintaining safety and economic efficiency compared to existing design proposals.

This paper investigates the L/G/B interactive buckling of laced built-up members under axial compression, with particular emphasis on column buckling occurring in the plane of the lacing system. The laced built-up columns consist of two hot-rolled C-sections arranged either tip-to-tip ([ ]) or back-to-back (] [), with both chords interconnected by double (X) flat lacing bars. Additionally, the lacing connectors are assumed to be riveted or bolted, and the built-up columns are subjected to axial loads under simply supported conditions. The spacing between the two C-sections ensures that the flexural buckling of the built-up section always occurs in the plane of the lacing system. The application of the O.I.C. is extended to the design of laced built-up sections that buckle in the plane of the lacing system, where a significant triple interaction mode occurs. This includes local buckling of the cross-section, global buckling of the chords between lacing connectors and built-up buckling of the overall member, all of which are examined through extensive numerical analyses. The extension of the O.I.C.-based design rule to account for the triple interaction is described in Section 5.2. The details and limitations of current design approaches are discussed in Section 5.3, while the numerical modeling procedure and validation study are presented in Section 5.4. Accordingly, O.I.C.-based design formulas for laced built-up members are proposed. The resistance values predicted by the O.I.C. approach, Eurocode 3, and the American Standards are compared against numerical and experimental results, accompanied by a reliability analysis in Section 5.5 and Section 5.6, respectively.

5.2 O.I.C.-based design rules

5.2.1 O.I.C.-based design rules for double interaction

The O.I.C. is based on the well-established resistance-instability interaction, utilizing a definition of generalized relative slenderness. It eliminates the need for cross-section classification and the E.W.M., treating all cross-section shapes uniformly at both the section and member levels. More specifically, the O.I.C. uses the plastic capacity of the section (N_{pl}) as a reference and introduces penalty factors (χ) to account for the detrimental effects of different buckling modes, imperfections, and their interactions.

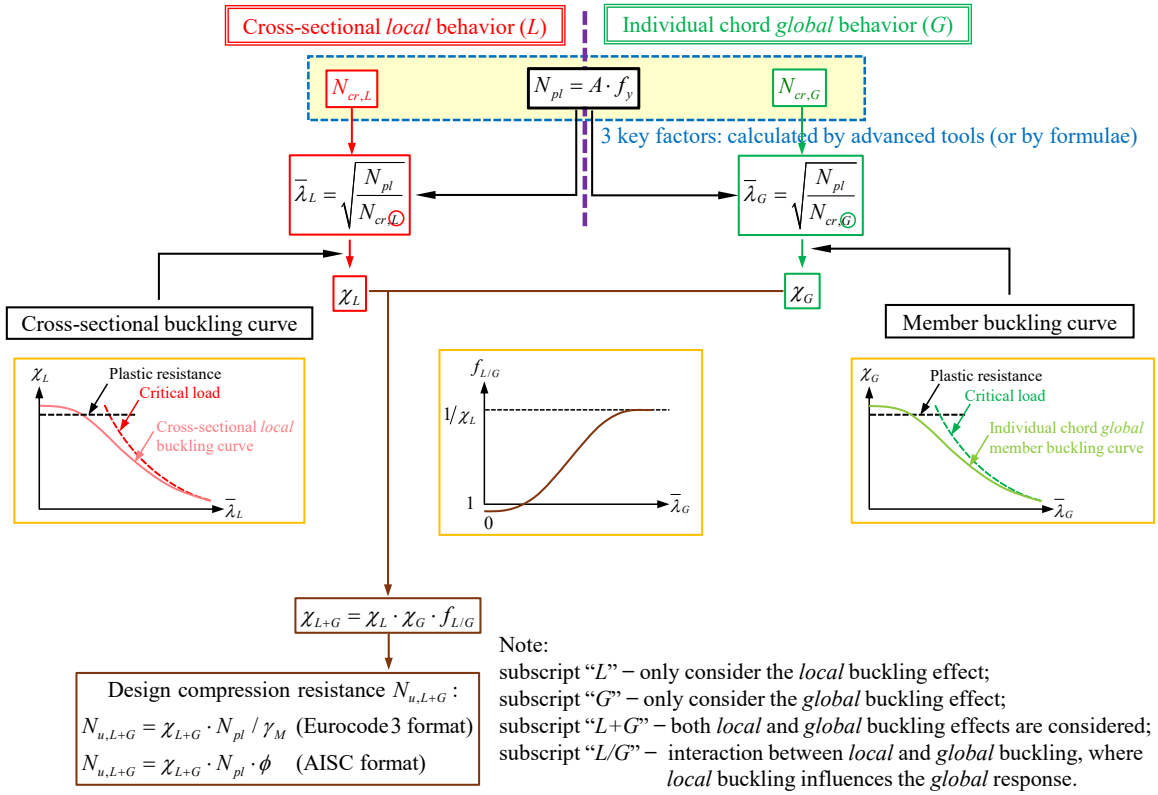

Figure 5.4 O.I.C. design flow chart for L/G interaction mode.

Figure 5.4 illustrates the O.I.C. design flow chart for double interaction mode, specifically for non-built-up members subjected to pure compression load, along with the calculation steps that need to be followed to determine the ultimate resistance. In this case, two buckling modes, i.e., local and global, have a significant effect on the capacity of members. First, the full plastic capacity (N_{pl}) of the member with the gross cross-sectional area $A_g = A$ is calculated using Eq. (5.1).

$$N_{pl} = A \cdot f_y \tag{5.1}$$

Then, the elastic local and global critical loads ($N_{cr,L}$ and $N_{cr,G}$) are determined, which represent the elastic buckling loads under local and global instability, respectively. It should be noted that these three key factors (N_{pl}, $N_{cr,L}$, and $N_{cr,G}$) are either calculated using formulas as addressed in [112], [113], [116], [183] or by advanced tools as proposed in [123]. Next, the generalized local and global relative slenderness ($\bar{\lambda}_L$ and $\bar{\lambda}_G$) are defined to balance the influence of material plasticity and instability caused by geometric non-linearities. The expressions of $\bar{\lambda}_L$ and $\bar{\lambda}_G$ are given in Eq. (5.2).

$$\bar{\lambda}_L = \sqrt{\frac{N_{pl}}{N_{cr,L}}} \quad \text{and} \quad \bar{\lambda}_G = \sqrt{\frac{N_{pl}}{N_{cr,G}}} \tag{5.2}$$

Separate reduction coefficients, specifically for local buckling $\chi_L = f^o(\lambda_L)$ and global buckling $\chi_G = f^o(\lambda_G)$, are determined to account for resistance-stability interactions and imperfections. Note that up to this point in the flowchart, L and G are fully independent; the L/G interaction has not been addressed yet. Finally, the ultimate compression resistance (N_u) is calculated by multiplying the plastic capacity (N_{pl}) by the reduction coefficients and a local/global interaction factor ($f_{L/G}$), which adjusts for the interaction between local and global effects. Therefore, when considering the effect of local/global instability, the ultimate load of a member is obtained from Eq. (5.3).

$$N_{u,L+G} = \chi_{L+G} \cdot N_{pl} \text{ where: } \quad \chi_{L+G} = \chi_L \cdot \chi_G \cdot f_{L/G} \tag{5.3}$$

In Eq. (5.3), χ_{L+G} is the penalty factor to account for the detrimental effects of local and global buckling modes (χ_L and χ_G), and their interactions ($f_{L/G}$). The O.I.C. method offers a comprehensive and unified approach to predict the behaviour of different cross-section types and loading conditions while accounting for the full range of structural responses, from stocky to slender sections. Besides, partial safety factors γ_M or ϕ may be incorporated to account for the reliability aspects of the proposed design equations, following either the European or American format, as shown in Figure 5.4.

5.2.2 Extension of O.I.C. design rules for L/G/B interaction

Following the O.I.C. concept in Figure 5.4, each buckling mode is addressed individually. Laced built-up members – the focus of this study – can exhibit multiple buckling behaviours, including local, global, and built-up buckling, as well as interactions among them (L/G/B interactions). Accordingly, the ultimate load $N_{u,L+G+B}$ is evaluated by Eq. (5.4).

$$N_{u,L+G+B} = \chi_{L+G+B} \cdot N_{pl} \quad \text{where:} \quad \chi_{L+G+B} = \chi_L \cdot \chi_G \cdot \chi_B \cdot f_{L/G/B} \tag{5.4}$$

In Eq. (5.4), χ_{L+G+B} stands as an overall reduction factor accounting for the combined effects of local, global, and built-up buckling. The terms χ_L, χ_G, and χ_B represent the reduction factors corresponding to the isolated (pure) local, global, and built-up buckling modes, respectively, without interaction. The interaction effects among these modes are captured through the factor $f_{L/G/B}$.

As discussed in Section 5.1, the ultimate resistance of laced built-up members may be significantly influenced by L/G/B interaction. Current design standards, such as Eurocode 3 and AISC, treat these interactions differently. Eurocode 3 addresses these effects by assuming that the strength of a built-up member is governed by the global buckling resistance of each individual chord segment between lacing connectors, while local buckling is handled through effective section properties based on section classification. In contrast, AISC treats built-up columns as a unified system, incorporating both global and built-up buckling effects into a modified slenderness ratio. Both standards handle local buckling in a similar manner through section classification and the use of the effective width method. More details on the implementation of these codes are provided in Section 5.3.

Consistent with the AISC approach, this study treats the laced built-up column as a unified system by incorporating the effects of global and built-up buckling into a combined reduction factor χ_{G+B}, while addressing local buckling separately. Therefore, the interaction factor $f_{L/G/B}$ in Eq. (5.4) can be written in the form of Eq. (5.5), where correspondence with the general O.I.C. flow chart is reached through $f_{G/B} = \dfrac{\chi_{G+B}}{\chi_G \cdot \chi_B}$ and $f_{L/GB} = \dfrac{\chi_{L+G+B}}{\chi_L \cdot \chi_{G+B}}$.

$$f_{L/G/B} = f_{L/GB} \cdot f_{G/B} \tag{5.5}$$

In Eq. (5.5), $f_{G/B}$ represents the interaction between global and built-up buckling – specifically, the influence of global buckling on built-up behaviour. The term $f_{L/GB}$ accounts for local interaction effects, capturing the influence of cross-sectional local buckling on the global/built-up buckling response of the member. The proposed O.I.C. design flow chart for L/G/B interaction of laced built-up column under compression load is presented in Figure 5.5. In this figure, the expressions of $\overline{\lambda}_L$ and $\overline{\lambda}_G$ are formulated based on the properties of an individual chord, while $\overline{\lambda}_B$ is calculated considering the properties of the full built-up configuration.

$$\bar{\lambda}_L = \sqrt{\left(\frac{N_{pl}}{N_{cr,L}}\right)_{ch}}\ ,\ \bar{\lambda}_G = \sqrt{\left(\frac{N_{pl}}{N_{cr,G}}\right)_{ch}}\ \text{and}\ \bar{\lambda}_B = \sqrt{\frac{N_{pl}}{N_{cr,B}}} \tag{5.6}$$

Here, N_{pl} at the local and global levels is determined using the gross cross-sectional area of an individual chord (A_{ch}), while N_{pl} at the built-up level is calculated based on the gross cross-sectional area of the entire built-up section (A). The values of $N_{cr,G}$ and $N_{cr,B}$ are defined by Eq. (5.7), where I_{ch} and I are the second moment of area of the individual chord section and the overall built-up section, respectively, and L_G and L_B represent the length of a chord segment between lacing connectors and the total length of the built-up member, respectively.

$$N_{cr,G} = \frac{\pi^2 E I_{ch}}{L_G^2}\ \text{, and}\ N_{cr,B} = \frac{\pi^2 E I}{L_B^2} \tag{5.7}$$

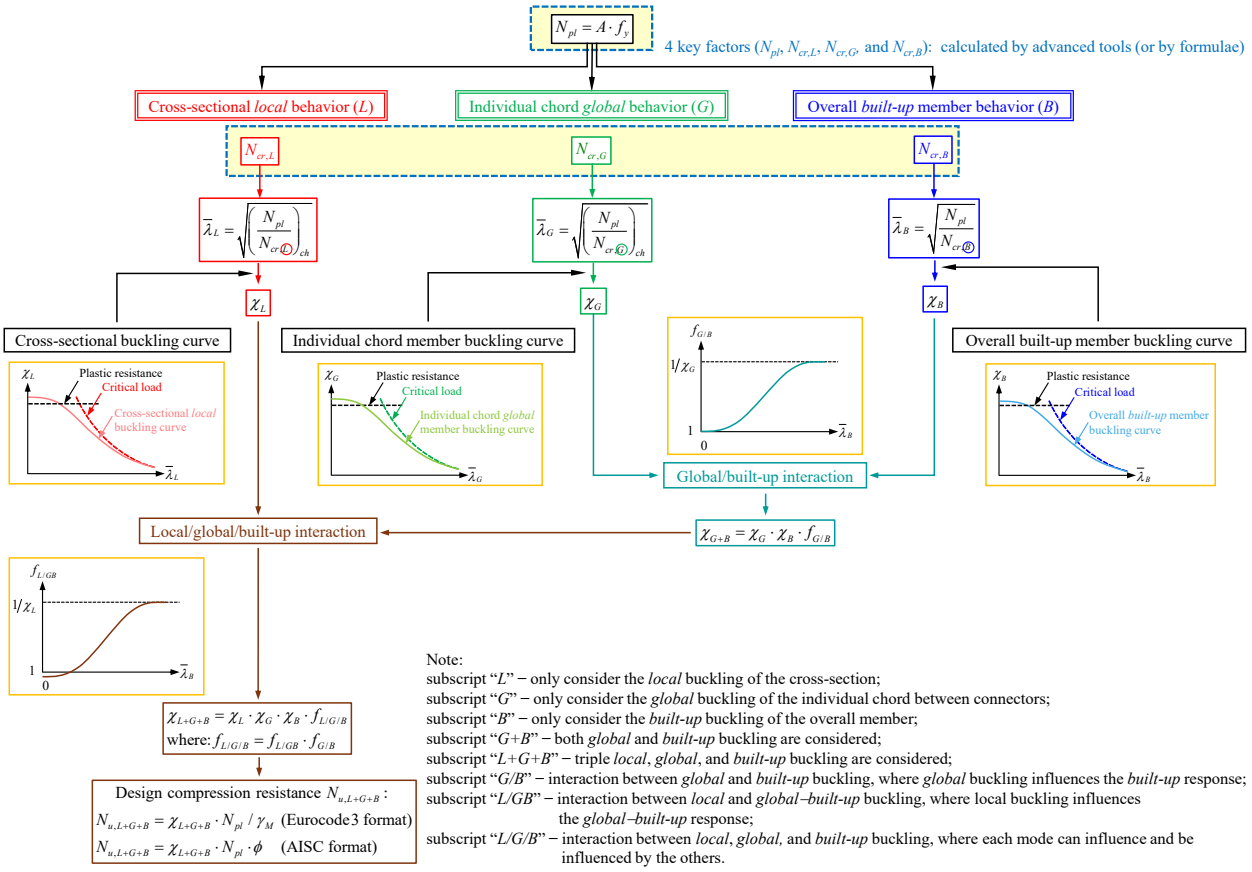

Figure 5.5 Proposed O.I.C. design flow chart for L/G/B interaction.

5.3 Current design rules for built-up members

5.3.1 American Standards (AISC and AAHTO Provisions)

To determine the ultimate resistance of built-up members, the American Standards, specifically AISC [112] and AASHTO Provisions [113], use a theory-based version of the modified slenderness ratio for members. The simplified expression for the slenderness ratio of a built-up member that accounts for shear deformations is expressed as Eq. (5.8).

$$\left(\frac{L_B}{r}\right)_m = \sqrt{\left(\frac{L_B}{r_{yo}}\right)^2 + 0.82\left(\frac{L_G}{r_{yi}}\right)^2} \approx \sqrt{\left(\frac{L_B}{r_{yo}}\right)^2 + \left(\frac{L_G}{r_{yi}}\right)^2} \tag{5.8}$$

This equation is determined for a built-up member with simply support conditions. In Eq. (5.8), L_B / r_{yo} is the slenderness ratio of the built-up member buckling in flexure (built-up buckling), determined using the built-up member length L_B and the radius of gyration of the built-up member r_{yo}. The second term, L_G / r_{yi}, is the slenderness ratio of individual chords in bending around their minor-axis (global buckling) between the lacing connectors where L_G is the distance between lacing connectors and r_{yi} is the radius of gyration of the individual chord. To clearly indicate the mode interaction of both standards, the subscript "*m*" of the modified slenderness of the built-up member is replaced with "G+B". By adopting a similar notation as in the O.I.C. flow chart and substituting Eq. (5.2) into Eq. (5.8), the modified slenderness of the built-up member is represented by Eq. (5.9).

$$\lambda_{G+B} = \sqrt{\lambda_G^2 + \lambda_B^2} \tag{5.9}$$

Details of the built-up member strength prediction in the American Standards are summarized in Table 5.1. Furthermore, the code prescribes to limit the slenderness of the individual chord, λ_G, to 75% of the built-up member slenderness λ_B to reduce the interaction between individual chord buckling and member buckling (G/B interaction), as this interaction can further decrease the member's buckling load, as suggested in the study presented in [103]. Additionally, to account for local buckling of cross-sections, the American Standards use the E.W.M. to assess their sensitivity to local buckling, dividing them into two groups: non-slender and slender sections, for members

subjected to pure compression loads. For cross sections with slender elements, which are affected by local buckling, the effective cross-sectional area A_{eff} must be used instead of the gross area A. In this case, A_{eff} is determined by applying the E.W.M. to calculate the effective width of the slender elements.

5.3.2 Eurocode 3

Compared to the American Standards, Eurocode 3 does not utilize a strength reduction factor when addressing the triple interaction behaviour. Instead, the code focuses on the capacity of the individual chord between the connectors, which is primarily influenced by local and global interactions. To account for the effect of built-up buckling, the code suggests verifying the performance of individual chord in-between the connectors ($N_{u,L+G}$) with the design force ($N_{ch,Ed}$) for each chord, where the force is determined from the applied compression load N_{Ed} and the bending moment M_{Ed} at the mid-height of the overall built-up member. The verification criterion is summarized by Eq. (5.10).

$$\frac{N_{ch,Ed}}{N_{u,L+G}} \leq 1 \tag{5.10}$$

Here, $N_{ch,Ed} = N_{Ed} + M_{Ed} / h_0$ where M_{Ed} / h_0 represents the load resulting from the bending of the overall built-up member and h_0 denotes the distance from chords' centroids. To clearly identify the ultimate resistance of the built-up member as influenced by local, global and built-up buckling, the ultimate strength can be defined when $N_{ch,Ed} / N_{u,L+G} = 1$.

$$N_{u,L+G+B} = N_{Ed} = N_{u,L+G} - \frac{M_{Ed}}{h_0} \tag{5.11}$$

In Eq (5.11), $N_{u,L+G+B}$ shall be calculated iteratively to achieve the condition $N_{ch,Ed} / N_{u,L+G} = 1$. Details of the design procedure are summarized in Table 5.1, where it is clearly seen that the Eurocode 3 design rule is not straightforward to determine the ultimate strength of built-up members affected by local/global/built-up interaction. This indicates that the strength reduction caused by built-up buckling of the overall member is considered independently of local and global buckling effects. Specifically, Eurocode 3 does not account for the interaction of local or global

buckling with built-up buckling behaviour, which may lead to an overestimation of the member's capacity.

5.3.3 Observations

It is clearly observed that the design recommendations provided by the American Standards overlook interactions between global buckling of the chord between connectors and built-up buckling of the overall member, only introducing an additional constraint to minimize this effect (G/B interaction). In contrast, Eurocode 3 considers only the local/global interaction behaviour of the chord between the connectors and fails to account for the built-up member interaction in strength reduction. These limitations may lead to overstrength predictions for built-up members, where the local/global/built-up interaction significantly affects the member's capacity. Therefore, both design approaches are seen to require improvements, particularly in (i) handling global/built-up interactions and (ii) addressing local/global/built-up interactions. As mentioned in the previous section, the O.I.C. design methodology is ideally suited to address both "local/global" and "local/global/built-up" coupled instabilities, as proposed in Section 5.2.2, and provides direct, continuous predictions of resistance, ranging from plastic to slender capacities, potentially incorporating complex interaction behaviour.

Table 5.1 Design procedures for the American Standards and Eurocode 3.

Code	AISC & AASHTO	Eurocode 3
Member slenderness	$\lambda_{G+B}=\sqrt{\lambda_G^2+\lambda_B^2}$; where $\lambda_G/\lambda_B \le 0.75$	$\lambda_G=\sqrt{A_{chh,eff}\cdot f_y / N_{cr,G}}$
Penalty factor	$\chi_{G+B}=\begin{cases}0.658^{\lambda_{G+B}^2} & \lambda_{G+B}\le 1.5\\ 0.877/\lambda_{G+B}^2 & \lambda_{G+B}>1.5\end{cases}$	$\phi_{L+G}=0.5\left[1+\alpha_{G,EC3}\left(\lambda_{L+G}-0.2\right)+\lambda_{L+G}^2\right]$ $\chi_{L+G}=\dfrac{1}{\phi_{L+G}+\sqrt{\phi_{L+G}^2-\lambda_{L+G}^2}}\le 1$
"L+G+B" resistance of member	$N_{u,L+G+B}=\chi_{G+B}\cdot A_{eff,L+G+B}\cdot f_y$	$N_{u,L+G+B}=N_{u,L+G}-M_{Ed}/h_0$; where: $N_{u,L+G}=\chi_{L+G}\cdot A_{ch,eff}\cdot f_y$

5.4 Numerical investigations

5.4.1 Key features and assumptions

Numerical models of laced built-up members were created using the non-linear Finite Element (F.E.) software ABAQUS [156] to perform parametric studies, with appropriate constraints applied to isolate specific buckling modes, as detailed in Section 5.5. These built-up sections consist of two longitudinal columns (chords) positioned either tip-to-tip ([ ]) or back-to-back (] [). The chords are linked by flat lacing bars arranged in an X-pattern (double lacing), with tie-plates reinforcing at both ends. To simulate the main chords, lacing bars and tie-plates, four-node shell elements (S4R) were utilized, as they have been widely employed in previous numerical studies, demonstrating high accuracy [130], [131], [157], [158]. Before performing F.E.-based analyses, a mesh sensitivity study was conducted for Geometrically and Materially Non-linear with Imperfection Analyses (G.M.N.I.A.). As shown in Figure 5.6a, a mesh size equivalent to $1/20^{th}$ of the web dimension of the chords was selected, as it provided an optimal balance between computational efficiency and numerical accuracy for further investigations. Besides, additional hollow beam sections and spring elements were introduced in the web-to-flange regions to (i) represent the actual geometry of the fillet areas, (ii) enhance the torsional rigidity of the section and (iii) prevent local buckling within the fillet radius [127]–[130] (see Figure 5.6b).

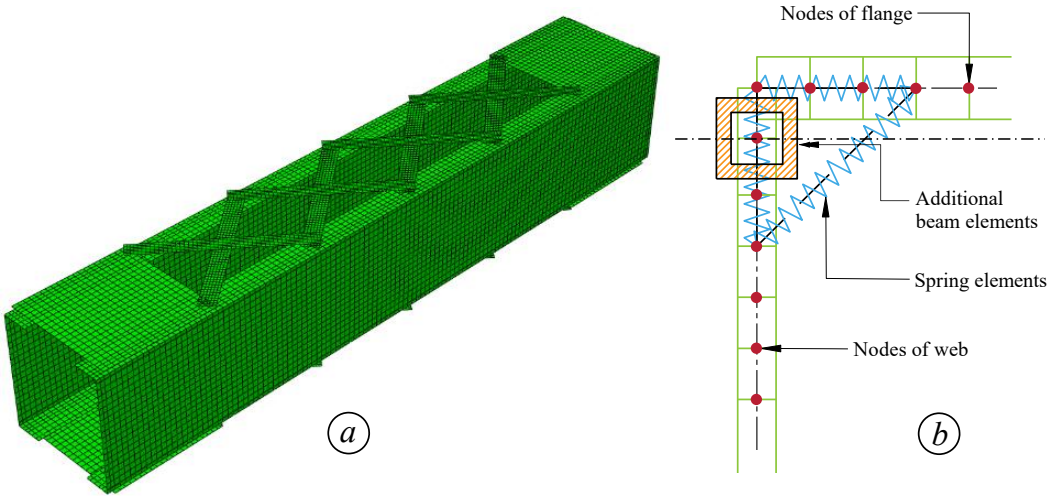

Figure 5.6 Numerical modeling – (a) Typical tip-to-tip arrangement with a double (X) lacing system – (b) Modeling of the area between the web and flange of chord members.

5.4.2 Material characteristics and imperfections

The material model was defined by a quad-linear stress-strain relationship [162]. This relationship was converted into true stress and logarithmic plastic strain and implemented in ABAQUS for validation and subsequent parametric analyses. The material imperfections were introduced in the chords of laced built-up sections by adopting a residual stresses proposed by Beyer et al. [100] for C-sections. In Figure 5.7a, the amplitude of residual stress is defined as $\sigma_{max} = 0.15 f_y$, where the factor $x_1 = 1 + bt_f / (ht_w)$ and $x_2 = 0.5$. Here, b represents the width of the C-section, h is the height of the section, and t_w and t_f are the thickness of web and flange, respectively.

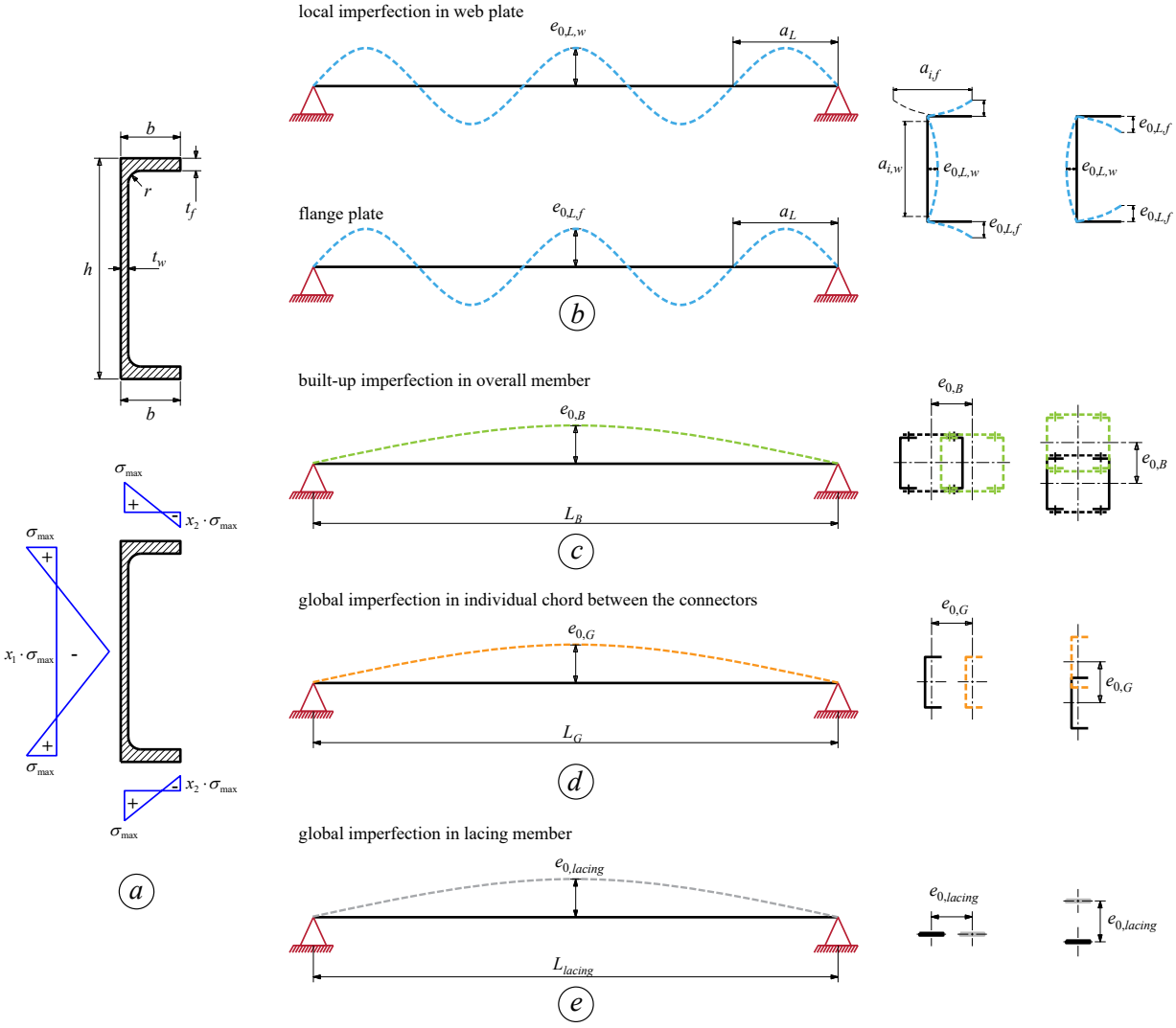

Figure 5.7 Definition of residual stresses and geometrical imperfections.

The local and global geometrical imperfections were incorporated into the F.E. shell models by adjusting node coordinates using sine-wave functions, as recommended in [184], [185]. As depicted in Figure 5.7b, local imperfections were introduced in the flange and web plates where the half-wavelength a_L of local imperfections is assumed to be associated with the web and flange flat (buckling) lengths ($a_{i,w}$ and $a_{i,f}$). These lengths are defined as $a_{i,w} = h - 2\,(t_f + r)$ and $a_{i,f} = 2\,(b - t_w - r)$. The amplitude of local imperfections for the web and flange is defined as $e_{0,L,w}$ and $e_{0,L,f}$, respectively. It should be noted that, to ensure the weakest cross-section remains at the mid-span of the member, an odd number of half-waves is chosen. More details can be found in [186]. According to Eurocode 3, the global imperfection of a built-up member is typically assumed to apply only to the overall structure. However, in this study, global imperfections are independently applied to (i) the overall built-up member, (ii) individual chords between the lacing connections, and (iii) the lacing members. This separation offers a more realistic representation of imperfect built-up members and is particularly effective for isolating the buckling modes of individual components (built-up member, chord, and lacing member), which will be incorporated into the O.I.C. proposal. Furthermore, as presented in Figure 5.7c, to Figure 5.7e, the half-wavelengths for global imperfections in the overall built-up member, individual chords between lacing connectors, and lacing members are defined as L_B, L_G, and L_{lacing}, respectively. Here, L_B, L_G, and L_{lacing} represent the length of the built-up member, the length of an individual chord between lacing connectors, and the length of a lacing bar, respectively. The amplitudes of global imperfections for the overall built-up member, individual chords, and lacing members are defined as $e_{0,B}$, $e_{0,G}$, and $e_{0,lacing}$, respectively. Such imperfections were applied along the minor axis of bending of the members and complemented by residual stress patterns. Section 5.4.4 provides further discussion on the effectiveness of using geometric imperfections suggested by Eurocode 3, as well as the combined geometric imperfections adopted in this study.

5.4.3 Lacing connections and boundary conditions

In most existing truss bridges composed of built-up members, connections between the chord, lacing, and tie-plate are typically riveted or bolted. These connections can be represented using a connection line, as shown in Figure 5.8a. The joint between the lacing member and the chord is modeled as a rivet connection, allowing free rotation within the plane of the lacing system. To achieve this, a kinematic constraint is applied along the connection line to control the movement

of the reference node (Node 1) and the coupling node (Node 2), ensuring they share the same translational and rotational degrees of freedom, except for rotation around the rivet's longitudinal axis (*y'* axis), which remains unconstrained. This modeling allows free rotation about the *y'* axis while fixing relative displacements in other directions. Additionally, the end tie-plates are attached to the chord members using a similar method, as shown in Figure 5.8b. However, in this case, the constraint ensures that all nodes in the connected region undergo the same displacements and rotations.

As presented in Figure 5.9, the built-up column was assumed to be loaded under simply supported conditions, with torsional rotation and translational movement in the *x* and *y* directions restricted at both ends ($u_x = u_y = \theta_z = 0$). Additionally, the axial load was applied at a reference point on one end, while axial displacement was blocked at the opposite end. Both reference points, positioned at the center of gravity of the cross-section, ensured that all nodes at each end shared the same displacement. Their positions could be adjusted translationally and longitudinally by specific distances (e_x and e_z), allowing the model to replicate actual experimental setups for numerical validation, see Section 5.4.4.

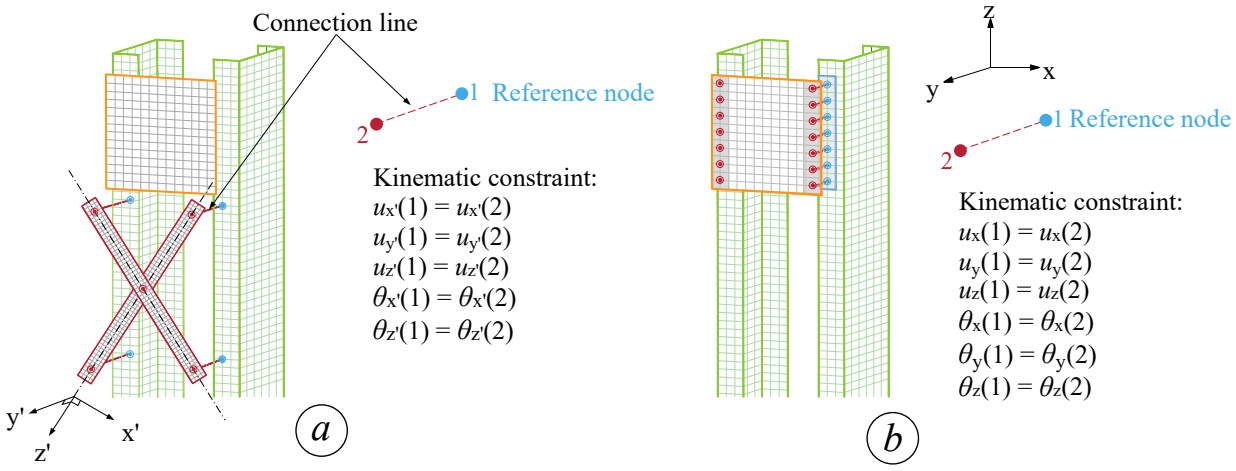

Figure 5.8 Connection modeling of – (a) lacing member to chord – (b) tie-plate to chord.

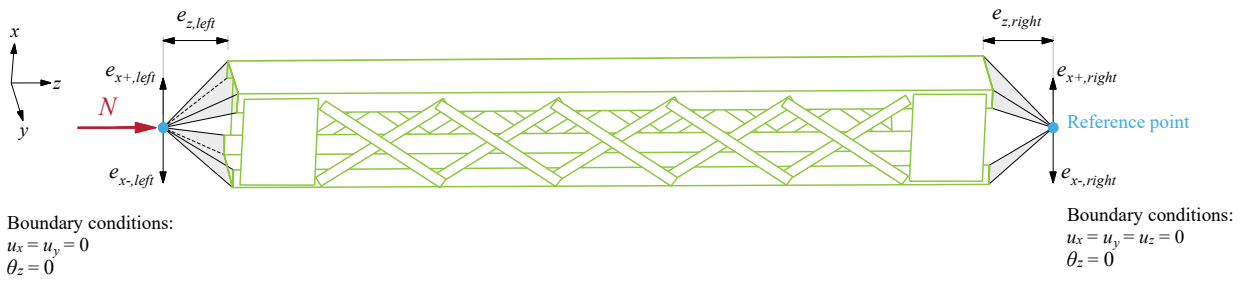

Figure 5.9 Boundary conditions of built-up members.

5.4.4 Validation of numerical models

The F.E. models were validated against experimental test conducted by Kleiser and Uang [148], Lee and Bruneau [150], Bonab et al. [164], and Kalochairetis et al. [165] before being used within parametric studies covering a large range of section dimensions and member slenderness. The test specimens contain both tip-to-tip and back-to-back built-up sections which their chords consisting of C-shaped sections and interconnected by lacing members. Table 5.2 summarizes the dimensions of specimens, member geometries and their material properties measured through coupon tests. Overall, a total of 23 test specimens were considered: three from [148] , seven from [150], nine from [164], and four from [165]. Note that all specimens were loaded under static load, except for test conducted in [148] and [150] where the specimens were loaded under cyclic loads following the ATC-24 loading protocol [163]. Besides, similar numerical validation investigations against these specimens were conducted in [161] showing that the overall difference of ultimate load obtained from the cyclic condition and the static condition is less than 2%. Yet, since this study focuses on the static behaviour of the compressive laced built-up members, all test specimens were subjected to static loading conditions. Note that, in Table 5.2, b_o is the total width of cross section, h is the total height of cross section, L is the total length of member, c is the distance between connector of lacing measured in the axial direction of built-up member, e is end distance from end of built-up member to edge of end tie-plate measured in axial direction of built-up member, b_p is the width of plate, h_p is the length of plate, and t_p is the thickness of plate. As outlined in Table 5.3, all specimens were loaded under simple supports, where the longitudinal distance between the support and the member's end is represented as e_z, and they were subjected to either concentric load ($e_x = 0$) or eccentric compression loads ($e_x \neq 0$). It should be noted that all specimens reported in [164] and [165] were restricted to prevent out-of-plane displacement ($u_x = 0$) at the mid-section.

Given the lack of information on actual measured geometrical imperfections for certain specimens, a sensitivity study was first conducted to identify suitable amplitudes for local imperfections in the cross-section and global geometric imperfections of the overall built-up member, the chord between lacing connector and the lacing member, respectively. These amplitudes were later used in numerical parametric studies which were incorporated into the model as described in Section 5.4.2. Two scenarios for combining these imperfections, namely with respect to their amplitudes, were investigated, including (i) the combination of local imperfections (in the cross-section) and global imperfections (of the overall built-up member), as suggested by Eurocode 3, i.e., $e_{0,L} + e_{0,B}$ (Case A), and (ii) the combination of local imperfections (in the cross-section), global imperfections (of the overall built-up member), global imperfections of the chord between connector and global imperfections of the lacing member, i.e., $e_{0,L} + e_{0,B} + e_{0,G} + e_{0,lacing}$ (Case B). For both cases, the amplitude of local imperfections was scaled based on the halfwave length, amplified by a factor of 1 / 200, as suggested by Eurocode 3 Part 1.5 [183], [184], [159]. Specifically, $e_{0,L} = a_L$ / 200, where the halfwave length is taken as $a_L = (a_{i,w} + a_{i,f})$ / 2. This 1 / 200th amplitude of the flat width was also adopted for open and hollow steel section [124], [131], [185], [159], [187], [188] in previous experimental and numerical studies, showing suitable for local imperfection amplitudes.

As recommended by Eurocode 3, the amplitude of global imperfections of the overall built-up member was set to 1 / 500th of the member's length in Case A. Therefore, only one amplification factor $e_{0,B}$ as given in Eq. (5.12) was considered. Yet, in Case B, three global amplitudes (1 / 500, 1 / 1000, and 1 / 1500) were investigated, as defined in Eq. (5.13).

$$e_{0,B} = \frac{L_B}{500} \tag{5.12}$$

$$\text{(i)}\ e_{0,B} = \frac{L_B}{500}, \quad e_{0,G} = \frac{L_G}{500}, \quad e_{0,lacing} = \frac{L_{lacing}}{500}$$

$$\text{(ii)}\ e_{0,B} = \frac{L_B}{1000}, \quad e_{0,G} = \frac{L_G}{1000}, \quad e_{0,lacing} = \frac{L_{lacing}}{1000} \tag{5.13}$$

$$\text{(iii)}\ e_{0,B} = \frac{L_B}{1500}, \quad e_{0,G} = \frac{L_G}{1500}, \quad e_{0,lacing} = \frac{L_{lacing}}{1500}$$

Table 5.3 presents the $N_{u,FE}$ / $N_{u,test}$ ratios of the ultimate load obtained from F.E. analyses compared to the test results. As shown in the "Global imperfection factor" column, the loads derived from the F.E. models show reasonable agreement with the test results, with an average $N_{u,FE}$ / $N_{u,test}$ ratio of 0.98 and a Coefficient of Variation (C.o.V.) of 6.8% for Case A. It is important to note that the results in Case A are based on the combination of local imperfections of the cross-section and global imperfections of the overall built-up member, specifically with a_L / 200 and L / 500. As expected, adopting a smaller amplification factor for the global imperfection results in a higher member capacity. This is clearly illustrated in Case B, where the $N_{u,FE}$ / $N_{u,test}$ ratio steadily increases for all specimens as the global imperfection amplitude decreases. When combining local imperfections with global imperfections of the overall built-up member, the chord between lacing and the lacing member, the results tend to be more conservative when maintaining the same global amplification factor (1 / 500) as in Case A, with the average $N_{u,FE}$ / $N_{u,test}$ ratio reduced to 0.94 and a C.o.V. of 7.0%. Additionally, for Case B, the results become unconservative when the global amplification factor is set to 1 / 1500, with an average strength prediction approximately 8% higher than in Case A. However, the global amplification factor of 1 / 1000 shows an improvement, with an average $N_{u,FE}$ / $N_{u,test}$ ratio of approximately 0.99 and a C.o.V. of 6.6%.

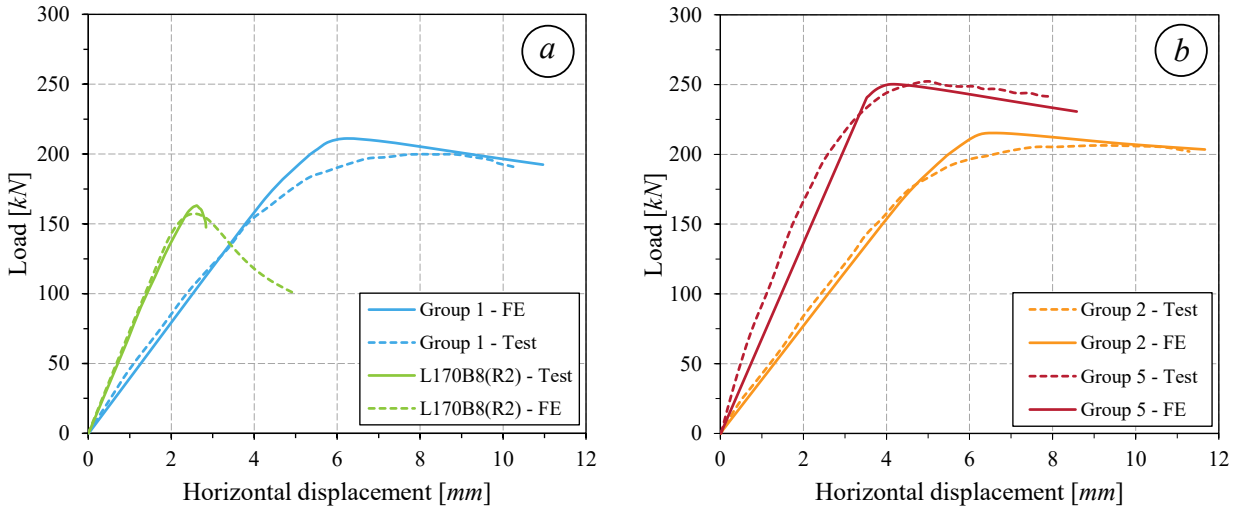

Figure 5.10 Load-displacement curves for – (a) specimens L170B8(R2) and Group 1 – (b) specimens Group 2 and Group 5, reported in [164] and [165].

As illustrated in Figure 5.10, the F.E. models effectively represent the initial stiffness, ultimate resistance, and post-peak behaviour of the specimens, as shown in the load-displacement curves

for L170B8(R2), Group 1, Group 2 and Group 4 specimens. Besides, Figure 5.11 shows that the numerical failure modes of Specimens 1 and 3 closely correspond to the experimental ones.

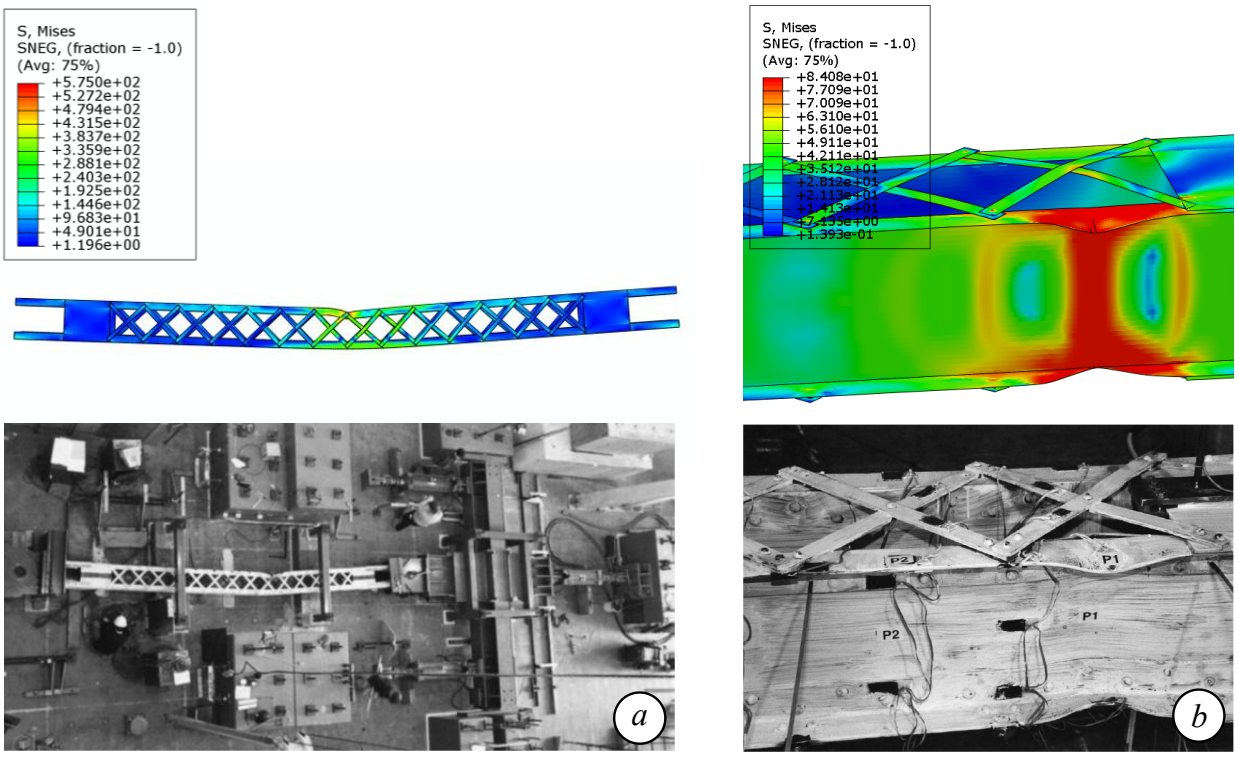

Figure 5.11 Comparison between F.E. and test failure modes for – (a) Specimen 3 – (b) Specimen 1 reported in [148] (Von Mises stress is in *ksi*).

A strong correlation between F.E. predictions and test results is observed for all specimens when using a combination of local imperfections ($e_{0,L} = a_L / 200$), global imperfections of the overall built-up member ($e_{0,B} = L_B / 1000$), global imperfections of the chord between connectors ($e_{0,G} = L_G / 1000$) and global imperfections of the lacing member ($e_{0,lacing} = L_{lacing} / 1000$). Consequently, this combination was selected for further parametric studies. These various results confirm that the developed numerical models can accurately predict ultimate resistances and effectively capture the buckling behaviour of laced built-up members, making them suitable for further parametric analyses. Specifically, under this selected imperfection set, the $N_{u,FE} / N_{u,test}$ ratio ranges from 0.88 to 1.11, as summarized in Table 5.3.

Table 5.2. Sections, cross-section dimensions, profiles, and material properties of each component of test specimens.

Specimens	Sections and geometric dimensions		Main chords			Lacing system and end tile-plates	
	Section	Cross-section dimensions	Profile / F_y / F_u [MPa]				
		b_o x h x L x c x e [mm]	Channel	Angle	Web plate [PL b_p x t_p, mm]	Lacing [PL b x t_p, mm]	End tile-plate [PL b_p x h_p x t_p, mm]
Specimen 1 [148], [149]	4L+2P	437 x 337 x 7146 x 365 x 530	-	L76x76x8 / 338 / 489	PL 330x8 / 324 / 478	PL 38x8 / 327 / 484	PL 441x553x7 / 327 / 484
Specimen 2 [148], [149]							
Specimen 3 [148], [149]							
By8-60 [150]	4L+2P	121 x 121 x 2445 x 108 x 0	-	L25x25x3.2 / 361 / 475	PL 121x3.3 / 323 / 384	PL 19x3.2 / 323 / 384	PL 121x495x9.5 / 253 / 349
By8-120 [150]		121 x 121 x 5035 x 108 x 0		L25x25x3.2 / 361 / 475	PL 121x3.3 / 323 / 384	PL 19x3.2 / 323 / 384	PL 121x495x9.5 / 253 / 349
By16-60 [150]		133 x 133 x 1838 x 95 x 0		L51x51x3.2 / 352 / 470	PL 133x3.3 / 323 / 384	PL 24x3.2 / 323 / 384	PL 133x560x9.5 / 253 / 349
By16-120 [150]		133 x 133 x 3835 x 95 x 0		L51x51x3.2 / 352 / 470	PL 133x3.3 / 323 / 384	PL 24x3.2 / 323 / 384	PL 133x560x9.5 / 253 / 349
Bx8-120 [150]		114 x 76 x 3683 x 102 x 0		L25x25x3.2 / 361 / 475	PL 76x3.3 / 323 / 384	PL 19x3.2 / 323 / 384	PL 114x394x9.5 / 253 / 349
Bx16-60 [150]		165 x 105 x 2432 x 133 x 0		L51x51x3.2 / 352 / 470	PL 105x3.3 / 323 / 384	PL 24x3.2 / 323 / 384	PL 165x527x9.5 / 253 / 349
Bx16-120 [150]		165 x 105 x 5055 x 133 x 0		L51x51x3.2 / 352 / 470	PL 105x3.3 / 323 / 384	PL 24x3.2 / 323 / 384	PL 165x527x9.5 / 253 / 349
L140B8(R1) [164]	2C	80 x 60 x 1400 x 56 x 0	UNP60 / 278 / 405	-	-	PL 10x3 / 278 / 405	PL 200x80x10 / 278 / 405
L140B8(R2) [164]		80 x 60 x 1400 x 56 x 0					
L140B8(R3) [164]		80 x 60 x 1400 x 56 x 0					
L140B10(R1) [164]		100 x 60 x 1400 x 56 x 0					
L170B7(R1) [164]		70 x 60 x 1700 x 56 x 0					
L170B7(R2) [164]		70 x 60 x 1700 x 56 x 0					
L170B7(R3) [164]		70 x 60 x 1700 x 56 x 0					
L170B8(R2) [164]		80 x 60 x 1700 x 56 x 0					
L170B8(R3) [164]		80 x 60 x 1700 x 56 x 0					
Group 1 [165]	2C	218 x 60 x 2020 x 400 x 0	UNP60 / 338 / 435	-	-	L25x25x3	-
Group 2 [165]		218 x 60 x 2020 x 200 x 0	UNP60 / 338 / 435				
Group 4 [165]		218 x 60 x 2020 x 400 x 0	UNP60 / 335 / 435				
Group 5 [165]		218 x 60 x 2020 x 400 x 0	UNP60 / 302 / 435				

Table 5.3. Summary of F.E. vs. test ultimate load of test specimens.

References	Specimens	Arrangements	Loading positions				Ultimate loads and ratios				
			$e_{x,left}$ $[mm]$	$e_{z,left}$ $[mm]$	$e_{x,right}$ $[mm]$	$e_{z,right}$ $[mm]$	$N_{u,test}$ $[kN]$	$N_{u,FE}$ / $N_{u,test}$ [-] Global imperfection amplitude			
								Case A	Case B		
								1 / 500	1 / 500	1 / 1000	1 / 1500
Kleiser and Uang [148]	Specimen 1	] [	381	400	0	400	928.79	0.96	0.94	1.05	1.11
	Specimen 2		127	400	0	400	1633.83	1.01	0.97	0.95	1.01
	Specimen 3		0	400	0	400	2885.12	0.95	0.91	0.98	1.05
Lee and Bruneau [150]	By8-120	] [	0	0	0	0	295.81	0.95	0.90	0.94	0.99
	By16-60		0	0	0	0	521.64	0.91	0.87	0.93	0.99
	By16-120		0	0	0	0	447.00	0.98	0.92	0.95	1.18
	Bx8-60		0	0	0	0	267.16	1.05	1.01	1.11	1.17
	Bx8-120		0	0	0	0	213.51	1.11	1.04	1.07	1.15
	Bx16-60		0	0	0	0	506.87	1.09	0.99	1.01	1.09
	Bx16-120		0	0	0	0	409.50	1.02	0.98	1.10	1.17
Bonab et al. [164]	L140B8(R1)	] [	0	140	0	140	204.76	0.97	0.92	0.98	1.07
	L140B8(R2)		0	140	0	140	183.86	1.01	0.97	1.01	1.09
	L140B8(R3)		0	140	0	140	159.09	1.01	0.96	1.02	1.08
	L140B10(R1)		0	95	0	95	289.05	0.88	0.84	0.88	0.90
	L170B7(R1)		0	95	0	95	151.95	0.91	0.85	0.90	0.91
	L170B7(R2)		0	95	0	95	135.19	0.88	0.82	0.89	0.92
	L170B7(R3)		0	95	0	95	124.32	0.91	0.86	0.96	0.97
	L170B8(R2)		0	95	0	95	162.40	0.94	0.89	0.98	0.95
	L170B8(R3)		0	95	0	95	146.29	0.97	0.91	0.96	0.98
Kalochairetis et al. [165]	Group 1	[ ]	100	162.5	100	162.5	200.00	1.06	1.02	1.06	1.10
	Group 2		100	162.5	100	162.5	206.00	1.05	1.01	1.06	1.11
	Group 4		100	162.5	-80	162.5	230.00	1.07	1.04	1.07	1.13
	Group 5		50	162.5	50	162.5	247.00	1.01	0.98	1.01	1.07
							Mean	0.98	0.94	0.99	1.06
							C.o.V.	6.8 %	7.0 %	6.6 %	8.3 %
							Min.	0.88	0.82	0.88	0.90
							Max.	1.11	1.04	1.11	1.18

[ ] = tip-to-tip arrangement

] [= back-to-back arrangement

5.4.5 Parametric studies

By using the validated F.E. models, comprehensive parametric studies were conducted to examine the potential effects of chord arrangements, section dimensions, and section/member slenderness on the cross-sectional and member resistance of laced built-up columns. The built-up section consisted of two hot-rolled C-shaped sections interconnected by double (X) flat lacing bars at intermediate spans and tie plates at both ends. These sections were arranged either tip-to-tip or back-to-back, with the lacing bars assumed to be connected to both chords using rivet connections. Each component of the built-up columns, including chords, lacing members, and tie plates, is assumed to have similar material properties with steel grade CSA G40.4 and a nominal yield strength f_y = 230 MPa. This grade was selected to represent a structural steel commonly used in Canada during the 1950s, ensuring consistency with the design standards and practices of that period, even though it is not aligned with current specifications. Moreover, studies [126], [127], [131] have shown that the steel grade has a relatively low influence on the buckling curve selection for hot-rolled and welded members, supporting this assumption.

A total of 300 channels and C-shapes sections were taken from standardized hot-rolled sections [189]–[191] as well as invented sections were considered for studying the local behaviour of cross-sections, the global behaviour of the chord between connectors, the built-up behaviour of the overall member and the local/global/built-up interaction behaviour. The properties of the invented C-sections were based on those of angle sections – two angles connected by a continuous plate forming a C-shape (Figure 5.1d). Note that the angle-based section serves only as a reference; the models represent equivalent C-sections with similar properties, not the angle sections themselves. For all sections, the height (h) varied from 152.5 *mm* to 1021 *mm*, while the width (b) ranged from 30.5 *mm* to 152.4 *mm*. The sections included both non-slender and slender elements, with the slenderness of the web plate (h / t_w) and flange plate (b / t_f) ranging from 6 to 96.95 and 4 to 10.7, respectively. It should be noted that the lacing members were designed to prevent failure before the built-up member fails, and the minimum inclination angle of the lacing relative to the axis of the built-up member was 25 degrees. Overall, approximately 5 000 G.M.N.I.A. simulations were conducted to determine the ultimate loads of the columns and the corresponding buckling reduction coefficients χ_L, χ_G, χ_B, and χ_{L+G+B}.

5.5 Proposed O.I.C. design rules

5.5.1 Local, global, and built-up member buckling curves

Using the numerical results obtained from the parametric studies discussed in Section 5.4, the proposed design buckling curves for cross-section local behaviour, global behaviour of the chord between the connectors and built-up behaviour of the overall member are presented in Figure 5.12 and Figure 5.13. Both figures plot the obtained results in "O.I.C. format", where the horizontal axis corresponds to the cross-section and members relative slenderness ($\overline{\lambda}_L$, $\overline{\lambda}_G$, and $\overline{\lambda}_B$) associated with the corresponding reduction factors χ_L, χ_G, and χ_B.

Local buckling:

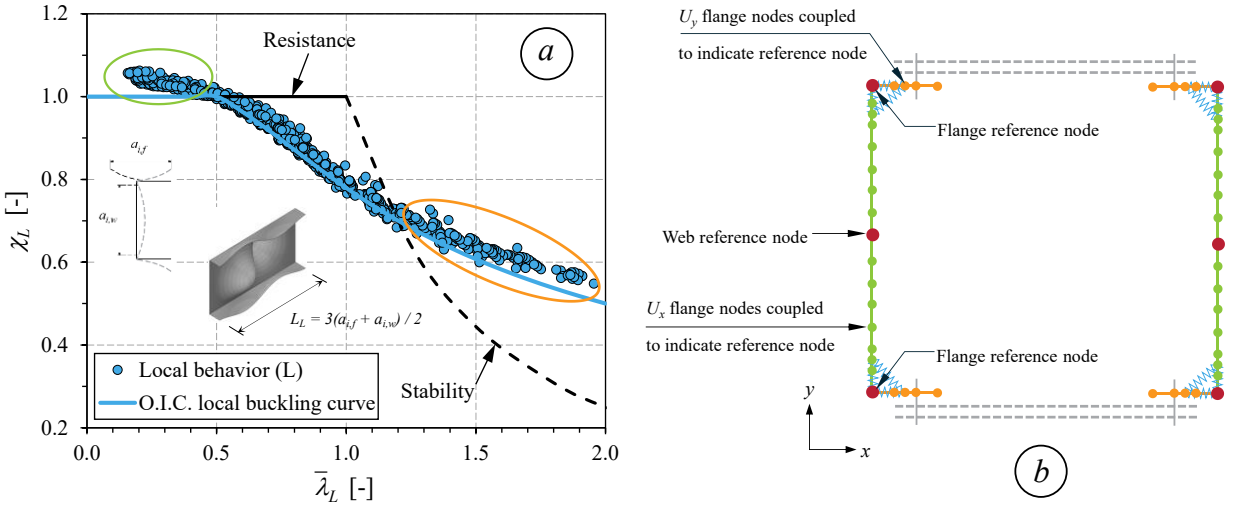

Figure 5.12 (a) O.I.C. buckling curve for cross-section resistance – (b) Plate buckling restraint.

Figure 5.12a illustrates the *local buckling behaviour* of the cross-section obtained from F.E. results in a $\chi_L - \overline{\lambda}_L$ format, along with two specific lines: (i) a horizontal solid line ($\chi_L = 1$), which indicates the plastic resistance, and (ii) a parabolic dashed line ($\chi_L = 1/\overline{\lambda}_L^2$), which represents the limit elastic plate buckling where the design assumes an ideal plate free of imperfections. As can be seen, across all range of λ_L, values of the penalty factor χ_L differ by less than 5%, indicating that a single local buckling curve is sufficiently accurate and appropriate for use. Additionally, as indicated in the orange ellipse in Figure 5.12a, most slender C-shaped cross-sections experience post-buckling effects, resulting in a χ_L value exceeding the stability limit. Furthermore, most

compact sections exceed their plastic capacity due to the benefit of strain-hardening effects (see green ellipse).

Global buckling:

To isolate the *pure global buckling* behaviour of a chord between connectors, a corresponding F.E. model was developed for a single chord with a total length of L_G, where L_G is the distance between lacing connections. To prevent local buckling in the cross-section and isolate global buckling, the vertical displacement (U_y) of each node along the flange plates was constrained to match the displacement of the reference node located at the corner of the section, while the horizontal displacement (U_x) of each node along the web plate was constrained to match the value of the reference node at the midpoint. Figure 5.12b illustrates the plate buckling constraint for a laced built-up member composed of two main chords. Note that in Figure 5.12b, a similar constraint is applied to isolate the global buckling of the chord between connectors, but only one chord is considered.

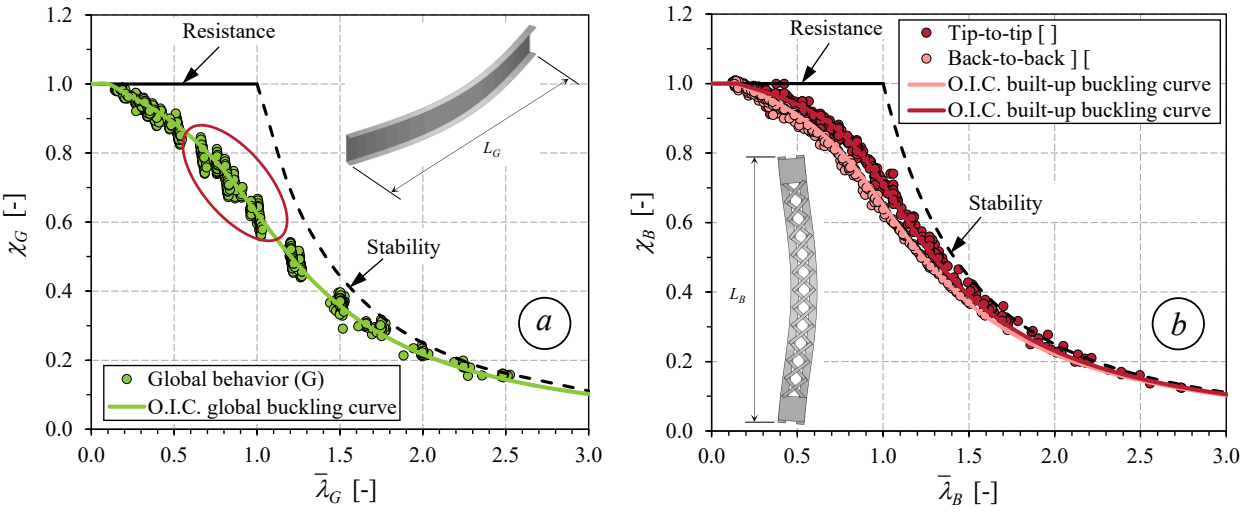

Figure 5.13 O.I.C. buckling curves for – (a) global buckling of chords between the connectors – (b) built-up buckling of the overall member.

The proposed O.I.C. buckling curve for global buckling of the chord between the connectors is presented in Figure 5.13a. The F.E. data exhibits a slight dispersion, particularly for members with $\overline{\lambda}_G$ varying from 0.5 to 1.0, where the effects of geometrical imperfections and residual stresses are more pronounced. This is clearly illustrated by the red ellipse in Figure 5.13a, where the deviation, approximately 8%, arises from the varying section dimensions of the C-shaped profiles

considered in this study. As expected, the resistance of long columns, specifically for $\overline{\lambda}_G > 1.5$ is primarily governed by global instability, with minimal influence from geometrical imperfections. This is evidenced by the fact that the results closely align with the "stability" limit line.

Built-up buckling:

Further, to ensure that only the *built-up buckling* of the overall member governs the behaviour, the F.E. models were complemented with 2 additional constraints to prevent (i) local buckling of the cross-section, as indicated in Figure 5.12b, and (ii) global buckling of the chord between the connectors (i.e., not within the cross-section). This was achieved by limiting the spacing of the lacing connectors, L_G, so that the global slenderness $\overline{\lambda}_G$ remains close to the ideal slenderness $\overline{\lambda}_{G,0}$, ensuring that $\chi_G \approx 1$. This implies that the chord retains its full axial capacity, with no significant loss of strength due to buckling between connectors. The F.E. results for the built-up buckling of the overall member are depicted in Figure 5.13b. Similarly, for built-up member resistance, the effects of residual stresses and imperfections are negligible in long members. Yet, clear trends can be observed for short and intermediate column lengths ($\overline{\lambda}_B < 1.5$) owing to different chord arrangements (tip-to-tip vs back-to-back). As illustrated in Figure 5.13b, the adoption of two separate buckling curves is therefore deemed fully appropriate, with an excellent level of consistency achieved, as indicated by the very limited scatter with respect to each curve.

The proposed O.I.C. design equations for local, global and built-up member buckling are presented in Table 5.4, in extension to the Ayrton-Perry format [192]. Each equation addresses a distinct buckling mode (local, global, or built-up), in order to evaluate their contributions separately, i.e., at this point, no coupling is accounted for. In accordance with this format, the proposed buckling curves for local buckling of the cross-section, global buckling of the chord between connectors and built-up buckling of the overall member are illustrated in Figure 5.12a, Figure 5.13a, and Figure 5.13b, respectively. These curves were precisely optimized by defining a set of key parameters: $\overline{\lambda}_0$, δ, and α; $\overline{\lambda}_0$ relates to the length of the "plateau" where χ = 1.0, δ considers any post-buckling strength and α is the generalized imperfection factor. For each buckling mode, α and $\overline{\lambda}_0$ are successively denoted as α_L, α_G, and α_B and $\overline{\lambda}_{0,L}$, $\overline{\lambda}_{0,G}$ and $\overline{\lambda}_{0,B}$; they lead to reduction factors (χ_L, χ_G, and χ_B) for each buckling mode. As a particular point regarding built-up buckling in the plane of the lacing systems, the imperfection factor for the back-to-back section

is greater than that of the tip-to-tip section, indicating that the proposed buckling curve for the back-to-back section is lower than that for the tip-to-tip section.

Table 5.4. Design procedure and key parameters for local, global, and built-up member buckling curves.

Buckling resistance	Key parameters	Reduction factor based on Ayrton-Perry format
Local buckling (L)	$\bar{\lambda}_{0,L} = 0.5$ $\alpha_L = 0.125$ $\delta_L = 0.7$	$\phi_L = 0.5 \cdot \left[1 + \alpha_L \left(\bar{\lambda}_L - \bar{\lambda}_{0,L} \right) + \bar{\lambda}_L^{\delta} \right]$ $\chi_L = \frac{1}{\phi_L + \sqrt{\phi_L^2 - \bar{\lambda}_L^{\delta}}} \leq 1$
Global buckling (G)	$\bar{\lambda}_{0,G} = 0.1$ $\alpha_G = 0.25$ $\delta_G = 2.0$	$\phi_G = 0.5 \cdot \left[1 + \alpha_G \left(\bar{\lambda}_G - \bar{\lambda}_{0,G} \right) + \bar{\lambda}_G^2 \right]$ $\chi_G = \frac{1}{\phi_G + \sqrt{\phi_G^2 - \bar{\lambda}_G^2}} \leq 1$
Built-up buckling (B)	$\bar{\lambda}_{0,B} = 0.15$ $\alpha_B = \begin{cases} 0.14 \text{ for tip-to-tip section [ ]} \\ 0.22 \text{ for back-to-back section] [} \end{cases}$ $\delta_B = 2.0$	$\phi_B = 0.5 \cdot \left[1 + \alpha_B \left(\bar{\lambda}_B - \bar{\lambda}_{0,B} \right) + \bar{\lambda}_B^2 \right]$ $\chi_B = \frac{1}{\phi_B + \sqrt{\phi_B^2 - \bar{\lambda}_B^2}} \leq 1$

5.5.2 Interaction factor $f_{L/G/B}$

In Section 5.5.1, the cross-section reduction factor (χ_L) and the member buckling reduction factors (χ_G and χ_B) were derived independently, without considering possible interactions between local, global, and built-up buckling. According to Eq. (5.5) and Figure 5.5, once local, global, and built-up buckling have been characterized separately, their potential interactions are incorporated through a coupling factor $f_{L/G/B}$. In this respect, a stepwise approach was adopted. First, the interaction between global and built-up buckling modes was characterized by coupling factor $f_{G/B}$. Once this interaction is determined, the local buckling interaction with global-built-up response can be incorporated by introducing an additional coupling factor $f_{L/GB}$. Values of $f_{G/B}$ and $f_{L/GB}$ can be obtained from the F.E. results of the parametric studies using Eq. (5.5), where χ_{G+B} is determined by applying constraints to prevent local buckling, while χ_{L+G+B} is obtained by relaxing all constraints. Their relationships with $\bar{\lambda}_B$ are depicted in Figure 5.14.

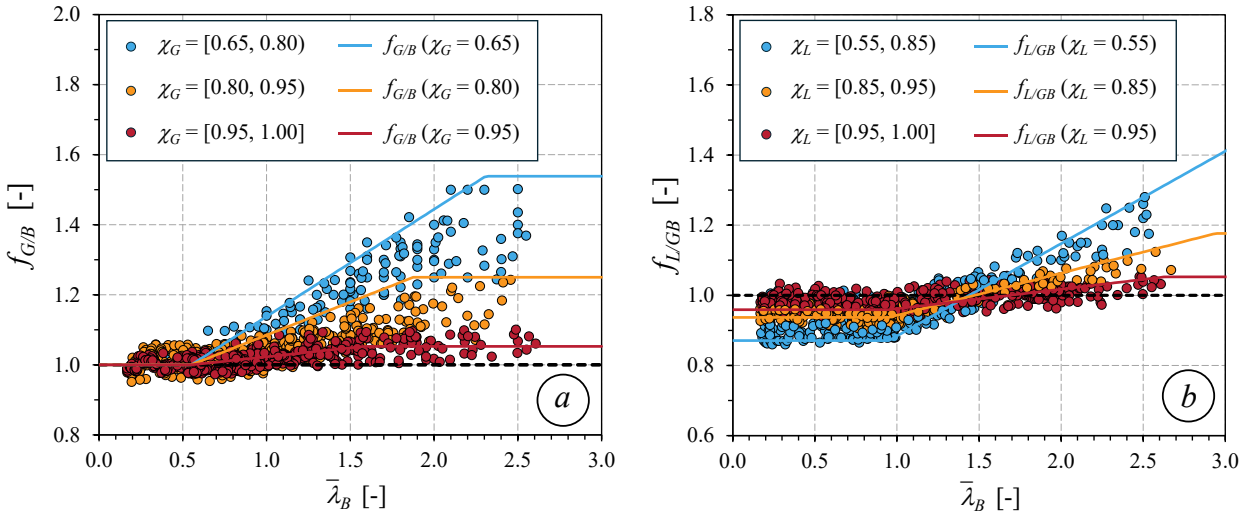

Figure 5.14 Interaction factors when considering – (a) Global/built-up interaction $f_{G/B}$ – (b) Local and global–built-up interaction $f_{L/GB}$.

Overall, Figure 5.14 shows that $f_{G/B}$ and $f_{L/GB}$ vary with the overall slenderness of the built-up member $\bar{\lambda}_B$. Figure 5.14a illustrates the interaction results when considering global/built-up interaction. The scatter plot illustrates the relationship $f_{G/B} = \chi_{G+B} / (\chi_G \cdot \chi_B)$, assuming local buckling is ignored. Here, $f_{G/B}$ represents the influence of global buckling on built-up buckling (G/B interaction), where χ_{G+B} is the reduction factor accounting for the combined global and built-up buckling effects. The terms χ_G and χ_B denote the individual reduction factors from pure global buckling of chord between connectors and from built-up buckling, respectively. If $f_{G/B} < 1$, the interaction is adverse, meaning the combined effect reduces the strength more than expected. When $f_{G/B} \approx 1$, the two buckling mode act independently, so $\chi_{G+B} \approx \chi_G \cdot \chi_B$. If $f_{G/B} > 1$, the interaction is favorable, often occurring when global buckling of the chord between connectors has a minimal or negligible effect – leading to $f_{G/B} \approx 1/\chi_G$. From these cases, the interaction factor satisfies the condition $1 < f_{G/B} < 1/\chi_G$, defining the range where the interaction is favorable but less than the limiting case dominated solely by global buckling. Trilinear, conservative design equations for $f_{G/B}$ are given in Eq. (5.14), and their bounds are validated against numerical results in Figure 5.14a.

$$f_{G/B}=\begin{cases}1 & \bar{\lambda}_B \le 0.55\\ \dfrac{\bar{\lambda}_B-0.55}{1.5/\chi_G-0.55}\left(1/\chi_G-1\right)+1 & 0.55<\bar{\lambda}_B\le 1.5/\chi_G\\ 1/\chi_G & \bar{\lambda}_B>1.5/\chi_G\end{cases} \tag{5.14}$$

After defining the global/built-up interaction, the effect of local buckling can be considered by introducing an additional coupling factor, $f_{L/GB}$, which accounts for the influence of local buckling on the built-up behaviour, the latter encompassing global buckling. The corresponding numerical results are presented in Figure 5.14b along with the proposed design equation for the $f_{L/GB}$ factor:

$$f_{L/GB}=\begin{cases}k_L=0.22\cdot\chi_L+0.75 & \bar{\lambda}_B \le 0.95\\ \dfrac{\bar{\lambda}_B-0.95}{2.5/\chi_L-0.95}\left(1/\chi_L-k_L\right)+k_L & 0.95<\bar{\lambda}_B\le 2.5/\chi_L\\ 1/\chi_L & \bar{\lambda}_B>2.5/\chi_L\end{cases} \tag{5.15}$$

The function $f_{L/GB}$ is defined as a piecewise tri-linear interpolation with respect to the normalized relative slenderness $\bar{\lambda}_B$. For $\bar{\lambda}_B \le 0.95$, $f_{L/GB}$ remains constant at k_L, a factor that quantifies the adverse influence of local buckling on built-up behaviour. In slender sections, where this effect is significant, k_L typically drops to around 0.75 and increases up to 0.97 as the section becomes stockier. Within the interval $0.95<\bar{\lambda}_B\le 2.5/\chi_L$, the $f_{L/GB}$ transitions linearly from k_L to $1/\chi_L$, ensuring continuity and smoothness, and remains constant at $1/\chi_L$ for $\bar{\lambda}_B > 2.5/\chi_L$.

In Figure 5.14b, it is revealed that for short columns ($\bar{\lambda}_B \le 0.55$), $f_{L/GB}$ remains below unity due to a significant impact of local buckling on the interactions. Similarly, for intermediate length columns ($\bar{\lambda}_B \le 0.95$), the built-up column is also affected by strong local interactions. This effect is more pronounced for built-up members with slender sections, i.e., sections with small χ_L values, where the interaction of local buckling results in relatively lower load-carrying capacities. Although $f_{L/G/B}$ continues to decrease as χ_L decreases, yet, in some cases, it tends to approach unity, particularly for compact sections where $\chi_L \approx 1$. This effect is accounted for by the coefficient k_L, as proposed in Eq. (5.15).

Besides, it is noticed that the interaction effect of local buckling is less pronounced for built-up members with high relative slenderness ratios $\overline{\lambda}_B$. Therefore, for very long members, $f_{L/GB}$ is set to tend to $1/\chi_L$ in order to disregard the impact of local buckling. Additionally, the local interaction behaviour should be accounted for intermediate length columns to fulfil the condition: $k_L < f_{L/GB} < 1/\chi_L$. As illustrated in Figure 5.14b, the proposed $f_{L/GB}$ expressions are compared to the F.E. results. It should be noted that each data point corresponds to their own $f_{L/GB}$ value. Here, only three upper bounds (safe) for $f_{L/GB}$ are presented.

Once the $f_{G/B}$ and $f_{L/GB}$ factors are defined, the local/global/built-up interaction factor $f_{L/G/B}$ can be determined through Eq. (5.5), where $f_{L/G/B} = f_{G/B} \cdot f_{L/GB}$. It is observed that the proposed $f_{L/G/B}$ values are conservative and suitable for built-up members with various lacing spacings where the shear deformation is adequately accounted for. Besides, the suggested equations are safe and suitable for members with various slender sections and can be considered for short, intermediate and long columns. A more detailed discussion of the overall performance of the proposed design equations is presented in the next paragraph.

5.5.3 Assessment of design proposal

A detailed comparison of the numerical results, the current design rules based on the American Standards (AISC & AASHTO) and Eurocode 3, and the proposed O.I.C.-based design approach for laced built-up columns with double (X) lacing systems is presented in the following. Figure 5.15 illustrates the performance of these current design rules and the proposed design approach for built-up columns, whose sections consist of two C-shaped sections arranged in both tip-to-tip ([ ]) and back-to-back (] [) configurations. As shown in Figure 5.15a, each scatter point represents a $\chi_{L+G+B,\text{Ref.}} / \chi_{L+G+B,\text{FE}}$ ratio associated to a unique member relative slenderness $\overline{\lambda}_B$, where “Ref.” denotes the reference standard (American Standard, Eurocode 3 or the proposed O.I.C. method). Additionally, Figure 5.15b presents the corresponding frequencies as a function of the $\chi_{L+G+B,\text{Ref.}} / \chi_{L+G+B,\text{FE}}$ ratio. Moreover, Table 5.5 provides statistical data related to the $\chi_{L+G+B,\text{Ref.}} / \chi_{L+G+B,\text{FE}}$ ratio, including the mean value, the C.o.V., the maximum and minimum values, and the percentage of predictions that exceed 5%, 10%, and 15% on the unconservative side. These percentages indicate which reference design proposal might misestimate the capacity

of members, leading to either unsafe or over-conservative resistance predictions. If the overestimation is significant, specifically, up to 10%, standard safety factors may not be sufficient to prevent failure. Deeper investigations on reliability aspects are presented in Section 5.6.

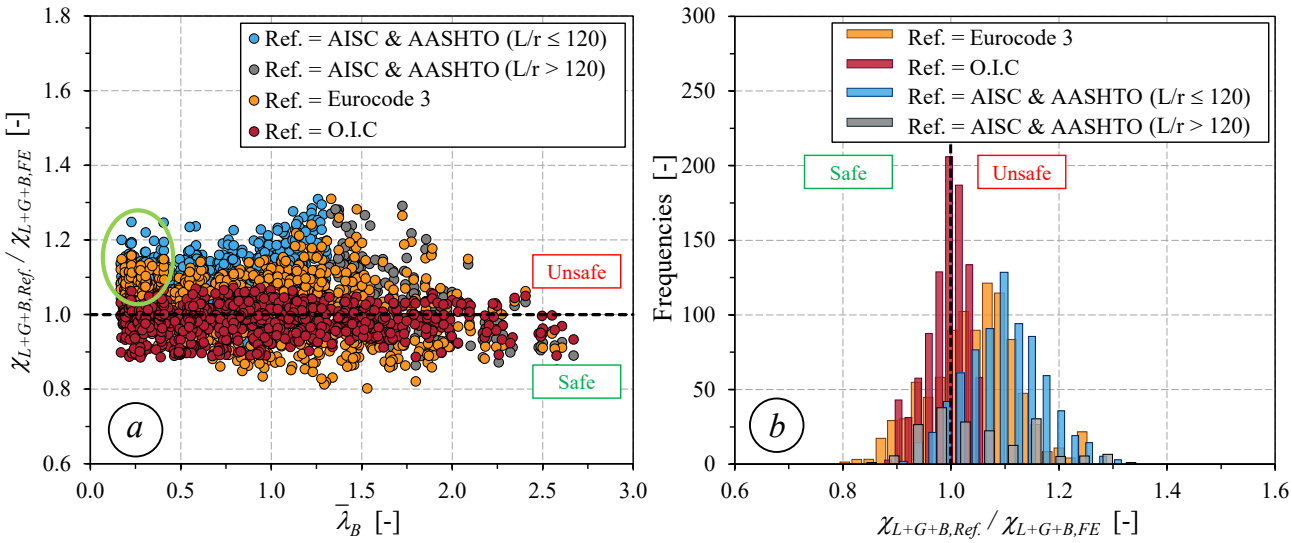

Figure 5.15 Analytical resistance predictions vs. numerical results.

Overall, the main observation from Figure 5.15 and Table 5.5 indicate that the O.I.C.-based design rules can capture accurate resistance prediction, with an excellent mean $\chi_{L+G+B,\text{Ref.}} / \chi_{L+G+B,\text{FE}}$ value of 0.99 and a very low C.o.V. of 3.9%, while the worse result remains within 7% on the unsafe side. In turn, Eurocode 3 provides less accurate results compared to the proposed O.I.C. design equations, with a mean value of 1.05 and a C.o.V. of 7.5%. It is found that Eurocode 3 overestimates the average strength prediction by approximately 6% compared to the O.I.C. A more detailed analysis of the results highlights two key factors affecting its accuracy:

- The capacity of built-up members primarily relies on the resistance of the chord between the connectors, while only local buckling and global buckling are considered by Eurocode 3. However, even when the interaction between global and built-up buckling modes is minimal and local buckling governs the response ($\bar{\lambda}_B \approx \bar{\lambda}_0 \approx 0.14$), the maximum of the $\chi_{L+G+B,\text{Ref.}} / \chi_{L+G+B,\text{FE}}$ ratio still remains approximately 20% on the unsafe side (see green ellipse in Figure 5.15a). This suggests that the combined use of the effective area A_{eff} along with multiple global buckling curves, as currently prescribed in the code, may lead to inaccurate predictions;

- Additionally, the code enforces a reduction in load due to the overall bending of built-up members but overlooks the interaction between local and global buckling coupled with built-up buckling behaviour. This limitation is particularly evident in members with intermediate lengths ($\overline{\lambda}_B \approx 1.25$), where the worst case results in an overestimation of up to 31% on the unsafe side. Despite this, Eurocode 3 appears to be the safest standard, especially for intermediate ($\overline{\lambda}_B$ from 0.8 to 1.6) and long columns ($\overline{\lambda}_B$ > 1.6), where about 11% and 18% of results fall below 0.9.

Further, AISC and AASHTO provisions exhibit quite worse results compared to Eurocode 3. Since AASHTO follows AISC recommendations for resistance predictions but imposes an additional constraint by limiting the slenderness ratio L / r to 120 for primary truss members, whereas AISC allows up to 200 for compression members, this restriction categorizes results into two sets: members that comply with the limit ($L / r \leq 120$) and those that exceed it ($L / r > 120$), which may not be acceptable under AASHTO provisions. It is observed that the overall results obtained from the American Standards are overly unconservative, with a mean $\chi_{L+G+B,\text{Ref.}} / \chi_{L+G+B,\text{FE}}$ ratio of 1.09 and a C.o.V. of 7.5% while the worse result reaching up to 31% on the unsafe side for members with $L / r \leq 120$. Yet, as reported in Table 5.5, approximately 66% of the results obtained from the American Standards, compared to the F.E. results, lie more than 5% on the unsafe side, whereas around 41% and 20% deviate up to 10% and 15% on the unsafe side, respectively. Furthermore, for members with $L / r > 120$, the American Standards also demonstrate a lack of consistency, with a mean $\chi_{L+G+B,\text{Ref.}} / \chi_{L+G+B,\text{FE}}$ ratio of 1.04 and a C.o.V. of 9.7%. Overall, in terms of lack of conservatism, the worst-case scenario reaches up to 31% on the unsafe side, with approximately 66%, 41%, and 20% of the data points remaining on the unsafe side at 5%, 10%, and 15%, respectively. Two main reasons may explain these results:

(i) The American Standards limit the slenderness of individuals chords to 75% of the built-up member's overall slenderness. This reduces the interaction between individual chord buckling and overall member buckling (G/B interaction), which can further decrease the buckling capacity of members;

(ii) Since the code enforces additional constraints to minimize G/B interactions, the handling of L/G/B interactions is overlooked. As clearly indicated in Figure 5.14b,

particularly for slender sections with χ_L ranging from 0.55 to 0.85 (represented by the blue line), this interaction reduces the member's resistance by approximately 10%.

In comparison, the O.I.C. approach provides excellent accuracy and better consistency, with a mean $\chi_{L+G+B,\mathrm{OIC}} / \chi_{L+G+B,\mathrm{FE}}$ ratio approximately equal to unity and a very low C.o.V. of around 4%. Besides, only 2.3% of the results exceed the 5% threshold on the unsafe side. Given the diverse member and section geometries considered, along with the complexity of local/global/built-up coupled instabilities analyzed in built-up members, the O.I.C. proposal proves to be a reliable design approach, ensuring accuracy, consistency, and safety.

Table 5.5 Statistical results of $\chi_{L+G+B,Ref.} / \chi_{L+G+B,FE}$ ratio for all columns in this study.

Relative slenderness	n	References	Mean	C.o.V. [%]	Max.	Min.	< 0.90 [%]	>1.05 [%]	>1.10 [%]	>1.15 [%]
$\bar{\lambda}_B \le 0.8$	455	AISC & AASHTO ($L/r \le 120$)	1.08	5.6	1.25	0.92	0.0	70.4	36.1	11.0
		Eurocode 3	1.03	5.3	1.16	0.86	1.1	43.4	10.1	0.2
		O.I.C.	0.98	4.1	1.07	0.89	5.6	2.7	0.0	0.0
$0.8 < \bar{\lambda}_B \le 1.6$	399	AISC & AASHTO ($L/r \le 120$)	1.10	8.5	1.31	0.91	0.0	70.3	48.8	29.7
		Eurocode 3	1.03	10.6	1.31	0.80	11.0	43.1	18.5	6.5
		O.I.C.	0.99	3.6	1.07	0.89	1.3	1.8	0.0	0.0
$\bar{\lambda}_B > 1.6$	108	AISC & AASHTO ($L/r > 120$)	1.04	9.7	1.29	0.85	5.6	22.2	12.0	5.6
		Eurocode 3	1.13	18.5	1.26	0.82	17.6	31.5	21.3	18.5
		O.I.C.	0.98	4.0	1.06	0.89	3.7	2.8	0.0	0.0
All values of $\bar{\lambda}_B$	952	AISC & AASHTO	1.09	7.5	1.31	0.85	0.6	65.6	40.7	19.7
		Eurocode 3	1.05	7.5	1.31	0.80	7.1	41.9	14.9	4.9
		O.I.C.	0.99	3.9	1.07	0.89	3.6	2.3	0.0	0.0

5.6 Reliability analyses

To estimate the degree of safety of the various design models considered herein, reliability analyses were carried out using (i) the Eurocode framework as described in Annex D of EN 1990 [193] with a simplified method reported in [194] to determine the partial safety factor γ_M and (ii) the American LRFD design framework originally developed by Ravindra and Galambos [195] to

determine the resistance factor ϕ. All uncertainties associated with load statistics, material properties, geometric variability, and inaccuracies in the design model approximations of the American Standards, Eurocode 3, and the O.I.C. proposals were considered. Besides, the Tail Approximation (T.A.) technique [196], [197] was adopted to improve the representativeness of the derived γ_M or ϕ factors and to avoid overly large or unnecessarily low values of the safety factors.

5.6.1 Reliability analysis in accordance with EN 1990 (Eurocodes)

The reliability analysis was carried out based on the recommendations of the First Order Reliability Method. Table 5.6 reports the results of the reliability analyses and the key statistical parameters considered, where n is the number of numerical and experimental results in each subset, $k_{d,n}$ is the design fractile factor, b is the mean value of the correction factor, $f_{y,mean}/f_{y,nom}$ is the material overstrength factor, and V_r is the combined coefficient of variation, which accounts for uncertainties from both the design model and the basic variables. The value of V_r was calculated using the following expression:

$$V_r^2 = V_\delta^2 + V_{rt}^2 \tag{5.16}$$

In Eq. (5.16), V_δ represents the C.o.V. of the uncertainties in the numerical and experimental resistance associated with the design models and $V_{r,t}$ is the C.o.V. of the uncertainties related to the k basic variables, where $V_{r,t}$ can be determined through Eq.(5.17) for each F.E. result, considering how the resistance depends on the variability of the two basic variables, i.e., geometry (V_{geom}) and material properties (V_{mat}).

$$V_{rt}^2 = V_{geom}^2 + V_{mat}^2 \tag{5.17}$$

In this study, statical data of material overstrength factor $f_{y,mean}/f_{y,nom}$ and the associated V_{mat}, along with V_{geom}, were adopted as recommended in Annex E of EN 1993-1-1 [116]. Finally, the mean partial safety factor required for the different cases considered was derived based on Eq. (5.18).

$$\gamma_M = \frac{1}{n}\sum_{i=1}^{n}\frac{r_{nom,i}}{r_{d,i}} \tag{5.18}$$

In Eq. (5.18), $r_{nom,i}$ is the nominal resistance calculated from F.E. models using the nominal values of material properties and $r_{d,i}$ is the design resistance determined as a function of the mean correction factor b and of the predicted resistance taken from the current standards and the O.I.C. proposal. More details about the calculation procedure can be found in [198].

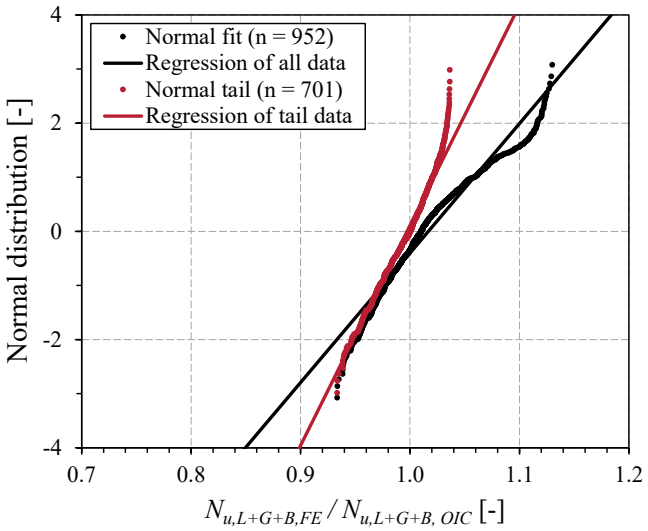

Figure 5.16 Example of a tail approximation for laced built-up members.

The T.A. approach helps correct the excessive conservatism that results from incorrectly assuming normality for the full dataset, thereby improving the accuracy of safety and resistance factor calibration. Figure 5.16 shows an example of adopting the T.A. technique, using a normal probability plot where the "normal distribution" is plotted on the vertical axis, alongside the ratio of the ultimate load obtained from the F.E. model to that obtained from the O.I.C. approach, denoted as "$N_{u,L+G+B,FE} / N_{u,L+G+B,OIC}$", on the horizontal axis. In this figure, the black dots represent the full dataset for all cases, which deviates noticeably from the regression line (solid black line) of a standard normal distribution, indicating that the overall data does not follow a normal distribution. To address this, the T.A. technique is applied by isolating the worst on the unsafe tail – 701 cases in this example, shown as red dots – which are more relevant for reliability-based design. It is observed that the regression line fitted to this subset (red solid line) closely follows a linear trend, suggesting that the lower tail can reasonably be modeled by a normal distribution. In contrast, the regression line for the complete dataset fails to align with a normal distribution, contradicting the assumptions of the statistical procedure in Annex E of EN 1993-1-1 [116].

Table 5.6 Summary of reliability analysis results based on the Eurocode approach.

Study cases	Proposals	n	$k_{d,n}$	b	$f_{y,mean} / f_{y,nom}$	V_{geom}	V_{mat}	V_δ	V_r	γ_M
Without T.A.	AISC & AASHTO	952	3.1	0.912	1.25	0.025	0.055	0.075	0.096	1.18
	Eurocode 3	952	3.1	0.953	1.25	0.025	0.055	0.075	0.097	1.13
	O.I.C.	952	3.1	0.986	1.25	0.025	0.055	0.040	0.072	1.01
With T.A.	AISC & AASHTO	701	3.104	0.888	1.25	0.025	0.055	0.052	0.080	1.15
	Eurocode 3	732	3.103	0.932	1.25	0.025	0.055	0.050	0.078	1.09
	O.I.C.	701	3.144	0.975	1.25	0.025	0.055	0.023	0.065	1.00

As reported in Table 5.6, without adopting the T.A. technique, the γ_M value for the O.I.C. proposal was found to be an excellent 1.01, due to lower overall uncertainty – particularly attributed to the variability in geometry and material properties. In contrast, γ_M values associated with the American Standards and Eurocode 3 are 1.18 and 1.13, respectively. These values exceed the typical recommended limit – Eurocode 3 specifies a partial safety factor of $\gamma_M = 1.00$, which implies no safety margin for the cross-section and member. The Eurocode 3 value found here ($\gamma_M = 1.13$) reflects the need for a safety margin above 10%; AISC and AASHTO adopt a resistance factor $\phi = 0.90$, corresponding to $\gamma_M \approx 1 / \phi \approx 1.11$. A careful analysis of these results indicates that these higher γ_M values primarily result from significant uncertainties in the design models, as reflected by a correction factor b lower than 1 and a higher V_δ.

Moreover, as shown in Figure 5.17, by applying the T.A. technique, γ_M factors for the American Standards and Eurocode 3 reduce to 1.16 and 1.10, respectively. This decrease is due to a drop in V_δ by disregarding the model uncertainty in the upper tail, thereby improving on previously conservative estimates of γ_M with more representative data. The O.I.C. method achieved a minimum γ_M of about 1.00, closely matching the actual resistance distribution. In conclusion, the O.I.C proposal shows more appropriate γ_M values compared to the other two proposals, suggesting it provides a more reliable design approach alongside superior accuracy, as discussed in previous paragraphs.

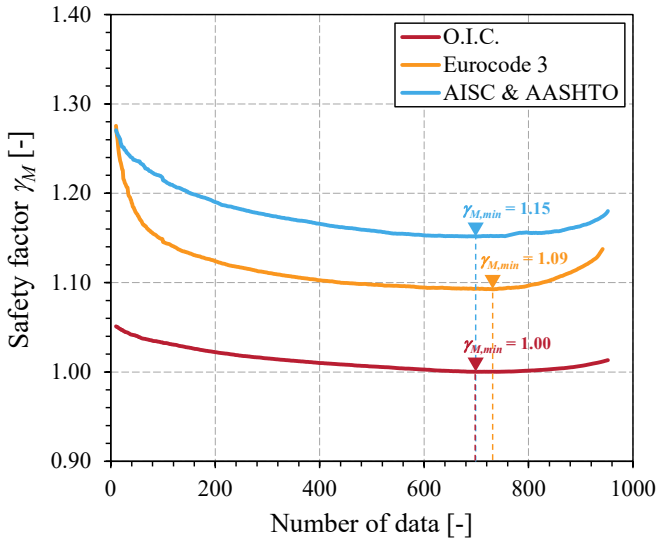

Figure 5.17 Safety factor variation with tail approximation.

5.6.2 Reliability analysis in accordance with AISC-LRFD approach

The AISC-LRFD approach was developed using first-order probabilistic principles. This simplified method uses two key statistical parameters, i.e., the mean and the C.o.V. of the relevant variables, together with their relationship to the safety index β, to determine the resistance factor ϕ. The values of both ϕ and β are determined as in Eq. (5.19).

$$\phi = \frac{R_m}{R_n}\exp\left(-\alpha\beta V_R\right) \tag{5.19}$$

In Eq. (5.19), R_m and R_n are the mean and nominal resistance and α is the separation factor. In this study, a value of $\alpha = 0.8$ was adopted, as suggested by [199] and [200]. As the AISC analyses take load statistics into account, the safety index β associated with load combination of $1.2D + 1.6L$, as described in [200] and [201], is given by Eq. (5.20).

$$\beta = \frac{1}{\sqrt{V_R^2 + V_Q^2}}\ln\left(\frac{R_m}{0.657\phi_2 R_n}\right) \tag{5.20}$$

In Eq. (20), V_R and V_Q are the C.o.V. values of the resistance and load effect, respectively. For this evaluation, a constant resistance factor $\phi_2 = 0.90$ is adopted. The value of V_Q was set to 0.22,

following the AISC assumption of a mean live-to-dead load ratio $L_m / D_m \approx 3.0$. The R_m / R_n ratio and V_R shall be calculated from Eqs. (5.21) and (5.22).

$$R_m / R_n = M_m \times F_m \times P_m \tag{5.21}$$

$$V_R = \sqrt{V_M^2 + V_F^2 + V_p^2} \tag{5.22}$$

In Eqs. (5.21) and (5.22), M_m reflects the mean ratio of the actual-to-specified yield stress (material properties), F_m represents the mean ratio of the actual-to-specified plastic section modulus (fabrication) and P_m is the mean ratio of test-to-predicted resistance (professional judgment), while V_M, V_F, and V_P are their corresponding C.o.V. values, respectively.

The results of reliability analyses based on the AISC-LRFD approach under the standard load combination ($1.2D + 1.6L$) are summarized in Table 5.7. It should be noted that the AISC design provisions are generally calibrated to achieve a target reliability index of approximately $\beta = 2.6$ for member design. In comparison, EN 1990 specifies a higher, stricter global target of $\beta = 3.8$ for a 50-year design life, corresponding to $\beta \approx 3.04$ for resistance only. Unlike EN 1990, AISC accounts for uncertainties in both resistance and load effects, resulting in a lower target [200]. Overall, without applying the T.A. technique, the resistance factors ϕ associated with the American Standards and Eurocode 3 were found to be 0.84, failing to reach the AISC's usual target of 0.90. These values correspond to reliability indices of $\beta = 2.27$ for the American Standards and of $\beta = 2.34$ for Eurocode 3, both below the minimum target value of 2.6. To ensure an acceptable level of safety, a minimum $\beta = 2.6$ was applied, resulting in a calibrated factor of $\phi = 0.82$. However, since this value is lower than the resistance factor currently used in the American Standards, it suggests that the design provisions may be unconservative, potentially overestimating safety. In contrast, the O.I.C. proposal achieves the highest reliability index and resistance factor, with $\beta = 2.70$ and $\phi = 0.93$, indicating a more reliable and potentially more accurate design approach. Furthermore, incorporating the T.A. technique (see Table 5.8) results in only marginal improvement in reliability, with resistance factors remaining virtually unchanged.

Table 5.7 Summary of reliability analysis results based on the AISC-LRFD framework.

Proposals	n	M_m	F_m	P_m	R_m / R_n	V_F	V_M	V_p	V_R	V_Q	β	ϕ
AISC & AASHTO	952	1.10	1.00	0.936	1.029	0.05	0.056	0.075	0.106	0.22	2.27	0.84 / 0.82*
Eurocode 3	952	1.10	1.00	0.974	1.071	0.05	0.056	0.102	0.127	0.22	2.34	0.84 / 0.82*
O.I.C.	952	1.10	1.00	1.017	1.118	0.05	0.056	0.040	0.085	0.22	2.70	0.93
* Value calculated based on $\beta = 2.6$												

Table 5.8 Safety factors ϕ obtained from the best tail approximation from different proposals.

Proposals	n_{tail}	ϕ
AISC & AASHTO	611	0.82
Eurocode 3	791	0.82
O.I.C.	880	0.93

5.7 Conclusions

This paper investigated the buckling behaviour of laced built-up columns subjected to pure compression loads, where buckling occurs within the plane of the lacing system. The built-up sections consisted of two main C-shaped sections interconnected by double (X) flat lacing bars. Results from extensive numerical analyses addressing local, global, and built-up buckling modes were presented. Non-linear shell F.E. models were carefully developed and validated against existing experimental results and subsequently used to conduct both preliminary and parametric studies. It was observed that laced built-up columns with slender elements are significantly influenced by cross-sectional local interactions and by complex local/global/built-up interaction modes. The original O.I.C.-based design approach was extended to address triple L/G/B interaction modes in laced built-up columns. This approach accounts for (i) local buckling of the cross-section of the chord, (ii) global buckling of the chord between lacing connectors, (iii) built-up buckling of the overall member and (iv) a local/global/built-up interaction factor $f_{L/G/B}$ to capture the interactions among the corresponding buckling modes. The performance and accuracy of the O.I.C. proposal, along with those of current design provisions, were evaluated against reference F.E. results. It was found that the American Standards and Eurocode 3 fail to adequately capture

local/global/built-up interaction effects, leading to unconservative and scattered resistance predictions. In contrast, the O.I.C.-based design approach showed improved accuracy and consistency to the other design recommendations. Furthermore, reliability analyses incorporating the T.A. technique, conducted in accordance with EN 1990 and the AISC-LRFD framework, confirmed that the proposed O.I.C. design rules offer a safe and reliable method for designing laced built-up columns.

5.8 Abbreviations and symbols

AASHTO	American Association of State Highway and Transportation Officials
AISC	American Institute of Steel Construction
C.o.V.	Coefficient of Variation
C.S.M	Continuous Strength Method
D.S.M.	Direct Strength Method
E.W.M.	Effective Width Method
EC 3	Eurocode EN 1993-1-1
F.E.	Finite Element
G.M.N.I.A.	Geometrically and Materially Non-linear with Imperfections Analysis
L.B.A.	Linear Buckling Analysis
O.I.C.	Overall Interaction Concept
T.A.	Tail Approximation
A	Total area of built-up section
A_{ch}	Area of individual chord section
$A_{ch,eff}$	Effective area of individual chord, calculated using E.W.M.
A_{eff}	Effective cross-sectional area, calculated using E.W.M.
a_L	Half-wavelength of local imperfections
$a_{i,f}$	Buckling length of flange plate

$a_{i,w}$	Buckling length of web plate
b	Width of C-sections (section geometry); mean value of the correction factor (reliability analysis)
b_o	Total width of cross-section
b_p	Width of tie-plate
D	Dead load
D_m	Mean value of dead load
E	Young's modulus
e	End distance from end of built-up member to edge of end tie-plate, measured along axial direction of built-up member
$e_{0,B}$	Amplitude of global imperfection in overall built-up member
$e_{0,G}$	Amplitude of global imperfection in individual chord segment between connectors
$e_{0,L}$	Amplitude of local imperfection in cross-section
$e_{0,L,f}$	Amplitude of local imperfection in flange plate
$e_{0,L,w}$	Amplitude of local imperfection in web plate
$e_{0,lacing}$	Amplitude of global imperfection in lacing bar
F_m	Mean ratio of actual-to-specified plastic section modulus
$f_{G/B}$	Interaction factor accounting for influences of global buckling on built-up buckling
$f_{L/G}$	Interaction factor accounting for influences of local buckling on global buckling
$f_{L/GB}$	Interaction factor accounting for influences of local buckling on built-up buckling
$f_{L/G/B}$	Interaction factor accounting for local, global, and built-up buckling interactions
f_y	Yield strength
$f_{y,mean}$	Mean value of yield strength
$f_{y,nom}$	Nominal value of yield strength

f_u	Ultimate tensile strength
h	Total height of cross-section
h_o	Distance between centroids of chords
h_p	Length of tie-plate
I	Second moment of area of built-up section
I_{ch}	Second moment of area of individual chord section
$k_{d,n}$	Design fractile factor
k_L	Factor accounting for the influence of local buckling
L	Length of test specimen (geometry); live load (reliability analysis)
L_B	Length of built-up member
L_G	Length of chord segment between connectors
L_L	Length of stub column
L_{lacing}	Length of lacing member measured between the centers of connection points
L_m	Mean value of live load
M_{Ed}	Design value of applied bending moment
M_m	Mean ratio of actual-to-specified yield stress
N	Axial compression load
$N_{ch,Ed}$	Design axial force for each chord
N_{cr}	Elastic critical load
$N_{cr,B}$	Elastic critical load corresponding specifically to built-up buckling
$N_{cr,G}$	Elastic critical load corresponding specifically to global buckling of chords segment between connectors
$N_{cr,L}$	Elastic critical load corresponding specifically to local buckling of cross-section
N_{Ed}	Design axial compression axial force

N_{pl}	Plastic capacity of built-up section
$N_{pl,ch}$	Plastic capacity of individual chord section
N_u	Ultimate load or peak load
$N_{u,F.E.}$	Ultimate load predicted by F.E. analysis
$N_{u,L+G}$	Ultimate load considering local and global buckling
$N_{u,L+G+B}$	Ultimate load considering local, global, and built-up buckling
$N_{u,Test}$	Ultimate load recorded during testing
n	Number of cases
n_{tail}	Number of cases using T.A. technique
P_m	Mean ratio of test-to-predicted resistance
R_m	Mean value of resistance
R_n	Nominal value of resistance
r	Fillet radius (section geometry); radius of gyration (section property)
t_f	Thickness of flange plate
t_p	Thickness of tie-plate
t_w	Thickness of web plate
V_F	C.o.V. of fabrication
V_{geom}	C.o.V. of section geometry
V_M	C.o.V. of material property (AISC-LRFD approach)
V_{mat}	C.o.V. of material property (European approach)
V_P	C.o.V. of professional judgment
V_Q	C.o.V. of load effect
V_R	C.o.V. of resistance
V_r	Combined C.o.V. of design model and basic variables

$V_{r,t}$	Combined C.o.V. of material and geometry variables
V_δ	C.o.V. of uncertainty of numerical and experimental resistance
x_1, x_2	Factor of residual stress
$x_o - x_o$	Strong axis of built-up section
$y_o - y_o$	Weak axis of built-up section
α	Imperfection factor (buckling curve); separation factor (reliability analysis)
α_B	Generalized imperfection factor for built-up buckling of overall member
α_G	Generalized imperfection factor for global buckling of chord segments between connectors
α_L	Generalized imperfection factor for local buckling of cross-section
β	Factor accounting for possible strain hardening effects (material behaviour); safety index (reliability analysis)
γ_M	Partial safety factor (EC 3 format)
δ	Factor accounting for potential post-buckling effect
χ	Generalized reduction factor
χ_B	Generalized reduction factor for built-up buckling of overall member
χ_G	Generalized reduction factor for global buckling of chord segments between connectors
χ_L	Generalized reduction factor for local buckling of cross-section
χ_{G+B}	Generalized reduction factor accounting for global and built-up buckling
χ_{L+G}	Generalized reduction factor accounting for local and global buckling
χ_{L+G+B}	Generalized reduction factor accounting for local, global, and built-up buckling
λ	Slenderness value corresponding to relevant buckling mode

$\overline{\lambda}_0$ Length of plateau of buckling curve

$\overline{\lambda}_B$ Generalized relative slenderness of built-up buckling of overall member

$\overline{\lambda}_G$ Generalized relative slenderness of global buckling of chord segments between connectors

$\overline{\lambda}_{G+B}$ Generalized relative slenderness of members including influence of global and built-up buckling

$\overline{\lambda}_L$ Generalized relative slenderness of local buckling of cross-section

$\overline{\lambda}_{L+G}$ Generalized relative slenderness of members including influence of local and global buckling

$\overline{\lambda}_{L+G+B}$ Generalized relative slenderness of members including influence of local, global, and built-up buckling

ϕ Resistance factor (AISC format)

ϕ_2 Constant resistance factor

ϕ_B Key parameter to determine χ_B

ϕ_G Key parameter to determine χ_G

ϕ_L Key parameter to determine χ_L

ϕ_{L+G} Key parameter to determine χ_{L+G}

$\sigma_{\max}$ Amplitude of residual stress

5.9 Acknowledgements

This research and development project would not have been possible without the contribution and collaboration of The Jacques Cartier and Champlain Bridges Incorporated.

CHAPTER 6 ARTICLE 3: O.I.C. DESIGN OF LACED BUILT-UP STEEL COLUMNS FOR OUT-OF-PLANE FLEXURAL BUCKLING

Oudom Chhoeng[a], Morane Chloé Mefande Wack[a], Nicolas Boissonnade[b, *], Robert Tremblay[a]

[a] Polytechnique Montréal, H3T 1J4, Montréal, QC, Canada

[b] Université Laval, G1V 0A6, Québec, QC, Canada

[*] Corresponding author

Email: oudom.chhoeng@polymtl.ca (O. Chhoeng), morane-chloe.mefande-wack@polymtl.ca (M. Wack), nicolas.boissonnade@gci.ulaval.ca (N. Boissonnade), robert.tremblay@polymtl.ca (R. Tremblay).

The paper was submitted to *Thin-Walled Structures* on 31 October 2025.

Abstract: This paper investigates the flexural buckling resistance of laced built-up steel columns subjected to compressive loading. These columns are quite sensitive to out-of-plane buckling due to the significant increase in overall cross-sectional width, defined as the distance between the main chords, introduced by the built-up configuration. A companion study [202] focused on the in-plane buckling of laced built-up columns, where global buckling of the chords between lacing connectors was shown to significantly reduce the load-carrying capacity. In contrast, this paper focuses on members that buckle out of the plane of the lacing systems. Two critical phenomena, often overlooked in current design codes, are examined: (i) the influence of shear deformations resulting from the global buckling of chords between connectors, and (ii) the effect of local buckling on the overall member behaviour. A finite element model was developed to accurately predict the resistance of laced built-up columns, and its accuracy was validated through comparison with 23 available experimental data. Extensive parametric studies were conducted to evaluate the impact of geometric variations, sectional arrangements, and member slenderness on the resistance. The numerical results were used to assess the merits of a design method for laced built-up columns that exhibit out-of-plane buckling of the lacing system, based on the Overall Interaction Concept (O.I.C.). This O.I.C.-based approach provides more accurate, consistent, and conservative strength

predictions compared to the Canadian, Eurocode 3, and American standards. Its reliability is further supported by statistical analyses in accordance with EN 1990 and AISC-LRFD design provisions.

Keywords: Laced built-up columns, Out-of-plane buckling, Overall interaction concept, Design proposal.

6.1 Introduction

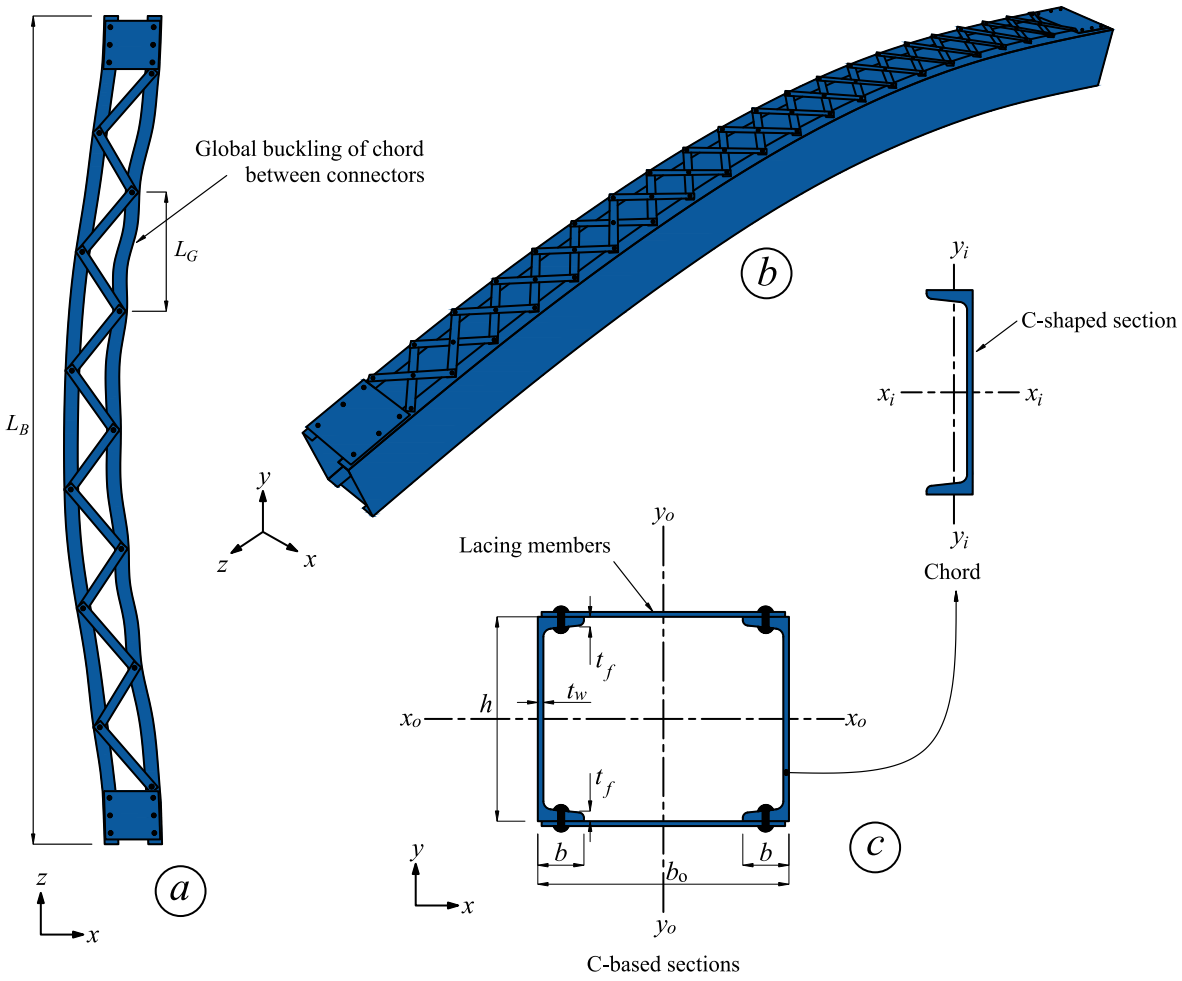

Figure 6.1 Buckling behaviour of laced built-up columns under axial compression – (a) In-plane buckling – (b) Out-of-plane buckling – (c) Notations.

This paper addresses the design of laced built-up columns that buckle out of the plane of the lacing system under compressive loading. Such members are typically characterized by a low height-to-width ratio (h / b_o), resulting from large chord spacing b_o (Figure 6.1). This geometry reduces the moment of inertia about the x-axis ($I_x < I_y$), making out-of-plane flexural buckling the governing mode. Accurate representation of this response is therefore essential for reliable design.

As shown in Figure 6.1, two distinct instabilities are relevant. In-plane buckling (see Figure 6.1a), which occurs within the lacing plane, often involves global (G) buckling of chord segments between connectors. This mode becomes critical when connector spacing is large or when the lacing lacks stiffness. Out-of-plane buckling (see Figure 6.1b), in contrast, involves lateral or torsional deformation of the overall built-up member perpendicular to the lacing plane, and is governed by the global flexural and torsional stiffness of the system. Current design provisions [112], [114], [154] remain limited, particularly in addressing shear-deformation effects associated with the global buckling of chords between lacing connectors, and in capturing the interaction between local (L) buckling of slender cross-sections and built-up (B) buckling of the overall member. These limitations are of practical importance, as many riveted built-up members fabricated for steel truss bridges in the late 19th and early 20th centuries are still in service today, especially in North America.

Early analytical work by Engesser [7], [8] established the critical load of simply supported built-up columns while incorporating shear deformation due to global buckling of chord segments. This formulation provided the basis for subsequent extensions by numerous researchers [6], [7], [22], [34], [45], [47], [57], [58], [61], [131], [199], including the incorporation of shear deformation and inelasticity effects [10], [11], [26], experimental and numerical studies on compact and double-angle members [61], [62], [203], criteria for stitch spacing and local buckling [49], [51], and the introduction of "equivalent slenderness" expressions for design [38], [64], [65], [135]. The concept of the equivalent slenderness ratio $(KL / r)_{eq}$ – a modified form of the classical slenderness ratio accounting for both chord buckling between connectors and overall built-up buckling – has since been widely adopted in design codes.

More directly relevant are investigations into out-of-plane buckling. Toossi [57] showed that neglecting out-of-plane effects in battened columns could lead to unsafe designs and provided analytical solutions accounting for batten and torsional properties. Subsequent studies emphasized the same need for explicit consideration: Johnston [36] demonstrated that tie plates can significantly increase buckling strength, while Dabaon et al. [204] experimentally validated out-of-plane behaviour and proposed extensions to the Direct Strength Method, and Stone and LaBoube [205] identified complex mode interactions. Hosseini Hashemi and Jafari [206], while focusing on stiffener formulas, indirectly highlighted the importance of such effects. Collectively, these studies confirm that neglecting out-of-plane buckling leads to unsafe or inaccurate designs. Yet, major

design codes still exhibit significant shortcomings in capturing the complex interaction between out-of-plane of the built-up member and local buckling of the cross section, as well as the associated uncertainty of global buckling of the chord segments between lacing connectors.

The present study extends the Overall Interaction Concept (O.I.C.) [123], [126]–[131], originally developed for non-built-up members, to laced built-up columns composed of two hot-rolled C-sections such as tip-to-tip ([ ]) or back-to-back (] [) interconnected with double (X) flat lacing bars. In this work, the concept is extended to laced built-up sections consisting of two hot rolled C-sections arranged either tip-to-tip ([ ]) or back-to-back (] [), with the chords interconnected by double (X) flat lacing bars. The lacing connectors are assumed to be riveted or bolted to the main chords. The paper first describes the development and validation of shell finite element (F.E.) models for built-up columns. Modelling details, including initial geometric imperfections and residual stresses, are also discussed (see Section 6.2). Then, Section 6.3 presents the parameters used in an extensive parametric study, which results in approximately 6 000 non-linear F.E. simulations. This section also provides a preliminary discussion of key concerns, such as the global buckling of chord segments between lacing connectors and the effect of local buckling interaction of the cross-section on the ultimate load capacity. These effects are compared for built-up members buckling in-plane and out-of-plane relative to the lacing system. The reference results serve as the foundation for evaluating the proposed design method described in Section 6.4. To assess its performance, the resistance values predicted by the O.I.C. approach, the American Standards, Eurocode 3, and Canadian Standards are compared with the numerical results, followed by a reliability analysis presented in Section 6.5.

6.2 F.E. modelling

6.2.1 Basic features: material, section modelling, support conditions and loading

The developed F.E. models of laced built-up members were created using the non-linear F.E. software ABAQUS [156] and have been shown to be adequate [161]. A similar modelling approach was adopted, and all mesh elements used in this work were previously confirmed to be suitable, particularly in terms of mesh density, aspect ratios, and geometric regularity. The intersection of web and flange in the cross-section was modeled using advanced features, including: (i) the

implementation of extra hollow beam elements to closely match the cross-sectional geometric properties, with particular emphasis on torsional stiffness, and (ii) the use of spring elements to ensure that the web-flange regions remain free from local buckling.

The connections between the lacing members and tie-plates to the main chord are represented by connection lines (see Figure 6.2). These connections are assumed to behave like rivets or bolts, modeled using modified kinematic constraints between the reference node (Node 1, located on the flange of the main chord) and the coupling node (Node 2, located on the lacing member or tie-plate), as described below:

(i) For the connection between lacing members and the main chord, kinematic constraints were applied to enforce equal translational and rotational degrees of freedom at both nodes, except for rotation about the local *y'*-axis. This allows free rotation around the *y'*-axis while constraining all other motions (see Figure 6.2a);

(ii) For the connection between tie-plates and the main chord, the same technique was used; however, all translational and rotational degrees of freedom were fully constrained to prevent any relative motion (see Figure 6.2b).

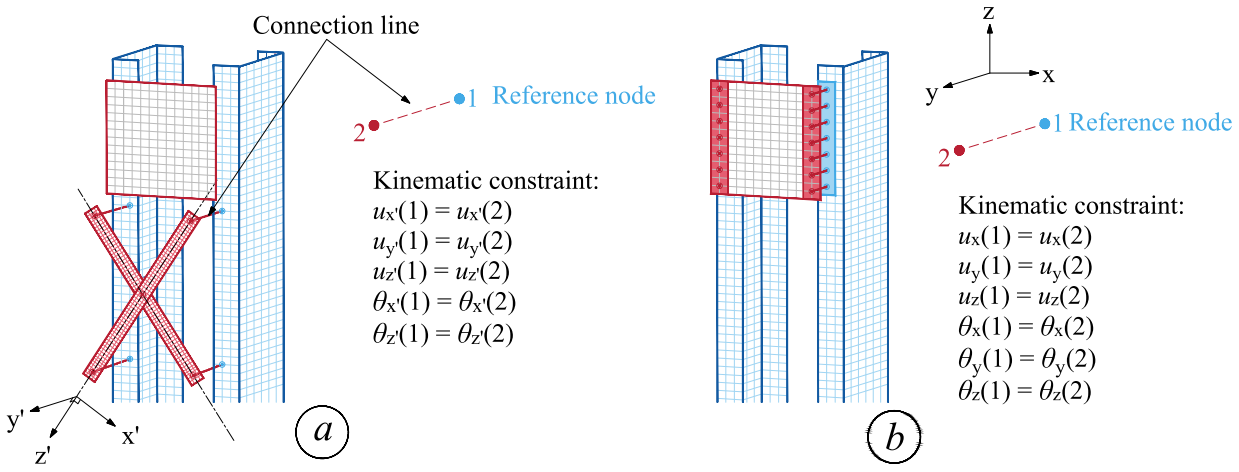

Figure 6.2 Connection modelling of – (a) Lacing member to chord – (b) Tie-plate to chord.

The application of axial compression is illustrated in Figure 6.3. The axial load was applied at a reference point on one end of the member, while axial displacement was restrained at the opposite end. Both reference points were constrained to control and share the degrees of freedom of all nodes along the corresponding cross-sectional ends. To replicate the experimental setup used for numerical validation in Section 6.2.3, the positions of these reference points were made

adjustable in the transverse and longitudinal directions by specified distances (e_x and e_y). For the parametric study, both reference points were positioned at the cross-section's center of gravity, and the column was assumed to be simply supported with fork-type supports at both ends, restricting torsional rotation and translational displacements in the x and y directions restricted at both ends ($u_x = u_y = \theta_z = 0$).

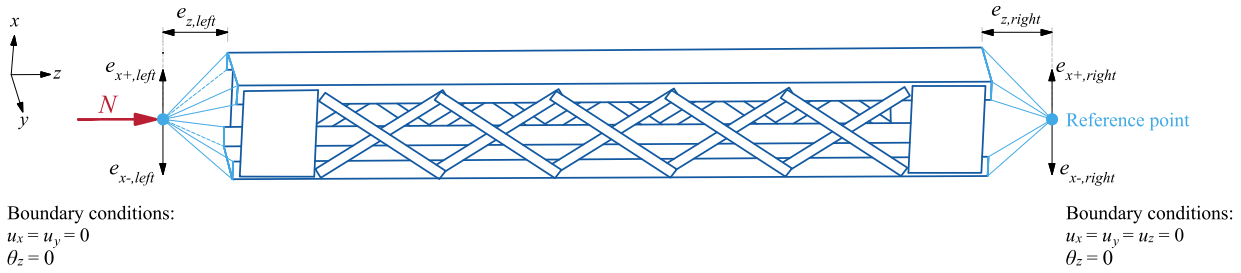

Figure 6.3 Support conditions and application of loading.

A standardized quad-linear stress–strain relationship, based on thousands of tensile test data [162], was adopted (see Figure 6.4). This relationship was converted into true stress and logarithmic plastic strain and implemented in ABAQUS for validation and subsequent parametric analyses. As illustrated in Figure 6.4, the constitutive model is defined by three primary input parameters: E, f_y, and f_u, where E is the Young's modulus, and f_y and f_u represent the yield stress and ultimate stress, respectively. The intermediate parameters ε_1, ε_2, and f_2 characterize the yield plateau and strain hardening stage. Further details can be found in [162].

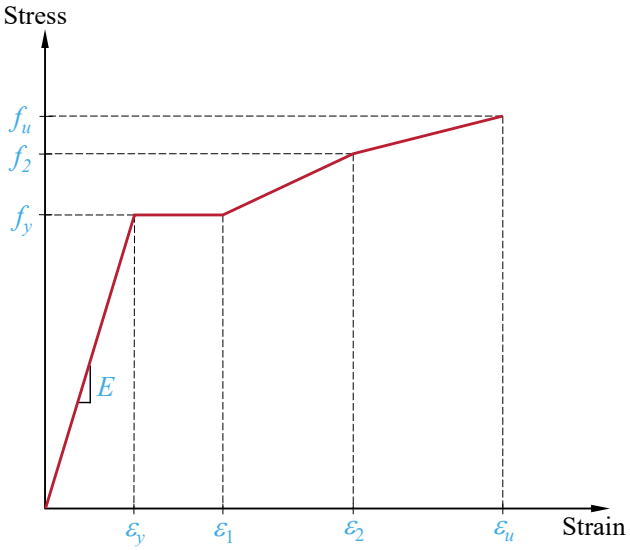

Figure 6.4 Quad-linear stress–strain relationship used in F.E. parametric studies.

6.2.2 Initial imperfections and residual stresses

Initial geometrical imperfections have been accounted for by means of adequate modification of node coordinates. A combination of both local and global geometrical imperfections was incorporated using sine-wave functions. Here, it should be noted that local imperfections refer to the imperfections of the web and flange plates of the cross-section, while global imperfections refer to the imperfections of individual components such as the main chord segment between the lacing connectors, lacing members, and the overall built-up member. Details about the implementation of imperfections are described as follows:

(i) Local imperfections, allowing the potential development of local instability, were introduced for the web and flange of the chord cross-section in both directions, with amplitudes of $e_{0,L,w} = a_{i,w} / 200$ and $e_{0,L,f} = a_{i,f} / 200$, as recommended from [159], where $a_{i,w}$ and $a_{i,f}$ are the web and flange buckling lengths, respectively (see Figure 6.5a). To ensure that the weakest cross-section remains at the mid-span of the member, an odd number of half-waves is chosen, associated with a half-wavelength of $a_L = (a_{i,w} + a_{i,f}) / 2$, as reported in [126], [128], [129], [131], [186], leading to reasonable and appropriate resistance predictions;

(ii) Global imperfections were introduced independently for the overall built-up member, the individual chord segments between lacing connections, and the lacing members, with amplitudes defined as $e_{0,B} = a_{glob.} \times L_B$, $e_{0,G,chord} = a_{glob.} \times L_G$, $e_{0,lacing} = a_{glob.} \times L_{lacing}$, respectively (see Figure 6.5b to Figure 6.5d), where $a_{glob.}$ is the global factor and L_B, L_G, and L_{lacing} are the total lengths of the corresponding members. In this study, global imperfection factors $a_{glob.}$ of 1 / 500, 1 / 1000 and 1 / 1500 were considered to evaluate and compare with experimental data, in order to select an appropriate coefficient for consecutive parametric studies. Details regarding the selection of these amplitudes are discussed in Section 6.2.3.

Residual stresses were introduced to the chords by adopting a residual stress pattern suggested by Beyer et al. [100] for hot-rolled C-sections with total height h, width b, web thickness t_w, and flange thickness t_f (see Figure 6.5e). The amplitude of the residual stress is defined as $\sigma_{max} = 0.15 f_y$, where $x_1 = 1 + b t_f / (h t_w)$ and $x_2 = 0.5$.

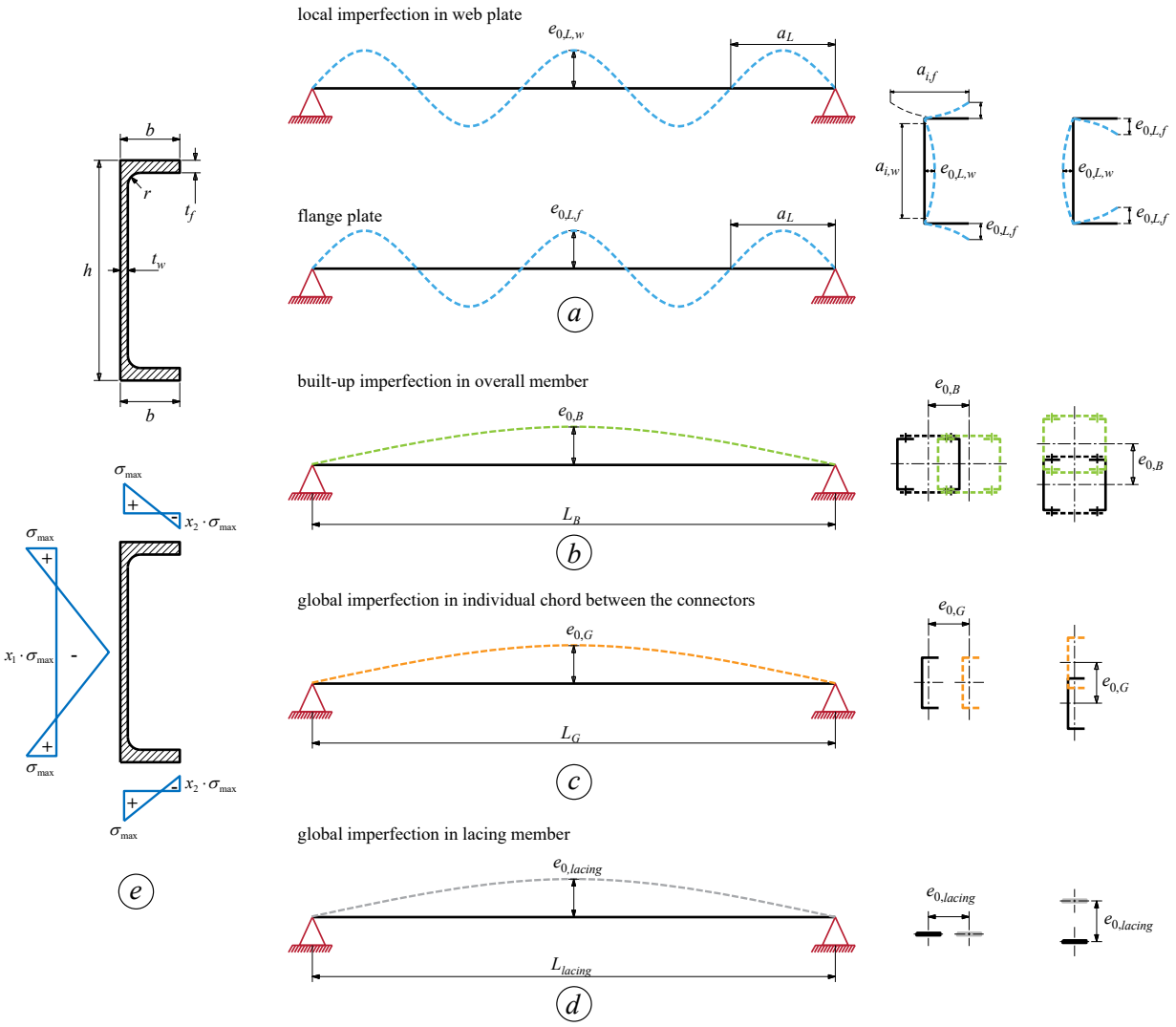

Figure 6.5 Sine-shaped initial geometrical imperfections and residual stresses.

6.2.3 Validation against experimental results

Analyses performed with the F.E. model described in previous paragraphs were compared against experimental test results on the laced built-up sections found in the literature. In this respect, the experimental results from Kleiser and Uang [148], Lee and Bruneau [150], Bonab et al. [164], and Kalochairetis et al. [165] on tip-to-tip ([ ]) and back-to-back (] [) laced built-up sections were considered. The dimensions of specimen and their material properties are reported in Table 6.1. With the exception of the tests reported in [148] and [150], all specimens in this study were subjected to static loading; in those two studies, cyclic loading was applied instead. To assess the impact of this difference, numerical validation was carried out in [161], indicating that the variation

in ultimate load between cyclic and static loading conditions was minimal. Therefore, for consistency and since this study focuses on static behaviour, all specimens analyzed here were loaded under static conditions.

All specimens were tested under simple support conditions, with the longitudinal distance from the support to the member end denoted as e_z. They were subjected to either concentric loading ($e_x = 0$) or eccentric compression ($e_x \neq 0$), see Table 6.2.

By incorporating the initial geometric imperfections and residual stress patterns described in Section 6.2.2, the F.E. model provides results for each specimen that can be directly compared with the corresponding experimental data. The ratios of ultimate load from the F.E. analysis to the test results ($N_{u,FE} / N_{u,test}$), corresponding to three values of the global amplification factor, are presented in Table 6.2. Overall, the numerical results show very good agreement with the experimental data, with the average $N_{u,FE} / N_{u,test}$ ratio ranging from 0.94 to 1.06 across all three cases, and a coefficient of variation (C.o.V.) between 6.6% and 8.3%. Among these, adopting a global factor of $a_{glob.} = 1 / 1000$ results in an average ratio of 0.99 and a C.o.V. of 6.6%, representing the highest level of accuracy among all cases.

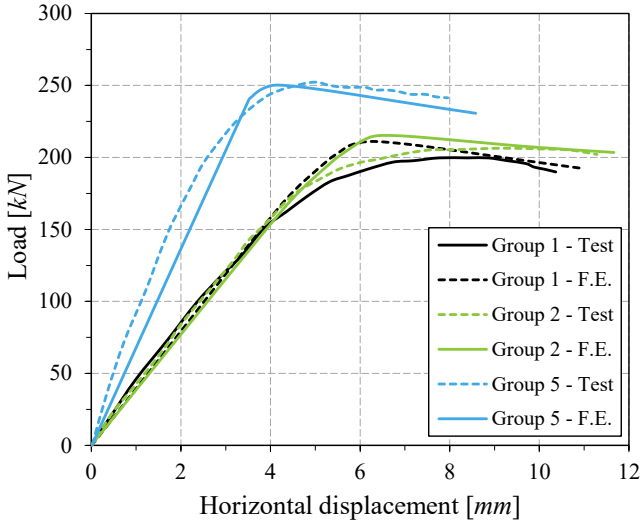

Figure 6.6 Load-displacement curves of specimens Group 1, Group 2 and Group 5, reported in [165], showing the F.E. results with amplitude factors of 1/200 for local and 1/1000 for global imperfections.

As a complement, Figure 6.6 presents representative load-displacement curves, demonstrating a strong correlation between the F.E. results and the reference test data in terms of ultimate load, initial stiffness, and post-peak behaviour. Additionally, Figure 6.7 illustrates the close agreement

between failure modes, both global and local, predicted by F.E. model and those observed experimentally for specimen Bx8-120, as reported in [150]. Accordingly, the developed F.E. model is considered suitable for accurately capturing both the ultimate load and the overall experimental behaviour of laced built-up members. This reliability is supported by the adoption of standard imperfection shapes associated with factors of 1 / 1000 for global and 1 / 200 for local imperfections, which closely reflect experimental observations. As a result, the model has been extensively employed in the numerical parametric studies presented in the following paragraph.

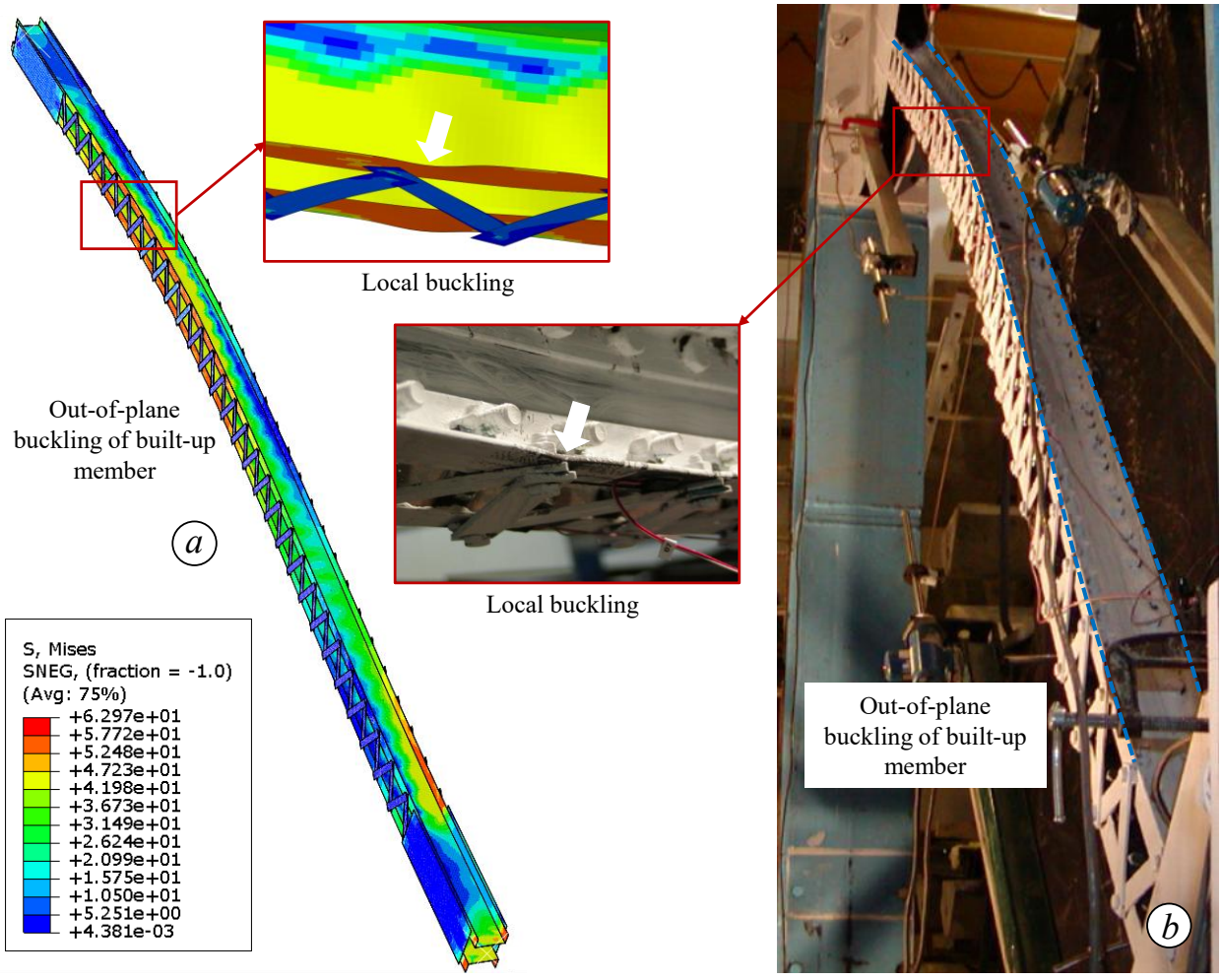

Figure 6.7 Failure mode of specimen Bx8-120 – (a) Obtained from F.E. model (von Mises stress shown in *ksi*) – (b) Observed experimentally, as reported in [150].

Table 6.1 Sections, cross-section dimensions, profiles, and material properties of each component of test specimens.

Specimens	Sections and geometric dimensions		Main chords			Lacing system and end tile-plates	
	Section	Cross-section dimensions	Profile / F_y / F_u [*MPa*]				
		b_o x h x L x c x e [*mm*]	Channel	Angle	Web plate [PL b_p x t_p, *mm*]	Lacing [PL b x t_p, *mm*]	End tile-plate [PL b_p x h_p x t_p, *mm*]
Specimen 1 [148], [149]	4L+2P	437 x 337 x 7146 x 365 x 530	-	L76x76x8 / 338 / 489	PL 330x8 / 324 / 478	PL 38x8 / 327 / 484	PL 441x553x7 / 327 / 484
Specimen 2 [148], [149]							
Specimen 3 [148], [149]							
By8-60 [150]	4L+2P	121 x 121 x 2445 x 108 x 0	-	L25x25x3.2 / 361 / 475	PL 121x3.3 / 323 / 384	PL 19x3.2 / 323 / 384	PL 121x495x9.5 / 253 / 349
By8-120 [150]		121 x 121 x 5035 x 108 x 0		L25x25x3.2 / 361 / 475	PL 121x3.3 / 323 / 384	PL 19x3.2 / 323 / 384	PL 121x495x9.5 / 253 / 349
By16-60 [150]		133 x 133 x 1838 x 95 x 0		L51x51x3.2 / 352 / 470	PL 133x3.3 / 323 / 384	PL 24x3.2 / 323 / 384	PL 133x560x9.5 / 253 / 349
By16-120 [150]		133 x 133 x 3835 x 95 x 0		L51x51x3.2 / 352 / 470	PL 133x3.3 / 323 / 384	PL 24x3.2 / 323 / 384	PL 133x560x9.5 / 253 / 349
Bx8-120 [150]		114 x 76 x 3683 x 102 x 0		L25x25x3.2 / 361 / 475	PL 76x3.3 / 323 / 384	PL 19x3.2 / 323 / 384	PL 114x394x9.5 / 253 / 349
Bx16-60 [150]		165 x 105 x 2432 x 133 x 0		L51x51x3.2 / 352 / 470	PL 105x3.3 / 323 / 384	PL 24x3.2 / 323 / 384	PL 165x527x9.5 / 253 / 349
Bx16-120 [150]		165 x 105 x 5055 x 133 x 0		L51x51x3.2 / 352 / 470	PL 105x3.3 / 323 / 384	PL 24x3.2 / 323 / 384	PL 165x527x9.5 / 253 / 349
L140B8(R1) [164]	2C	80 x 60 x 1400 x 56 x 0	UNP60 / 278 / 405	-	-	PL 10x3 / 278 / 405	PL 200x80x10 / 278 / 405
L140B8(R2) [164]		80 x 60 x 1400 x 56 x 0					
L140B8(R3) [164]		80 x 60 x 1400 x 56 x 0					
L140B10(R1) [164]		100 x 60 x 1400 x 56 x 0					
L170B7(R1) [164]		70 x 60 x 1700 x 56 x 0					
L170B7(R2) [164]		70 x 60 x 1700 x 56 x 0					
L170B7(R3) [164]		70 x 60 x 1700 x 56 x 0					
L170B8(R2) [164]		80 x 60 x 1700 x 56 x 0					
L170B8(R3) [164]		80 x 60 x 1700 x 56 x 0					
Group 1 [165]	2C	218 x 60 x 2020 x 400 x 0	UNP60 / 338 / 435	-	-	L25x25x3	-
Group 2 [165]		218 x 60 x 2020 x 200 x 0	UNP60 / 338 / 435				
Group 4 [165]		218 x 60 x 2020 x 400 x 0	UNP60 / 335 / 435				
Group 5 [165]		218 x 60 x 2020 x 400 x 0	UNP60 / 302 / 435				

Table 6.2 Summary of F.E. vs. test ultimate load of test specimens.

References	Specimens	Sections	Loading positions				Ultimate loads and ratios			
			$e_{x,left}$	$e_{z,left}$	$e_{x,right}$	$e_{z,right}$	$N_{u,test}$	$N_{u,FE}$ / $N_{u,test}$ [-]		
								Global amplification factor, $a_{glob.}$		
			[mm]	[mm]	[mm]	[mm]	[kN]	1 / 500	1 / 1000	1 / 1500
Kleiser and Uang [148]	Specimen 1	] [	381	400	0	400	928.79	0.94	1.05	1.11
	Specimen 2		127	400	0	400	1633.83	0.97	0.95	1.01
	Specimen 3		0	400	0	400	2885.12	0.91	0.98	1.05
Lee and Bruneau [150]	By8-120	] [	0	0	0	0	295.81	0.90	0.94	0.99
	By16-60		0	0	0	0	521.64	0.87	0.93	0.99
	By16-120		0	0	0	0	447.00	0.92	0.95	1.18
	Bx8-60		0	0	0	0	267.16	1.01	1.11	1.17
	Bx8-120		0	0	0	0	213.51	1.04	1.07	1.15
	Bx16-60		0	0	0	0	506.87	0.99	1.01	1.09
	Bx16-120		0	0	0	0	409.50	0.98	1.10	1.17
Bonab et al. [164]	L140B8(R1)	] [	0	140	0	140	204.76	0.92	0.98	1.07
	L140B8(R2)		0	140	0	140	183.86	0.97	1.01	1.09
	L140B8(R3)		0	140	0	140	159.09	0.96	1.02	1.08
	L140B10(R1)		0	95	0	95	289.05	0.84	0.88	0.90
	L170B7(R1)		0	95	0	95	151.95	0.85	0.90	0.91
	L170B7(R2)		0	95	0	95	135.19	0.82	0.89	0.92
	L170B7(R3)		0	95	0	95	124.32	0.86	0.96	0.97
	L170B8(R2)		0	95	0	95	162.40	0.89	0.98	0.95
	L170B8(R3)		0	95	0	95	146.29	0.91	0.96	0.98
Kalochairetis et al. [165]	Group 1	[ ]	100	162.5	100	162.5	200.00	1.02	1.06	1.10
	Group 2		100	162.5	100	162.5	206.00	1.01	1.06	1.11
	Group 4		100	162.5	-80	162.5	230.00	1.04	1.07	1.13
	Group 5		50	162.5	50	162.5	247.00	0.98	1.01	1.07
							Mean	0.94	0.99	1.06
							C.o.V.	7.0 %	6.6 %	8.3 %
							Min.	0.82	0.88	0.90
							Max.	1.04	1.11	1.18

[ ] = tip-to-tip arrangement

] [= back-to-back arrangement

6.3 Numerical parametric studies

6.3.1 Overview of key parameters

The parameters considered in these extensive parametric studies were selected to closely reflect practical applications. Considerations related to production, construction, and service conditions were also factored into the choice of parameter values. The selected parameters are presented as follows:

(i) 2 chord section arrangements were considered: tip-to-tip ([ ]) and back-to-back (] [). In each case, the chord consists of two C-shaped sections connected by double X-shaped flat lacing bars, with tie plates provided at both ends. The spacing between the two main chords was selected to be relatively wide, resulting in a ratio of I_{yo} / I_{xo} ranging from 1.05 to 2.82. This configuration increases the member's sensitivity to out-of-plane buckling;

(ii) 4 different values of the relative slenderness of the lacing bars λ_{lacing} were considered, ranging from 0.6 to 1.8. These lacing bars were selected to ensure sufficient stability, remaining unbuckled up to the peak load of the built-up member;

(iii) 5 different values of the inclination angle of the lacing bars relative to the built-up members' longitudinal axis were chosen, ranging from 20^{o} to 60^{o}. These angles were selected to adjust the spacing of lacing bars;

(iv) 30 cross-sections were considered, including standard C-shaped profiles and invented sections, covering a wide range of sizes. The overall height (h) varied from 152.5 *mm* to 1021 *mm*, while the flange width (b) ranged from 30.5 *mm* to 152.4 *mm*. The web slenderness ratio (h / t_w) ranged from 6 to 96.95, while the flange slenderness ratio (b / t_f) varied from 4 to 10.7;

(v) 2 steel grades: CSA G40.4 with f_y = 230 *MPa* and CSA G40.21 with f_y = 350 *MPa*;

(vi) 6 different lengths of the built-up members (L_B) were considered to represent a wide range of relative slenderness value, from short columns and for quite long ones. Such column lengths were selected to remain realistic and representative of practical structural applications.

In this paper, two types of numerical simulations were investigated for all cases by performing (i) Linear Buckling Analysis (L.B.A.) to estimate the elastic critical load of column under ideal conditions and (ii) Geometrically and Materially Non-linear with Imperfection Analysis (G.M.N.I.A.) to determine the ultimate strength of columns taking into account material yielding, residual stresses, initial geometric imperfections, and all relevant interaction effects.

6.3.2 Observations

Given that a full parametric study would involve approximately 29 000 simulations, sub-studies on selected key parameters were first carried out, as described in Section 6.3.3, aiming to determine whether certain parameters (e.g., yield strength) have a strong or limited impact, and can therefore be reduced or fixed without compromising the overall conclusions. In addition, Section 6.3.4 examines the key buckling modes and their interactions in laced built-up columns subjected to compression. The focus is on how each mode, especially the global buckling of the chord between lacing connectors, influences the column's ultimate resistance and how the buckling modes interact with one another, including in-plane and out-of-plane buckling within the laced system. It should be noted that in Figure 6.8, Figure 6.9 and Figure 6.10, the subscripts indicate the buckling modes considered in each case:

- "*L*" refers to local buckling of the cross-section only;
- "*G*" refers to global buckling of the chord between lacing connectors only;
- "*B*" refers to built-up buckling of the overall member only;
- "*L*+*B*" indicates that both local buckling of the cross-section and global buckling of the chord between lacing connectors are considered;
- "*G*+*B*" indicates that both global buckling of the chord and built-up buckling of the overall member are considered;
- "*L*+*G*+*B*" indicates that all local, global, and built-up buckling are considered.

Following this preliminary investigation, the study was refined to approximately 4 000 simulations. The results from these simulations were then used as reference data to support the development and evaluation of the proposed design method, detailed in Section 6.4.

6.3.3 Studies on selected key parameters

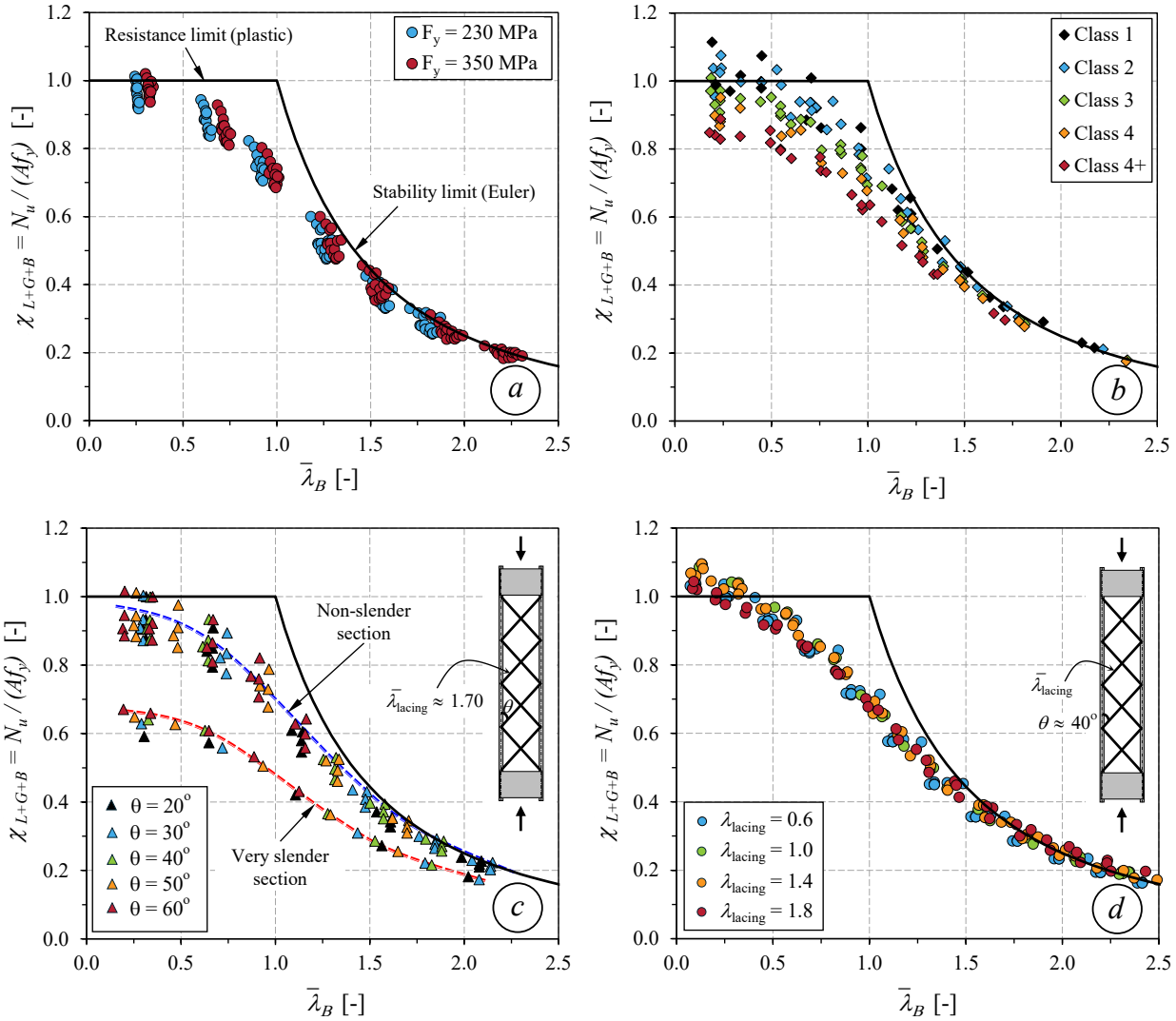

Figure 6.8 Influence of selected key parameters on ultimate resistance – (a) Yield strength – (b) Cross-section geometry – (c) Inclination angle of lacing – (d) Slenderness ratio of lacing.

Figure 6.8 presents results from sub-studies on selected key parameters, including yield strength, cross-section geometry, lacing inclination, and the slenderness ratio of lacing. The purpose of these sub-studies is to evaluate the relative influence of each parameter on the compressive resistance to out-of-plane buckling. All results illustrated from Figure 6.8a to Figure 6.8d are presented in terms of the reduction factor for compressive resistance (χ_{L+G+B}) plotted against the relative slenderness of column ($\bar{\lambda}_B$). The $\chi_{L+G+B} = 1.0$ line is shown as reference, representing the plastic limit, i.e., full cross-sectional capacity in the absence of buckling. The classical Euler curve is also included

as a stability limit, derived from elastic buckling theory and based on an ideal member with no imperfection and no yielding. In some cases, results exceed $\chi_{L+G+B} = 1.0$ due to strain hardening, although this effect remains limited. Additionally, for high $\bar{\lambda}_B$ values, some results slightly scatter above the Euler curve. This can be attributed to deviations from the assumption of Euler theory, such as the presence of large rotations.

6.3.3.1 Influence of yield strength

Figure 6.8a presents a series of results for laced built-up columns with a double (X) lacing system under compressive loading, considering two steel grades: CSA G40.4 with $f_y = 230$ *MPa* and CSA G40.21 with $f_y = 350$ *MPa*. The objective is to investigate whether steel grade influences the compressive resistance to out-of-plane buckling. For a given set of parameters, as described in Section 6.3.1, the results show similar trends for both grades. As expected, the steel grade with higher yield strength ($f_y = 350$ *MPa*) produces results that slightly scatter above those of the lower grade, due to the reduced influence of residual stresses and the horizontal shift in the buckling response caused by the increase in f_y while the elastic modulus E remains constant. Across the full range of relative column slenderness ($\bar{\lambda}_B$), the difference in the reduction factor for compressive resistance (χ_{L+G+B}) between the two yield strengths remains below 5%. Overall, the influence of yield strength is therefore well captured within the $\chi_{L+G+B} - \bar{\lambda}_B$ framework, suggesting that the adoption of a single buckling curve for out-of-plane buckling could be considered adequate regardless of the influence of steel grade used.

6.3.3.2 Influence of cross-section geometry

Figure 6.8b shows the buckling behaviour of laced built-up columns with different chord section classes: non-slender sections (Class 1, 2, and 3), slender sections (Class 4), and very slender sections (Class 4+). Overall, the variation in the plotted data reflects the influence of cross-sectional classification on axial resistance. As expected, for very low slenderness values ($\bar{\lambda}_B < 0.25$), most sections, except Class 4 and 4+, achieve resistance close to the full plastic capacity, with minimal variation due to limited influence from local buckling. As the section class increases, specifically with increasing width-to-thickness ratios (h / t_w and b / t_f), the scatter among data points becomes more noticeable, particularly for Class 4 and 4+ sections. This trend is attributed to the higher sensitivity of slender sections to local buckling, which reduces the effective cross-sectional area

before global member buckling occurs. Additionally, imperfections such as residual stresses and initial geometric deviations play a significant role, especially for $\overline{\lambda}_B$ ranging from 0.5 to 1.5. For Class 4 and 4+ sections, this effect is further amplified due to the pronounced influence of local buckling. At high slenderness levels ($\overline{\lambda}_B > 1.5$), the influence local buckling diminishes, as the plots for all section classes remain close to the Euler buckling curve.

6.3.3.3 Influence of lacing parameters: inclination angle and slenderness ratio

This section examines the effect of lacing characteristics on the compressive resistance of laced built-up columns, focusing on two key parameters: the inclination angle of the lacing, θ (see Figure 6.8c), and the slenderness ratio of lacing bares $\overline{\lambda}_{\text{lacing}}$ (see Figure 6.8d). For a given $\overline{\lambda}_{\text{lacing}} \approx 1.7$ (Figure 6.8c), variations in θ do not significantly alter the overall trend of the buckling curve, although affecting the values of $\overline{\lambda}_B$ and the associated reduction factor χ_{L+G+B}. The observed scatter among data points is primarily attributed to the cross-sectional classification, non-slender vs. very slender, as highlighted by the two distinct dashed trend lines in Figure 6.8c. Additionally, for the specific case of $\theta \approx 40°$ (Figure 6.8d), with changes in lacing slenderness $\overline{\lambda}_{\text{lacing}}$, this parameter can be reasonably omitted from the definition of the out-of-plane buckling curve without significant loss of accuracy. Overall, a comparison between Figure 6.8c and d shows that the influence of both θ and $\overline{\lambda}_{\text{lacing}}$ on the response to compressive response of laced built-up column with a double (X) lacing system remains negligible, provided the buckling behaviour is properly captured in the buckling curve definition.

6.3.4 Key buckling and interaction behaviours: in-plane and out-of-plane buckling

6.3.4.1 Effect of global buckling of chords between lacing connectors

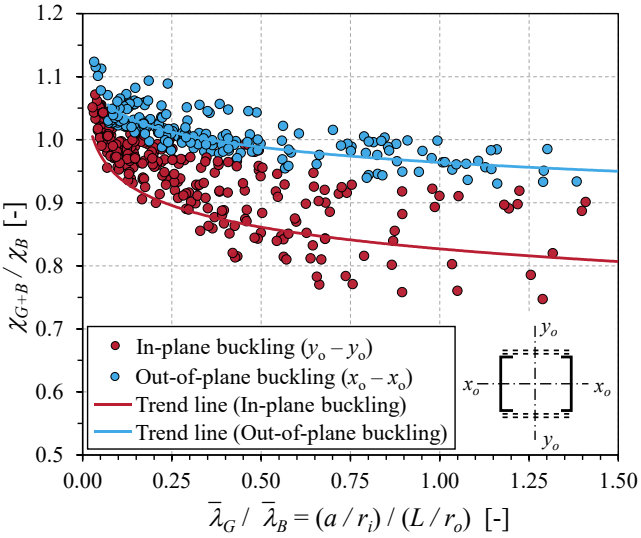

Figure 6.9 Effect of global buckling of the chord between lacing connectors.

Figure 6.9 presents a series of results on various selected parameters described in Section 6.3.1, under compression and for two different types of chord arrangements ([ ] and] [). The figure illustrates the influence of global buckling of chords between lacing connectors, comparing in-plane (buckling about $x_o - x_o$) and out-of-plane (buckling about $y_o - y_o$) buckling behaviours. The vertical axis represents the ratio χ_{G+B} / χ_B, which quantifies the reduction in resistance of built-up members when both the global buckling of the chord between connectors and the built-up buckling of the overall member are considered, relative to built-up buckling alone. The horizontal axis represents a normalized relative slenderness ratio $\bar{\lambda}_G / \bar{\lambda}_B$, reflecting the relative slenderness of the chord between lacing connectors compared to that of the built-up member. Note that a larger $\bar{\lambda}_G / \bar{\lambda}_B$ indicates that the member geometry is more sensitive to global buckling of the chord, whereas a lower $\bar{\lambda}_G / \bar{\lambda}_B$ reflects reduced sensitivity to global buckling of the chord. For both in-plane and out-of-plane buckling, each data series – blue and red points – is fitted with a separate logarithmic trend line. These trend lines indicate the predominance of global chord buckling on overall member buckling in reducing the compressive resistance, as $\bar{\lambda}_G / \bar{\lambda}_B$ increases. In-plane

buckling shows a more significant reduction, up to approximately 20%, due to global buckling of the chord between connectors; in contrast, this effect is less pronounced for out-of-plane buckling, with the overall strength reduction remaining below 5%.

6.3.4.2 Effect of local buckling interactions

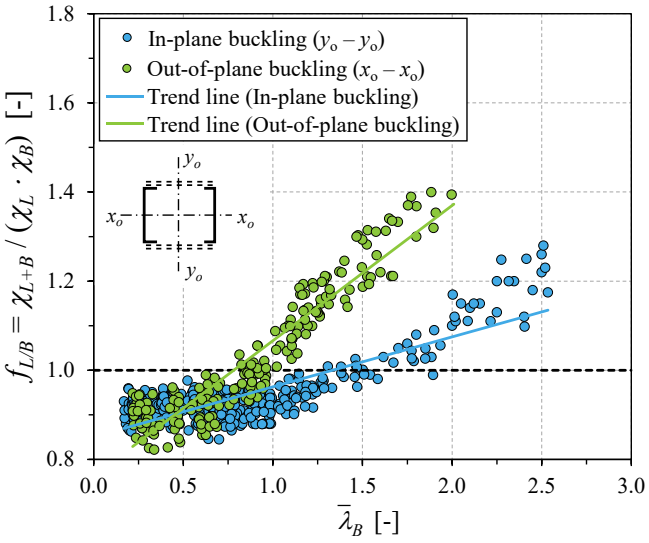

Figure 6.10 Effect of local buckling interaction.

The plot in Figure 6.10 illustrates the influence of cross-sectional local buckling interactions on the ultimate strength of laced built-up columns with a double (X) lacing system subjected to axial compression. The horizontal axis, $\bar{\lambda}_B$, denotes the slenderness ratio of the built-up member. The vertical axis, $f_{L/B}$, represents the interaction factor between local and built-up buckling, indicating how local buckling affects the overall built-up response. Values of $f_{L/B} < 1$ correspond to a strong influence of local buckling, which occurs mainly in short columns with Class 4 and 4+ cross-sections, whereas $f_{L/B} > 1$ indicates a weaker effect, particularly for long column columns. Results are presented for both in-plane and out-of-plane buckling modes. The in-plane buckling, associated with buckling about the $y_o - y_o$ axis, is shown as a blue scatter series with its corresponding linear trend line, while the out-of-plane buckling about the $x_o - x_o$ axis is depicted in green. A clear divergence in behaviour is observed between the two modes as the relative slenderness ($\bar{\lambda}_B$) increases with respect to the interaction factor $f_{L/B}$. When $f_{L/B} < 1$, the ultimate resistance of the built-up column is reduced by up to 20% due to the interaction among local and built-up buckling modes, reflecting an “erosion” of the ultimate load caused by these coupled effects. Conversely,

$f_{L/B} \geq 1$ suggests that the interaction effect is less severe, as the column behaviour is dominated by built-up buckling modes. The influence of local buckling on the overall column response depends on the column slenderness. Notably, this effect is more pronounced in short columns for both in-plane and out-of-plane built-up buckling. As $\overline{\lambda}_B$ increases, the out-of-plane buckling shows a more rapid rise in $f_{L/B}$ compared to in-plane buckling, as indicated by the steeper trend line. This highlights that the out-of-plane buckling mode is less sensitive to local buckling interactions, primarily because such interactions are concentrated in the flange. It underscores the need to differentiate between in-plane and out-of-plane responses when formulating interaction models.

Further comparing Figure 6.9 and Figure 6.10, it is evident that global buckling of the chord between lacing connectors has a strong influence on the in-plane buckling resistance. In contrast, its influence on the out-of-plane buckling resistance of the laced built-up column with a double (X) lacing system appears to be limited, particularly when the lacing bars are properly designed to remain stable until the built-up member reaches its ultimate load. Additionally, the results show that the out-of-plane buckling mode is less sensitive to local buckling interactions compared to the in-plane buckling behaviour, suggesting that adopting a distinct treatment of the interaction for each buckling plane is appropriate.

6.3.5 Isolating built-up resistance of the overall member

In the O.I.C. approach, local, global, and built-up buckling are first treated as independent, with their reduction factors χ_L, χ_G, and especially χ_B obtained from F.E. analysis. Interaction factors such as $f_{L/G/B}$ are then introduced to quantify the extent to which local and global buckling of chords between the connectors influences the built-up buckling response. This section describes how the reduction factor χ_B is obtained from F.E. analysis. To isolate flexural buckling of the overall built-up member through its reduction factor χ_B, the F.E. shell models were modified to prevent (i) local instability and (ii) global instability of individual chords between the lacing connectors. Figure 6.11a illustrates the constraints adopted in the F.E. models to prevent local cross-sectional buckling. Specifically, displacements of each node were constrained: flange *y*-displacements were constrained to web-flange junctions (reference nodes at the section corners), and web *x*-displacements were linked to a central node along the web. These constraints ensured the cross-section moved as a single unit, preventing any local deformation. As results, only built-up buckling

of the overall member and global buckling of individual chords between connectors could occur. Additionally, to eliminate global buckling of chords between connectors, the spacing between lacing connections L_G was limited so that the relative slenderness $\bar{\lambda}_G \le \bar{\lambda}_{G,0}$ (see Figure 6.11b). Here, $\bar{\lambda}_{G,0}$, also called the end-of-plateau slenderness, defines the threshold below which global buckling does not occur. This ensures that $\chi_G \approx 1$, meaning no significant strength loss occurred due to buckling between connectors. Therefore, only χ_B is considered.

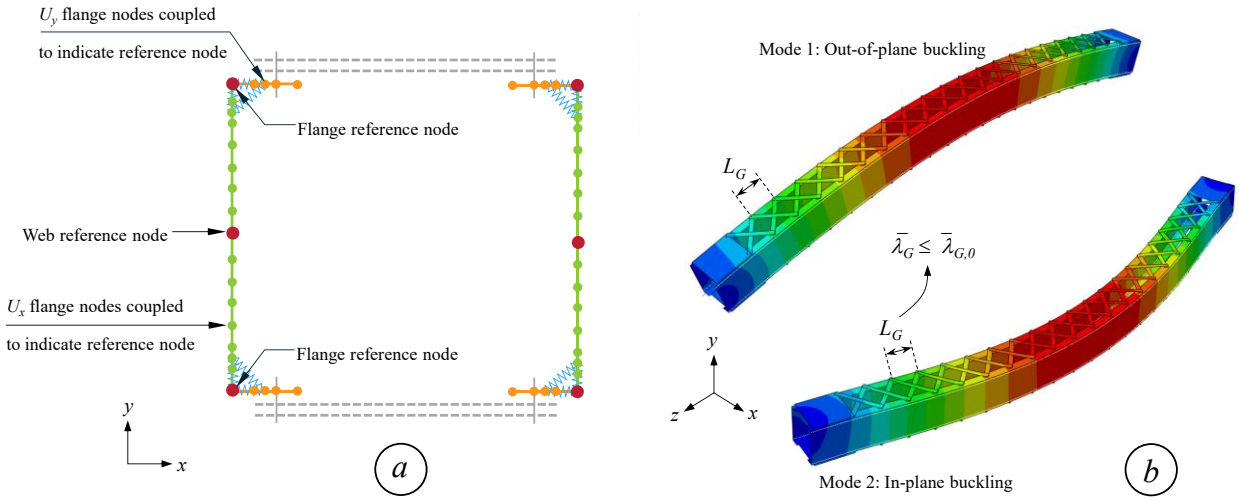

Figure 6.11 Constraints adopted in the F.E. models for reduction factor χ_B: (a) local instability and (b) global instability of individual chords between connectors.

6.4 Proposed O.I.C.-based design approach

6.4.1 Principle and application steps

6.4.1.1 Full interaction framework: L/G/B interaction

Before presenting the proposed approach, it is useful to recall the full O.I.C. interaction approach as applied to built-up columns, specifically for design of laced built-up steel columns under in-plane flexural buckling. As illustrated in Figure 6.12, laced built-up members can experience local, global, and built-up buckling, including interactions among them (L/G/B interaction). The ultimate load can be determined as follows:

$$N_{u,L+G+B} = \chi_L \cdot \chi_G \cdot \chi_B \cdot f_{L/G/B} \cdot N_{pl} \tag{6.1}$$

where χ_L, χ_G, and χ_B are the reduction factors for pure local, global, and built-up buckling, and $f_{L/G/B}$ accounts for their interaction effects. This interaction factor can be further decomposed as:

$$f_{L/G/B} = f_{L/GB} \cdot f_{G/B} \tag{6.2}$$

with $f_{G/B}$ representing global/built-up interaction, while $f_{L/GB}$ captures the influence of local buckling on global/built-up behaviour. A detailed design procedure can be found in [202].

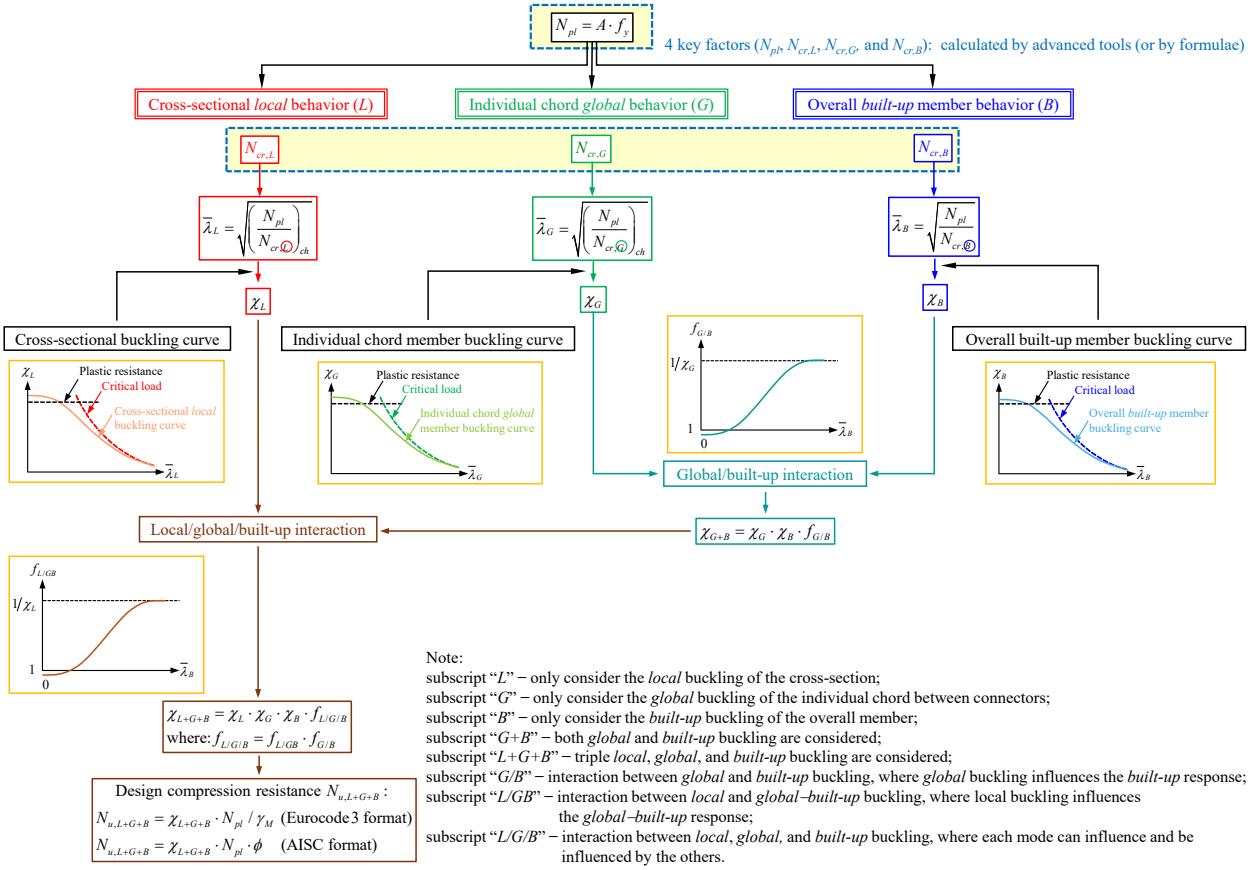

Figure 6.12 O.I.C. design flow chart for L/G/B interaction.

As previously discussed in Section 6.3.4, global buckling of the chord between lacing connectors can be neglected for the laced built-up columns considered in this study. In particular, out-of-plane global buckling has a minor effect, reducing the overall strength by less than 5%, whereas in-plane global buckling is more pronounced, causing a strength reduction of up to approximately 20%. This distinction justifies the adoption of a reduced O.I.C. proposal, focusing exclusively on local/built-up interaction. The proposed reduced L/B interaction procedure is presented in the following section.

6.4.1.2 Reduced interaction framework: L/B interaction

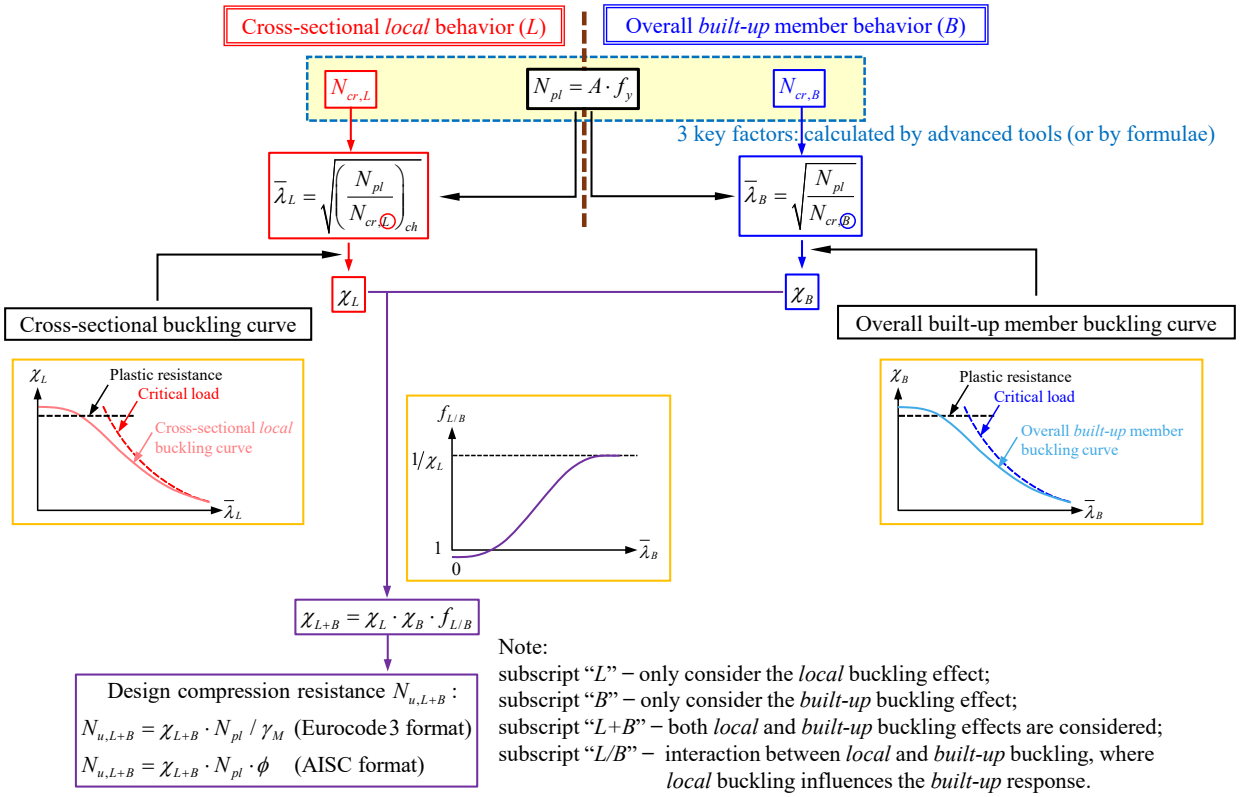

Figure 6.13 O.I.C. design flowchart for L/B interaction.

The O.I.C. offers a unified method for calculating the resistance of steel members by considering both resistance and instability through a generalized relative slenderness. Unlike the traditional approach adopted by current design codes, which is based on cross-section classification, the O.I.C. treats all section shapes in a consistent way. This method uses the plastic capacity of a section as a baseline and applies penalty factors – χ_L for cross-sectional resistance and χ_B for overall built-up member resistance – to account for buckling, imperfections, and their interactions. This allows it to accurately evaluate all section types, from non-slender (stocky) to slender. Figure 6.13 presents the proposed O.I.C. design flowchart to determine the resistance of laced built-up members with a double (X) lacing system, specifically addressing cases governed by out-of-plane buckling. In this method, the possibility of global buckling of the chord segments between lacing connectors is intentionally disregarded, as discussed in Section 6.3.4. The figure presents the calculation steps required to determine the ultimate resistance where two buckling modes, i.e., local and built-up,

have a significant effect on the capacity of members. Further insights into applying the proposed design approach are provided below:

- Step 1: determine the full plastic capacity N_{pl} of built-up members using the total gross cross-sectional area A;
- Step 2: calculate the elastic cross-sectional critical load $N_{cr,L}$ for local buckling of the individual chord's cross-section, and $N_{cr,B}$ for out-of-plane built-up buckling of the overall member, given by $N_{cr,B} = \pi^2 EI_{xo} / L_B^2$, where I_{xo} is the second moment of area of the built-up section about the out-of-plane (governing) buckling axis. The parameters N_{pl}, $N_{cr,L}$, and $N_{cr,B}$ may also be determined using simplified expression in [112], [114], [154], while more accurate values can be obtained through computational tools [123];
- Step 3: evaluate the relative slenderness $\bar{\lambda}_L$ for local resistance and $\bar{\lambda}_B$ for built-up resistance to reflect the balance between plasticity and instability. It is worth noting that, $\bar{\lambda}_L$ is determined based on the properties of an individual chord, whereas $\bar{\lambda}_B$ is derived from the characteristic of the full built-up configuration. Their expressions are given by:

$$\bar{\lambda}_L = \sqrt{\left(\frac{N_{pl}}{N_{cr,L}}\right)_{ch}} \quad \text{and} \quad \bar{\lambda}_B = \sqrt{\frac{N_{pl}}{N_{cr,B}}} \tag{6.3}$$

- Step 4: compute reduction factor χ_L from the standard local buckling curve, and χ_B from the standard built-up buckling curve, both incorporating the effects of initial imperfections and instability;
- Step 5: calculate the ultimate compressive capacity $N_{u,L+B}$ of laced built-up columns by multiplying the plastic capacity N_{pl} with the reduction factors for local and built-up buckling (χ_L and χ_B) and an interaction factor $f_{L/B}$. The interaction factor $f_{L/B}$ accounts for the influence of local buckling on the overall buckling behaviour of the built-up member through their multiplicative coupling effect. In addition, $f_{L/B}$ also incorporates the impact of imperfections, such as residual stresses and initial geometric deviations, which may otherwise be considered multiple times in the design process. The result formula is:

$$N_{u,L+B} = \chi_L \cdot \chi_B \cdot f_{L/B} \cdot N_{pl} \tag{6.4}$$

The O.I.C. method provides a unified framework for predicting the compressive resistance of various cross-section types and loading conditions, covering the full range from stocky to slender members. Besides, in Eq. (6.4), partial safety factors (e.g., γ_M in Eurocode 3 or ϕ in AISC) may be incorporated to address reliability requirements, depending on the chosen design format – see Section 6.5.

6.4.2 Local and built-up buckling curves

The proposed design approach is based on the concept of buckling curves, which is commonly used to reflect the interaction between structural resistance and instability. This relationship is typically defined in terms of the non-dimensional parameters χ (reduction factor) and $\overline{\lambda}$ (relative slenderness ratio). In the context of the O.I.C. framework, the resistance function $\chi = f\left(\overline{\lambda}\right)$ is derived from the Ayrton-Perry format [192], which rigorously accounts for the effects of geometric imperfections, non-linear buckling behaviour, and post-buckling strength reserves through the systematic calibration of key parameters. The generic O.I.C. formulation is given in Eq. (6.5):

$$\chi = \frac{1}{\phi + \sqrt{\phi^2 - \overline{\lambda}^{\delta}}} \tag{6.5}$$

where $\phi = 0.5 \cdot \left(1 + \alpha\left(\overline{\lambda} - \overline{\lambda}_0\right) + \overline{\lambda}^{\delta}\right)$

In this expression, $\overline{\lambda}_0$ defines the length of plateau where $\chi = 1$, α captures the influence of residual stresses and geometric imperfections on both the cross-section and built-up member behaviour, and δ characterizes the instability limit and reflects possible post-buckling strength reserves at the local level. The proposed O.I.C. design buckling curves, representing both the local behaviour of the cross-section and the built-up behaviour of the overall member, are presented in Figure 6.14, with each curve including two references lines:

- a horizontal solid line ($\chi = 1$), indicating the plastic resistance;

- a parabolic dashed line ($\chi = 1/\bar{\lambda}^2$), representing the elastic limit associated with ideal plate buckling in stub columns and ideal column buckling, both assuming perfectly elastic behaviour and the absence of imperfections.

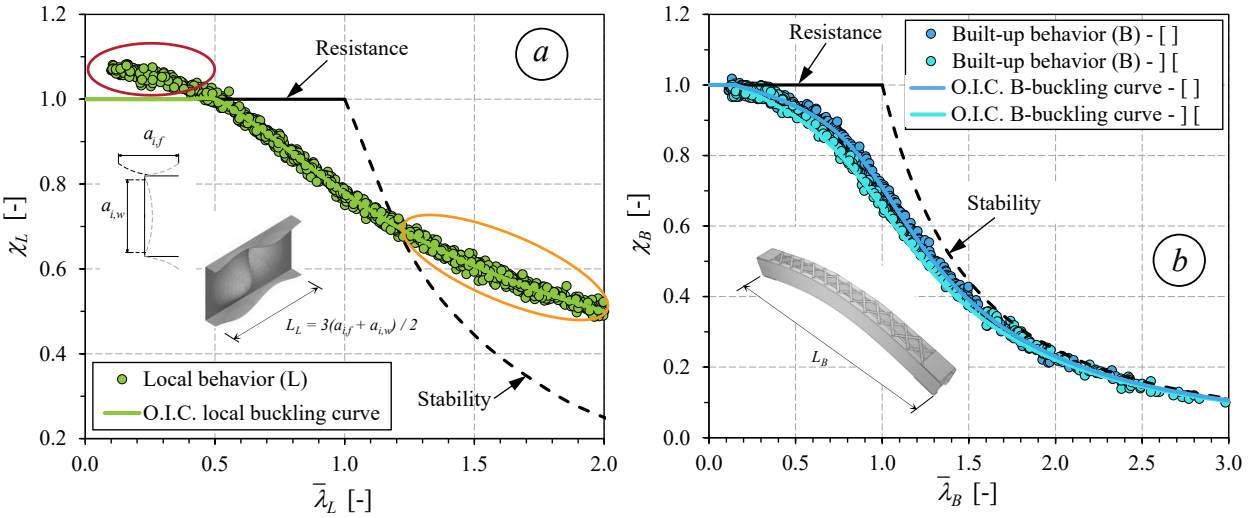

Figure 6.14 O.I.C. buckling curves for: (a) cross-section resistance – (b) overall built-up member resistance.

As discussed in Section 6.3.3, only a single steel grade (f_y = 350 *MPa*) is adopted for the analysis, as the influence of yield strength on the reduction factor is minor (less than 5%) across the range of column slenderness, allowing all cross-sections to be represented with a single representative case. As can be seen in Figure 6.14a, the F.E. results for cross-section resistance were obtained by assuming that the stub column length L_L corresponds to three half-waves lengths, i.e., $L_L = 3 \cdot \left(a_{i,f} + a_{i,w}\right) / 2$, consistently with [126]–[128], [130], [131]. This choice ensures that the weakest section develops at mid-height, with a column length that is sufficiently short to eliminate global flexural buckling, yet long enough to minimize the influence of boundary conditions on the ultimate resistance [131], [118]. As illustrated in Figure 6.14a, variations in the penalty factor χ_L remain below 5% across the full range of $\bar{\lambda}_L$, indicating that a single buckling curve can be applied with sufficient accuracy.-In some cases ($\bar{\lambda}_L < 0.5$), the data points scatter above 1.0 (see red ellipse) for very stocky sections, since some fibers in the cross-section may strain harden while others remain elastic. When a significant portion of the section reaches this stage, the average resistance may slightly exceed the nominal load (Af_y), making $\chi_L > 1$ physically plausible for very low $\bar{\lambda}_L$. However, in very slender members, built-up buckling typically governs failure before strain

hardening develops in local buckling. For members of intermediate slenderness, the interaction of local and built-up buckling further limits this effect. Accordingly, χ_L is limited to 1.0, ensuring the design resistance does not exceed the plastic load.

Besides, as marked in the orange ellipse, for sections with large slenderness ($\bar{\lambda}_L > 1.3$), most sections exhibit post-buckling effects, resulting in χ_L values (i.e., resistances) notably exceeding the stability limit ($\chi_L > 1/\bar{\lambda}_L^2$). While such high slenderness values are uncommon in practical applications, post-buckling effects are typically accounted for indirectly in design through established formulations (e.g., the effective width method through the Winter equation [207]), rather than being modeled explicitly.

For the built-up resistance of the overall member, Figure 6.14b presents two series of F.E. results for both tip-to-tip and back-to-back configurations. It can be observed that for built-up buckling, the data trends vary with the section arrangement, with differences up to 7% if a single safe-side curve is used. Therefore, two design curves are proposed: $\alpha_B = 0.14$ for the tip-to-tip configuration and $\alpha_B = 0.22$ for the back-to-back configuration, to reflect their distinct behaviours, noting that even slender sections (Class 4) can reach $\chi_B = 1.0$ without a χ_L reduction. The clustering of data points around the generalized reduction factor $\chi_B = 1$ indicates that most of the built-up members are able to reach, or nearly reach, their full plastic axial capacity under compression. This behaviour typically occurs in very short members with $\bar{\lambda}_B < 0.2$, where buckling effects are minimal and the response is governed primarily by material yielding. The downward trend in resistance values, particularly in the range $0.5 \le \bar{\lambda}_B \le 1.5$, reflects typical reductions caused by geometric imperfections and residual stresses, which lower the ultimate strength of the members. For long columns ($\bar{\lambda}_B > 1.7$), points appear close to the stability limit line ($\chi_B \approx 1/\bar{\lambda}_B^2$), which corresponds to the Euler elastic critical load, indicating that the strength is governed by elastic capacity due to lower sensitivity to the effects of geometric imperfection and residual stresses.

Overall, the O.I.C. adopts an extended Ayrton-Perry format, with all key parameters calibrated to fit the proposed buckling curves against the numerical results, ensuring both conservatism and safe-side predictions. The detailed O.I.C.-based design equations for both local buckling and built-up buckling are provided in Table 6.3.

Table 6.3 Design procedure and key parameters for local and built-up member buckling curves.

Buckling resistance	Local buckling	Built-up buckling
Key parameters	$\bar{\lambda}_0 = 0.5$ $\alpha_L = 0.125$ $\delta = 0.7$	$\bar{\lambda}_0 = 0.15$ $\alpha_B = \begin{cases} 0.14, \text{ tip-to-tip section } [\,] \\ 0.22, \text{ back-to-back section }] \, [\end{cases}$ $\delta = 2.0$
Reduction factor based on Ayrton-Perry format	$\phi_L = 0.5 \cdot \left[1 + \alpha_L \left(\bar{\lambda}_L - \bar{\lambda}_0 \right) + \bar{\lambda}_L^{\delta} \right]$ $\chi_L = \frac{1}{\phi_L + \sqrt{\phi_L^2 - \bar{\lambda}_L^{\delta}}} \le 1$	$\phi_B = 0.5 \cdot \left[1 + \alpha_B \left(\bar{\lambda}_B - \bar{\lambda}_0 \right) + \bar{\lambda}_B^2 \right]$ $\chi_B = \frac{1}{\phi_B + \sqrt{\phi_B^2 - \bar{\lambda}_B^2}} \le 1$

6.4.3 Local/built-up interaction factor $f_{L/B}$

6.4.3.1 Limit cases and theoretical considerations

The local/built-up interaction factor $f_{L/B}$ is introduced to account for the interaction between local buckling of the cross section and built-up buckling in the overall member. Therefore, the effect of this interaction can be expressed as a function of $\bar{\lambda}_B$, since at large $\bar{\lambda}_B$ the member is so slender that overall built-up buckling dominates, and the contribution of cross-section interaction becomes negligible. The $f_{L/B}$ relationship, defined by Eq. (6.6), is based on the O.I.C. design flow chart shown in Figure 6.13. Here, χ_{L+B} is numerically determined by relaxing all constraints to capture the full combined local and built-up buckling response.

$$f_{L/B} = \frac{\chi_{L+B}}{\chi_L \cdot \chi_B} \tag{6.6}$$

In Eq (6.6), the behaviour of $f_{L/B}$ can be characterized by examining limit cases of column relative slenderness: (i) for short columns (small), where $\bar{\lambda}_B$ the built-up buckling of the overall member is minimal ($\chi_B \approx 1$), local buckling of the cross-section dominates, and the interaction factor is primarily governed by the cross-section resistance, (ii) for long columns (large $\bar{\lambda}_B$), the elastic capacity is governed by the built-up buckling of the overall member, and local buckling of the cross section does not influence the load at which χ_B is reached, so $f_{L/B}$ tends toward $1/\chi_L$, and (iii) for intermediate columns, the interaction is partial, and the factor satisfies $1 < f_{L/B} < 1/\chi_L$. These limit

cases provide a framework for understanding how cross-section slenderness and built-up member slenderness interact, emphasizing conceptual trends rather than specific design adjustments.

6.4.3.2 Numerical results and discussion

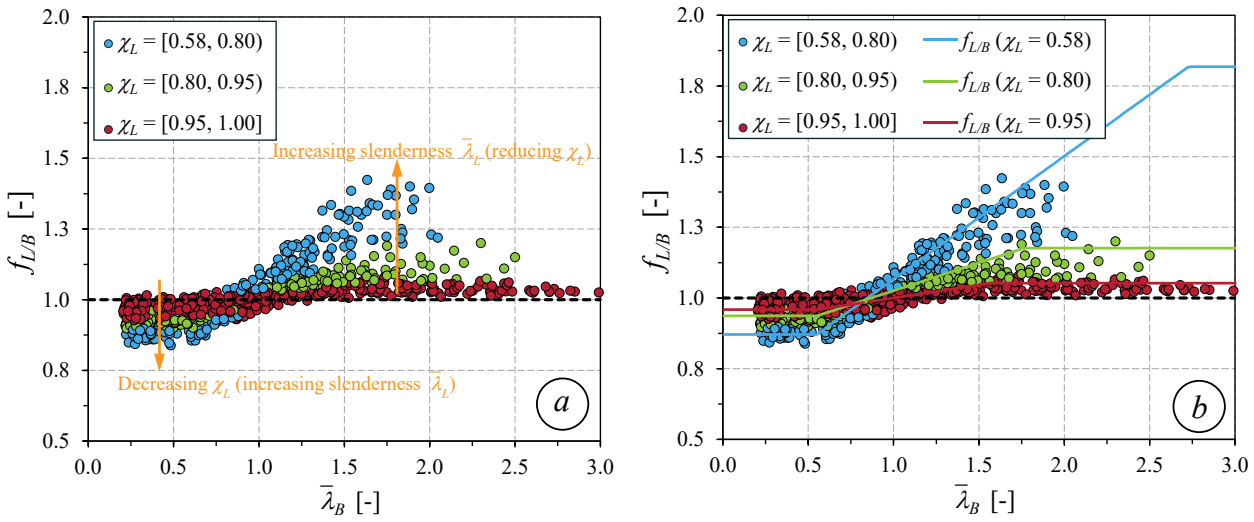

Figure 6.15 Local/built-up interaction factor $f_{L/B}$.

To facilitate a clearer investigation, the series of F.E. results in Figure 6.15 were categorized into three cases based on the value of χ_L: (i) (very) slender $\chi_L = [0.58, 0.80)$, (ii) moderately slender $\chi_L = [0.80, 0.95)$, and (iii) nearly compact $\chi_L = [0.95, 1.00]$. Note that χ_L represents the reduction factor for cross-section resistance – where a smaller value indicates a more slender section, while a value closer to 1.0 corresponds to a non-slender section. It is clearly seen that the slenderness of the cross-section has significant effects on the local/built-up coupling factor. Figure 6.15a highlights several key points:

- For short built-up columns ($\bar{\lambda}_B \leq 0.55$), increasing the cross-section slenderness $\bar{\lambda}_L$ (i.e., decreasing χ_L) leads to a reduction in the $f_{L/B}$, reflecting the strong interaction between local and built-up buckling. When the local/built-up interaction is less pronounced – as observed for $\chi_L = [0.95, 1.00]$ – $f_{L/B}$ remains close to 1.0. In contrast, when the local/built-up interaction becomes strongly coupled, typical of $\chi_L = [0.58, 0.80)$, $f_{L/B}$ falls substantially below 1.0, reflecting a notable reduction in resistance due to the intensified interaction between local and overall buckling;

- Conversely, increasing the cross-section slenderness $\bar{\lambda}_L$ at high $\bar{\lambda}_B$ results in a gradual rise in the $f_{L/B}$ value. This occurs because, for long columns, the elastic capacity is governed by the overall buckling mode, and local buckling does not influence the load level at which χ_B is reached. Therefore, the factor $f_{L/B}$ should be defined to account for the effect of built-up buckling, χ_B, on the member's resistance. In particular, when $\chi_L < 1$, $f_{L/B}$ may be expressed as $1/\chi_L$, which corresponds to the behaviour for long columns (higher $\bar{\lambda}_B$), where the influence of local buckling dominates and $f_{L/B}$ tends toward $1/\chi_L$;
- For intermediate column lengths, the factor lies between the two extremes: $1 < f_{L/B} < 1/\chi_L$.

6.4.3.3 Proposed design equation for $f_{L/B}$

As observed in Figure 6.15a, a set of trilinear design equations was developed for the factor $f_{L/B}$, as expressed in Eq (6.7). This proposed equation is derived through curve fitting of the numerical data. The formula is compared with the numerical results in Figure 6.15b, where only the upper-bound curves for $f_{L/B}$, corresponding to $\chi_L = 0.58$, $\chi_L = 0.80$, and $\chi_L = 0.95$, are presented. Note that in Figure 6.15b, the lower-bound curves are shown for illustration. Each data point corresponds to a slightly different $f_{L/B}$, so the curve may appear smoother than the actual discrete results. While these curves show the general trend, the proposed formula provides a more accurate representation than the figure suggests.

$$f_{L/B} = \begin{cases} k_L & \bar{\lambda}_B \le 0.55 \\ \dfrac{\bar{\lambda}_B - 0.55}{1.5/\chi_L - 0.55}\left(1/\chi_L - k_L\right) + k_L & 0.55 < \bar{\lambda}_B \le 1.5/\chi_L \\ 1/\chi_L & \bar{\lambda}_B > 1.5/\chi_L \end{cases} \tag{6.7}$$

where the factor k_L is given as follows:

$$k_L = 0.22\chi_L + 0.75 \tag{6.8}$$

This factor quantifies the effect of local buckling in short columns, particularly when $\bar{\lambda}_B \le 0.55$. When the interaction is strong, typically in slender sections, χ_L is relatively low and k_L approaches

0.75. As χ_L increases and the interaction becomes less pronounced, k_L rises toward 0.97, indicating a reduced impact on the resistance due to local/built-up interaction.

As shown in Figure 6.15b, the proposed trilinear equation demonstrates good agreement with the numerical results across all considered cases. For each selected value of χ_L, the corresponding upper-bound design curve closely follows the distribution of the numerical data, particularly in the moderate to high slenderness range. The equation effectively captures the influence of the local/built-up interaction through the parameters k_L and χ_L, providing a consistent and conservative estimate of the interaction factor $f_{L/B}$. Overall, the proposed expression offers a practical and reliable tool for design applications, accurately reflecting the reduction in resistance due to coupled buckling effects in laced built-up columns.

6.4.4 Assessment of design proposal

To offer a more explicit numerical evaluation of the O.I.C. design proposal, Figure 6.16 illustrates the performance of the O.I.C. design proposal and current standards (AISC [112], Eurocode 3 [154], and CSA S16 [114]) – collectively referred to as Reference (Ref.) – in comparison with F.E. results. Figure 6.16a presents a variation of the $\chi_{L+B,\mathrm{Ref.}} / \chi_{L+B,FE}$ ratio to assess the overall accuracy of each design proposal relative to the slenderness of built-up columns $\overline{\lambda}_B$, while Figure 6.16b further displays the frequency distribution across intervals of the same $\chi_{L+B,\mathrm{Ref.}} / \chi_{L+B,FE}$ ratio. It should be noted that $\chi_{L+B,\mathrm{Ref.}} / \chi_{L+B,FE} = N_{u,L+B,\mathrm{Ref.}} / N_{u,L+B,FE}$, representing the predicted-to-real resistance obtained from the F.E. results. A ratio below 1.0 corresponds to safe resistance estimates, whereas those exceeding 1.0 suggest potentially unsafe predictions.

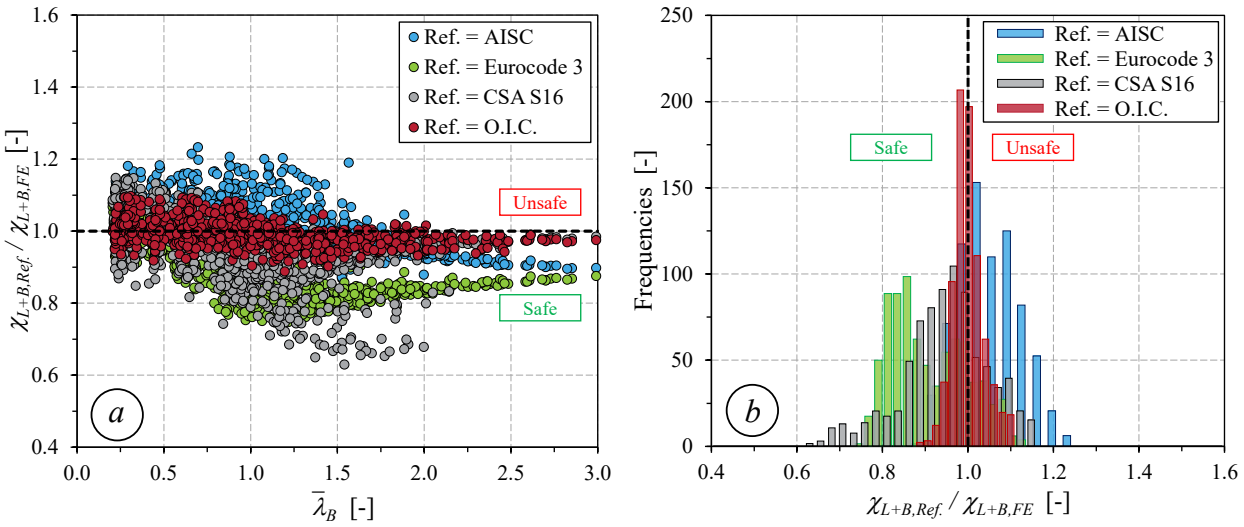

Figure 6.16 Analytical resistance vs. numerical results.

Results show that the O.I.C. design proposal exhibits a tightly clustered distribution around the ideal value of 1.0, indicating close agreement with F.E. results and minimal deviation. Compared to other standards, the O.I.C. method provides less scatter, with values predominantly near or slightly below 1.0. Besides, the frequency distribution for the O.I.C. proposal is sharply peaked around 1.0, emphasizing its consistency and precision.

A more refined statistical assessment of the O.I.C and current design proposals is presented in Table 6.4. The results of each method are categorized into three slenderness ranges corresponding to short ($\bar{\lambda}_B \leq 0.75$), intermediate ($0.75 < \bar{\lambda}_B \leq 1.5$) and long columns ($\bar{\lambda}_B > 1.5$). Based on 791 F.E. results across full range of $\bar{\lambda}_B$, the data indicate that the O.I.C. design proposal provides excellent accuracy, with an average $\chi_{L+B,O.I.C} / \chi_{L+B,F.E.}$ ratio of 0.99 and a C.o.V. of 3.5%, reflecting a high degree of precision and consistency. The most conservative estimate in the dataset is 0.89, which remains within an acceptable safety margin. Notably, no critically unsafe predictions are observed. Only a small fraction of cases (6.4%) exceeded a ratio of 1.05, with a maximum of 1.10, corresponding to the worst-case unsafe prediction (10% above the expected value). These findings confirm that the O.I.C. method offers reliable and consistently conservative estimates for the compressive resistance of laced built-up columns.

Table 6.4 Summary of statistical results of $\chi_{L+G+B,\mathrm{Re}f.} / \chi_{L+G+B,FE}$ ratio for laced built-up columns based on relative slenderness $\overline{\lambda}_B$.

Relative slenderness	Number of cases	Proposals	Mean	C.o.V. [%]	Max.	Min.	< 0.90 [%]	>1.05 [%]	>1.10 [%]
$\overline{\lambda}_B \le 0.75$	302	AISC	1.06	5.2	1.23	0.94	0.0	56.3	**24.2**
		Eurocode 3	0.98	5.7	1.13	0.84	7.9	14.2	1.0
		CSA S16	1.01	**7.1**	1.15	0.82	7.3	33.4	10.9
		O.I.C.	**1.01**	**3.4**	1.10	0.92	0.0	10.9	0.0
$0.75 < \overline{\lambda}_B \le 1.50$	327	AISC	1.04	6.4	1.24	0.9	0.0	37.0	**19.9**
		Eurocode 3	**0.85**	7.3	1.0	0.75	79.2	0.0	0.0
		CSA S16	**0.88**	**8.3**	1.05	0.65	59.0	0.0	0.0
		O.I.C.	**0.99**	**3.5**	1.08	0.89	0.30	5.5	0.0
$\overline{\lambda}_B > 1.50$	162	AISC	1.01	15.7	1.22	0.88	4.9	16.0	**16.0**
		Eurocode 3	**0.84**	2.8	0.90	0.78	99.4	0.0	0.0
		CSA S16	**0.91**	**10.6**	0.99	0.63	22.8	0.0	0.0
		O.I.C.	**0.97**	**1.9**	1.02	0.92	0.0	0.0	0.0
All values of $\overline{\lambda}_B$	791	AISC	**1.04**	**8.7**	1.24	0.88	1.0	39.9	**20.5**
		Eurocode 3	0.90	9.7	1.13	0.75	56.1	5.4	0.4
		CSA S16	0.93	**10.5**	1.15	0.63	31.9	12.8	4.2
		O.I.C.	**0.99**	**3.5**	1.10	0.89	0.1	6.4	0.0

In comparison, Eurocode 3 provides the most conservative estimates among all standards across the full range of column lengths, with an average $\chi_{L+B,Eurocode3} / \chi_{L+B,F.E.}$ ratio of 0.90 and a C.o.V. of 9.7%. More than 55% of its predictions fall below 0.90, highlighting its conservative bias. The greatest level of conservatism is observed for columns of intermediate length, where the minimum ratio reaches as low as 0.75. CSA S16 exhibits a similar trend, with an average $\chi_{L+B,CSAS16} / \chi_{L+B,F.E.}$ ratio of 0.93 and a higher C.o.V. of 10.5%. Its most conservative prediction is 0.63, while the most unconservative case reaches a maximum ratio of 1.15. In contrast, the AISC design provisions tend to be the most unconservative among the evaluated standards, though still within acceptable limits. The average $\chi_{L+B,AISC} / \chi_{L+B,F.E.}$ ratio is 1.04 with a C.o.V. of 8.7%, indicating a slight overestimation relative to the F.E. results. The most conservative results is 0.88, while the most unconservative reaches 1.24. Additionally, over 20% of the predictions exceed a ratio of 1.10, reflecting a noticeable portion of potentially unsafe predictions, particularly for long members.

All three standards (AISC, Eurocode 3, and CSA S16) exhibit relatively high variability, with C.o.V. exceeding 10% when evaluated within specific slenderness categories (i.e., short, intermediate, and long columns), even though the overall scatter is lower. Such elevated dispersion

may undermine the consistency of the design method, indicating uneven performance across different column lengths. Consequently, higher C.o.V. values may require more conservative safety factors or targeted modifications to ensure adequate safety margins. Given the observed variability and safety concerns, the following section presents a reliability analysis to evaluate the required safety factors for the O.I.C. design proposal as well as for the current design standards.

6.5 Reliability analyses

6.5.1 Reliability analyses in accordance with EN 1990 (Eurocodes)

In this section, the Eurocode framework outlined in Annex D of EN 1990 [193] is employed to determine the partial safety factor γ_M. This factor accounts for variability and uncertainties in material properties, geometric dimensions, imperfections, and the simplifications inherent in design models, covering both cross-section and member resistance verifications. The reliability assessment was performed following the guidelines of the First Order Reliability Method. The analysis focused on quantifying the uncertainty and safety margins associated with both numerical results and the evaluated design proposals, which include AISC, Eurocode 3, CSA S16, and the proposed O.I.C. method. According to Clause 6.1 of Eurocode 3 Part 1-1, a recommended target value of γ_M = 1.0 is specified for both cross-sectional and member level checks. Equivalently, this corresponds to a resistance factor $\phi = 1/\gamma_M = 1.0$. For comparison, AISC adopts $\gamma_M \approx 1.1$, or $\phi = 0.90$.

As reported in Table 6.5, each design proposal was evaluated based on a consistent set of statical parameters including: the number of data points *n*, the design fractile factor $k_{d,n}$, the bias factor *b*, and the material overstrength factor $f_{y,mean}/f_{y,nom}$. The total uncertainty in resistance prediction was characterized by the combined coefficient of variation V_r, which incorporates variability from material, geometric, and model sources and can be calculated as follows:

$$V_r^2 = V_\delta^2 + V_{rt}^2 \tag{6.9}$$

$$V_{rt}^2 = V_{mat}^2 + V_{geom}^2 \tag{6.10}$$

where V_δ denotes the C.o.V. associated with model uncertainty, V_{mat} represents the C.o.V. due to material variability, and V_{geom} is the C.oV. due to geometric variability. In this study, V_{mat} and V_{geom} were taken as 0.05 and 0.025, respectively, following the recommendations in [197].

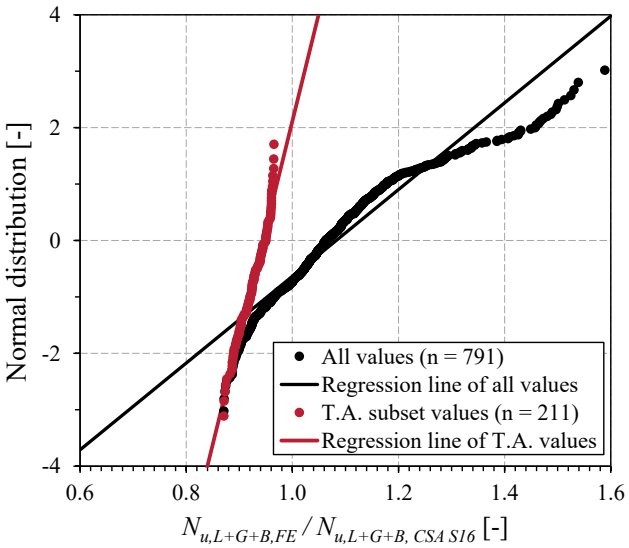

Figure 6.17 Example of tail approximation for CSA S16.

To improve the accuracy in the tail region, particularly for high reliability targets, a Tail Approximation (T.A.) technique was employed as a supplementary method. This approach addresses the incorrect assumption that resistance predictions follow a log-normal distribution by refining the behaviour of the lower tail of the resistance data, where greater scatter and deviations from the ideal distribution are typically observed. These deviations can undermine standard statistical assumptions and affect the reliability of safety assessments. The T.A. allows the statistical model to remain valid by better capturing the lower-bound resistance values that influence design safety factors. To clearly illustrate this, an example of applying the T.A. technique to CSA S16 is presented in Figure 6.17. The figure presents a normal probability plot of the resistance ratio $N_{u,L+B,FE} / N_{u,L+G+B,CSA\ S16}$, used to assess the statistical characteristics of the prediction accuracy. The full dataset (n = 791) is shown as black markers, with a corresponding regression line indicating approximate normality. A lower-tail subset (n = 211), highlighted in red, was selected for the T.A. technique. As shown by the black regression line, the full dataset initially exhibits a noticeable deviation from linearity in the lower tail, indicating non-normal behaviour. After applying TA, the red line demonstrates a nearly linear trend, suggesting that TA effectively mitigates this deviation. This deviation supports the application of T.A. to more accurately

characterize low-probability strength predictions, particularly in the unsafe region where $N_{u,L+B,FE} / N_{u,L+G+B,CSA\ S16} < 1$.

Table 6.5 Results of reliability analyses based on the Eurocode approach.

Study cases	Proposals	n	$k_{d,n}$	b	$f_{y,mean} / f_{y,nom}$	V_{geom}	V_{mat}	V_{δ}	V_r	γ_M
Without T.A.	AISC	791	3.103	0.953	1.20	0.025	0.05	0.083	0.100	1.19
	Eurocode 3	791	3.103	1.064	1.20	0.025	0.05	0.096	0.111	1.10
	CSA S16	791	3.103	1.020	1.20	0.025	0.05	0.110	0.123	1.20
	O.I.C.	791	3.103	1.010	1.20	0.025	0.05	0.033	0.065	1.01
With T.A.	AISC	654	3.105	0.946	1.20	0.025	0.05	0.073	0.092	1.17
	Eurocode 3	297	3.123	0.996	1.20	0.025	0.05	0.044	0.071	1.04
	CSA S16	211	3.134	0.949	1.20	0.025	0.05	0.040	0.069	1.09
	O.I.C.	698	3.104	1.006	1.20	0.025	0.05	0.028	0.063	1.00

As shown in Table 6.5, the calibrated partial safety factors (γ_M) for AISC, Eurocode 3, and CSA S16 without applying T.A. are 1.19, 1.10, and 1.20, respectively. These values result from the calibration procedure and reflect the methodology used, which may differ from the standard target values of 1.0 or 1.1 recommended by the codes. When T.A. is applied, the γ_M values decrease slightly to 1.17, 1.04, and 1.09. These γ_M values are obtained from the most representative subset of each dataset, corresponding to the lowest ratio of design resistance to experimental resistance within that subset. The reduction observed after applying T.A. is a result of refined estimation in the lower range of the resistance distribution, which influences the characterization of rare but critical failure cases. According to the design provisions, AISC and CSA S16 target a safety factor of $\gamma_M = 1 / \phi \approx 1.1$, while Eurocode 3 specifies $\gamma_M = 1.0$. When comparing these targets to the calibrated values obtained from applying T.A. technique, the safety factor for Eurocode 3 is slightly higher than its target (1.04 vs. 1.0), indicating a mildly conservative prediction. For CSA S16, the calibrated value is approximately equal to the target, suggesting a generally well-aligned design approach with a minor conservative margin. In contrast, the calibrated safety factor for AISC is noticeably higher than the target value, reflecting that the current AISC provision tends to produce multiple unsafe predictions. To compensate for these problematic results, the calibration increases γ_M, ensuring overall conservative design predictions. Besides, the O.I.C. method yields a

minimum γ_M of approximately 1.00, improving from 1.01 when the T.A. procedure is applied, based on a selected subset of 698 cases. This indicates that the T.A. approach slightly enhances the accuracy of the predictions, bringing the minimum predicted-to-real resistance closer to the ideal value of 1.0. Figure 6.18 further illustrates how γ_M varies with the number of data points retained in the tail approximation, highlighting its responsiveness to changes in performance across all design proposals.

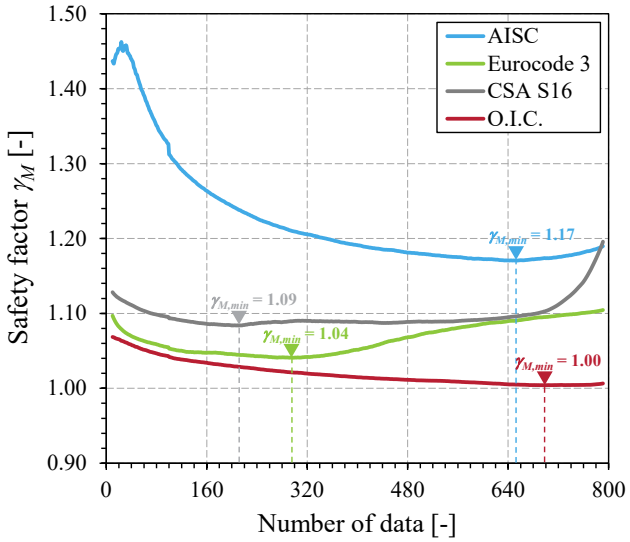

Figure 6.18 Variation of safety factor γ_M with tail data using EN 1990 approach.

6.5.2 Reliability analyses in accordance with the AISC-LRFD approach

The AISC-LRFD method is based on a probability-based limit states framework, where reliability is measured by a reliability index β, assuming a lognormal distribution as defined by Ravindra and Galambos [195]. The reliability index can be estimated using the following expression:

$$\beta = \frac{1}{\sqrt{V_R^2 + V_Q^2}} \ln\left(\frac{R_m}{Q_m}\right) \tag{6.11}$$

where R_m and Q_m denote the mean resistance and the mean total load effect, respectively, while V_R and V_Q represent their corresponding C.o.V.s. To account for the statistical characteristics of the total load effect, the Eq. (6.12) can be expressed as:

$$\beta = \frac{1}{\sqrt{V_R^2 + V_Q^2}} \ln\left(\frac{R_m}{0.657\phi_2 R_n}\right) \tag{6.12}$$

This formulation was calibrated based on the load combination 1.2*D* + 1.6*L*, as described in [201] and [200], where V_Q was taken as 0.22, particularly for cases with a mean live-to-dead load ratio L_m / D_m = 3.0. The ratio R_m / R_n and V_R can be defined using Eqs. (6.13)and (6.14), respectively. In this context, M_m represents the mean ratio of actual-to-specified yield stress (capturing material variability), F_m refers to the mean ratio of actual-to-specified plastic section modulus (representing fabrication effects), and P_m corresponds to the mean ratio of test-to-predicted resistance (reflecting professional judgment). The C.o.V. for these parameters are given by V_M, V_F, and V_P, respectively.

$$R_m / R_n = M_m \cdot F_m \cdot P_m \tag{6.13}$$

$$V_R = \sqrt{V_M^2 + V_F^2 + V_p^2} \tag{6.14}$$

In this study, the statistical parameters for material variability, M_m and V_M, were adopted based on recommendations in [208], while those for fabrication variability, F_m and V_F were taken from the data reported in [209]. The resistance factor was then approximated as:

$$\phi = \frac{R_m}{R_n} \exp\left(-\alpha\beta V_R\right) \tag{6.15}$$

where the separation factor α, representing the margin between mean and design resistance, was taken as 0.8. According to Commentary Section B3.1 of AISC 360-22, the LRFD method was calibrated at a L_m / D_m = 3.0, where the resistance factor ϕ is specified as 0.90, corresponding to a minimum reliability index β of approximately 2.6 for member design. The resistance factor ϕ is related to the partial safety factor γ_M through $\phi \approx 1/\gamma_M$. For comparison, EN 1990 uses a higher target global reliability index $\beta = 3.8$ for a 50-year design life of building structures, which corresponds to a resistance-only reliability index of approximately 3.04. Unlike EN 1990, the AISC framework considers uncertainties from both resistance and load effects, resulting in a lower, more permissive, β target for members. Therefore, the β values derived here are not directly comparable to those based on EN 1990, as they are obtained using the simplified approximation $\phi \approx 1/\gamma_M$.

While this provides a practical estimate, it does not account for all factors considered in the standard.

Table 6.6 Results of reliability analyses based on the AISC-LRFD approach.

Proposals	n	M_m	F_m	P_m	R_m / R_n	V_F	V_M	V_p	V_R	V_Q	β	ϕ
AISC	791	1.10	1.00	0.969	1.066	0.05	0.056	0.080	0.110	0.22	2.40	0.86 / 0.84*
Eurocode 3	791	1.10	1.00	1.124	1.237	0.05	0.056	0.095	0.121	0.22	2.94	0.93
CSA S16	791	1.10	1.00	1.083	1.191	0.05	0.056	0.115	0.137	0.22	2.70	0.88
O.I.C.	791	1.10	1.00	1.016	1.117	0.05	0.056	0.033	0.082	0.22	2.71	0.93

* Value calculated based on $\beta = 2.60$

Table 6.7 Resistance factor ϕ according to best tail approximation for different proposals.

Proposals	n_{tail}	ϕ
AISC	781	0.84
Eurocode 3	753	0.93
CSA S16	653	0.91
O.I.C.	782	0.93

Adopting the procedure from [200], the resistance factor ϕ_2 in Eq. (6.12) was fixed at 0.90 to enable direct comparison across different proposals when estimating the reliability index β. A higher β correspond to higher safety levels and lower probabilities of failure. In this context, a minimum reliability index of 2.6 is required to ensure an adequate safety margin. Table 6.6 presents the results of reliability analysis based on the AISC-LRFD approach. It should be noted that the resistance factor ϕ shown in the table applies solely to member design. As indicated, Eurocode 3 and CSA S16 have reliability index values β exceeding the minimum requirement, with values of 2.94 and 2.70, respectively. Their corresponding resistance factors ϕ are 0.93 for Eurocode 3 and 0.88 for CSA S16. In contrast, the AISC standard has a reliability index of 2.40, which falls below the required minimum of 2.60. To meet this requirement, the resistance factor for AISC is recalculated based on $\beta = 2.6$, resulting in a more conservative value of 0.84, compared to the previously specified value of 0.86. Applying this recalculated $\phi = 0.84$ in the AISC design equations ensures that the resulting design satisfies the minimum required safety level. As summarize in Table 6.7, the resistance factors obtained with and without the application of the T.A. technique show minimal improvement across all design proposals, except for CSA S16, where ϕ

increases from 0.88 to 0.91. In contrast, the resistance factor obtained for AISC ($\phi = 0.84$) still fails to meet the recommended target value of 0.90, indicating that the design provision may be unconservative and inconsistent, highlighting the need for further calibration to ensure adequate safety and reliability. In comparison, the O.I.C. proposal shows a reliability index β of 2.71, meeting the minimum reliability criterion, and a resistance factor ϕ of 0.93. With ϕ exceeding 0.90, the O.I.C. proposal demonstrates a more reliable, consistent, and accurate design approach. The observed difference in the O.I.C. proposal when using the EN1990 and AISC LRFD frameworks arises from different assumptions on material overstrength (1.2 vs. 1.1) and reliability indices. Consequently, the resulting factors cannot be directly compared, as they reflect different safety margins and target reliabilities.

6.6 Conclusions

This study has addressed the out-of-plane flexural buckling behaviour of laced built-up steel columns with a double (X) lacing system subjected to axial compression. The investigated built-up sections are characterized by low height-to-width ratios h / b_o, resulting from a large spacing b_o between the main chords. This geometry reduces the flexural stiffness about the weak axis and increases susceptibility to out-of-plane buckling. A comprehensive parametric study was conducted to quantify the influence of section classifications, steel grades, chord arrangement, lacing angle, lacing slenderness, and member length proportions on the out-of-plane resistance. A validated F.E. model was developed to investigate key buckling phenomena, including local buckling, built-up buckling, and their interaction. Based on the numerical findings, a design approach based on the O.I.C. was proposed. The method provides more reliable, consistent, and conservative predictions than those given by AISC, Eurocode 3 and CSA S16. Its validity is supported by reliability analyses in accordance with EN 1990 and AISC LRFD, confirming its suitability for practical design of laced built-up columns subject to out-of-plane buckling failure.

6.7 Acknowledgement

This research and development project would not have been possible without the contribution and collaboration of The Jacques Cartier and Champlain Bridges Incorporated.

CHAPTER 7 GENERAL DISCUSSION

7.1 Overview of integrated findings

The studies presented in this thesis were undertaken to evaluate the compressive strength of built-up steel members, with particular emphasis on those used in truss bridges constructed in the 1950s and currently managed by JCCBI. The primary objective of the project was to develop simple and efficient tools for evaluating the compressive strength of these truss members. The investigation focused on built-up members composed of two C-shaped sections interconnected by lacing systems. While each article addressed a specific aspect, their integration provides a comprehensive understanding of the governing mechanisms.

Through extensive numerical investigations, supported by available experimental data, consistent trends were identified regarding the influence of second-order effects on shear forces within built-up members, as well as the interaction of complex buckling modes of the individual components – local, global, and overall built-up interactions – on the ultimate resistance. Each study also resulted in formulations and equations to quantify shear forces, compressive resistance, and buckling interactions, providing a quantitative framework to assess member behaviour.

The findings revealed that the geometry and slenderness of lacing systems and the built-up members themselves do not always comply with current fabrication limits specified in modern construction standards. Furthermore, bridge members were often assembled from multiple components such as angles, plates, and channel sections, whose buckling behaviour is highly sensitive to interaction effects. The results also indicated that current design provisions are, in some cases, either overly conservative or unconservative when applied to laced built-up members.

Collectively, these findings provide a comprehensive understanding of the factors controlling the compressive behaviour and failure modes of laced built-up members, integrating insights from the stability of the lacing system under second-order effects, buckling interactions, and the design approach developed in this thesis.

7.2 Methodological considerations

Assessing the compressive strength of built-up steel members can be approached in several ways. Different methods offer varying levels of accuracy, generality, and practicality, depending on the

complexity of the members and the interactions being considered. These approaches can be broadly categorized as follows:

(i) Traditional methods in design codes, such as AISC, EC3, CSA, and AASHTO, rely on analytical or empirical formulas that estimate resistance using slenderness, effective length, and reduction factors. While straightforward, these approaches often simplify or neglect complex interactions between lacing systems and member components;

(ii) Experimental testing offers direct insights into failure modes and ultimate resistance, but it is limited by the number of specimens, parameter coverage, and practical constraints;

(iii) Numerical modeling, particularly FE analysis, provides a systematic means to study a wide range of geometries/slenderness, lacing/section arrangements, and interaction effects that would be difficult to capture experimentally or with simplified code formulas;

(iv) Modern advanced methods integrate numerical modeling with systematic interaction approaches, such as the O.I.C. method, to capture complex buckling interactions, including local, global member behaviour, providing a more comprehensive and accurate assessment of compressive strength, particularly for members with non-standard geometries or existing bridge members beyond code limits.

The methodology adopted in this thesis primarily relies on modern advanced techniques integrated with numerical modeling. The O.I.C. approach was employed to derive equations for assessing the compressive strength of laced built-up members. To achieve this, numerical analyses were conducted and validated against available experimental data from the literature. Geometric imperfections were calibrated based on experimental results, residual stresses were adopted from established proposals in previous studies, and boundary conditions were idealized to remain consistent with the test configurations. This sequential process of calibration, validation, and parametric analysis ensured that the finite element models accurately captured the behaviour of laced built-up members under compression. In particular, the extended O.I.C. approach was implemented to capture triple-interaction buckling modes, encompassing local, global, and overall member behaviour. This positions the present methodology closer to advanced numerical approaches than to traditional code-based formulas or purely experimental methods.

Another important aspect of the buckling behaviour in laced built-up members is the instability of the lacing system itself. The lacing system enables shear transfer between the main components of the built-up column; however, designing it to prevent premature buckling – buckling that occurs before the main chords fail – remains challenging, particularly when its stiffness is considered. Unlike traditional approaches based on simplified empirical formulations, the modern advanced approach used in this study integrates numerical modeling to derive simple yet effective equations. This is not merely because the method is F.E.-based, but rather because the buckling behaviour of lacing systems is inherently complex. Empirical formulas often lead to complicated expressions and may fail to adequately capture the influence of lacing slenderness and arrangement on member performance.

In this thesis, the instability of the lacing system was first investigated to clearly understand the magnitude of the forces transferred through it, enabling the design of lacing systems that can resist buckling before the main components fail. This investigation allows for a systematic evaluation of second-order effects influenced by lacing slenderness, lacing arrangement, chord configuration, and cross-section slenderness. The outcome is a set of comprehensive design equations that enhance the understanding and assessment of lacing system stability across a wide range of built-up members. Subsequently, the extensive framework of the O.I.C. approach was developed to formulate equations for predicting the ultimate resistance of laced built-up members subjected to buckling in both the in-plane and out-of-plane directions of the lacing system. Compared with other approaches in the literature, the adopted methodology offers a balance between reliability and generality, providing confidence in the F.E. model's predictions across a wide range of parameters.

7.3 Contribution to literature and practice

The overall contribution of this thesis lies in providing a comprehensive understanding of the actual buckling response of laced built-up steel members under compression, bridging the gap between conventional design assumptions and actual structural behaviour. The primary failure modes of laced built-up steel members can be classified as follows: (i) local buckling of the cross-section, (ii) global buckling of the main chord between lacing connections, (iii) overall built-up buckling of the member, and (iv) failure of the lacing system and (v) interaction effects involving buckling, yielding, geometric imperfections, and residual stresses.

This thesis makes several original contributions to the understanding and design of laced built-up steel members. A first key contribution lies in investigating the stability of the lacing system due to second-order effects (see Paper 1 in Chapter 4); this work provides a systematic method to evaluate forces in the lacing system, enabling engineers to account for the effects of lacing slenderness, lacing arrangement (single and double lacing system), and cross-section slenderness across a wide range of member lengths when designing lacing systems. There is a lack of studies addressing these factors, and although current design codes specify limits for slenderness and geometry, many existing bridge members exceed these limits. This contribution therefore addresses a gap identified in the literature review and provides an original and more effective tool for evaluating shear forces, which are then used to design the lacing systems in laced built-up members.

Besides, as reported in Paper 2 and 3 (see Chapter 5 and 6), this research quantifies the ultimate compressive resistance of laced built-up members and identifies the governing buckling behaviour under axial loads, considering variations in yield strength, cross-section slenderness, lacing slenderness, chord arrangements, and member slenderness. This extends existing knowledge to members whose geometries exceed current design limits and provides extensive guidance for assessing older bridge steel members. A further contribution is the proposal of an extensive O.I.C. approach to capture the triple-interaction buckling modes, encompassing local, global, and overall member buckling. This approach provides a comprehensive understanding of complex buckling behaviour, offers practical design equations for laced built-up members, and highlights factors governing failure that are often neglected in conventional design approaches. In addition, a reliability study was conducted for the proposed equations to assess their safety factors and demonstrate the robustness and applicability of the proposed formulation.

From a practical standpoint, the findings enable an evaluation of the safety levels of built-up members relative to current design codes, including AISC, EC3, CSA, and AASHTO. In doing so, the thesis provides engineers with evidence-based guidance on the safety levels of laced built-up columns relative to current design codes. Finally, the extensive development of the O.I.C. approach to address triple-interaction buckling provides a reference methodology for future researchers, offering a framework for handling complex buckling modes not only in built-up members but also in structural members with complex shapes and buckling behaviours, serving as the underlying philosophy for further studies.

7.4 Practical implications and limitations

The findings of this study have important implications for the design and assessment of laced built-up steel members in existing bridge structures, particularly those managed by JCCBI. The proposed design equations primarily address built-up columns composed of two C-shaped sections, arranged either tip-to-tip or back-to-back, and interconnected by single (diagonal) or double (X) lacing systems. For members with a single lacing system, the study provides equations for estimating forces in the lacing systems; however, their overall compressive strength is not directly addressed, as such members are rarely found in JCCBI-managed bridges, including the Jacques Cartier and Quebec Bridges. The study also covers built-up members whose main components consist of angle sections joined with a continuous web plate, as illustrated in Figure 1.3. In these cases, the riveted connections between the angle legs and the web plate are assumed to be sufficiently rigid to ensure composite action, such that the angles and web plate act together as C-sections. The slenderness ratios of the web and flange plates, defined as h / t_w and b / t_f, range from 6 to 96.95 and from 4 to 10.7, respectively. The lacing members were proportioned to remain elastic and to avoid failure prior to that of the built-up member. In addition, the minimum inclination angle of the lacing bars relative to the longitudinal axis of the built-up member was 25°. Accordingly, the proposed equations can be applied to similar members in other JCCBI-managed bridges, provided that all critical connections (including both the main chord–lacing connections and, for main chords composed of angles joined by a web plate, the connections between the angles and the web plate) remain sufficiently rigid and that slippage effects are negligible. While member deterioration, such as corrosion, may reduce overall strength, this does not invalidate the equations; appropriate reinforcement measures can maintain structural performance under such conditions.

Overall, the study provides a framework for assessing and designing laced built-up members in existing steel bridges under realistic constraints, while explicitly acknowledging the limitations associated with experimental uncertainties and deteriorated conditions. The proposed design equations remain applicable for members in good condition, whereas reinforcement techniques can address the effects of degradation without modifying the fundamental formulations. However, it is important to note that the method, in its current state of development, has the following limitations:

(i) The numerical analyses relied on residual stresses and calibrated initial geometric imperfections taken from available experimental data. While these

assumptions improve model accuracy, they may still differ from field conditions, where variability in residual stresses, fabrication tolerances, and other imperfections can influence member behaviour;

(ii) The possible slippage, looseness or failure of connections, particularly in built-up members whose individual chords are composed of two angles interconnected by continuous plates, was not modeled. This connection behaviour, combined with the potential effects of corrosion and material degradation over time, can influence the force distribution between components, reduce effective stiffness, and affect the overall stability and load-carrying capacity of aged structures;

(iii) The thesis primarily focused on members subjected to pure axial compression with simple support conditions. The dynamic behaviour, reinforcement solutions, combined influence of load eccentricities, connection flexibility, and the effect of gusset plates and boundary conditions on the effective length factor were not explicitly modeled. In real bridge truss joints, these factors can influence force distribution and capacity of members. These limitations do not undermine the validity of the findings but define the boundaries of their applicability.

7.5 Ongoing research

Future experimental work could involve testing both historical built-up members with batten plates and newly fabricated built-up members with lacings. Specifically, it could include approximately seven specimens (built-up members with batten plates) taken from the original Champlain Bridge, to characterize material properties, geometric imperfections, residual stress patterns, and connection behaviour, as well as to investigate buckling and failure under axial compression. In addition, testing three built-up members with lacing systems, representative of existing bridges such as the Jacques Cartier Bridge, would provide further insight into the behaviour of laced built-up members. The results from these experiments could be used to validate and refine the numerical models and analytical framework developed in this thesis, offering a more comprehensive understanding of both historical and modern built-up members and supporting the development of more accurate design recommendations.

CHAPTER 8 CONCLUSIONS AND RECOMMENDATIONS

8.1 Conclusions

The studies presented in this thesis were undertaken to evaluate the compressive strength of built-up steel members, with particular emphasis on those used in truss bridges constructed in the 1950s and currently managed by JCCBI. The investigation focuses on built-up members composed of two C-shaped sections interconnected by lacing systems. The main objective was to propose an original design approach for both the lacing system and the laced built-up steel members themselves, based on the O.I.C. framework, considering the possible local, global, and built-up interactions under simple loading conditions.

A comprehensive review of the factors influencing the resistance of built-up members was presented in Chapter 2. In addition, the historical development of buckling behavior and interactions was concisely reviewed, alongside a description of the methodologies adopted in current design standards. Overall, ensuring the stability of laced built-up columns under compression requires verifying two key aspects: (i) that the lacing system can effectively transfer shear forces within the column prior to failure, and (ii) that the main components of the built-up member can adequately resist axial loads.

To achieve this, a numerical shell F.E. model was first developed and carefully validated using *23 available experimental test results* conducted across four different laboratories. The developed model demonstrated an excellent capability to accurately replicate the experimental response and resistance. Accordingly, the validated F.E. models were further employed in extensive parametric studies, resulting in a database comprising *more than 20 000 simulation results*. This database was used to assess the stability of both the lacing system and the laced built-up members, as detailed in Chapters 4 to 6. The F.E. models were designed to cover all cross-section classifications, chord section arrangements, lacing configurations, lacing slenderness ratios, various member lengths, connector spacings, and steel grades, in order to represent the practical geometries of truss bridges constructed during the 1950s.

The research then began by investigating the stability of the lacing system and its influence on the ultimate resistance of laced built-up members, as detailed in Article 1. The objective was to propose an original equation for predicting the shear force transferred through the lacing system, accounting

for the effects of cross-section geometry, lacing slenderness, lacing configuration, and chord arrangement. This equation was developed to be applicable to a wide range of member geometries beyond the limitations of current design standards. Moreover, it enables engineers to design the lacing system such that failure does not occur before the main member reaches its ultimate capacity. The research then proceeded to investigate the ultimate resistance of laced built-up members under compression, with particular focus on members incorporating a double (X) lacing system, using the O.I.C. framework. A new extended O.I.C. framework was proposed to account for the triple interaction effect, i.e., L/G/B interaction. The studies specifically address: (i) members buckling in the plane of the lacing system, as detailed in Article 2, and (ii) members buckling out of the plane of the lacing system, as detailed in Article 3. The objective was to propose an original equation for designing the compressive resistance of laced built-up members, accounting for the potential L/G/B buckling interactions, which are often overlooked by current design rules.

The main conclusions of the research are summarized as follows:

1. **2nd order effects and shear forces in laced built-up columns**

   Shear forces induced by initial imperfections were found to significantly affect the behaviour of laced built-up members. Their magnitude depends on lacing arrangement, lacing and chord slenderness, and member length. The research led to the development of practical design equations for predicting shear force-to-ultimate load ratios, including both complete and simplified formulations, ensuring reliable and broadly applicable design while preventing premature lacing failure;

2. **Local/global/built-up interaction**s

   The study revealed that buckling behaviour is strongly influenced by complex interactions among local, global, and built-up modes, particularly in slender members. The O.I.C. framework was extended to incorporate a unified interaction factor $f_{L/G/B}$, enabling accurate prediction of combined effects on compressive resistance. Compared to existing standards (AISC, Eurocode 3, CSA S16), the proposed approach provides improved accuracy, consistency, and safety;

3. **Out-of-plane flexural buckling**

   Columns with low overall height-to-width ratios due to large chord spacing are more susceptible to out-of-plane flexural buckling. Parametric studies demonstrated that section geometry, lacing angle, lacing slenderness, chord arrangement, steel grade, and member length influence the out-of-plane resistance. The results also showed that out-of-plane buckling is less sensitive to local buckling interactions compared to in-plane behaviour, suggesting that a distinct treatment of local/global/built-up interactions for each buckling plane is appropriate. The proposed O.I.C.-based design method accounts for these effects, providing conservative and practical design rules validated through numerical simulations and reliability analyses in accordance with EN 1990 and AISC-LRFD frameworks.

4. **Practical design recommendations**

   The proposed design approaches enable engineers to predict the behaviour of laced built-up columns with higher reliability and consistency than current standards, while remaining applicable to a wide range of practical geometries. By integrating validated numerical modeling, extensive parametric studies, and reliability-based verification, the methods offer a robust framework for safe and efficient design of laced built-up steel members.

Overall, this thesis provides a comprehensive framework for understanding and designing laced built-up steel columns, integrating 2nd order effects, complex buckling interactions, and both in-plane and out-of-plane instability phenomena. These contributions advance the state of the art in both theoretical and practical aspects of stability design for built-up members.

8.2 Recommendations for further studies

Based on the findings and limitations identified throughout this thesis, and particularly in the previous chapter, several directions for future research are proposed:

(i) Incorporate the effect of early buckling of the lacing system to assess the ultimate resistance of laced built-up members with a single lacing configuration. As discussed in Section 4.3.4 of Article 1, the lacing geometry (slenderness ratio) was found to have a significant influence on the ultimate compressive strength of laced built-up members, resulting in more than a 20% variation in compressive capacity,

whereas members with a double lacing system showed no such influence. Since the proposed design approach for the compressive resistance of laced built-up members in the current study primarily focuses on members with double (X) lacing systems, accounting for the effect of early buckling in single (diagonal) lacing systems is important – particularly for older bridge members that do not comply with current fabrication standards. This could be achieved by extending the proposed O.I.C.-based framework to include more complex buckling interactions that consider all possible mechanisms, including local buckling of the cross-section, global buckling of individual chords between connectors, built-up buckling of the overall member, and global buckling of the lacing bars;

(ii) The flexural buckling behaviour of compressive built-up members in steel truss bridges requires careful consideration, particularly the interaction effects between bending about the strong and weak axes caused by global imperfections of the overall built-up members. Current design codes often assume that buckling along each axis occurs independently and adopt the minimum axial buckling resistance as the governing strength. When the resistances along both axes are comparable, this assumption can lead to unconservative predictions. Quantifying the interaction of amplification factors about both axes and evaluating their impact on load-carrying capacity would provide valuable insights for defining more accurate strength reduction factors and improving the design and assessment of compressive built-up members in steel truss bridges;

(iii) The effective length factor of compressive members in steel truss bridges requires careful consideration. The current design proposals in this thesis assume pinned-pinned end conditions, whereas in reality, both ends are typically connected via bearing plates. These connections can influence buckling behaviour and modify the effective length factor, affecting the member's axial resistance. Considering the interaction between end-plate stiffness and connection details behaviour allows for a more accurate determination of effective lengths and improves the design of compressive members in steel truss bridges, though this approach requires a detailed analysis of the connection behaviour;

(iv) The effects of long-term material degradation, such as corrosion, residual stresses, or initial imperfections in older bridges, shall be incorporated into the assessment of laced built-up member performance;

(v) More accurate modeling of connectors, such as lacing bars, tie-plates, and main chords, should be incorporated. The simplified assumptions used in this study may not fully capture the stiffness, slip, or load transfer behaviour of these connections, which can also influence the buckling and failure response of built-up members;

(vi) While this thesis considered L/G/B interactions under pure compression, it is recommended to also develop an approach for combined compression and flexural loading to better capture the behaviour of compressive members under various service conditions.

REFERENCES

[1] Transport Canada, “Champlain Bridge: Historical Overview and Structural Description,” Transport Canada, Ottawa, Canada, 2018.

[2] Jacques Cartier and Champlain Bridges Inc. (JCCBI), “Official Report on the Champlain Bridge Deconstruction,” JCCBI, Montreal, Canada, 2019.

[3] CBC News, “Dismantling of old Champlain Bridge to begin later this year,” CBC/Radio-Canada. [Online]. Available: https://www.cbc.ca/news/canada/montreal/dismantling-of-old-champlain-bridge-to-begin-later-this-year-1.5027590

[4] Expedia, “Jacques Cartier Bridge in Ville-Marie,” Expedia, Inc.

[5] T. V. Galambos, *Guide to Stability Design Criteria for Metal Structures*, 4th ed. New York: Wiley, 1988.

[6] Galbraith and Holgate Derry, *Royal Commission on Quebec Bridge Inquiry*. 1908.

[7] F. Engesser, “Zum Einsturz der Brücke über den St. Lorenzstrom bei Quebec,” *Zentralblatt Bauverwalt.*, vol. 27, p. 609, 1907.

[8] F. Engesser, “Die Knickfestigkeit gerader Stäbe,” *Cent. Bauverwalt.*, vol. 11, no. 49, p. 483, 1891.

[9] H. Ziegler, “Arguments for and against Engesser’s buckling formulas,” *Ing.-Arch.*, vol. 52, no. 1–2, pp. 105–113, 1982, doi: 10.1007/BF00536318.

[10] S. P. Timoshenko, “Problems concerning elastic stability in structures,” *Trans. Am. Soc. Civ. Eng. Trans ASCE*, vol. 94, no. 1, pp. 1000–1020, 1930.

[11] F. Bleich, *Buckling Strength of Metal Structures*. McGraw-Hill, 1952.

[12] L. Mann, “Statische Berechnung steifer Viereckknetze,” *Z. Für Bauwes.*, vol. 59, pp. 539–568, 1909.

[13] K. Ljungberg, “Auf Knickung beanspruchte Gitterstabe,” *Eisenbau*, vol. 13, pp. 100–105, 1922.

[14] R. von Mises and J. Ratzersdorfer, “Die Knicksicherheit von Fachwerken,” *Z. Für Angew. Math. Mech.*, vol. 5, no. 3, pp. 218–235, 1925.

[15] R. von Mises and J. Ratzersdorfer, “Die Knicksicherheit von Rahmentragwerken,” *Z. Für Angew. Math. Mech.*, vol. 6, no. 3, pp. 181–199, 1926.

[16] E. Chwalla, “Die Stabilität des Rahmenstabes,” *Sitzungsberichte Akad. Wiss. Wien*, vol. 136, pp. 487–529, 1927.

[17] W. Wentzel, “Über die Stabilität des Gleichgewichtes ebener elastischer Stabwerke und die Knickfestigkeit des Gitterträgers,” Berlin, 1929.

[18] L. (Editor) Tall, *Structural Steel Design*, 2nd ed. New York: Ronald Press Company, 1974.

[19] H. Müller-Breslau, “Über exzentrisch gedrückte gegliederte Stäbe,” *Sitz. Phys.-Math. Cl.*, vol. 17, pp. 166–181, 1910.

[20] Petermann, “Müller-Breslaus Knickversuche mit Rahmenstäben,” *Bauing.*, vol. 7, no. 51, 52, pp. 979–981, 1009–1016, 1926.

[21] Petermann, “Knickversuche mit Rahmenstäben aus St. 48,” *Bauing.*, vol. 12, no. 28, pp. 509–515, 1931.

[22] D. H. Young, “Rational design of steel columns,” *Trans. ASCE*, vol. 101, pp. 422–451, 1936.

[23] M. Holt, “Tests on built-up columns of structural aluminum alloy,” *Trans. Am. Soc. Civ. Eng.*, vol. 105, pp. 196–219, 1940.

[24] A. J. S. Pippard, “The critical load of a battened column,” *Philos. Mag. 7th Ser.*, vol. 39, no. 228, pp. 58–66, 1948.

[25] A. J. S. Pippard, “The critical load of a battened column,” in *Studies in elastic structures*, London: Edward Arnold & Co., 1952, pp. 193–201.

[26] S. P. Timoshenko and J. M. Gere, *Theory of Elastic Stability*. Courier Corporation, 1961.

[27] W. H. Ng, “The behaviour and design of battened structural members,” Ph.D. thesis, Cambridge University, Cambridge, England, 1947.

[28] W. H. Ng, “The behaviour and design of battened structural members,” *Weld. Res.*, vol. 5, no. 3, pp. 175r–188r, 1951.

[29] B. D. Jones, “A theory for struts with lattice or batten bracing,” *Struct. Eng.*, vol. 30, no. 5, pp. 108–113, 1952.

[30] F. Koenigsberger and M. E. Mohsin, “Design and load carrying capacity of welded battened struts,” *Struct. Eng.*, vol. 34, no. 6, pp. 183–203, 1956.

[31] M. E. Mohsin, “The critical load of unsymmetrical welded battened struts,” *Struct. Eng.*, vol. 43, no. 11, pp. 379–385, 1965.

[32] M. E. Moshin, “The critical load of battened columns,” *Assiut Sci. Technol. Bull.*, vol. 1, pp. 23–40, 1958.

[33] J. Y. Tamayo and M. Ojalvo, “Buckling of three-legged columns with batten bracing,” *ASCE J. Struct. Div.*, vol. 91, no. ST1, pp. 141–153, 1965.

[34] R. A. Williamson and M. N. Margolin, “Shear effects in design of guyed towers,” *ASCE J. Struct. Div.*, vol. 92, no. ST5, pp. 213–235, 1966.

[35] F. J. Lin, E. C. Glauser, and B. G. Johnston, “Behaviour of laced and battened structural members,” *ASCE J. Struct. Div.*, vol. 96, no. ST7, pp. 1377–1401, 1970.

[36] B. G. Johnston, “Spaced steel columns,” *ASCE J. Struct. Div.*, vol. 97, no. ST5, pp. 1465–1479, 1971.

[37] J. B. Kennedy and M. K. S. Madugula, “Buckling of steel angle and tee struts,” *ASCE J. Struct. Div.*, vol. 98, no. ST11, pp. 2507–2522, 1972.

[38] G. Ballio and F. M. Mazzolani, *Theory and design of steel structures*. London, England: Chapman and Hall, Ltd., 1983.

[39] V. Gioncu, “Buckling of built up members,” presented at the International Colloquium on Stability of Steel Structures, Budapest, Hungary, 1990, pp. 41–60.

[40] C. Libove, “Sparsely connected built-up columns,” *ASCE J. Struct. Eng.*, vol. 111, no. 3, p p. 609–627, 1985.

[41] J. S. Chang, “Buckling and post-buckling behaviour of sparsely connected built-up columns,” Ph.D. Dissertation, Syracuse University, Syracuse, NY, 1984.

[42] J. S. Chang, “On the tangent modulus theory of inelastic buckling of built-up columns,” *J. Chin. Inst. Eng.*, vol. 14, no. 1, pp. 65–72, 1991.

[43] F. R. Shanley, “Inelastic column theory,” *J. Aeronaut. Sci.*, vol. 14, no. 5, pp. 261–268, 1947.

[44] M. C. Temple, J. A. Schepers, and D. J. L. Kennedy, “Interconnection of starred angle compression members,” *Can. J. Civ. Eng.*, vol. 13, no. 6, pp. 606–619, 1986.

[45] M. C. Temple, D. C. McClosky, and J. M. Calabrese, “Interconnection of boxed angle compression members,” *Can. J. Civ. Eng.*, vol. 14, no. 4, pp. 534–541, 1987.

[46] M. C. Temple and J. C. Tan, “Interconnection of widely spaced angles,” *Can. J. Civ. Eng.*, vol. 15, no. 4, pp. 732–741, 1988.

[47] G. J. Krige and K. T. Wolmarans, “The battening of starred angle struts,” *Civ. Eng. South Afr.*, vol. 33, no. 4, p. 1991.

[48] A. Astaneh-Asl and S. C. Goel, “Cyclic in-plane buckling of double angle bracing,” *ASCE J. Struct. Eng.*, vol. 110, no. 9, pp. 2036–2055, 1984.

[49] F. Aslani and S. Goel, “An analytical criterion for buckling strength of built-up compression members,” *Eng. J.*, vol. 28, pp. 159–168, 1991.

[50] A. Astaneh-Asl, S. C. Goel, and R. D. Hanson, “Cyclic Out-of-Plane Buckling of Double-Angle Bracing,” *J. Struct. Eng.*, vol. 111, no. 5, pp. 1135–1153, May 1985, doi: 10.1061/(ASCE)0733-9445(1985)111:5(1135).

[51] F. Aslani and S. C. Goel, “Stitch Spacing and Local Buckling in Seismic-Resistant Double-Angle Braces,” *J. Struct. Eng.*, vol. 117, no. 8, pp. 2442–2463, Aug. 1991, doi: 10.1061/(ASCE)0733-9445(1991)117:8(2442).

[52] A. Gjelsvik, “Buckling of Built-Up Columns with or without stay plates,” *J. Eng. Mech.*, vol. 116, no. 5, pp. 1142–1159, May 1990, doi: 10.1061/(ASCE)0733-9399(1990)116:5(1142).

[53] A. Gjelsvik, “A new theory of built-up columns,” in *Proceedings of Papers Presented at the Structures Congress ’93*, Irvine, CA: ASCE, Apr. 1993, pp. 1462–1465.

[54] M. Paul, “Theoretical and experimental investigation of buckling of built-up columns,” Ph.D. Dissertation, Columbia University, New York, 1993.

[55] M. Paul, “Buckling loads for built-up columns with stay plates,” *ASCE J. Eng. Mech.*, vol. 121, no. 11, pp. 1200–1208, 1995.

[56] M. Paul, “Theoretical and experimental study on buckling of built-up columns,” *ASCE J. Eng. Mech.*, vol. 121, no. 10, pp. 1098–1105, 1995.

[57] M. Toossi, “On the out-of-plane buckling of battened columns,” *Int. J. Mech. Sci.*, vol. 14, no. 8, pp. 511–521, 1972.

[58] S. Kitipornchai and H. W. Lee, “Inelastic buckling of single-angle, tee and double-angle struts,” *J. Constr. Steel Res.*, vol. 6, no. 1, pp. 3–20, Jan. 1986, doi: 10.1016/0143-974X(86)90018-0.

[59] AISC, *Load and resistance factor design specification for structural steel buildings. Part 6 of Manual of steel construction. Load and resistance factor design*, 1st ed., vol. I. Chicago, IL: American Institute of Steel Construction, 1986.

[60] C. J. Zahn and G. Haaijer, “Effect of connector spacing on double angle compressive strength,” presented at the Materials and Member Behaviour. Proceedings of the Sessions at Structures Congress ’87, Structural Division of the American Society of Civil Engineers, 1987, pp. 199–212.

[61] C. J. Zahn and G. Haaijer, “Effect of connector spacing and flexural-torsional buckling on double-angle compressive strength,” *Eng. J. AISC*, vol. 25, no. 3, pp. 109–118, 1988.

[62] R. Zandonini, “Stability of compact built-up struts: experimental investigation and numerical simulation,” *Construzione Met.*, no. 4, pp. 202–224, 1985.

[63] AISC, *Load and resistance factor design specification for structural steel buildings. Part 6 of Manual of steel construction. Load and resistance factor design*, 2nd ed., vol. 1. Chicago, IL: American Institute of Steel Construction, 1993.

[64] M. C. Temple and G. Elmahdy, “Equivalent slenderness ratio for built-up members,” *Can. J. Civ. Eng.*, vol. 20, no. 4, pp. 708–711, Aug. 1993, doi: 10.1139/l93-087.

[65] M. C. Temple and G. Elmahdy, “Local effective length factor in the equivalent slenderness ratio,” *Can. J. Civ. Eng.*, vol. 22, no. 6, pp. 1164–1170, Dec. 1995, doi: 10.1139/l95-134.

[66] W. T. Koiter, “Over de stabiliteit van het elastsch evenwicht (On the stability of elastic equilibrium),” Ph.D. thesis, Delft University of Technology, Amsterdam, 1945.

[67] A. van der Neut, “The interaction of local buckling and column failure of thin-walled compression members,” in *Proceedings of the 12th International Congress on Applied Mechanics*, Stanford, CA, 1968, pp. 389–399.

[68] T. R. Graves-Smith, “The ultimate strength of locally buckled columns of arbitrary length,” in *Thin Walled Steel Structures: Their Design and Use in Building*, K. C. Rockey and V. H. Harold, Eds., London: Crosby Lockwood & Son Ltd., 1969, pp. 35–60.

[69] W. T. Koiter and G. D. C. Kuiken, “The interaction between local buckling and overall buckling on the behaviour of built-up columns,” 447, 1971.

[70] J. M. T. Thompson and G. M. Lewis, “On the optimum design of thin-walled compression members,” *J. Mech. Phys. Solids*, vol. 20, no. 2, pp. 101–109, 1972.

[71] S. E. Svensson and J. G. A. Croll, “Interaction between local and overall buckling,” *Int. J. Mech. Sci.*, vol. 17, no. 4, pp. 307–321, 1975.

[72] Q. S. Fan, “Interaction of buckling modes of panels with symmetric cross section,” *ASCE J. Eng. Mech.*, vol. 115, no. 11, pp. 2526–2542, 1989.

[73] G. V. Palassopoulos, “Optimization of imperfection-sensitive structures,” *ASCE J. Eng. Mech.*, vol. 115, no. 8, pp. 1663–1682, 1989.

[74] G. V. Palassopoulos, “Reliability-based design of imperfection-sensitive structures,” vol. 117, no. 6, pp. 1220–1240, 1991.

[75] G. V. Palassopoulos, “New approach to buckling of imperfection-sensitive structures,” *ASCE J. Eng. Mech.*, vol. 119, no. 4, pp. 850–869, 1993.

[76] K. Ikeda and K. Murota, “Critical initial imperfection of structures,” *Int. J. Solids Struct.*, vol. 26, no. 8, pp. 865–886, 1990.

[77] Y. Migita, T. Aoki, and Y. Fukumoto, “Local and interaction buckling of polygonal section steel columns,” *ASCE J. Struct. Eng.*, vol. 118, no. 10, pp. 2659–2675, 1992.

[78] V. Gioncu, E. Fleseriu, and I. Munteanu, “Theoretical investigation on the interaction between flexural-torsional buckling and local buckling,” in *Proceedings of the 3rd International Colloquium on Stability of Metal Structures*, Paris, 1983, pp. 219–226.

[79] M. Pignataro and A. Luongo, “Simultaneous buckling modes and imperfection sensitivity of channels in compression,” in *Euromech. 200*, Mátrafüred, Hungary, 1985, pp. 233–252.

[80] K. J. R. Rasmussen and G. J. Hancock, “Nonlinear analyses of thin-walled channel section columns,” *Thin-Walled Struct.*, vol. 13, no. 1–2, pp. 145–176, 1991.

[81] K. J. R. Rasmussen and G. J. Hancock, “The flexural behaviour of fixed-ended channel section columns,” *Thin-Walled Struct.*, vol. 17, no. 1, pp. 45–63, 1993.

[82] J. M. T. Thompson and G. W. Hunt, *A general theory of elastic stability*. London, England: John Wiley and Sons, 1973.

[83] J. M. T. Thompson and G. W. Hunt, “Dangers of structural optimization,” *Eng. Optim.*, vol. 1, pp. 99–110, 1974.

[84] R. F. Crawford and J. M. Hedgepeth, “Effects of initial waviness on the strength and design of built-up structures,” *AIAA J.*, vol. 13, no. 5, pp. 672–675, 1975.

[85] E. Byskov, “Applicability of an asymptotic expansion for elastic buckling problems with mode interaction,” *AIAA J.*, vol. 17, no. 6, pp. 630–633, 1979.

[86] R. K. Miller and J. M. Hedgepeth, “The buckling of lattice columns with stochastic imperfections,” *Int. J. Solids Struct.*, vol. 15, no. 1, pp. 73–84, 1979.

[87] R. F. Crawford and M. D. Benton, “Strength of initially wavy lattice columns,” *AIAA J.*, vol. 18, no. 5, pp. 581–584, 1980.

[88] S. E. Svensson and J. Kragerup, “Collapse Loads of Laced Columns,” *J. Struct. Div.*, vol. 108, no. 6, pp. 1367–1384, Jun. 1982, doi: 10.1061/JSDEAG.0005972.

[89] S. E. Svensson and J. Kragerup, “Interaction effects in two-flange built-up columns,” in *Proceedings of the 3rd International Colloquium on Stability of Metal Structures*, 1983, pp. 55–60.

[90] N. Bälut, D. Porumb, and N. Rennon, “Interaction between individual buckling of the chords and overall buckling of laced columns,” in *Proceedings of the 3rd International Colloquium on Stability*, Timișoara, Romania, 1982, pp. 240–247.

[91] V. Gioncu, “Coupled instabilities in bar structures, phenomenon, theory, practice,” in *Proceedings of the 4th International Colloquium, North America Session, on Stability of Metal Structures*, New York City, NY, 1989, pp. 357–369.

[92] G. S. Tong and S. F. Chen, “An interactive buckling theory for built-up beam-columns and its application to centrally compressed built-up members,” *J. Constr. Steel Res.*, vol. 14, no. 3, pp. 221–241, 1989.

[93] Z. P. Bazant and L. Cedolin, *Stability of Structures: Elastic, Inelastic, Fracture, and Damage Theories*. New York: Oxford University Press, Inc., 1991.

[94] L. Duan, M. Reno, and C.-M. Uang, “Effect of compound buckling on compression strength of built-up members,” *Eng. J.*, vol. 39, pp. 30–37, Mar. 2002.

[95] R. D. Ziemian, *Guide to Stability Design Criteria for Metal Structures*. John Wiley & Sons, 2010.

[96] L. S. Beedle and L. Tall, “Basic Column Strength,” *ASCE J. Struct. Div.*, vol. 86, no. ST5, pp. 139–173, 1960.

[97] P. Može, L.-G. Cajot, F. Sinur, K. Rejec, and D. Beg, “Residual stress distribution of large steel equal leg angles,” *Eng. Struct.*, vol. 71, pp. 35–47, Jul. 2014, doi: 10.1016/j.engstruct.2014.03.040.

[98] H. Ban, G. Shi, Y. Shi, and Y. Wang, “Residual Stress Tests of High-Strength Steel Equal Angles,” *J. Struct. Eng.*, vol. 138, no. 12, pp. 1446–1454, Dec. 2012, doi: 10.1061/(ASCE)ST.1943-541X.0000585.

[99] J. Lindner and T. Glitsch, “Vereinfachter Nachweis für I- und U-Träger – beansprucht durch doppelte Biegung und Torsion,” *Stahlbau*, vol. 73, no. 9, pp. 704–715, 2004, doi: 10.1002/stab.200490174.

[100] A. Beyer, N. Boissonnade, A. Khelil, and A. Bureau, “Influence of assumed geometric and material imperfections on the numerically determined ultimate resistance of hot-rolled U-shaped steel members,” *J. Constr. Steel Res.*, vol. 147, pp. 103–115, Aug. 2018, doi: 10.1016/j.jcsr.2018.03.021.

[101] ECCS, *Manual on Stability of Steel Structures*. 1976.

[102] T. Geng-Shu and C. Shao-Fan, “An interactive buckling theory for built-up beam-columns and its application to centrally compressed built-up members,” *J. Constr. Steel Res.*, vol. 14, no. 3, pp. 221–241, Jan. 1989, doi: 10.1016/0143-974X(89)90074-6.

[103] L. Duan, M. Reno, and C.-M. Uang, “Effect of Compound Buckling on Compression Strength of Built-up Members,” *Eng. J.*, vol. 39, pp. 30–37, Mar. 2002.

[104] K. E. Kalochairetis and C. J. Gantes, “Numerical and analytical investigation of collapse loads of laced built-up columns,” *Comput. Struct.*, vol. 89, no. 11, pp. 1166–1176, Jun. 2011, doi: 10.1016/j.compstruc.2010.10.018.

[105] M. A. El Aghoury, A. H. Salem, M. T. Hanna, and E. A. Amoush, “Experimental investigation for the behaviour of battened beam-columns composed of four equal slender angles,” *Thin-Walled Struct.*, vol. 48, no. 9, pp. 669–683, Sep. 2010, doi: 10.1016/j.tws.2010.03.007.

[106] M. A. El Aghoury, A. H. Salem, M. T. Hanna, and E. A. Amoush, "Ultimate capacity of battened columns composed of four equal slender angles," *Thin-Walled Struct.*, vol. 63, pp. 175–185, Feb. 2013, doi: 10.1016/j.tws.2012.07.019.

[107] Y. Li, W. Cheng, B. Wang, and Y. Ren, "Investigation on Elastic Compound Buckling of Latticed Columns Considering Eccentricity and Geometric Imperfections," *Adv. Mech. Eng.*, vol. 11, no. 5, p. 1687814019847400, May 2019, doi: 10.1177/1687814019847400.

[108] Y. Li, F. Liu, and W. Cheng, "Influence of lacing bars on the buckling capacity of four-legged latticed columns considering geometric imperfections," *Sci. Prog.*, vol. 104, no. 2, p. 00368504211025905, Apr. 2021, doi: 10.1177/00368504211025905.

[109] R. M. Korol, A. Rutenberg, and D. Bagnariol, "On primary and secondary stresses in triangulated trusses," *J. Constr. Steel Res.*, vol. 6, no. 2, pp. 123–142, Jan. 1986, doi: 10.1016/0143-974X(86)90002-7.

[110] C. Higgins, A. Hafner, O. T. Turan, and T. Schumacher, "Experimental Tests of Truss Bridge Gusset Plate Connections with Sway-Buckling Response," *J. Bridge Eng.*, vol. 18, no. 10, pp. 980–991, Oct. 2013, doi: 10.1061/(ASCE)BE.1943-5592.0000433.

[111] L. Zheng, X. Qu, Y. Gao, and H. Guo, "The In-Plane Effective Length Factor of Web Members of the Steel Truss," *Int. J. Steel Struct.*, vol. 21, no. 3, pp. 800–819, Jun. 2021, doi: 10.1007/s13296-021-00474-1.

[112] AISC, *Specification for Structural Steel Buildings*. ANSI/AISC 360-22, American Institute of Steel Construction, Chicago, IL, 2022.

[113] American Association of State Highway and Transportation Officials, Ed., *LRFD bridge design specifications*, 9th edition. Washington, DC: American Association of State Highway and Transportation Officials, 2020.

[114] Canadian Standards Association, *CSA S16:24 – Design of Steel Structures*. Toronto, Ontario, Canada: CSA Group, 2024.

[115] CSA-S6, *Canadian Highway Bridge Design Code*. CAN/CSA-S6:19. Canadian Standards Association (CSA), Mississauga, Ont, 2019.

[116] European Committee for Standardization (CEN), *prEN 1993-1-1: Eurocode 3 - Design of steel structures - Part 1-1: General rules and rules for buildings*.

[117] L. Gardner, "The Continuous Strength Method," presented at the Proceedings of the Institution of Civil Engineers, Institution of Civil Engineers, 2008.

[118] L. Gérard, "Contribution to the Design of Steel I and H-Sections Members by Means of the Overall Interaction Concept," Ph.D. thesis, Laval University, 2020. [Online]. Available: https://hdl.handle.net/20.500.11794/68162

[119] B. W. Schafer, "Review: The Direct Strength Method of cold-formed steel member design," *J. Constr. Steel Res.*, vol. 64, no. 7, pp. 766–778, Jul. 2008, doi: 10.1016/j.jcsr.2008.01.022.

[120] B. W. Schafer, "Project: Cross-section Stability of Structural Steel," Johns Hopkins University, Baltimore.

[121] B. Young, P. B. Dinis, and D. Camotim, “CFS lipped channel columns affected by L-D-G interaction. Part I: Experimental investigation,” *Comput. Struct.*, vol. 207, pp. 219–232, Sep. 2018, doi: 10.1016/j.compstruc.2017.03.016.

[122] P. B. Dinis, D. Camotim, B. Young, and E. M. Batista, “CFS lipped channel columns affected by L-D-G interaction. Part II: Numerical simulations and design considerations,” *Comput. Struct.*, vol. 207, pp. 200–218, Sep. 2018, doi: 10.1016/j.compstruc.2017.03.017.

[123] N. Boissonnade, M. Hayeck, E. Saloumi, and J. Nseir, “An Overall Interaction Concept for an alternative approach to steel members design,” *J. Constr. Steel Res.*, vol. 135, pp. 199–212, Aug. 2017, doi: 10.1016/j.jcsr.2017.02.030.

[124] J. Nseir, “Development of a New Design Method for the Cross-Section Capacity of Steel Hollow Sections,” Ph.D. thesis, University of Applied Sciences of Western Switzerland - Fribourg, University of Liège, Saint-Joseph University Beirut, 2015.

[125] H. Michel, “Development of a New Design Method for Steel Hollow Section Members Resistance,” Ph.D. thesis, University of Applied Sciences of Western Switzerland - Fribourg, University of Liège, Saint-Joseph University Beirut, 2016.

[126] L. Li and N. Boissonnade, “Local/global coupled instabilities of slender I-sections under compression,” *Thin-Walled Struct.*, vol. 172, p. 108842, Mar. 2022, doi: 10.1016/j.tws.2021.108842.

[127] L. Li, L. Gérard, M. Kettler, and N. Boissonnade, “The Overall Interaction Concept for the design of hot-rolled and welded I-sections under combined loading,” *Thin-Walled Struct.*, vol. 172, p. 108623, Mar. 2022, doi: 10.1016/j.tws.2021.108623.

[128] L. Gérard, L. Li, M. Kettler, and N. Boissonnade, “Steel I-sections resistance under compression or bending by the Overall Interaction Concept,” *J. Constr. Steel Res.*, vol. 182, p. 106644, Jul. 2021, doi: 10.1016/j.jcsr.2021.106644.

[129] A.-S. Gagné, L. Gérard, and N. Boissonnade, “Design of stainless steel cross-sections for simple load cases with the O.I.C.,” *J. Constr. Steel Res.*, vol. 168, p. 105936, May 2020, doi: 10.1016/j.jcsr.2020.105936.

[130] L. Li, L. Gérard, S. Langlois, and N. Boissonnade, “O.I.C.-based design of mono-symmetric I-sections under simple load cases,” *Thin-Walled Struct.*, vol. 174, p. 109134, May 2022, doi: 10.1016/j.tws.2022.109134.

[131] L. Li, M. Fafard, and N. Boissonnade, “Local and global instabilities of rolled T-section columns under axial compression,” *Thin-Walled Struct.*, vol. 178, p. 109517, Sep. 2022, doi: 10.1016/j.tws.2022.109517.

[132] L. Li, S. Dahboul, P. Verma, P. Dey, M. Fafard, and N. Boissonnade, “O.I.C.-Based Design of Aluminum Circular Hollow Sections under Compression or Pure Bending,” *Eng. Proc.*, vol. 43, no. 1, Art. no. 1, 2023, doi: 10.3390/engproc2023043031.

[133] S. Dahboul, T. Coderre, L. Li, and N. Boissonnade, “Behaviour and Design of I-Shaped Aluminium Sections,” *Eng. Proc.*, vol. 43, no. 1, Art. no. 1, 2023, doi: 10.3390/engproc2023043035.

[134] S. Dahboul, L. Li, T. Coderre, and N. Boissonnade, "O.I.C.-based design of extruded and welded aluminum I-sections," *Structures*, vol. 58, p. 105504, Dec. 2023, doi: 10.1016/j.istruc.2023.105504.

[135] M. C. Temple and G. Elmahdy, "Buckling of built-up compression members in the plane of the connectors," *Can. J. Civ. Eng.*, vol. 20, no. 6, pp. 895–909, Dec. 1993, doi: 10.1139/l93-122.

[136] B. Hosseini Hashemi and M. A. Jafari, "Experimental evaluation of elastic critical load in batten columns," *J. Constr. Steel Res.*, vol. 65, no. 1, pp. 125–131, Jan. 2009, doi: 10.1016/j.jcsr.2008.02.016.

[137] B. Hosseini Hashemi and A. Poursamad Bonab, "Experimental investigation of the behaviour of laced columns under constant axial load and cyclic lateral load," *Eng. Struct.*, vol. 57, pp. 536–543, Dec. 2013, doi: 10.1016/j.engstruct.2013.09.033.

[138] L. Duan and W.-F. Chen, "Design rules of built-up members in load and resistance factor design," *J. Struct. Eng.*, vol. 114, no. 11, pp. 2544–2554, Nov. 1988, doi: 10.1061/(ASCE)0733-9445(1988)114:11(2544).

[139] A. Sato and C.-M. Uang, "Modified slenderness ratio for built-up members," *Eng. J. N. Y.*, vol. 44, pp. 269–280, Sep. 2007.

[140] A. G. Razdolsky, "Revision of Engesser's Approach to the Problem of Euler Stability for Built-Up Columns with Batten Plates," *J. Eng. Mech.*, vol. 140, no. 3, pp. 566–574, Mar. 2014, doi: 10.1061/(ASCE)EM.1943-7889.0000677.

[141] A. Gjelsvik, "Buckling of Built-Up Columns with or without stay plates," *J. Eng. Mech.*, vol. 116, no. 5, pp. 1142–1159, May 1990, doi: 10.1061/(ASCE)0733-9399(1990)116:5(1142).

[142] C. J. Gantes and K. E. Kalochairetis, "Axially and transversely loaded Timoshenko and laced built-up columns with arbitrary supports," *J. Constr. Steel Res.*, vol. 77, pp. 95–106, Oct. 2012, doi: 10.1016/j.jcsr.2012.05.004.

[143] M. A. Dar, D. R. Sahoo, and A. K. Jain, "Interaction between chord compactness and lacing slenderness in CFS built-up columns," *Structures*, vol. 30, pp. 985–995, Apr. 2021, doi: 10.1016/j.istruc.2021.01.065.

[144] M. A. El Aghoury, A. H. Salem, M. T. Hanna, and E. A. Amoush, "Experimental investigation for the behaviour of battened beam-columns composed of four equal slender angles," *Thin-Walled Struct.*, vol. 48, no. 9, pp. 669–683, Sep. 2010, doi: 10.1016/j.tws.2010.03.007.

[145] I. J. Baláž, Y. P. Koleková, and L. O. Moroczová, "Behaviour of steel laced built-up columns," in *Advances and Trends in Engineering Sciences and Technologies III*, 1st ed., M. Al Ali and P. Platko, Eds., CRC Press, 2019, pp. 29–35. doi: 10.1201/9780429021596-5.

[146] I. Baláž, Y. Koleková, and L. Moroczová, "Built-up CFS column with lacings and battens," *MATEC Web Conf.*, vol. 310, p. 00025, 2020, doi: 10.1051/matecconf/202031000025.

[147] L. Duan, M. Reno, and J. Lynch, “Section Properties for Latticed Members of San Francisco–Oakland Bay Bridge,” *J. Bridge Eng.*, vol. 5, no. 2, pp. 156–164, May 2000, doi: 10.1061/(ASCE)1084-0702(2000)5:2(156).

[148] M. Kleiser and C.-M. Uang, “Steel Latticed Members under Cyclic Axial and Flexural Actions,” *J. Struct. Eng.*, vol. 125, no. 4, pp. 393–400, Apr. 1999, doi: 10.1061/(ASCE)0733-9445(1999)125:4(393).

[149] A. Astaneh-Asl, R. A. Dameron, A. Itani, A. Krimotat, and C.-M. Uang, “Proof-Testing of Latticed Members and Their Connections on SFOBB,” Art. no. UCB/CEE-STEEL-98-03, 1998.

[150] K. Lee and M. Bruneau, “Seismic vulnerability evaluation of axially loaded steel built-up laced members I: experimental results,” *Earthq. Eng. Eng. Vib.*, vol. 7, no. 2, pp. 113–124, Jun. 2008, doi: 10.1007/s11803-008-0831-x.

[151] S. W. Cho and A. Astaneh-Asl, “Compressive behaviour of critical members of the Golden Gate Bridge,” 1994, pp. 713–722.

[152] C. M. Bowen, S.-W. Cho, and A. Astaneh-Asl, *Post buckling behaviour of laced members and main tower legs of the Golden Gate Bridge*. 1996, pp. 487–496.

[153] A. Astaneh-Asl, “Preservation of historical bridges in USA: The Golden Gate Bridge and The Albion River Bridge cases,” Jul. 2017.

[154] prEN 1993-1-1:2020, *Eurocode 3: Design of Steel Structures – Part 1-1: General Rules and Rules for Buildings*. Doc. CEN-TC250-SC3_N3023, 2019.

[155] AS 4100:2020, *Steel Structures, Standards Australia*. Sydney.

[156] “Abaqus/CAE,” Dassault Systèmes, Version 2022, 2022. [Online]. Available: https://www.3ds.com/products-services/simulia/products/abaqus/

[157] B. Huang and W. F. Zhang, “Local-overall interactive buckling of high strength steel welded I-section columns under axial compression,” *Thin-Walled Struct.*, vol. 157, p. 106964, Dec. 2020, doi: 10.1016/j.tws.2020.106964.

[158] Y. Wang, M. A. Bradford, and X. Liu, “Strength design of welded high-strength steel beams considering coupled local and global buckling,” *Thin-Walled Struct.*, vol. 149, p. 106391, Apr. 2020, doi: 10.1016/j.tws.2019.106391.

[159] L. Gérard, L. Li, M. Kettler, and N. Boissonnade, “Recommendations on the geometrical imperfections definition for the resistance of I-sections,” *J. Constr. Steel Res.*, vol. 162, p. 105716, Nov. 2019, doi: 10.1016/j.jcsr.2019.105716.

[160] G. Iskander, E. Soliman, and E. Sayed-Ahmed, “Design of built-up steel beam-columns composed of two-channel sections,” *Can. J. Civ. Eng.*, vol. 48, no. 11, pp. 1508–1522, Nov. 2021, doi: 10.1139/cjce-2020-0151.

[161] O. Chhoeng, M. C. M. Wack, R. Tremblay, and N. Boissonnade, “Stability and response of lacing systems in laced built-up truss bridge columns,” 2025, Accessed: Jun. 13, 2025. [Online]. Available: https://files.ssrcweb.org/proceedings/2025/Chhoeng_et_al_SSRC_2025.pdf

[162] X. Yun and L. Gardner, “Stress-strain curves for hot-rolled steels,” *J. Constr. Steel Res.*, vol. 133, pp. 36–46, Jun. 2017, doi: 10.1016/j.jcsr.2017.01.024.

[163] ATC, “Guidelines for Cyclic Seismic Testing of Components of Steel Structures,” Redwood City, Calif., No. ATC-24, 1992.

[164] A. P. Bonab, B. H. Hashemi, and M. Hosseini, “Experimental evaluation of the elastic buckling and compressive capacity of laced columns,” *J. Constr. Steel Res.*, vol. 86, pp. 66–73, Jul. 2013, doi: 10.1016/j.jcsr.2013.03.014.

[165] K. E. Kalochairetis, C. J. Gantes, and X. A. Lignos, “Experimental and numerical investigation of eccentrically loaded laced built-up steel columns,” *J. Constr. Steel Res.*, vol. 101, pp. 66–81, Oct. 2014, doi: 10.1016/j.jcsr.2014.04.032.

[166] R. V. Southwell, “On the analysis of experimental observations in problems of elastic stability,” *Proc. R. Soc. Lond. Ser. Contain. Pap. Math. Phys. Character*, vol. 135, no. 828, pp. 601–616, Jan. 1997, doi: 10.1098/rspa.1932.0055.

[167] T. Geng-Shu and C. Shao-Fan, “An interactive buckling theory for built-up beam-columns and its application to centrally compressed built-up members,” *J. Constr. Steel Res.*, vol. 14, no. 3, pp. 221–241, Jan. 1989, doi: 10.1016/0143-974X(89)90074-6.

[168] T. von Kármán, E. E. Sechler, and L. H. Donnell, “The Strength of Thin Plates in Compression,” *Trans. Am. Soc. Mech. Eng.*, vol. 54, no. 2, pp. 53–56, Apr. 2023, doi: 10.1115/1.4021738.

[169] M. Seif and B. W. Schafer, “Local buckling of structural steel shapes,” *J. Constr. Steel Res.*, vol. 66, no. 10, pp. 1232–1247, Oct. 2010, doi: 10.1016/j.jcsr.2010.03.015.

[170] L. Gardner, A. Fieber, and L. Macorini, “Formulae for Calculating Elastic Local Buckling Stresses of Full Structural Cross-sections,” *Structures*, vol. 17, pp. 2–20, Feb. 2019, doi: 10.1016/j.istruc.2019.01.012.

[171] T. Usami and Y. Fukumoto, “Welded box compression members,” *J. Struct. Eng. J Struct Eng*, vol. 110, no. 10, pp. 2457–2470, 1984.

[172] L. Gardner, X. Yun, and F. Walport, “The Continuous Strength Method – Review and outlook,” *Eng. Struct.*, vol. 275, p. 114924, Jan. 2023, doi: 10.1016/j.engstruct.2022.114924.

[173] B. Young and K. J. R. Rasmussen, “Behaviour of cold-formed singly symmetric columns,” 1999, Accessed: Jan. 29, 2025. [Online]. Available: http://hub.hku.hk/handle/10722/150128

[174] B. Young and J. Yan, “Channel Columns Undergoing Local, Distortional, and Overall Buckling,” *J. Struct. Eng.*, vol. 128, no. 6, pp. 728–736, Jun. 2002, doi: 10.1061/(ASCE)0733-9445(2002)128:6(728).

[175] P. B. Dinis and D. Camotim, “Local/distortional/global mode interaction in simply supported cold-formed steel lipped channel columns,” *Int. J. Struct. Stab. Dyn.*, vol. 11, no. 05, pp. 877–902, Oct. 2011, doi: 10.1142/S0219455411004385.

[176] P. B. Dinis, E. M. Batista, D. Camotim, and E. S. dos Santos, “Local–distortional–global interaction in lipped channel columns: Experimental results, numerical simulations and

design considerations," *Thin-Walled Struct.*, vol. 61, pp. 2–13, Dec. 2012, doi: 10.1016/j.tws.2012.04.012.

[177] P. B. Dinis, D. Camotim, E. Batista, and E. Santos, "Local / distortional / global mode coupling in fixed lipped channel columns: Behaviour and strength," *Adv. Steel Constr.*, vol. 7, no. 4, pp. 113–130, 2011.

[178] E. Souza dos Santos, E. de Miranda Batista, and D. Camotim, "Cold-formed steel columns under L-D-G interaction," *Steel Constr.*, vol. 7, no. 3, pp. 193–198, 2014, doi: 10.1002/stco.201410034.

[179] E. S. Santos, E. M. Batista, and D. Camotim, "Experimental investigation concerning lipped channel columns undergoing local–distortional–global buckling mode interaction," *Thin-Walled Struct.*, vol. 54, pp. 19–34, May 2012, doi: 10.1016/j.tws.2012.02.004.

[180] D. Cava, D. Camotim, P. B. Dinis, and A. Madeo, "Numerical investigation and direct strength design of cold-formed steel lipped channel columns experiencing local–distortional–global interaction," *Thin-Walled Struct.*, vol. 105, pp. 231–247, Aug. 2016, doi: 10.1016/j.tws.2016.03.025.

[181] M. V. Anil Kumar and V. Kalyanaraman, "Interaction of Local, Distortional, and Global Buckling in CFS Lipped Channel Compression Members," *J. Struct. Eng.*, vol. 144, no. 2, p. 04017192, Feb. 2018, doi: 10.1061/(ASCE)ST.1943-541X.0001935.

[182] D. Camotim, A. D. Martins, P. B. Dinis, B. Young, M.-T. Chen, and A. Landesmann, "Mode interaction in cold-formed steel members: state-of-art report," *Steel Constr.*, vol. 13, no. 3, pp. 186–207, 2020, doi: 10.1002/stco.202000044.

[183] European Committee for Standardization (CEN), *prEN 1993-1-5: Eurocode 3 - Design of steel structures - Part 1-5: Plated structural elements*.

[184] CEN, European Committee for Standardization, *Eurocode 3: Design of Steel Structures – Part 1-14: Design Assisted by Finite Element Analysis*, prEN 1993-1-14:2020, Brussels., 2021.

[185] B. Johansson, R. Maquoi, G. Sedlacek, C. Müller, and D. Beg, "Commentary and Worked Examples to EN 1993-1-5 Plated Structural Elements," 2007. [Online]. Available: https://publications.jrc.ec.europa.eu/repository/handle/JRC38239

[186] M. C. Mefande Wack, O. Chhoeng, R. Tremblay, and N. Boissonnade, "On the definition of geometric imperfections in the FE modelling of local buckling in hot-rolled channel sections," in *Proceedings of the Annual Stability Conference Structural Stability Research Council, SSRC 2025*, SSRC, 2025. Accessed: Jul. 10, 2025. [Online]. Available: https://publications.polymtl.ca/66106/

[187] M. Kettler, "Elastic-Plastic Cross-Sectional Resistance of Semi-Compact H-and Hollow Sections," Graz University of Technology, 2008.

[188] D. Beg, U. Kuhlmann, and L. Davaine, *ECCS Eurocode Design Manual: Design of Plated Structures*. 2010.

[189] *Handbook of Steel Construction*, 12th, 2nd Revised Printing ed. Canadian Institute of Steel Construction, 2023.

[190] *Handbook of Structural Steelwork: Eurocode Edition*. The British Constructional Steelwork Association Ltd and The Steel Construction Institute, 2013.

[191] *Steel Construction Manual*, 15th ed. Chicago: American Institute of Steel Construction (AISC), 2017.

[192] W. E. Ayrton and J. Perry, "On struts," *The Engineer*, vol. 62, 1886.

[193] CEN (European Committee for Standardization), *EN 1990:2002 Eurocode – Basis of Structural Design*. Brussels, Belgium.

[194] T. Tankova, L. Simões da Silva, L. Marques, C. Rebelo, and A. Taras, "Towards a standardized procedure for the safety assessment of stability design rules," *J. Constr. Steel Res.*, vol. 103, pp. 290–302, Dec. 2014, doi: 10.1016/j.jcsr.2014.09.010.

[195] M. K. Ravindra and T. V. Galambos, "Load and Resistance Factor Design for Steel," *J. Struct. Div. ASCE*, vol. 104, no. ST9, 1978.

[196] M. Kettler, "Elastic-Plastic Cross-Sectional Resistance of Semi-Compact H- and Hollow Sections," Ph.D. thesis, Graz University of Technology, Graz, Austria, 2008.

[197] A. Taras, V. Dehan, L. S. da Silva, L. Marques, T. Tankova, "SAFEBRICTILE: Standardization of Safety Assessment Procedures Across Brittle to Ductile Failure Modes," 2016.

[198] SAFEBRICTILE, "Standardization of safety assessment procedures across brittle to ductile failure modes," SAFEBRICTILE Project, Guideline Deliverable D1.1, 2016.

[199] "Basis of Design and Actions on Structures: Background and Application of Eurocode 1," in *IABSE Colloquium*, Delft, The Netherlands: International Association for Bridge and Structural Engineering (IABSE), 1996.

[200] M. Su, "Behaviour and design of aluminium alloy structural elements," Doctor of Philosophy, The University of Hong Kong, Pokfulam Road, Hong Kong SAR, 2014. doi: 10.5353/th_b5328036.

[201] C. A. Rogers and G. J. Hancock, "Ductility of G550 Sheet Steels in Tension - Elongation Measurements and Perforated Tests," University of Sydney, Sydney, Australia, Research Report R735, 1996.

[202] O. Chhoeng, M. C. Mefande Wack, R. Tremblay, and N. Boissonnade, "O.I.C.-based design for local/global/built-up interaction in laced built-up steel columns".

[203] A. Astaneh-Asl, S. C. Goel, and R. D. Hanson, "Cyclic Out-of-Plane Buckling of Double-Angle Bracing," *J. Struct. Eng.*, vol. 111, no. 5, pp. 1135–1153, May 1985, doi: 10.1061/(ASCE)0733-9445(1985)111:5(1135).

[204] M. Dabaon, E. Ellobody, and K. Ramzy, "Nonlinear behaviour of built-up cold-formed steel section battened columns," *J. Constr. Steel Res.*, vol. 110, pp. 16–28, Jul. 2015, doi: 10.1016/j.jcsr.2015.03.007.

[205] T. A. Stone and R. A. LaBoube, "Behaviour of cold-formed steel built-up I-sections," *Thin-Walled Struct.*, vol. 43, no. 12, pp. 1805–1817, Dec. 2005, doi: 10.1016/j.tws.2005.09.001.

[206] B. Hosseini Hashemi and M. A. Jafari, “Evaluation of Ayrton–Perry formula to predict the compressive strength of batten columns,” *J. Constr. Steel Res.*, vol. 68, no. 1, pp. 89–96, Jan. 2012, doi: 10.1016/j.jcsr.2011.07.007.

[207] G. Winter, “Strength of Thin Steel Compression Flanges,” *Trans. Am. Soc. Civ. Eng.*, vol. 112, no. 1, pp. 527–554, Jan. 1947, doi: 10.1061/TACEAT.0006092.

[208] F. M. Bartlett, R. J. Dexter, M. D. Graeser, J. J. Jelinek, B. J. Schmidt, and T. V. Galambos, “Updating Standard Shape Material Properties Database for Design and Reliability,” *Eng. J.*, vol. 40, no. 1, Art. no. 1, Mar. 2003, doi: 10.62913/engj.v40i1.800.

[209] B. Ellingwood, T. V. Galambos, J. G. Mac Gregor, and C. A. Cornell, “Development of a Probability-Based Load Criterion for American National Standard A58,” National Bureau of Standards, Washington, D.C., 577, 1980.